Characterisation of mass transfer behaviour in continuous gas/liquid/solid catalysed processes including packed bed for predictive scale up/down

Ilias Stamatiou

Submitted in accordance with the requirements for the degree of

Doctor of Philosophy

The University of Leeds

School of Chemical and Process Engineering

July 2018

The candidate confirms that the work submitted is his own, except where work which has formed part of jointly authored publications has been included. The contribution of the candidate and the other authors to this work has been explicitly indicated below. The candidate confirms that appropriate credit has been given within the thesis where reference has been made to the work of others.

The work in section 4.3 of the thesis has been appeared in publication as follows:

Determination of Mass Transfer Resistances of Fast Reactions in Three-Phase Mechanically Agitated Slurry Reactors, January 2017, Ilias K. Stamatiou and Frans L. Muller, AIChE Journal.

I was responsible for the whole work related to the above publication.

Frans L. Muller had the supervision of the project and his contribution to the work related to the above publication was advisory.

Acknowledgements

First and foremost, I would like to thank my supervisor Professor Frans Muller for entrusting me this research project and mentoring me over the four prior years. Of course, I cannot forget my co-supervisors; Dr. Antonia Borissova and Dr. Richard Bourne for their input into the project. The EPSRC and the University of Leeds are acknowledged for providing the funding and facilities without which this project could not have been accomplished.

I would like to thank all my colleagues in the iPRD for making my days better. I owe my special thanks to Dr. Mary Bayana and Dr. William Reynolds for their every-day assistance and their advices. I'm grateful to Matthey Broadband for his mechanic expertise which made my calculations and designs real. I would like to thank Jonathan White for his help running the TBR and for his input into the calculation of the pellets, glass beads sizing and ICP-MS.

I would also like to acknowledge Syngenta for the financial support and for hosting me in their research centre in Jealott's Hill. I would like to thank my industrial supervisor Dr. Colin Brennan for all the support he provided; the whole team of process studies group, particularly Dr. George Hodge, Dr. Rachel Donkor and Dr. Hazmi Tajuddin for making my life there productive and enjoyable.

Last but not the least, I would like to thank my family, especially my Father who made me love studying, my Father-in-law who taught me that nothing impossible, and of course my Wife, Μαρία, for her patience and support when the life gets hard.

Abstract

Hydrogenation is a very frequently occurring example of heterogeneously catalysed reaction widely used in the production routes of the High Value Chemical Manufacturing (HVCM) sector and it is currently based on batch processes, despite the potential benefits from the switching to continuous flow. This mainly occurs due to the luck of an established methodology for transferring quickly such processes from batch to continuous flow.

Throughout this research project, the effort to investigate the principles which govern the heterogeneously catalysed hydrogenation led in the development of a new methodology for determining the mass transfer resistances of three-phase reactions in semi-batch Stirred Tank Reactors (STR).

The characterisation of the semi-batch STR was found adequate for predicting the concentration profiles of styrene during its hydrogenation over Pd/C in the Continuous Stirred Tank Reactor (CSTR). On the other hand, due to the different behaviour of mass transfer between the STR and the Trickle Bed Reactor (TBR), the transfer of the styrene hydrogenation from the semi-batch STR to TBR was found more demanding; and consequently, a new methodology for characterising the mass transfer behaviour of the TBR was developed.

The hydrogenation of styrene over Pd/C in the semi-batch STR, CSTR and TBR was simulated by using the mass transfer coefficients approximated by the new methodologies.

Table of Contents

List of Tables

List of Figures

Nomenclature

A   Area available for mass transfer, $[m^2]$

C   Molar concentration, $[mol/m^3 liquid]$

$C_{H_2,i}$ Concentration of hydrogen in gas-liquid interphase, $[mol/m^3 liquid]$

$C_{H_2,L}$ Concentration of hydrogen in liquid phase, $[mol/m^3 liquid]$

$C_{H_2,S}$ Concentration of hydrogen at the outer surface of active pellet, $[mol/m^3 liquid]$

C_{St} Concentration of styrene, $[mol/m^3 liquid]$

C_{Eth} Concentration of ethylbenzene, $[mol/m^3 liquid]$

$\mathfrak{D}$ Molecular diffusion coefficient, $[m^2/s]$

D_{ax} Axial dispersion coefficient, $[m^2/s]$

D_e Effective diffusion coefficient in porous structures, $[m^2/m\ solid \cdot s]$

$D_{m,e}$ Effective diffusion coefficients of molecular diffusion, $[m^2/s]$

$D_{k,e}$ Effective diffusion coefficients of Knudsen diffusion, $[m^2/s]$

D   Dispersion coefficient in porous structures, $[m^2/s]$

d   Diameter, $[m]$

E   Surface-age distribution, $[1/s]$

F   Molar flow rate, $[mol/s]$

f   Overall wetting efficiency of the bed, $[-]$

H	Height of liquid in the STR, [m]
H_E	Henry constant, $[\text{Pa} \cdot \text{m}^3/\text{mol}]$
HL_{fd}, HL_{st}	Free draining and stagnant liquid holdup, $[\text{m}^3\text{liquid}/\text{m}^3\text{voids}]$
J	Molar flux, $[\text{mol}/\text{m}^2 \cdot \text{s}]$
k	Specific mass transfer coefficient, [m/s]
k_L	Specific gas-liquid mass transfer coefficient related to liquid side film, $[\text{m/s}]$
k_S	Specific liquid-solid mass transfer coefficient, $[\text{m/s}]$
K_{H_2}, K_{St}, K_{Eth}	Chemisorption equilibrium constants of hydrogen, styrene and ethylbenzene, $[\text{m}^3\text{liquid}/\text{mol}]$
$k'_{obs,1^{st}order}$	Observed rate constant for 1st-order reaction based on unit Pd weight in the bed, $[\text{m}^3\text{liquid}/\text{g cat} \cdot \text{s}]$ Equal to $k'_{obs}/\sqrt{C_{H_2,S}}$
$k'^{Pd}_{obs,1^{st}order}$	Observed rate constant for 1st-order reaction based on unit Pd weight in the bed, $[\text{m}^3\text{liquid}/\text{g Pd} \cdot \text{s}]$ Equal to $k'^{Pd}_{obs}/\sqrt{C_{H_2,S}}$
k'^{Pd}_{obs}	Observed rate constant for a competitive Langmuir-Hinshelwood reaction when styrene is in excess based on unit weight of palladium, $[\sqrt{\text{mole} \cdot \text{m}^3\text{liquid}}/\text{g Pd} \cdot \text{s}]$ Equal to $\left(k'^{Pd}_1 \cdot \sqrt{K_{H_2}}\right)/\left(K_{St} \cdot C_{St,S}\right)$
k'_{obs}	Observed rate constant for a competitive Langmuir-Hinshelwood reaction when styrene is in excess based on

unit weight of catalyst particle (either pellet or fine particles),
$[\sqrt{mole \cdot m^3 liquid}/g\, cat \cdot s]$

Equal to $\left(k_1' \cdot \sqrt{K_{H_2}}\right)/\left(K_{St} \cdot C_{St,s}\right)$

k_1 Intrinsic chemical reaction rate constant based on unit volume of liquid, $[mole/m^3 liquid \cdot s]$

k_1' Intrinsic chemical reaction rate constant based on unit weight of catalyst, $[mole/g\, cat \cdot s]$

k_1'' 1st-order chemical reaction rate constant based on unit surface area of catalyst, $[m^3 liquid/m^2 cat \cdot s]$

L Characteristic length of catalytic particle, $[m]$

L_b Length of reactor bed, $[m]$

M Molar mass of diffusing species, $[g/mol]$

MTR Mass transfer rate, $[mol/m^3 liquid \cdot s]$

N Stirrer speed, $[rpm]$

N_{im} Number of impellers

N_P Power number, $[-]$

N_T Number of tanks in series

n Molar amount, $[mol]$

P Pressure, $[bar]$ and Power, $[J/min]$ in section 4.3.4

Q_L Volumetric flow rate of liquid, $[m^3 liquid/s]$

R' Reaction rate based on unit weight of catalyst, $[mol/g\, cat \cdot s]$

R'^{Pd} Reaction rate based on unit weight of palladium, $[mol/g\, Pd \cdot s]$

r	Pore radius, [m]
r^2	Coefficient of determination
s	Rate of renewal of surface of liquid, [1/s]
S_s	Specific surface area of supporting material, $[m^2/g]$
$ş$	Rate of renewal of surface of liquid, [1/s]
$\mathcal{S}$	Cross sectional area of the reactor, $[m^2]$
T	Temperature, [K]
t	Time, [s]
U	Superficial velocity of liquid or gas, $[m/s$ or $g/m^2 \cdot s]$
V	Volume of liquid phase in the reactor, $[m^3]$
v_L	Kinematic viscosity of liquid phase, $[m^2/s]$
W	Weight, [g]

Greek letters

α	Gas-liquid mass transfer area of stirred tank reactor per unit volume of liquid, $[m^2/m^3 \text{ liquid}]$
$α_s$	Liquid-solid mass transfer area of stirred tank reactor per unit weight of catalyst, $[m^2/g \text{ cat}]$
$α_{bed}$	External mass transfer area of the bed per unit volume of bed, $[m^2 bed/m^3 \text{ bed}]$
$α_{act.pel}^{\prime Pd}$	Overall external mass transfer area of active pellets per unit weight of palladium in the bed, $m^2/g \text{ Pd}$
β	Vita factor, [-]

γ	Shape factor, [-]
ΔG	Activation free energy, [kJ/mole]
ΔH	Energy released during reaction, [kJ/mole]
Δx	Distance, [m]
δ	Film thickness, [m]
ε	Effectiveness factor, [-]
θ	Fraction of active sites
ϵ	Energy dissipation, [J/kg$\cdot$min]
μ_L	Dynamic viscosity, [kg/m $\cdot$ s]
ρ	Density, [kg/m^3]
τ	Residence time, [s]
$\tilde{\tau}$	Tortuosity, [-]
ϕ_b	Bed void, [-]
ϕ_p	Internal void of supporting material, [-]
Ω	Mass transfer resistance, [s]

Subscripts

C	Catalyst
Dec	Decane
Eth	Ethylbenzene
Exp	Experimental
G	Gas

GB	Glass beads
H_2	Hydrogen
i	Gas-liquid interface
in, out	reactor inlet and outlet
L	Liquid phase
p	particle
Pd	Palladium
R	Reaction
r	reactor
S	Solid phase
Sim	Simulated
St	Styrene
tot	Overall or total

Abbreviations

CSTR	Continuous Stirred Tank Reactor
FID	Flame ionization detector
ICP-MS	Inductively coupled plasma mass spectroscopy
MFC	Mass Flow Controller
STR	Stirred Tank Reactor
TBR	Trickle Bed Reactor

Dimensionless numbers

$$Bo = \frac{U_L \cdot d_{GB}}{D_{ax}}$$ Bodenstein number, [-]

$$Fr_L = \frac{U_L}{g \cdot d_p}$$ Froude number of liquid, [-]

$$Ga_L = \frac{d_p^3 \cdot g \cdot \rho_L^2}{\mu_L^2}$$ Galileo number of liquid, [-]

$$Mo_L = \frac{g \cdot \mu_L^4}{\rho_L \cdot \sigma_L^3}$$ Morton number of liquid, [-]

$$Re_L = \frac{U_L \cdot d_p \cdot \rho_L}{\mu_L}$$ Reynolds number of liquid, [-]

$$Re_{im} = \frac{N \cdot D_{im}^2 \cdot \rho_L}{\mu_L}$$ Reynolds number of impeller, [-]

$$Stk_L = \frac{U_L \cdot \mu_L}{g \cdot d_p^2 \cdot \rho_L}$$ Reynolds number of liquid, [-]

$$Sc = \frac{\mu_L}{D \cdot \rho_L}$$ Schmidt number, [-]

$$Sh = \frac{k_S \cdot d_p}{D}$$ Sherwood number, [-]

$$We_L = \frac{d_p \cdot U_L^2 \cdot \rho_L}{\sigma_L}$$ Weber number of liquid, [-]

1. Introduction

1.1. Chapters outline

The present Thesis consists of eight main chapters, namely; Introduction, Background theory and literature review, Theoretical aspects of hydrogenation models, Three-phase semi-batch Stirred Tank Reactor, STR, Three-phase Continuous Stirred Tank Reactor, CSTR, Trickle Bed Reactor, TBR, Design of continuous three-phase hydrogenators, Conclusions and future work.

First in the Introduction chapter, the research background is given, in which the importance of the scientific and economic perspectives of the research topic are highlighted, and the research question identified to be answered is formulated. Then, in the same chapter, the research structure, which was followed to conclude to the findings answering the research question, is described.

Following this, in the next chapter, a summary of the appropriate background theory and review of existing literature into the heterogeneous catalysed hydrogenation, the three-phase reactors and the underlying phenomena associated with gas/liquid/solid chemical reactions is presented.

Before critically presenting the findings of the research related to the semi-batch and continuous flow reactors, the theoretical aspects of the hydrogenation models, are developed based on the background theory. These includes the mass transfer in series models for the stirred tank reactors and the trickle bed reactor, the surface model of styrene hydrogenation and the stirred tank and trickle bed reactors' models.

Chapter 4, Chapter 5 and Chapter 6 are dedicated to critically presenting the work related to the three-phase semi-batch stirred tank reactors, the three-phase continuous stirred tank reactor and the trickle bed reactor, respectively. Each one is structured in three main sections. The first section of each one presents the materials and methods, by which the experimental investigations into the different reactors were conducted. The second section of each one focuses on the experimental investigations which were conducted on the different reactors and the latter section is dedicated to the modelling and simulation of the heterogeneously catalysed styrene hydrogenation in the different reactors.

Then, in Chapter 7, an effort, to consolidate the findings of batch experimentation and those related to the continuous flow reactors (CSTR and TBR) in a methodology for designing the continuous three-phase hydrogenation, is made.

At the end of the Thesis, the conclusions of the research are summarised and the gaps which this research leaves are presented leading to the suggestions for future work.

1.2.   Research background

Although the first time that the word 'Catalysis' came to light was in 1836 by Berzelius and the first industrial catalytic process took place in 1875 when sulfuric acid was produced using platinum catalyst, today's society depends on catalysts more than ever [1, 2]. Everyday life is based on goods which are produced through catalysed processes. From fuels, which move our vehicles, to specialty chemicals, which are used in pharmaceutical and agrochemical production. In figures form, around 80% of chemicals are produced according to a catalytic chemical pathway, from economic perspective, their annual sales reach approximately $10 billions [3]. In addition, the value added by the chemicals industry and end-users is estimated to be ca. 21% of UK GDP, contributing ca. 15% of UK export goods [4]. Therefore, without any doubt, the importance of catalytic processes is significant from both points of view; social and economic.

But what is the catalyst and which is its function?

Catalysts are materials which are able to speed up reactions without being consumed or produced during the reaction [5]. Their ability comes from the fact that they provide different reaction paths through which lower amounts of energy are needed to trigger reactants to be transformed into products. Catalysts can be classified into two different categories: homogeneous and heterogeneous. Homogeneous catalysts participate in reaction mixture in the same phase as the reactants, while heterogeneous catalysts are in a different phase from the reactants; they are usually in solid phase. Due to the ease of separation from product stream, heterogeneous catalysis is preferred [5].

Since catalyst is usually in solid phase and the most reactants are either in liquid or gas or many times in both phases, the use of multiphase reactors is inevitable. For example, hydrogenation of unsaturated oils and fats are performed in food industry; Fischer-Tropsch processes, oxidation and hydrogenation of unsaturated hydrocarbons are used widely in fine chemical and petroleum industry; and polymerization reactions involve three-phase reactions [6].

The three-phase reactions take place in three-phase catalytic reactors which are vessels designed to bring gas, liquid and the solid catalyst into contact, using several mixing configurations [7]. They can be divided into different categories based on several characteristics. According to the catalyst type, they are divided into two main categories: slurry reactors and fixed bed reactors [8]. As its name discloses fixed bed reactors are packed with coarse particles of catalyst which constitute the stationary bed through which gas and liquid phase flow in several regimes. In the case of slurry reactors, the catalyst is in the form of fine particles and it is suspended in the liquid phase [6]. From operating perspective, fixed bed reactors operate in continuous flow where gas and liquid insert reactor in concurrent or counter current flow. On the other hand, slurry reactors are operated in batch, semi-batch or continuous flow.

Continuous flow reactors present some crucial advantages. They are released from the time-consuming procedures of starting-up and shutting-down in contrast to batch reactors [9]. In contrast to batch reactors, continuous flow reactors benefit from improved thermal management and mixing control [10]. Despite the development of new control strategies, undoubtedly, even today continuous reactors offer safer, more reliable control and more reproducible

results in terms of selectivity and yield, since they run in steady state conditions as far as the reactor is supplied with reactants [11]. Using continuous flow reactors, it is more facile to automate multi-step processes and discard manual procedures. This fact leads to two main advantages: first, minimisation of the likelihood for the operators to be exposed to hazardous chemicals; and second, reduction of labour cost [12].

Lonza Group Ltd. performed a campaign to assess if the current batch processes which they run could be boosted from continuous flow processes. In their analysis 22 large scale processes took place and 86 different reactions performed. According to the campaign outcomes, half of them would be boosted by switching to continuous flow [13]. Particularly, hydrogenation reactions in presence of metal catalyst would benefit in terms of the required reaction time and the reduction of catalyst, hydrogen and solvent amounts [14].

A significant need for switching batch reactions to continuous flow for pharmaceutical and fine chemicals production has been already come in the forefront. The question which rises from this need is how to transfer a three-phase reaction from batch to continuous flow.

A heterogeneously catalysed reaction is a complicated combination of physical and chemical processes. Regarding the physical processes, a three-phase reaction involves mass transfer from gas to liquid phase, from liquid to solid phase and within solid phase [15, 16]. The chemical reaction takes place on catalyst surface involving interactions of the gas and liquid reactants with the active sites of catalyst. Each of the physical and chemical processes contribute to the overall reaction rate in different extent. An indication of how

much each individual process affects the overall reaction rate is given by the mass transfer coefficients and the intrinsic reaction rate constant.

Taking into account that the design and the scale up of a reactor lies on the overall reaction rate, the switching of a three-phase reaction from batch to continuous flow implies the development of methodologies for the characterisation of mass transfer behaviour of the three-phase reactors.

There are many heterogeneously catalysed reaction systems. Hydrogenation is a very frequently occurring example widely used in the organic synthesis [2].

Hence the key question identified to be answered is distilled in the following:

What information do we need for transferring a heterogeneously catalysed hydrogenation from batch to continuous flow?

1.3.   Research structure
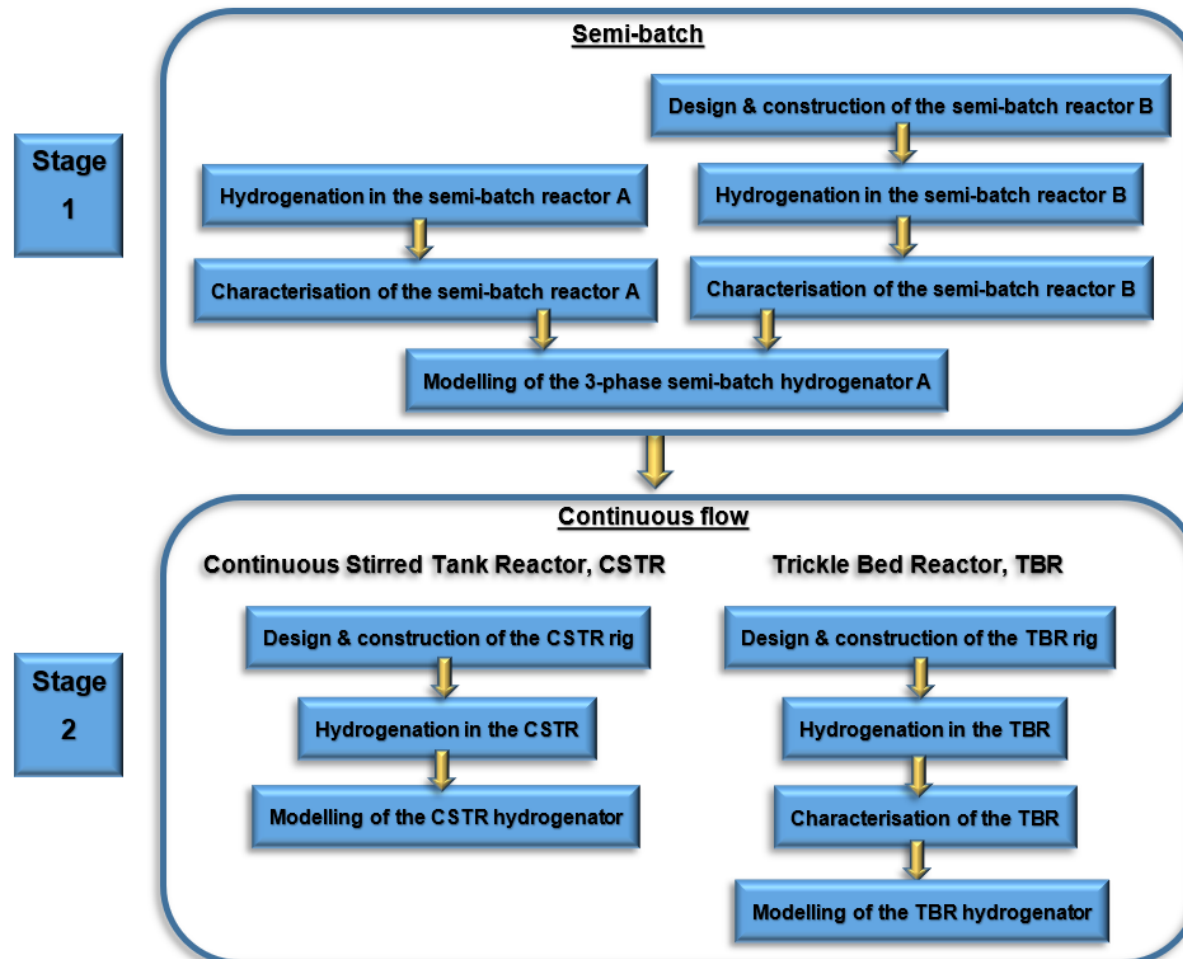
Figure 1.1: Research structure flow chart.

During the research, experiments are conducted in four different reactor rigs.

Stage 1 (Chapter 4)

The first stage of the research involves the development of a new methodology for characterising the mass transfer behaviour of the semi-batch stirred tank reactors.

At this stage two semi-batch stirred tank reactors were used (Chapter 4). The design and construction of the first rig did not constitute part of this project. This rig was used for the styrene hydrogenation over palladium on activated carbon. The chemical system was selected among others because of its fast-intrinsic reaction rate which allowed the observation of liquid-solid mass transfer resistance.

The design and construction of the second rig constituted part of this project, as a need for assessing the independence of the new methodology from equipment. For this reason, the scale and the impeller of the second reactor was different from those of the first.

The modelling of the semi-batch three-phase hydrogenation constituted the last part of the first stage of the project. The simulation of the semi-batch three-phase hydrogenation of styrene was based on mass transfer coefficients and intrinsic reaction rate constant which had been previously calculated using the developed methodology.

Stage 2

The second stage of the research involves the process transfer to continuous flow reactors.

Part 1 (Chapter 5)

First, the design and assembly of the continuous stirred tank reactor was carried out. The hydrogenation of styrene over palladium on activated carbon was conducted in this equipment. The similarity of the mass transfer behaviour between the semi-batch and continuous flow stirred tank reactors allowed the assumption that the mass transfer coefficients of the semi-batch and continuous flow are the same at the same agitation.

Therefore, the model of the continuous flow hydrogenation was based on the calculated mass transfer coefficients and intrinsic reaction rate constant of the semi-batch process. The experimental and the simulated concentration profiles verify this assumption.

Part 2 (Chapter 6)

The design, construction and assembly of a continuous flow trickle bed reactor rig was carried out. The equipment was used for the experimentation for developing a new methodology to characterise the mass transfer behaviour of the trickle bed reactor. The hydrogenation of styrene over palladium on activated carbon was used as a case study.

Chapter 2

2. Background theory and literature review

2.1. Introduction

This chapter presents a summary of the appropriate background and review of existing literature into the heterogeneous catalysed hydrogenation, the three-phase reactors and the underlying phenomena associated with gas/liquid/solid chemical reactions.

2.2. Heterogeneous catalysed hydrogenation

2.2.1. Significance of hydrogenation

The catalytic hydrogenation is one of the most significant reactions. Referring to hydrogenation, it is meant the addition of hydrogen atoms into organic molecules with at least one multiple bond. Consequently, a wide range of organic molecules are able to be hydrogenated such as alkenes, alkynes, aldehydes and ketones, acids, anhydrides and esters, nitriles, anilines, phenols and nitro compounds [7]. Hydrogenation is a reaction applied by a wide range of chemical industries such as fine chemical, pharmaceuticals, food, plastic and petroleum industry [17, 18]. In the next few paragraphs some examples which indicate the significance of the hydrogenation are introduced.

To begin with olefins hydrogenation, it is a well-known reaction among petroleum industry. High quality gasoline presents antiknock characteristics that it is covetable as they protect cars' engine. Antiknock characteristics are related to high percentage of octanes in gasoline. On the other hand,

petroleum distillates are rich of octenes, therefore by hydrogenating them, fuels rich in octanes are produced [19].

Acetylenes constitute significant raw or intermediate material for many synthetic utilities, for example, they are used in vitamins production and in hydro-purification of olefins [20]. Acetylene hydrogenation is a consecutive reaction that first produces cis-olefin and then paraffin. But due to the higher adsorption rate of acetylene on catalyst surface the reaction is characterised by high selectivity to olefin [7].

In addition, aldehydes and ketones are hydrogenated to primary and secondary alcohols, respectively. In particular, two examples are presented to underline the importance of the hydrogenation of these chemical compound groups. First, the catalytic hydrogenation of amino ketones is highlighted as the most cost effective way to produce optically active amino alcohols, a group of compounds contained in a wide range of active pharmaceutical substances [21]. Second, the hydrogenation of cinnamaldehyde has come in the front as its products meet great interest among fine chemical industry [22].

Hydrogenation of edible oils is a widely known process within food industry which is implemented in order to increase oil life and produce margarines and spreads [23, 24].

Finally, amino group in aromatic organic compounds is used in many intermediates within pharmaceutical and fine chemicals industry. Catalytic hydrogenation of aromatic nitro compounds is a widely used method to insert the amino group [25]. Moreover, hydrogenation of nitrobenzene leads to aniline production which is used in plastic industry [26].

2.2.2. Catalyst in heterogeneous hydrogenation

2.2.2.1. What is a catalyst?

The rate of chemical transformation of reactants to products is related to the amount of energy which needs to be overcome during the process of the chemical transformation. The free activation energy, ΔG, is an indication of this amount of energy. As higher the activation free energy, as slower the reaction is. The reaction rate can be dramatically increased by adding appropriate substances in the reaction mixture. These substances are known as catalysts [27]. Catalysts are materials which affect reactions' rate but they are neither consumed nor transport the reaction equilibrium which depends only on the thermodynamics of the reacting system [28].

Catalysts reduce ΔG by the following ways [27]:

- Changing reactant form in such a way that they are less stable

- Making the transition state more stable

- Changing reaction mechanism by providing a new reaction pathway with lower activation energy
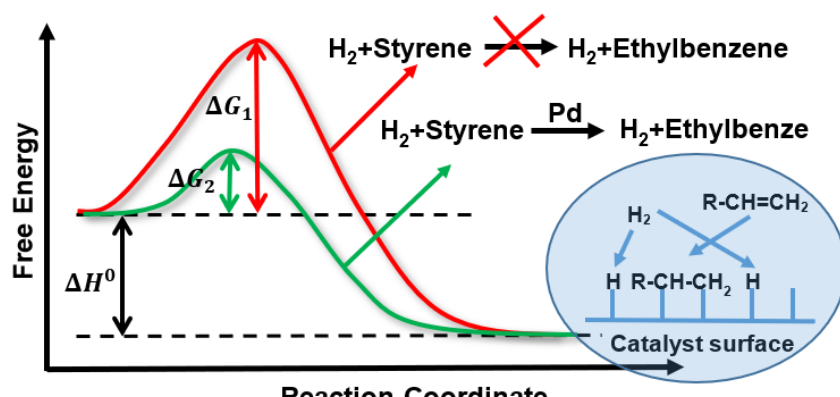
Figure 2.1: Qualitative diagram of activation free energy for catalysed & non-catalysed hydrogenation.

Figure 2.1 illustrates a qualitative diagram of activation free energy for a catalysed and non-catalysed hydrogenation. For example, the activation free energy for the styrene hydrogenation catalysed by palladium ranges between 15 kJ/mole and 55 kJ/mole [29-33].

2.2.2.2. Types of catalysts

The catalysts usually consist of two components: the active phase and the supporting material. The active phase is usually a platinum group metal (Ru, Rh, Pd, Os, Ir and Pt) and it is present in the form of discrete crystallites in the scale of a few nanometres in diameter [34]. The supporting material is catalytically inactive and operates as the carrier of the active phase which constitutes from 0.1 to 20% of the whole catalyst mass [35]. The most used supporting materials are carbon, alumina, silica, alkaline earth carbonates and sulphates, zinc, asbestos, and silk [7]. Because of their pore structure, they increase the surface area on which the active phase may be coated [7, 35]. The supporting material makes the catalysts less prone to poisoning comparing to unsupported catalysts [7].

Active phase location

As it has been mentioned the supporting materials are porous materials with several shapes. There are three different types of catalysts based on the location of the active phase. First, the eggshell catalysts, in which the active phase is present only on the outer surface of the supporting material. Second, the intermediate catalysts, in which the active phase is located not only on outer surface but also deeper within the pore structure. Final, the uniform catalysts, which are dispersed with active phase evenly throughout the supporting material [34].

The location of active phase affects the activity of the catalyst. As the active phase of the catalyst is deeper within the supporting material as less approachable is from the reactants. Consequently, for catalysts of the same active phase content, the eggshell catalysts show higher activity at low pressures. In the case of the intermediate and uniform type of catalysts, the activity increases with pressure because more active phase is exposed to the reactants [34].

When the active phase is located deeper within the pore is less prone to poisoning because the poison's molecules are usually weightier than the reactants' molecules and they face higher resistance to penetrate the pores [34]. On the other hand, the pore diffusion may affect the reaction rate and alter the selectivity and/or the yield of the reaction.
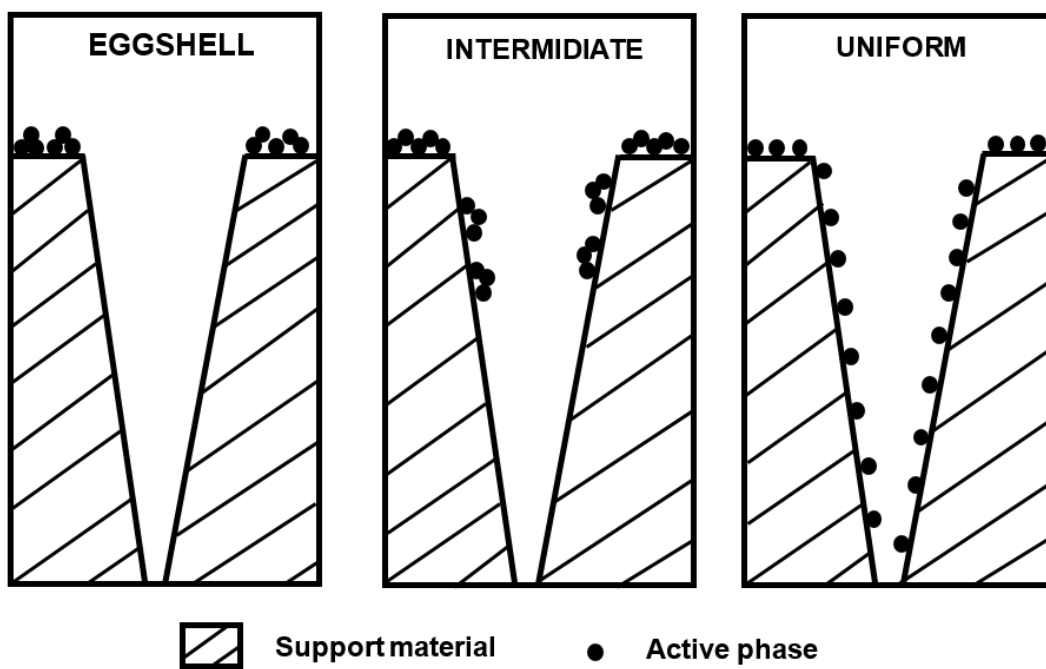
Figure 2.2: Illustration of the different catalysts based on active phase location [34].

Size of catalysts

According to their size, the supporting material is categorized to fine particles, the size of which is in the scale of microns and to coarse particles the size of which is few millimetres. Catalysts in the form of fine particles are preferred when the catalyst needs to be mobile, for example, in the case of slurries where the solid catalyst is suspended in a liquid solvent. On the other hand, coarse catalysts are preferable when the catalyst is fixed either creating a bed or in a mesh basket [7, 36]. From mechanical perspective, supporting materials for use in packed beds should present high resistance to crushing to withstand the forces developed by the moving fluids. Otherwise, they are powdered, resulting in pressure drop increase along the bed. Regarding the mobile catalysts, they should present law friction since they rub against each other [36].

Given the significant breakthroughs of material science and technology in nanoscale field, efforts have been made for the development of nano-catalysts in the size from 1 to 1.5 nm of active phase, appropriate for hydrogenation reactions. Some of the advantages which they present are: the enhanced exposed area of catalyst to reactant species, the minimization of sintering and internal diffusional resistance due to the relative large size of supporting material pore that varies from 3 to 30nm [37].

2.2.3. Heterogeneous hydrogenation process scheme-Slurry reactors

During the heterogeneous catalytic hydrogenations in slurry reactors, three phases are present:

- hydrogen (gas phase),
- substrate solution (liquid phase) and

- catalyst (solid phase)

Liquid is the continuous phase, in which, hydrogen is dispersed and fine particles of catalyst are suspended, because of the mixing.

The chemical reaction takes place on active phase of the catalyst. Therefore, molecules of liquid and gas reactant should be transferred into the active phase surface in order to react. From hydrogen molecules perspective, this transfer is described from the following steps [8]:

1. Diffusion of H_2 into the gas-liquid interface through the bubbles area

2. Diffusion of H_2 from the gas-liquid interface into bulk liquid phase

3. Diffusion of H_2 from the bulk liquid phase to the outer surface of the supporting material

4. Diffusion through the catalyst pore structure to the active phase surface (in-pore diffusion)
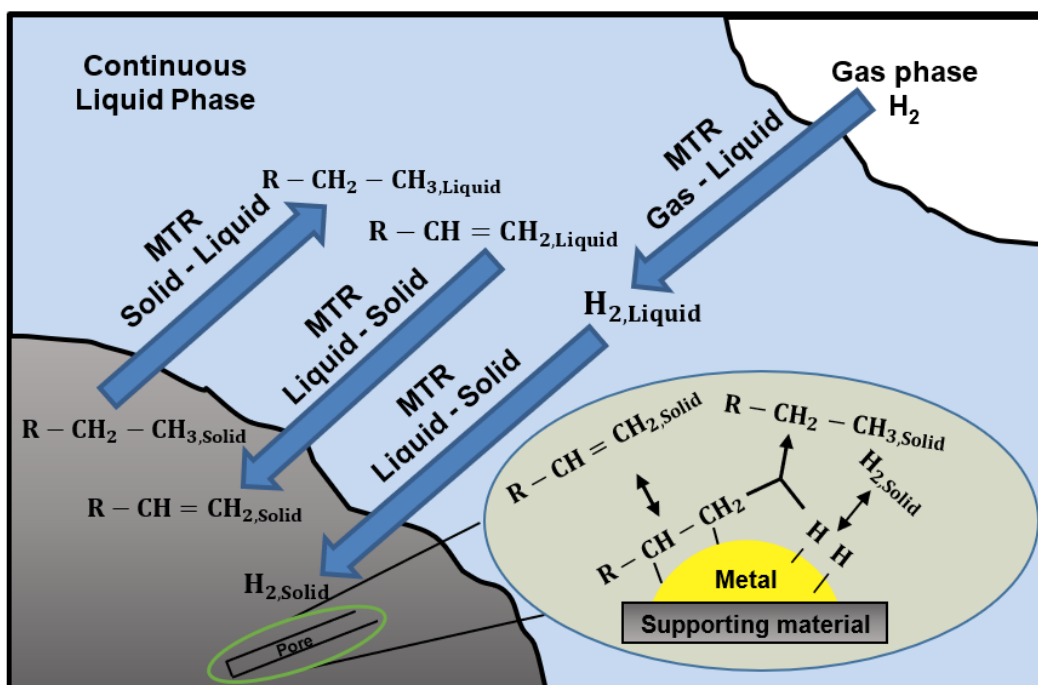
Figure 2.3: Process scheme of heterogeneous catalysed hydrogenation in slurry reactors.

The source of substrate molecules is in the bulk liquid. Therefore, they need first to diffuse to the external particle surface and then through the catalyst pore structure to the active phase surface.

After the in-pore diffusion, the reactants molecules interact with the metal surface of the catalyst. Hydrogen chemisorbs dissociatively onto the most transition metals [38]. The substrate may chemisorb onto metal surface or adsorbed physically without any chemical interaction with the metal.

2.2.4.   Heterogeneous hydrogenation process scheme-TBR

As in the case of the slurry reactors, during the heterogeneous catalytic hydrogenations in trickle bed reactors three phases are present; hydrogen (gas phase), substrate solution (liquid phase) and catalyst (solid phase). However, gas is the continuous phase, in which the liquid is dispersed developing thin rivulets around the coarse particles of catalyst. Hydrogen and liquid substrate need to follow the same steps as in the case of slurry reactors in order the reaction to take place on the active phase surface.
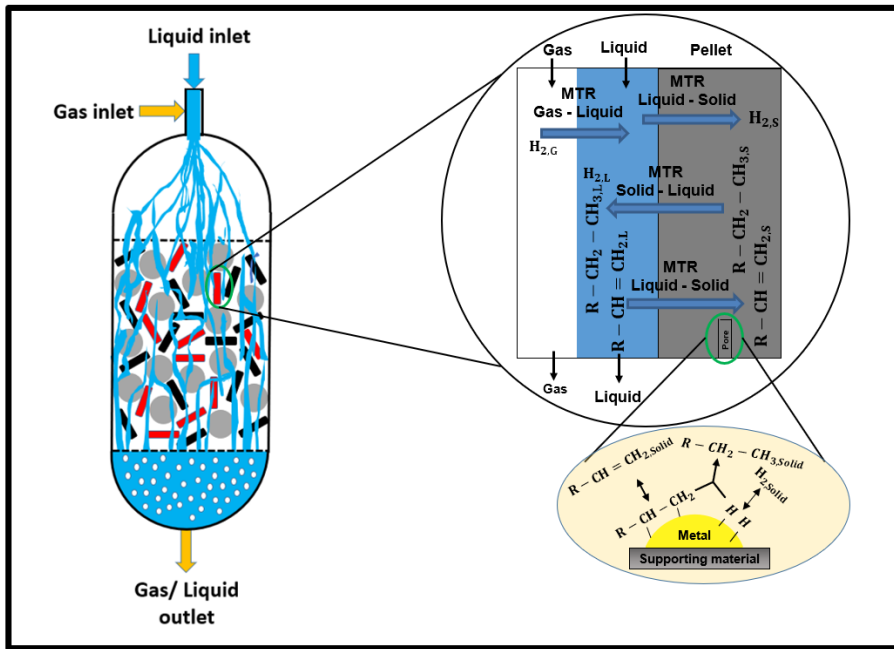
Figure 2.4: Process scheme of heterogeneously catalysed hydrogenation in TBR.

2.3.   Three-phase chemical reactors

Three-phase reactors are vessels which have been designed to bring hydrogen, catalyst and substrate into contact using several mixing configurations [7].

They can be divided into different categories based on several characteristics. In this work, they are categorised according to the catalyst movability. Hence, they are divided into two main categories: slurry reactors and fixed bed reactors [8]. As its name discloses fixed bed reactors are packed with coarse particles of catalyst, which constitute the stationary bed through which gas and liquid phase flow in several regimes. In the case of slurry reactors, fine particles of the catalyst are suspended in the liquid phase and the catalyst is easily removable from the reactor vessel.

In the next pages, an effort to present and describe different types of three-phase reactors is made.

2.3.1. Slurry reactors

The major advantages and disadvantages of slurry reactors are summarised in Table 2.1.

Table 2.1: Advantages and disadvantages of slurry reactors.

ADVANTAGES	DISADVANTAGES
Not complicated configuration and low capital cost.	Difficulty to obtain high degrees of conversion because residence time distribution patterns approach those of CSTR
High enough mass transfer rates which usually eliminate external gas-liquid mass transfer resistance without too high energy consumption.	Need of downstream separation of liquid and fine particles of catalyst
Catalyst effectiveness factor may reach unity.	Higher consumption of catalyst compared to fixed bed
Low energy consumption because of the low pressure drop	The high ratio of liquid to solid in slurry reactors allows homogeneous side-reactions to become more important, if any is possible.
Well-mixed conditions which result in uniform temperature in reactor and avoidance of hot spots.	

Table continues at the next page.

Continue of table 2.1

More facilitate temperature control of
exothermic reactions due to the large
amount of liquid.

Facilitate remove and addition of
catalyst from and to reactor vessel.

Powdered catalysts are often less
expensive than the same in pellet form.

Higher catalyst efficiency which leads to
lower amount of catalyst compared to
fixed bed.

2.3.1.1. Stirred tank slurry reactors

The stirred tank slurry reactors operate in continuous, semi-batch or batch
mode while mixing is provided by the installation of several configurations of
agitation systems. Regarding, batch reactors, they are well known among fine
chemical and pharmaceutical industry due to the need of multipurpose
reactors. They are also widely used by food industry because the large variety
of oil composition in feed stream does not allow the use of continues
processes [12, 39]. There are two main categories of edible oils
hydrogenators; the first is known as Wibuschewitsch Type and the second as
Normann Type. The major difference between them is the continuous phase,
in the first type liquid oil phase is sprayed into hydrogen atmosphere while in
Normann Type the hydrogen is sparged into the liquid oil [39]. Regarding
hydrogen feed, there are two types of reactor systems: circulating and dead-

end. The first is fed with large volumes of hydrogen, the amount of hydrogen that is not consumed is recirculated and supplied as feed again. In latter systems, the hydrogen is supplied in a flow rate equal to its consumption rate.

On the other hand, continuous stirred tank reactors, CSTRs, for three-phase hydrogenations present similar characteristics of CSTRs that are used in homogenous processes. Undoubtedly, the core difference is the duty of the agitation system. In the case of heterogeneously catalysed hydrogenation, not only does it have to stir liquid but also it has to suspend fine particles of catalyst and disperse gas bubbles sufficiently in order to maximise mass transfer rates [40].

Figure 2.5 shows a flow diagram of a three-phase CSTR. Recirculation loop of gas phase is used in order to increase residence time of gas.
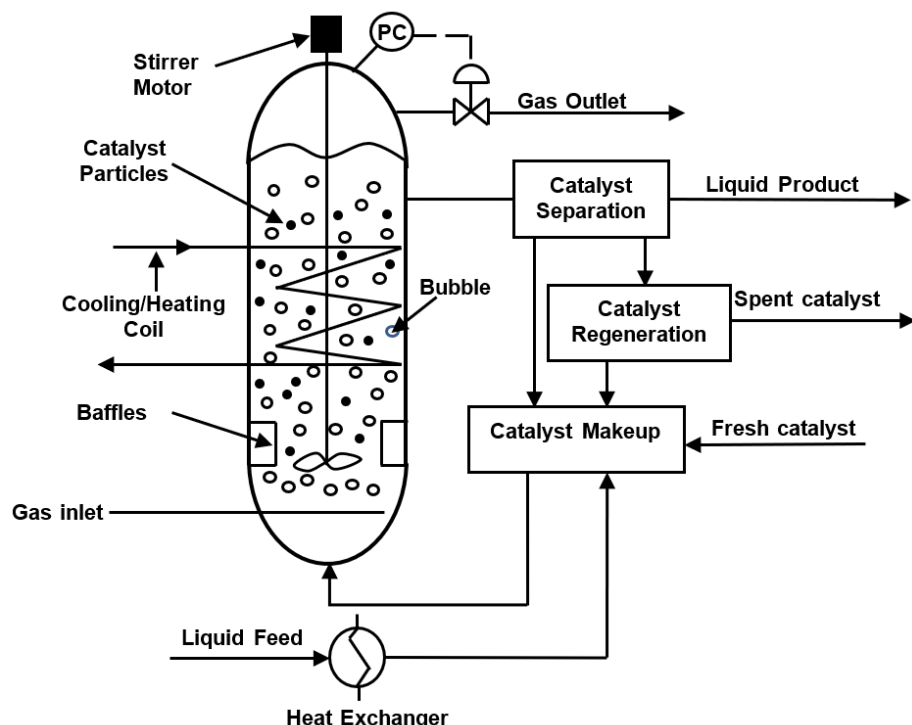
Figure 2.5: Flow diagram of three-phase CSTR [40].

2.3.1.2. Three-phase sparged reactors

This type of three-phase reactors includes any reactor which does not use any mechanical agitation for providing mixing to bring in contact the three phases. Instead, mixing is provided by the flow of either gas or liquid [41]. The sparged reactors can be further divided into three categories, with respect to the axial profile of solid concentration and to the phase which creates the mixing conditions, as: Gas-Sparged Slurry, Three-Phase Bubble Column, and Three-Phase Fluidized Bed reactors [42]. Regarding the flow regimes and depending on superficial gas velocity, the sparged reactors may operate in bubble flow regime, in churn-turbulent regime or in slug flow regime [43].

Gas-sparged slurry reactors

In gas-sparged slurry reactors, catalyst particles are maintained suspended by the upward flow of rising bubbles. There are not axial solids concentration gradients; therefore, a uniform distribution of particles dominates in the reactor column even under low gas velocities. Regarding momentum, liquid and suspended solids can be manipulated as a uniform fluid, because of zero relative velocity between them [42]. In this type of reactors, the solid particles are inserted and withdrawn continuously.
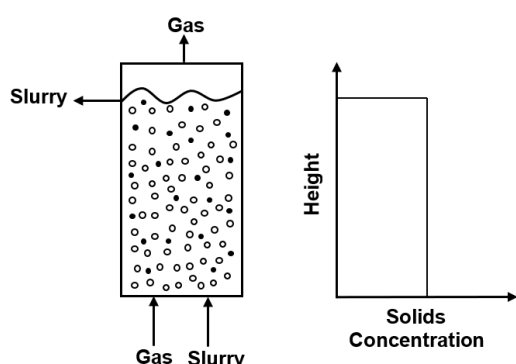
Figure 2.6: Gas-sparged reactor and axial concentration profile of solids [42].

Bubble column slurry reactors

Apart from the larger size of the particles which are used in three-phase bubble column reactors, they are same as the gas-sparged slurry reactors. They constitute a category of three-phase reactors in which fine particles of catalyst are remained suspended by rising bubbles of gas while liquid velocity is lower than the minimum fluidisation velocity [44]. They are usually designed for concurrent upflow of slurry and gas phase but in the presence of fast reaction kinetics, slurry downflow can be used [45]. Catalyst concentration is incrementally decreased from the bottom to the top of the column as a result of the tendency of solid particles to sink. This is because the gravitational forces which act on catalytic particles are higher than the forces caused by rising bubbles [42]. There is a radial liquid velocity gradient; at the centre of the column, the liquid velocity reaches its maximum value but it starts decreasing away from the centre and exhibits a minimum value near the wall. This behaviour of liquid makes the solids to circulate in the column, following an upward movement in the centre and downward near the wall [46]. The column is operated with gas phase in continuous flow while slurry can be either in batch or continuous mode [42].
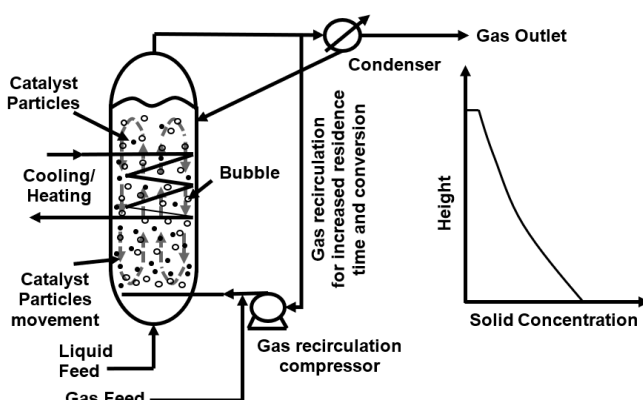
Figure 2.7: Flow diagram of bubble column showing the circulation of solids (left) and axial concentration profile (right) [40, 42].

Three-phase fluidised bed reactors

The three-phase fluidised bed reactors can be also found as three-phase liquid fluidisation in literature and they referred to three-phase reactors in which suspension of catalytic particles is achieved by upward flow of liquid and gas or liquid only [42, 44, 45]. There is no gradient of axial solid concentration but solids are uniformly distributed up to a certain height, known as bed height, lower than the total height of the column [40, 42]. The rest of column height contains only liquid and gas. The height of bed depends on fluid velocity and on size, shape and weight of particles. Therefore, if a column is filled with different particles, different layers of bed can be developed from the bottom to the top of the column. This fact leads to design one hardware in which different reactions can occur simultaneously in different axial column sections [40].
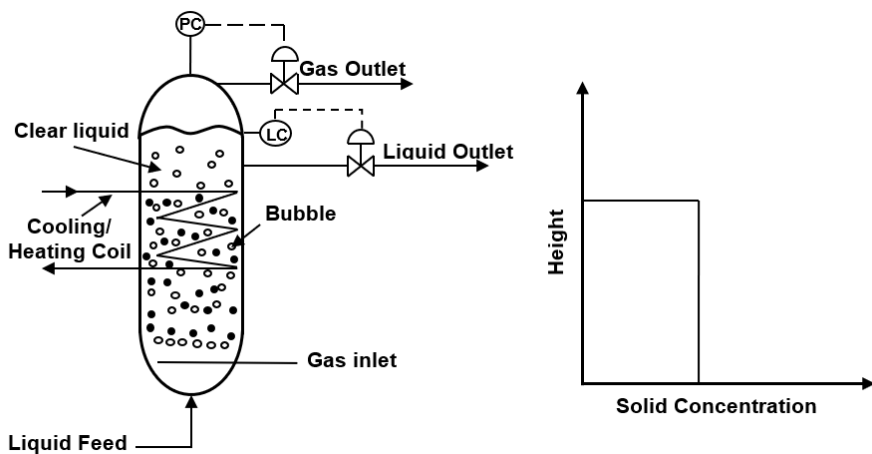
Figure 2.8: Flow diagram of fluidised bed reactor and axial concentration profile [42].

One more advantage of three-phase fluidised bed reactors is that the product does not require excessive separation from solids because this separation has been already fulfilled in the column [40]. Regarding solid phase, this type of reactors operate only in batch mode [42]. Particular case of three-phase

fluidised bed reactors constitutes the Ebullated-Bed reactor and the Three-Phase Transport Reactor. In the first case, solid suspension is achieved only by upward flow of liquid and the expansion of the bed due to the liquid flow reaches 100% [40].

2.3.1.3. Three-phase plate reactor

The plate reactor consists of a series of special plates that are placed one over the other. The plates have channels in which process and utilities streams flow. Appropriate design of channels promotes optimum mixing and heat transfer performance. This feature makes plate reactor too attractive especially for three-phase processes in which mixing conditions determine yield and selectivity. Plate reactor combines two significant characteristics of two different process units: the high heat transfer capabilities of the plate heat exchanger and the efficient mixing which microreactors presents [47].

Figure 2.9: Alfa Laval plate reactor and a plate of the reactor.

2.3.2. Fixed bed reactors

As it has been already mentioned Fixed Bed Reactors are referred to catalytic reactors in which catalyst is packed in the reactor vessel and it constitutes a stationary solid phase. FBRs may be categorised based on several characteristics, in this work, they are categorised into two main categories,

depending on either liquid or gas phase continuity in the reactor. Hence, fixed bed reactors with continuous gas phase and dispersed liquid phase are known as Trickle Bed Reactors. On the other hand, when the gas phase is dispersed in continuous liquid phase, the fixed bed reactor is referred to as Fixed Bed Bubble Reactor [40, 48].

Because of the stationary character of the solid phase, both categories of fixed bed reactors face difficulties of high pressure drop. This fact leads to the use of larger particles of supporting material although their use creates low values of effectiveness factor. The effectiveness factor is defined as the ratio of actual reaction rate over the ideal reaction rate if pores were not present [5] and it is discussed in section 2.4.2. Design of fixed bed reactors should compromise the pressure drop and the effectiveness factor.
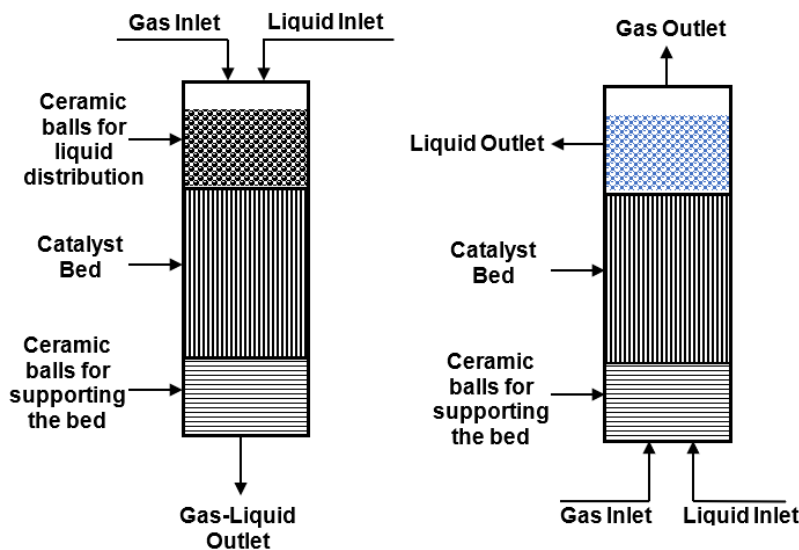
Figure 2.10: Trickle bed reactor concurrent flow (left) and fixed bed bubble reactor (right).(right).

2.3.2.1. Trickle bed reactors

Trickle bed reactors can operate in concurrent downflow or in counter current flow with upward gas flow, with one or several fixed beds of catalysts. TBRs

have taken their name of the trickle flow regime which are developed under moderate gas and liquid velocities as it is the most common flow regime which is applied in fixed bed concurrent downflow and counter current flow reactors.

Regarding the flow regimes which can be developed in a trickle bed reactor, they are apparently dependent on fluids velocities. Initially, at moderate mass flow velocities of gas and liquid phase, gas phase is continuous while liquid trickles down forming films or rivulets [8, 40]. As the gas flow rate is gradually increased while flow rate of liquid is kept constant two regimes are developed; initially the slug or pulsing regime, and after that, the spray regime. The first is an intermediate unsteady regime characterised by the formation of alternate slugs which are rich in liquid and gas. In spray regimes liquid droplets are dispersed in continuous gas phase [8]. Flow maps of gas-liquid flows have been developed by Satterfield [49], Midoux et al. [50] and Cheng et al. [51].

Comparing concurrent flow to counter current, the latter is preferred when large heat of reaction is involved because it reduces axial temperature gradients [48]. Moreover, counter current mode offers larger surface area for gas-liquid mass transfer and higher ratio of exposed active sites to reactants per reactor volume. Because of the increased surface area to volume ratio, for the same conversion, when counter current flow is used the catalyst loading ranges between 20-25% of the vessel volume, while in the case of concurrent flow it is three times higher, ranges between 60-70% [48]. On the other hand, counter current flow cannot operate at high liquid flow rates because of flooding. Although counter current flow reduces axial temperature gradients, it presents high axial dispersion of the liquid phase [48]. The

following table introduces the most significant pros and cons of trickle bed reactors.

Table 2.2: Advantages and disadvantages of concurrent TBRs [48].

Advantages	Disadvantages
Several flow regimes using one hardware.	Minimum particle size depends on liquid flow rate to keep the pressure drop at low levels.
High conversions due to plug flow of liquid phase.	Large particle size reduces effectiveness factor of catalyst.
Low catalyst loss and pressure drop which leads to lower operating cost.	If reactor diameter/particle size <25, channelling of liquid phase at low liquid flow rates may occur which leads to ineffective catalyst regions.
Simple construction due to presence of no moving part.	Trickle bed reactors cannot be used for viscous or foaming liquids.
Low liquid-solid volume ratio which leads to minimisation of homogeneous side-reactions and reduce of solvent use.	
High pressure and temperature operating conditions.	
Liquid rate can vary based on catalyst wetting, heat and mass transfer resistances.	

2.3.2.2. Fixed bed bubble reactor

As it has been already mentioned in fixed bed bubble reactors liquid phase is the continuous phase where the gas is dispersed with relatively moderate gas and liquid flow rates [40, 48]. They operate typically in upward concurrent flow and as in the case of trickle bed reactors; they have taken their name from the most applied regime of upward concurrent fixed bed reactors. They are also known as upflow reactors, upflow concurrent reactors, packed-bubble columns, upflow packed bubble columns or flooded fixed-bed reactors [48].

Regarding the flow regimes, at moderate gas and liquid flow rates bubble flow regime is observed. In order to prevent fluidisation of the bed by the increasing gas flow rate, hold-down screens or bed limiters should be used. Increasing the gas flow rate, the first regime which is developed is known as slug or pulsing regime that is also observed in trickle bed reactors. Further increasing of gas flow rate leads to spray regime [40]. As it is obvious, fixed bed bubble reactor is the only mode of fixed bed that can operate with bubbling flow of gas. Hence, it is a suitable reactor in cases where liquid reactants are treated with a relatively small amount of hydrogen such as in hydrogenations of nitrocompounds and olefins or if relatively large residence time of liquid is needed to achieve desired conversion degree [48].

Table 2.3: Main categories of three-phase reactors

THREE-PHASE REACTORS								
FIXED BED REACTORS Stationary catalyst bed				**SLURRY REACTORS** Suspended catalyst in liquid phase				
TRICKLE BED REACTORS		**FIXED BED BUBBLE REACTORS**		**STIRRED TANK REACTORS**		**3-PHASE SPARGED REACTORS**		**PLATE REACTOR**
Concurrent downflow	Counter current flow Upflow: Gas phase Downflow: Liquid phase	Concurrent upflow	Counter current flow Upflow: Gas phase Downflow: Liquid phase	Batch	Continuous	Gas-sparged slurry	Bubble column slurry Or 3-phase bubble fluidisation	3-phase liquid fluidisation Or 3-phase fluidised bed	Alfa Laval

2.4.   Mass transfer in three-phase reactions

As it has been already mentioned in sections 2.2.3 and 2.2.4, the heterogeneous catalytic hydrogenation is a complicated combination of physical and chemical processes. Regarding the physical processes, a three-phase reaction involves mass transfer from gas to liquid phase, from liquid to solid phase (external mass transfer or external diffusion) and within the solid phase (intraparticle or pore diffusion). The chemical reaction takes place on catalyst surface and involves interactions of the gas and liquid reactants with the active sites of catalyst. Theories, describing the mass transfer from eddies and bubble scale to molecular scale, are presented and interpreted in this section.

2.4.1.   External mass transfer or external diffusion

Imagine a container which is separated into two parts by a moving plate; if the first part contains, for example hydrogen, while the other part contains nitrogen, and the plate which separates the two parts is removed, then hydrogen and nitrogen will start being transferred from the one side to the other in order to minimize the inequality in composition between the two parts.

This is a simple example of mass transfer and as one understands the driving force for the mass transfer is the concentration gradient between the rich and poor regions of substance. Noyes and Whitney [52] studied the dissolution rate of solid substances to their own solutions and they concluded that the rate of mass transfer due to the dissolution was proportional to the difference of molar concentration in substance rich and substance poor regions. The proportionality constant between the mass transfer and the molar concentration difference is known as mass transfer coefficient.

Noyes and Whitney [52] equation:

$$\frac{dC}{dt} = k \cdot (C_{rich\ region} - C_{poor\ region}) \qquad \text{Equation 2.1}$$

Where, C = Molar concentration, $[mol/m^3 liquid]$

      k = mass transfer coefficient, [1/s]

      t = Time, [s]

In the form of molar flux, this can be expressed by Equation 2.2.

$$J_{H_2} = \frac{F_{H_2}}{A} = k \cdot (C_{rich\ region} - C_{poor\ region}) \qquad \text{Equation 2.2}$$

Where, J_{H_2}= Molar flux of hydrogen, $[mol/m^2 \cdot s]$

      F_{H_2}= Molar flow rate of hydrogen, [mol/s]

      A = Area available for mass transfer, $[m^2]$

Mass transfer is the result of two mechanisms; the molecular diffusion and the convection, which may occur simultaneously. The first mechanism is described by the 1st Fick's law (Equation 2.3) which defines the molar flux (a) proportional to the concentration difference between the substance rich and substance poor regions and (b) inversely proportional to the distance which the molecules of the substance have gone through.

$$J_{H_2} = \frac{F_{H_2}}{A} = \mathfrak{D} \cdot \frac{(C_{rich\ region} - C_{poor\ region})}{\Delta x} \qquad \text{Equation 2.3}$$

Where, $\mathfrak{D}$ = Molecular diffusion coefficient, $[m^2/s]$

      Δx = Distance, [m]

On the other hand, according to the second mechanism, the mass is transferred due to the bulk motion of the fluid which is a result of velocity gradients between the regions. The velocity gradients may be naturally caused by pressure, density and concentration gradients between the regions; or may be the fluid is forced to move by the use of an external source such as a pump or an agitation system. To describe the convective mass transfer between two phases, three major theories have been developed; the two-film theory, the penetration theory and the surface-renewal theory.

2.4.1.1. The two-film theory

The two-film theory is the first and simplest theory which was developed to describe mass transfer of a substance through different phases [53]. W. Nerst in 1904 was the first researcher who used the diffusion layer or film concept to explain why a two-phase reaction is performed slower than what the intrinsic kinetics indicate [54]. However, the two-film theory was developed by Whitman [55]. It ignores any turbulent conditions near the interface supposing that the mass transfer takes place only by molecular diffusion through the stagnant films on either side of the interface [56]. The resistance to mass transfer is caused only by the films. Moreover, it is assumed that the total time of contact is long enough to consider that the required time to achieve establishment of concentration gradients in both films and equilibrium at the interface is short. As a result steady-state diffusion is assumed, consequently, the molar flux is given by 1st Fick's law in Equation 2.3 [56].
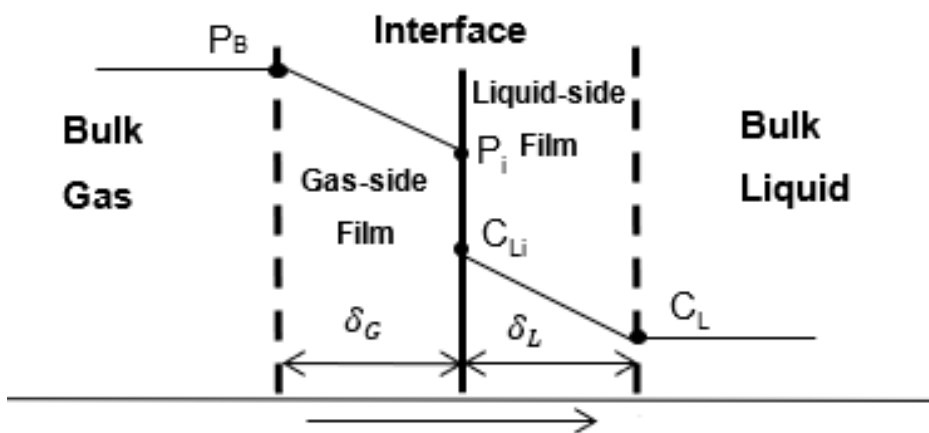
Figure 2.11: Schematic representation of the two-film theory.

Gas-Side

Transfer is taken place in gas-side film due to the difference of pressure between the bulk gas and the interface; therefore the driving force of transfer is considered the differential pressure $P_B - P_i$, which is converted into concentration difference using the Henry's law $(P = H_E \cdot C)$ [55]. As a result, using Equation 2.3, gas molar flux in gas-side film is given by Equation 2.4.

$$J_{H_2,G} = \frac{F_{H_2,G}}{A} = \mathfrak{D} \cdot \frac{(P_B - P_i)}{\delta_G} \cdot \frac{1}{H_E}$$ Equation 2.4

Where, $J_{H_2,G}$ = Molar flux from bulk gas to gas-liquid interface, $[mol/m^2 \cdot s]$

$F_{H_2,G}$ = Molar flow rate of hydrogen, $[mol/s]$

A = Area available for mass transfer, $[m^2]$

$\mathfrak{D}$ = Molecular diffusion coefficient, $[m^2/s]$

P_B, P_i = Pressure in bulk gas and gas-side film, respectively, $[Pa]$

δ_G = Thickness of gas-side film, $[m]$

H_E = Henry constant, $[Pa \cdot m^3/mol]$

Liquid-Side

In the same way, the driving force of the mass transfer in liquid-side film is considered the difference of molecular density (concentration) of gas between the interface and the bulk liquid [55]. Therefore, using Equation 2.3 gas molecular flux in liquid-side film is given by Equation 2.5.

$$J_{H_2,L} = \frac{F_{H_2,L}}{A} = \mathfrak{D} \cdot \frac{(C_{Li} - C_L)}{\delta_L}$$ Equation 2.5

Where, $J_{H_2,L}$ = Molar flux from gas-liquid interface to bulk liquid, $[mol/m^2 \cdot s]$

$F_{H_2,L}$ = Molar flow rate of hydrogen, $[mol/s]$

C_{Li} = Concentration at interface, $[mol/m^3]$

C_L = Concentration in bulk liquid, $[mol/m^3]$

δ_L = Thickness of liquid-side film, $[m]$

Comparing Equation 2.4 and Equation 2.5 to Equation 2.2, the gas-side and liquid-side gas-liquid mass transfer coefficients, k_G and k_L, are defined as $\mathfrak{D}/\delta_G$ and $\mathfrak{D}/\delta_L$, respectively.

The importance of film theory lies in its simplicity. It is a simple theory which quickly provides information about the resistances against the mass transfer and how they are affected by external factors, e.g. mixing intensity.

2.4.1.2. Penetration theory

As there is not any physical reason of turbulence conditions lack near the interface, Higbie in 1936 proposed the penetration model, assuming that gas-liquid interface consists of many small liquid elements (eddies), which fall onto interface from bulk liquid and return to bulk liquid because of the mixing [56, 57]. Three more main assumptions of penetration model are:

- As long as the liquid elements stay at surface are stagnant,

- dissolved gas concentration in eddies is equal to the bulk liquid concentration,

- all eddies stay at the interface for the same time intervals, equal to $t^* = d/u_b$, where d represents the vertical length of the bubble and u_b its velocity.

Therefore, gas is absorbed from the liquid elements to bulk liquid under unsteady state molecular diffusion which is described by the 2nd Fick's law (Equation 2.6).

$$\mathfrak{D} \cdot \frac{\partial^2 C}{\partial x^2} = \frac{\partial C}{\partial t} \qquad \text{Equation 2.6}$$

Where, dt= the time interval the eddies stay at the interface

x= depth in bulk liquid
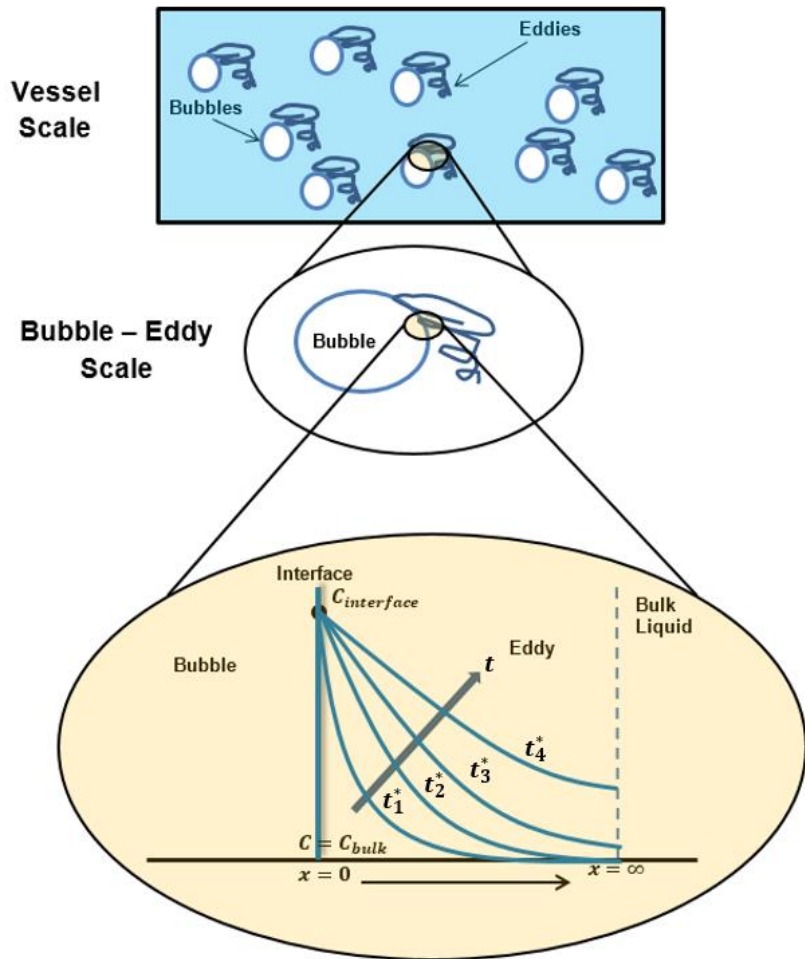
Figure 2.12: Schematic representation of penetration theory.

Figure 2.12 describes the penetration theory. Let us assume that hydrogen needs to be transferred to the bulk liquid. Initially, the concentration of hydrogen in bulk liquid is zero. A fresh eddy come from the bulk liquid, fall onto the interface, stays stagnantly there for t^* and returns back to the bulk liquid, having an increased concentration of hydrogen. Now this eddy falls onto another bubble, creates an interface, stays stagnantly there for t^* and returns back to the bulk liquid having an even more increased concentration of hydrogen. This happens for all eddies and bubbles in the vessel until all eddies have the same concentration of hydrogen as the bubbles.

Solving the differential Equation 2.6 with the following boundary conditions, the concentration C is expressed by Equation 2.7.

- At t=0, x>0: C=C$_{bulk\ Liq}$, at the beginning of contact and in any distance far from interface concentration equals the bulk liquid concentration.
- At t>0, x=0, C=C$_{interface}$, at any time, concentration at interface equals the interface concentration.
- x tends to infinity, C is bounded

$$\frac{C_{interface} - C}{C_{interface} - C_{bulk}} = erf\left(\frac{x}{2\sqrt{\mathcal{D} \cdot t}}\right)$$ Equation 2.7

The concentration gradient at the interface is given by Equation 2.8.

$$-\left(\frac{\partial C}{\partial x}\right)_{x=0} = \frac{C_{interface} - C_{bulk}}{\sqrt{\mathcal{D} \cdot \pi \cdot t}}$$ Equation 2.8

Therefore, the flux for an eddy at the interface during time t is defined by Equation 2.9

$$J_{H_2} = \frac{F_{H_2}^{x=0}}{A} = -D \cdot \left(\frac{\partial C}{\partial x}\right)_{x=0} = (C_{interface} - C_{bulk}) \cdot \sqrt{\frac{\mathcal{D}}{\pi \cdot t}}$$ Equation 2.9

Where, $F_{H_2}^{x=0}$ = Molar flow rate of hydrogen at interface, [mol/s]

The flux of an eddy during its whole life, t=t*, is given by Equation 2.10.

$$\left(J_{H_2} = \frac{F_{H_2}^{x=0}}{A}\right)_{av} = \frac{1}{t^*} \cdot \int_0^{t^*} \frac{MTR_{H_2}^{x=0}}{A} = (C_{interface} - C_{bulk}) \cdot 2 \cdot \sqrt{\frac{\mathcal{D}}{\pi \cdot t^*}}$$ Equation 2.10

Comparing Equation 2.10 to Equation 2.2, mass transfer coefficient k is proportional to the square root of diffusivity, $\mathcal{D}$.

2.4.1.3. Surface-renewal theory

Danckwerts [58] evolved the penetration theory introducing the random surface renewal theory. His model is based on penetration theory but it takes

into account that in a turbulent motion each eddy is impossible to spend same time at the gas-liquid interface. Therefore, Danckwerts [58] inserted probability function to represent the age of an eddy at the interface.

Consequently, the average flux is given by Equation 2.11.

$$\left(J_{H_2} = \frac{F_{H_2}^{x=0}}{A} \right)_{av} = (C_{interface} - C_{bulk}) \cdot \sqrt{\frac{\mathfrak{D}}{\pi \cdot t}} \cdot E(t) \cdot dt \qquad \text{Equation 2.11}$$

Where, $E(t)$= surface-age distribution function

$E(t) \cdot dt$ = gives the fraction of the total surface which is made up of elements whose age is larger than t and smaller than (t+dt)

$$\int_0^\infty E(t) \cdot dt = 1 \qquad \text{Equation 2.12}$$

$$E = \mathfrak{s} \cdot e^{-\mathfrak{s} \cdot t} \qquad \text{Equation 2.13}$$

Where, $\mathfrak{s}$ = rate of renewal of surface of liquid, [1/s]

Hence, the mean flux of gas absorption is defined by Equation 2.14.

$$\left(J_{H_2} = \frac{F_{H_2}^{x=0}}{A} \right)_{av} = (C_{interface} - C_{bulk}) \cdot \sqrt{\mathfrak{D}} \cdot \int_0^\infty \frac{\mathfrak{s} \cdot e^{-\mathfrak{s} \cdot t}}{\sqrt{\pi \cdot t}} dt$$

$$\text{Equation 2.14}$$

$$= (C_{interface} - C_{bulk}) \cdot \sqrt{\mathfrak{D} \cdot \mathfrak{s}}$$

Comparing Equation 2.14 to Equation 2.2 the mass transfer coefficients k is proportional to the square root of diffusivity, $\mathfrak{D}$.

Table 2.4: Summary of mass transfer theories.

Theory	Assumptions	Mass Transfer Coefficient definition
Film Theory	• No turbulent conditions near the interface • mass transfer by molecular diffusion through stagnant films • steady-state diffusion	$k = \mathfrak{D}/\delta$
Penetration Theory	• G-L interface consisted of eddies • As long as the liquid elements stay at surface are stagnant • dissolved gas concentration in eddies is equal to bulk liquid concentration • all elements stay at interface for same time intervals	$k = \sqrt{\dfrac{\mathfrak{D}}{\pi \cdot t^*}}$
Surface-Renewal Theory	• probability function to represent the age of an eddy at interface	$k = \sqrt{\mathfrak{D} \cdot \mathfrak{s}}$

2.4.2. Internal or pore diffusion

2.4.2.1. Mass transfer within porous supporting material

In section 2.4.1, a description of mass transfer at the scale of bubbles and eddies was given. In this section, an effort to describe the mass transfer at the particle scale is made.

Although Langmuir-Hinshelwood and Eley-Rideal models describe very well the reactions which take place on catalyst surface, to demonstrate and explain

what happens in catalysts' pores, power rate law is used, since it fits adequately most catalytic conversion data and it is much simpler [59].

As it has been already mentioned, in most cases catalysts consist of the porous supporting material and the metal active phase. Imagine a pore; its surface has been partially coated by a layer of metal active phase. Apparently, reactant molecules should penetrate inside the pore to reach active sites of catalyst and be anchored there on, in order to react. Molecules can penetrate into pores following three different diffusion mechanisms, based on the size of catalyst pore. Figure 2.13 depicts the influence of pore size diffusion mechanism and Table 2.5 summarises the pore diffusion mechanisms.

Internal or pore diffusion is described by 1st Fick's Law which is given by Equation 2.15.

$$J_{H_2} = D_e \cdot \frac{dC_{H_2}}{dx}$$
<div align="right">Equation 2.15</div>

Where, J_{H_2} = Molar flux of hydrogen diffusion, $[mol/m^2 \cdot s]$

D_e = Effective diffusion coefficient in porous materials, $[m^2/s]$

C_{H_2} = Concentration of hydrogen, $[mol/m^3]$

x = diffusion coordinate, $[m]$

The effective diffusion coefficient, which is given by Equation 2.16, is a combination of the molecular and Knudsen diffusion coefficients and it is applied when macro pores supporting materials are used [60].

$$\frac{1}{D_e} = \frac{1}{D_{m,e}} + \frac{1}{D_{k,e}}$$
<div align="right">Equation 2.16</div>

$$D_{m,e} = \frac{\mathfrak{D} \cdot \Phi_p}{\tilde{\tau}}$$

Equation 2.17

$$D_{k,e} = 0.194 \cdot \frac{\Phi_p{}^2}{\tilde{\tau}} \cdot \frac{1}{S_s \cdot \rho_p} \cdot \sqrt{\frac{T}{M}}$$

Equation 2.18

Where, $D_{m,e}$, $D_{k,e}$ = Effective diffusion coefficients of molecular and Knudsen diffusion, respectively, $[m^2/s]$

$\mathfrak{D}$ = Molecular diffusion coefficient, $[m^2/s]$

Φ_p = Internal void fraction of supporting material, in absence of experimental data a value of ca. 0.5 is attributed, [-]

$\tilde{\tau}$ = Tortuosity, in absence of experimental data a value of ca. 4 is attributed, [-]

S_s = Specific surface area of supporting material, $[m^2/g]$

ρ_p = Density of supporting material, $[kg/m^3]$

T = Temperature, [K]

M = Molar mass of diffusing species, [g/mol]

Table 2.5: Summary of mass transfer mechanisms in pore materials [60].

Molecular diffusion	Stands if the pore diameter, $\mathbf{d_{pore}}$, is much larger than the mean free path, λ, of diffusing molecules.
Knudsen diffusion	Stands if $d_{pore} \cong \lambda$. Collisions between the diffusing molecules and pore wall are more frequent than those among molecules.
Configurational diffusion	Stands if d_{pore} is close to molecule size. Molecules are continuously in contact with pore wall and they are free to move only parallel to pore channel.
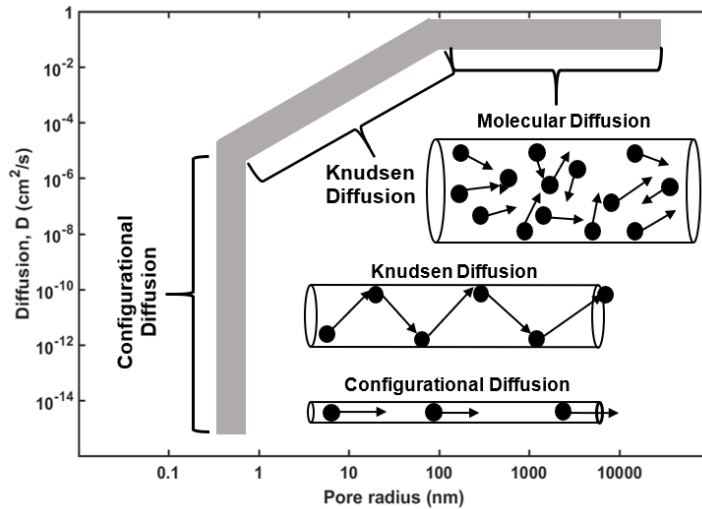
Figure 2.13: Influence of pore size on diffusivity regimes [5].

Reaction in porous materials

At this point a consideration based on Levenspiel [59] is used to describe how pore diffusion affects reactant concentration.

Consider a porous particle of radius r and having a cylindrical pore of length L on which active phase is partially coated. Hydrogen, H_2, diffuses into the pore, then, it finds the catalyst active sites and a 1st-order reaction takes place on the surface and product diffuses out of the pore.

If the reaction rate based on catalyst surface is given by the law which is described by Equation 2.19 and calculating the material balance of hydrogen at steady state for an elementary section of the cylindrical pore, the concentration of hydrogen is given by Equation 2.20.

The first term of Equation 2.20 gives the change of hydrogen concentration along the pore due to the effects of diffusion. On the other hand, the second term gives the change of hydrogen concentration because of the reaction kinetics.

$$-R''_{H_2} = -\frac{1}{S}\frac{dn_A}{dt} = k''_1 \cdot C_{H_2} \qquad \text{Equation 2.19}$$

$$\frac{\partial^2 C_{H_2}}{\partial x^2} - \frac{2 \cdot k''_1}{D_e \cdot r} \cdot C_{H_2} = 0 \qquad \text{Equation 2.20}$$

Where, $-R''_{H_2}$ = Reaction rate based on catalyst surface area, $[\text{mol/m}^2\text{cat} \cdot \text{s}]$

S = Surface area of catalyst, $[\text{m}^2\text{cat}]$

k''_1 = 1st-order chemical reaction rate constant based on unit surface area of catalyst, $[\text{m}^3\text{liquid/m}^2\text{cat} \cdot \text{s}]$

C_{H_2} = Molar concentration of hydrogen, $[\text{mol/m}^3\text{liquid}]$

D_e = Effective diffusion coefficient, $[\text{m}^2/\text{m solid} \cdot \text{s}]$

r = radius of cylindrical pore, $[\text{m}]$

To eliminate pore radius from Equation 2.20, the Equation 2.21, which describes the interrelation between reaction rate constants based on (a) volume of voids in the reactor, k_1, (b) weight of catalyst, k'_1, and (c) catalyst surface, k''_1, is used.

$$k_1 \cdot V = k'_1 \cdot W = k''_1 \cdot S \qquad \text{Equation 2.21}$$

Solving Equation 2.21 for k_1 and substituting in Equation 2.20 the material balance of hydrogen at steady state for a given elementary volume of pore and reaction rate based on volume of voids in the reactor is given by Equation 2.22.

$$\frac{\partial^2 C_{H_2}}{\partial x^2} - \frac{k_1}{D_e} \cdot C_{H_2} = 0 \qquad \text{Equation 2.22}$$

To analyse the effect of the reaction kinetics and pore diffusion on the concentration evolution of hydrogen along the pore, Equation 2.22 was

integrated using the following initial condition. The evolution of hydrogen concentration is described by Equation 2.23 and it is illustrated in the qualitative Figure 2.14.

Initial conditions:

- At the pore entrance, x=0, $C_{H_2} = C_{H_2,o}$
- At the end of the pore and supposing a closed outlet of pore so that no flux of material takes place, x=L, $\frac{\partial C_{H_2}}{\partial x}=0$

$$\frac{C_{H_2}}{C_{H_2,o}} = \frac{e^{m(L-x)} + e^{m(L-x)}}{e^{mL}+e^{-mL}} = \frac{\cosh[m(L-x)]}{\cosh[mL]}$$

Equation 2.23

Thiele Modulus: $$m \cdot L = L \cdot \sqrt{\frac{k_1}{D_e}} = L \cdot \sqrt{\frac{2k_1''}{D_e \cdot r}}$$

Equation 2.24
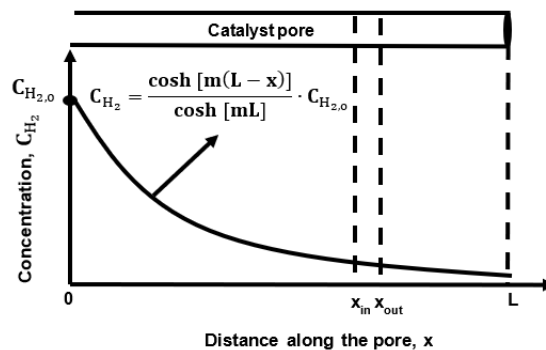
Figure 2.14: Qualitative scheme of concentration drop along the pore.

From Equation 2.23, one concludes to the followings:

- For a given porous material structure and reaction kinetics, concentration of hydrogen along the pore depends on the distance x lengthwise the pore. Concentration of hydrogen drops lengthwise the pore due to the diffusion and reaction effect.
- For a given pore structure with characteristic size L, the concentration drop lengthwise the pore depends on factor m. In other words, it depends on reaction rate constant and effective diffusion constant. By

increasing m, concentration drop is faster. But increase of factor m can occur because of either reason: (a) increase of rate constant (fast reaction), (b) decrease of effective diffusion constant (slow diffusion-i.e. high resistance to diffusion). As it is discussed later a careful consideration should be made to compromise these two factors and select the appropriate catalyst for a given reaction.

2.4.2.2. Effectiveness factor

To define how much pore diffusion affects the reaction rate or in other words, how much reaction rate is lowered by the resistance to pore diffusion, the effectiveness factor is used and it is defined as [59]:

$$\text{effectiness factor,} \qquad \varepsilon = \frac{\text{actual mean reaction rate within pore}}{\text{rate in absence of pore diffusion}}$$

In the case of 1st-order reaction, the effectiveness factor is expressed by Equation 2.25.

$$\varepsilon = \frac{\overline{C}_A}{C_{As}} = \frac{\tanh(mL)}{mL} \qquad\qquad \text{Equation 2.25}$$

Relationship between effectiveness factor and Thiele modulus is introduced in Figure 2.15.
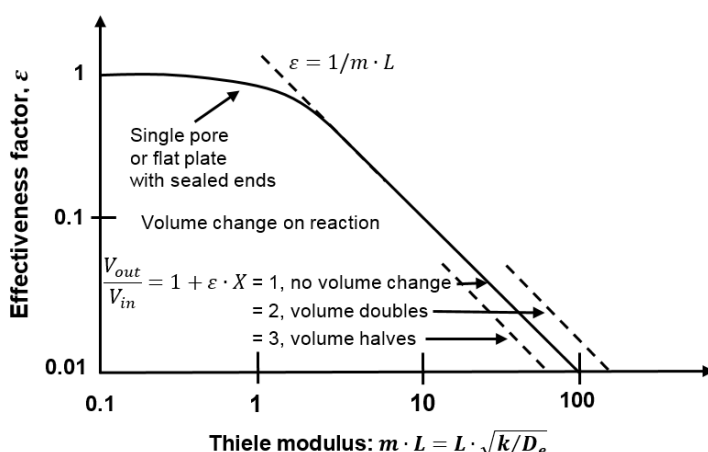
Figure 2.15: Effectiveness factor for 1st-order reaction with respect to Thiele modulus [59].

- If $m \cdot L < 0.4$, effectiveness factor is almost equal to unity. This means that pore diffusion does not actually affect the overall rate. Substituting m with $\sqrt{k/D_e}$ and rearranging appropriately, $k < 0.16 \cdot D_e/L$. This justifies that reaction is not too fast to be slowed by diffusion for the particular catalyst particle. Moreover, small value of Thiele modulus indicates: short pore, slow reaction or rapid diffusion [59].

- If $m \cdot L > 0.4$, effectiveness factor is given by the reciprocal of Thiele modulus. In this regime, reactant concentration drops quickly to zero, without approaching the end of the pore. In analogous way, in this case $k > 16 \cdot D_e/L$, indicating too fast reaction that is slowed by pore diffusion. This regime is known as strong pore resistance [59]. In particular cases where reaction rate is too high and pore long enough, unused catalyst regions longwise the pore can be created which may result in the formation of by-products.

2.4.2.3. Pore effectiveness factor

Equation 2.26 correlates the penetration depth of the pore, beyond which the concentration hydrogen is zero, to the Thiele modulus, for a 1st-order reaction taking place in a cylindrical pore.

$$\frac{x}{L} = \frac{1}{L}\sqrt{\frac{D_e}{k'' \cdot} \cdot \frac{r}{2}} = \frac{1}{\text{Thiele modulus}}$$

Equation 2.26

Figure 2.16 shows how Thiele modulus affects the concentration drop over the distance along the catalyst pore. At the same penetration depth inside the pore, as Thiele modulus increases, concentration of reactant has been decreased more. On the other hand, if Thiele modulus is too high so that reactant concentration drops to zero without using the whole catalyst pore, reactions between products may occur if they are promoted of the catalyst and reaction conditions. This may give the chance for by-product formation from any consecutive reaction leading to product loss.
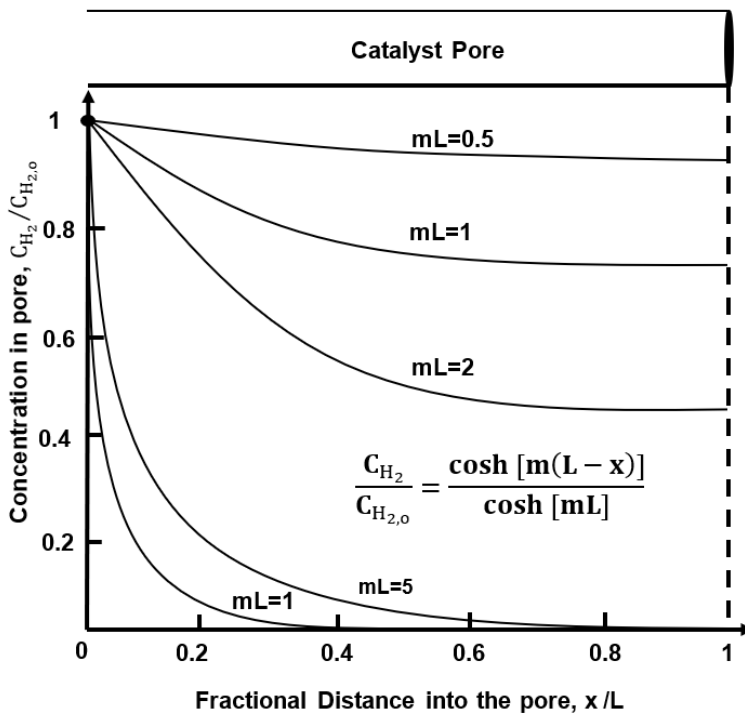
Figure 2.16: Reactant concentration drop along pore for different values of Thiele Modulus [59].

Table 2.6: Effectiveness factor for different particle shapes [59, 61].

Particle Shape	Effectiveness Factor, ε
Flat Plate	$\dfrac{\tanh(mL)}{mL}$
Cylinders	$\dfrac{1}{mL} \cdot \dfrac{I_1(2 \cdot mL)}{I_0(2 \cdot mL)}$ Where, I_1 and I_2 is Bessel Function
Spheres	$\dfrac{1}{mL} \cdot \left[\dfrac{1}{\tanh(3 \cdot mL)} - \dfrac{1}{3 \cdot mL} \right]$

2.4.3. Surface models of heterogeneous hydrogenation

In section 2.4.1 and 2.4.2, a description of mass transfer at the bubble scale and particle scale was given, respectively. In this section, an effort to describe

the mass transfer at the molecular scale is made and the Langmuir-Hinshelwood and Eley-Rideal models for bimolecular reactions are presented.

Although in the last century significant research effort has been made, catalyst function in heterogeneous reaction is still ambiguous [28]. Heterogeneous catalytic reactions take place on catalyst surface. The vast majority of catalysts which are used in hydrogenation are platinum group metals. It is known that metals are crystalline, therefore, their atoms build well-structured bonds in arranged arrays. It is usual phenomenon many metals to present defects in their crystal grid. Localised atoms in defected areas of the grid have higher energy than those in well-structured area of crystal. Moreover, it has been observed that atoms on crystal defects have fewer neighbours than on average in the crystal grid [28]. The last two facts may cause a higher reactivity of these atoms. The concept that high-energy atoms act as active sites for catalytic reactions is generally accepted today. But there is not still any way to calculate accurately the number of active centres of catalyst which may give us the opportunity for precise kinetic models of heterogeneous catalysed reactions [28].

Despite the fact of unmeasurable active centres, kinetic models of heterogeneous catalysed processes have been proposed. Langmuir-Hinshelwood and Eley-Rideal models are the two most significant and widely used models which describe the heterogeneous catalysed hydrogenation [25, 62, 63].

As hydrogenations are heterogeneously catalysed, hydrogen and the compound which is to be hydrogenated should be transferred to active phase surface. This is done by adsorption processes. There are two ways for a

substance to be adsorbed on the surface of a solid; either chemically or physically, depending on the bonds which are developed between the solid's surface and adsorbed substance. In the first case, electron interactions take place between the external layers of crystal grid of the metal and the adsorbed substance [36]. This type of adsorption results in rearrangements of the electrons within the molecules, so, it is called chemical adsorption or chemisorption and it is considered as a chemical reaction. The latter type of adsorption occurs when Van der Waals forces take place which result in less strong interaction without any molecular alteration [36].

2.4.3.1. Langmuir-Hinshelwood model

The Langmuir-Hinshelwood model implies the chemisorption of the gas and liquid substances onto catalyst active sites while each site can adsorb only one molecule. In addition, all the active sites have the same probability to take part in the chemisorption, in other words, they are energetically equivalent. Before the chemisorption onto active sites, there is not any interaction between the gas and liquid reactant, however, the gas and liquid reactants may compete, or not, for adsorbing onto the same active sites.

According to Langmuir-Hinshelwood model, reaction on catalyst surface is progressed at three steps while reaction at surface constitutes the rate limiting step [59, 61]:

- Chemisorption of the unsaturated compound and hydrogen onto active phase surface.
- Reaction between them on active phase surface.
- Products desorption from the active phase site to the bulk pore.

Dissociative chemisorption of H₂

The active phase of most of the catalyst consists of transition metal in which hydrogen is dissociatively chemisorbed [64-68]. If one considers the chemisorption as a reversible chemical reaction, it is expressed as below:

$$H_{2,S} + \square \quad \square \quad \overset{K_{H_2}}{\longleftrightarrow} \quad 2 \cdot H - \square$$
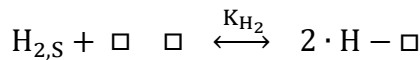
Where $H_{2,S}$ is the hydrogen at the outer surface of the catalytic particle, the open square, $\square$, denotes the active sites, and the $H - \square$ represents the complex between one active site and one atom of hydrogen. If the fraction of active sites which are occupied by hydrogen is denoted by θ_{H_2} and the fraction of vacant active sites is denoted by $\theta_\square$, the equilibrium constant is given by Equation 2.27.

$$K_{H_2} = \frac{\theta_{H_2}^2}{\theta_\square^2 \cdot C_{H_2,S}} \qquad \qquad \text{Equation 2.27}$$

Non-competitive adsorption

In a same manner, the chemisorption of the liquid compound, which chemisorbed in a different type of active sites, is described in the form of a reversible chemical reaction as below:

$$B_S + o \quad \overset{K_{St}}{\longleftrightarrow} \quad B - o$$
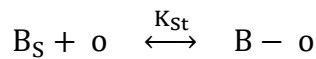
Where B_S is the liquid compound at the outer surface of the catalytic particle, the open circle, o, denotes the active sites which are available for being occupied by the liquid compound, and the $B - o$ represents the complex between one active site and one molecule of the liquid compound. If the fraction of active sites which are occupied by B is denoted by θ_B and the

fraction of vacant active sites is denoted by θ_o, the equilibrium constant is given by Equation 2.28.

$$K_B = \frac{\theta_B}{\theta_o \cdot C_{B,S}}$$

Equation 2.28

As the Langmuir-Hinshelwood model implies, the chemical reaction takes place between the chemisorbed compounds. Therefore, it is written as below:

$$2 \cdot H - \square + B - o \quad \overset{K_{St}}{\longleftrightarrow} \quad BH_2 + o + \square$$
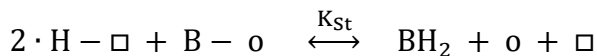
Equation 2.29 and Equation 2.30 give the material balance for the two types of active sites, in terms of the fractional coverages.

$$\theta_{H_2} + \theta_\square = 1$$

Equation 2.29

$$\theta_B + \theta_o = 1$$

Equation 2.30

Solving for the fractional coverages of the hydrogen and the liquid compound Equation 2.27 and Equation 2.28, respectively, and eliminating the expressions of vacant sites fractions using Equation 2.29 and Equation 2.30, the fractional coverage of hydrogen and liquid compound are expressed by Equation 2.31 and Equation 2.32, respectively, as functions of the equilibrium constants and the concentrations of the hydrogen and liquid compound at the outer surface of the catalytic particle.

$$\theta_{H_2} = \frac{\sqrt{C_{H_2,S} \cdot K_{H_2}}}{1 + \sqrt{C_{H_2,S} \cdot K_{H_2}}}$$

Equation 2.31

$$\theta_B = \frac{C_{B,S} \cdot K_{St}}{1 + C_{B,S} \cdot K_{St}}$$

Equation 2.32

Competitive adsorption

In the case of competitive chemisorption, hydrogen and liquid compound compete for the same active sites. Therefore, the chemisorption of the liquid

compound, is described in the form of a reversible chemical reaction as below, the equilibrium constant is defined by Equation 2.33 and the material balance of the active sites, in terms of the fractional coverages by Equation 2.34.

$$B_S + \square \overset{K_{St}}{\longleftrightarrow} B - \square$$
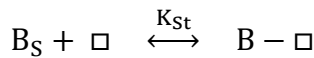
$$K_B = \frac{\theta_B}{\theta_\square \cdot C_{B,S}}$$
Equation 2.33

$$\theta_{H_2} + \theta_B + \theta_\square = 1$$
Equation 2.34

Following the same manner, the fractional coverages are expressed as functions of (a) the equilibrium constants and (b) the concentrations of the hydrogen and liquid compound at the outer surface of the catalytic particle, they are defined by Equation 2.35 and Equation 2.36.

$$\theta_{H_2} = \frac{\sqrt{C_{H_2,S} \cdot K_{H_2}}}{1 + \sqrt{C_{H_2,S} \cdot K_{H_2}} + C_{B,S} \cdot K_B}$$
Equation 2.35

$$\theta_{St} = \frac{C_{B,S} \cdot K_{St}}{1 + \sqrt{C_{H_2,S} \cdot K_{H_2}} + C_{B,S} \cdot K_B}$$
Equation 2.36

Reaction rate law

The reaction rate is expressed, in terms of the fractional coverages of hydrogen and liquid compound, θ_{H_2} and θ_{St}, respectively, by Equation 2.37.

$$R = k_1 \cdot \theta_{H_2} \cdot \theta_B$$
Equation 2.37

The suitable expression of the fractional coverage of the hydrogen and liquid compound needs to be substituted in Equation 2.37 depending on if the adsorption is competitive or not. This is ascertained experimentally by observing the reaction rate in different concentrations of hydrogen and liquid compound. In the case of non-competitive adsorption, in excess of liquid compound the reaction rate is independent of liquid compound concentration.

In contrast, if the hydrogen and liquid compound compete for the same active sites, in excess of liquid compound, is inversely proportional to the liquid compound concentration.

Non-competitive:
$$R = k_1 \cdot \frac{\sqrt{C_{H_2,S} \cdot K_{H_2}} \cdot C_{B,S} \cdot K_B}{\left(1 + \sqrt{C_{H_2,S} \cdot K_{H_2}}\right) \cdot \left(1 + C_{B,S} \cdot K_B\right)}$$
Equation 2.38

Competitive:
$$R = k_1 \cdot \frac{\sqrt{C_{H_2,S} \cdot K_{H_2}} \cdot C_{B,S} \cdot K_B}{\left(1 + \sqrt{C_{H_2,S} \cdot K_{H_2}} + C_{B,S} \cdot K_{St}\right)^2}$$
Equation 2.39

2.4.3.2. Eley-Rideal model

Eley-Rideal model implies that only one of the reactants is chemisorbed on the catalyst surface while the other reacts directly from bulk gas or it is adsorbed physically [63, 69, 70].

In this case, the chemisorbed hydrogen reacts with the substrate B which is either in the outer surface of the catalyst or has been physically adsorbed in the active sites. Therefore, the reaction rate is given by Equation 2.40.

$$R = k_1 \cdot \theta_{H_2} \cdot C_{B,S}$$
Equation 2.40

Substituting the hydrogen fractional coverage, the reaction rate is described by Equation 2.41.

$$R = k_1 \cdot \frac{\sqrt{C_{H_2,S} \cdot K_{H_2}}}{1 + \sqrt{C_{H_2,S} \cdot K_{H_2}} + C_{B,S} \cdot K_B} \cdot C_{B,S}$$
Equation 2.41

Chapter 3

3.   Theoretical aspects of hydrogenation models

3.1.   Mass transfer in series model

In section 2.2.3 and 2.2.4, the process scheme of the heterogeneous hydrogenation in the slurry and trickle bed reactors were introduced. As the process schemes describes, the heterogeneous catalytic hydrogenation is a complicated combination of physical and chemical processes which proceeds in four steps. Sections 2.4.1 and 2.4.2 offered an insight into the interphase mass transfer and the intraparticle diffusion by reviewing the most significant models which describe them. In Section 2.4.3, the two most significant models which describe the surface chemical reaction were introduced. In this section, an effort to give a model which describes the overall heterogeneous hydrogenation including all the steps is made.

To do so, the mass transfer in series model is adopted [59]. According to this model, the interphase mass transfer, the intraparticle diffusion and the chemical reaction on active sites take place consecutively, under the same rate which is defined by the slowest process, referred as limiting step. The mass transfer proceeds from the region with the highest concentration to the region with the lowest concentration. In addition, each of the physical and chemical processes obstruct the mass transfer in a different extent. This obstruction is referred to as resistance against the mass transfer and an analogy to Ohm's law related to the electrical circuit is used. According to this analogy, the mass transfer rate is likened to the current, I; the concentration

gradient to the voltage, V; and the mass transfer resistances, the definition of which is given later, to the electrical resistances, Ω.
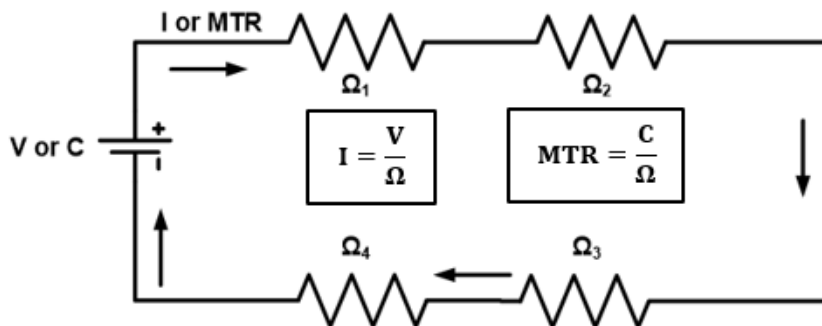
Figure 3.1: Schematic representation of mass transfer resistances in series model in analogy to Ohm's law.

3.1.1. Global mass transfer rate in stirred tank reactors

As it has been already mentioned in section 2.2.3, in stirred tank reactors, in which the catalyst is in the form of fine particles suspended in the continuous liquid phase creating a slurry, molecules of hydrogen should be transferred to the catalyst active phase in order to react with the substrate. Therefore, hydrogen molecules transfer is broken down to the following steps [8]:

1.   Diffusion of H_2 from gas phase into the gas-liquid interface

2.   Diffusion of H_2 from the gas-liquid interface into bulk liquid phase

3.   Diffusion of H_2 from the bulk liquid phase to the external particle surface

4.   Diffusion through the catalyst pore structure to the active phase surface (intraparticle diffusion)

While the hydrogen is found in gas, liquid and solid phase, substrate molecules are present in bulk liquid and solid phase. Therefore, they need first to diffuse to the external particle surface and then through the catalyst pore structure to the active phase surface.

Figure 3.2 illustrates the evolution of reactants concentration along the direction of mass transfer while the external mass transfer is described by the film theory. Table 3.1 summarises the mathematical expressions of each step.

The external mass transfer expressions are based on Equation 2.2. In contrast to the surface reaction models of either Langmuir-Hinshelwood or Eley-Rideal, the chemical step is expressed by a 1st order reaction rate law in order to make easy the combination of chemical reaction step with the external mass transfer steps, a manipulation inspired by [59].
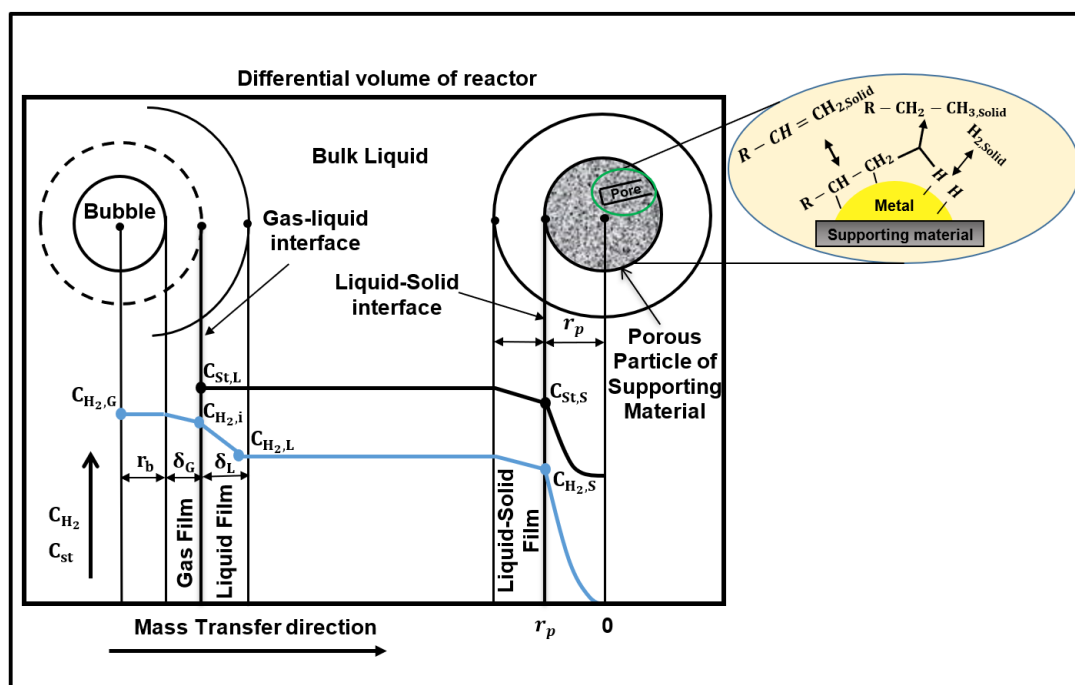
Figure 3.2: Concentration profiles of hydrogen and substrate along mass transfer direction in a STR.

Table 3.1: Summary of rate expressions of hydrogen and styrene in a STR.

Step	Mathematical expression	
Rate of hydrogen diffusion from gas phase to gas-liquid interface	$MTR_{H_2,G-i}^{STR} = k_G \cdot \alpha \cdot H_E \cdot \left[\dfrac{P_{H_2,G}}{H_E} - \dfrac{P_{H_2,i}}{H_E} \right]$	Equation 3.1
Rate of hydrogen diffusion from gas-liquid interface to bulk liquid	$MTR_{H_2,i-L}^{STR} = k_L \cdot \alpha \cdot \left(C_{H_2,i} - C_{H_2,L} \right)$	Equation 3.2
Rate of hydrogen diffusion from bulk liquid to catalyst surface	$MTR_{H_2,L-S}^{STR} = k_{s,H_2} \cdot \alpha_s \cdot \dfrac{W_C}{V_L} \cdot \left(C_{H_2,L} - C_{H_2,S} \right)$	Equation 3.3
Rate of hydrogen diffusion through the catalyst pore structure and reaction on catalyst active sites	$MTR_{H_2,R}^{STR} = \varepsilon \cdot \dfrac{W_C}{V_L} \cdot k'_{obs,1^{st}order} \cdot C_{H_2,S}$	Equation 3.4
Rate of styrene diffusion from bulk liquid to catalyst surface	$MTR_{St,L-S}^{STR} = k_{s,St} \cdot \alpha_s \cdot \dfrac{W_C}{V_L} \cdot \left(C_{St,L} - C_{St,S} \right)$	Equation 3.5
Rate of styrene diffusion through the catalyst pore structure and reaction on catalyst active sites	$MTR_{St,R}^{STR} = \varepsilon \cdot \dfrac{W_C}{V_L} \cdot k'^{St}_{obs,1^{st}order} \cdot C_{St,S}$	Equation 3.6

HYDROGEN (Equations 3.1–3.4)

STYRENE (Equations 3.5–3.6)

Global mass transfer rate of hydrogen

Assuming that the steady state of the three-phase reaction is reached quickly, comparing to the overall reaction time, the mass transfer and the chemical reaction take place under the same rate.

$$\text{MTR}_{H_2,G-i}^{STR} = \text{MTR}_{H_2,i-L}^{STR} = \text{MTR}_{H_2,L-S}^{STR} = \text{MTR}_{H_2,R}^{STR} = \text{MTR}_{H_2}^{STR} \qquad \text{Equation 3.7}$$

Transforming appropriately Equation 3.1, Equation 3.2, Equation 3.3 and Equation 3.4, the overall or global mass transfer rate of hydrogen which takes into account all the steps of the three-phase reaction is defined by Equation 3.9. The first step has been eliminated because when pure hydrogen or slightly soluble gases are used, the hydrogen diffusion from gas phase to gas-liquid interface is unlikely to be the limiting step. The gas-liquid interfacial concentration of hydrogen is assumed in equilibrium with the gas phase pressure of hydrogen based on Henry's law which is given by Equation 3.8.

$$P_{H_2} = C_{H_2,i} \cdot H_E \qquad \text{Equation 3.8}$$

$$\text{MTR}_{H_2}^{STR} = \cfrac{1}{\cfrac{1}{k_L \cdot \alpha} + \cfrac{1}{k_{s,H_2} \cdot \alpha_s \cdot \cfrac{W_C}{V_L}} + \cfrac{1}{\varepsilon \cdot k'_{obs,1^{st}order} \cdot \cfrac{W_C}{V_L}}} \cdot \cfrac{P_{H_2}}{H_E} \qquad \text{Equation 3.9}$$

Where, $\text{MTR}_{H_2}^{STR}$ = Mass transfer rate of hydrogen, $[mol/m^3 liquid \cdot s]$

k_L = Specific gas-liquid mass transfer coefficient related to liquid side film, $[m/s]$

α = Gas-liquid mass transfer area of stirred tank reactor per unit volume of liquid, $[m^2/m^3 \ liquid]$

α_s = Liquid-solid mass transfer area of stirred tank reactor per unit weight of catalyst, $[m^2/g \ cat]$

k_{s,H_2} = Specific liquid-solid mass transfer coefficient of hydrogen, [m/s]

$k'_{obs,1^{st}order}$ = Observed rate constant for 1st-order reaction based on unit Pd weight in the bed, [m^3liquid/g Pd $\cdot$ s]

ε = Effectiveness factor, [-]

P_{H_2}= Partial pressure of hydrogen in the reactor, [Pa]

H_E = Henry constant, [Pa $\cdot$ m^3/mol]

V_L = Volume of liquid phase in the reactor, [m^3]

W_C = Weight of catalyst, [g]

The three components at the denominator of Equation 3.9 act as barriers to the mass transfer rate, the higher they are the slower the rate is.

The denominator of Equation 3.9 describes the overall mass transfer resistance of hydrogen which consists of three components (Equation 3.10). The first component is related to the mass transfer resistance because of the film which is developed between the gas and liquid phases. The second term is related to the mass transfer resistance because of the film which is developed around the catalyst particle and the third component is related to the resistance because of the pore diffusion and the chemical reaction kinetics.

$$\Omega^{STR}_{H_2,tot} = \frac{P_{H_2}/H_E}{MTR_{H_2}}$$

$$= \frac{1}{k_L \cdot \alpha} + \frac{1}{k_{s,H_2} \cdot \alpha_s \cdot \frac{W_C}{V_L}} + \frac{1}{\varepsilon \cdot k'_{obs,1^{st}order} \cdot \frac{W_C}{V_L}} \qquad \text{Equation 3.10}$$

Where, $\Omega^{STR}_{H_2,tot}$ = Mass transfer resistance of hydrogen, [s]

Table 3.2: Summary of Mass transfer resistances of hydrogen in STR.

	Description	Expression	Definition
External mass transfer resistances	Resistance of gas-liquid interface	$\Omega_{H_2,i-L}^{STR}$	$\dfrac{1}{k_L \cdot \alpha}$
	Resistance of liquid - solid interface	$\Omega_{H_2,L-S}^{STR}$	$\dfrac{1}{k_{s,H_2} \cdot \alpha_s \cdot \dfrac{W_C}{V_L}}$
Resistance of internal catalyst pore structure and surface chemical reaction		$\Omega_{H_2,R}^{STR}$	$\dfrac{1}{\varepsilon \cdot k_{obs,1^{st}order}' \cdot \dfrac{W_C}{V_L}}$

Global mass transfer rate of substrate

In a same manner as in hydrogen case, assuming that the steady state of the three-phase reaction is reached quickly, comparing to the overall reaction time, the mass transfer and the chemical reaction take place under the same rate.

$$MTR_{St,L-S}^{STR} = MTR_{St,R}^{STR} = MTR_{St}^{STR}$$

Equation 3.11

Following the same procedure as we have shown in the case of hydrogen, we conclude to the expressions of the overall mass transfer rate and overall mass transfer resistance of substrate in Equation 3.12 and Equation 3.13, respectively.

$$MTR_{St}^{STR} = \frac{1}{\dfrac{1}{k_{s,St} \cdot \alpha_s \cdot \dfrac{W_C}{V_L}} + \dfrac{1}{\varepsilon \cdot \dfrac{W_C}{V_L} \cdot k_{obs,1^{st}order}'^{St}}} \cdot C_{St,L}$$

Equation 3.12

Where, MTR_{St}^{STR} = Mass transfer rate of styrene, $[mol/m^3 liquid \cdot s]$

$k_{s,St}$ = Specific liquid-solid mass transfer coefficient of styrene, [m/s]

$k'^{St}_{obs,1^{st}order}$ = Observed rate constant of styrene for 1st-order reaction based on unit Pd weight in the bed, $[m^3 liquid/g\ Pd \cdot s]$

$C_{St,L}$ = Concentration of styrene in liquid phase, $[mol/m^3 liquid]$

The two components at the denominator of Equation 3.12 act as barriers to the mass transfer rate, the higher they are the slower the rate.

The denominator of Equation 3.12 describes the overall mass transfer resistance of styrene which consists of two components (Equation 3.13). The first is related to the mass transfer resistance because of the film which is developed around the catalyst particle. The second component is related to the resistance because of the pore diffusion and the chemical reaction kinetics.

$$\Omega^{STR}_{St,tot} = \frac{C_{St,L}}{MTR_{H_2}} = \frac{1}{k_{s,sub} \cdot \alpha_s \cdot \frac{W_C}{V_L}} + \frac{1}{\varepsilon \cdot \frac{W_C}{V_L} \cdot k'^{St}_{obs,1^{st}order}} \qquad \text{Equation 3.13}$$

Where, $\Omega^{STR}_{St,tot}$ = Mass transfer resistance of styrene, [s]

Table 3.3: Summary of mass transfer resistances of styrene in the STR.

Description	Expression	Definition
Resistance of liquid-solid interface	$\Omega^{STR}_{St,L-S}$	$\dfrac{1}{k_{s,H_2} \cdot \alpha_s \cdot \frac{W_C}{V_L}}$
Resistance of internal catalyst pore structure and surface chemical reaction	$\Omega^{STR}_{St,R}$	$\dfrac{1}{\varepsilon \cdot \frac{W_C}{V_L} \cdot k'^{St}_{obs,1^{st}order}}$

3.1.2. Global mass transfer rate in trickle bed reactors

As in the case of stirred tank reactor, hydrogen has to overcome two external mass transfer processes before the reaction take place on catalyst active phase, however, in the trickle bed reactor gas is the continuous phase in which liquid is dispersed developing thin rivulets around the coarse particles of catalyst.

Figure 3.3 illustrates the evolution of reactants concentration along the direction of mass transfer while the external mass transfer is described by the film theory. Table 3.4 summarises the mathematical expressions of each step.

As in the case of the stirred tank reactor, the external mass transfer expressions are based on Equation 2.2. and the chemical step is expressed by a 1st order reaction rate law in order to make easy the combination of chemical reaction step with the external mass transfer steps as Levenspiel [59] suggests.

The bed is comprised of (a) the glass beads, (b) the active pellets and (c) the non-active pellets. The gas-liquid mass transfer takes place in the surface area which is developed around all the types of solids; glass beads, active and non-active pellets. On the other hand, the chemical reaction takes place on active sites of the catalyst, which means that only the surface area developed around the active pellets contributes to the liquid-solid mass transfer.
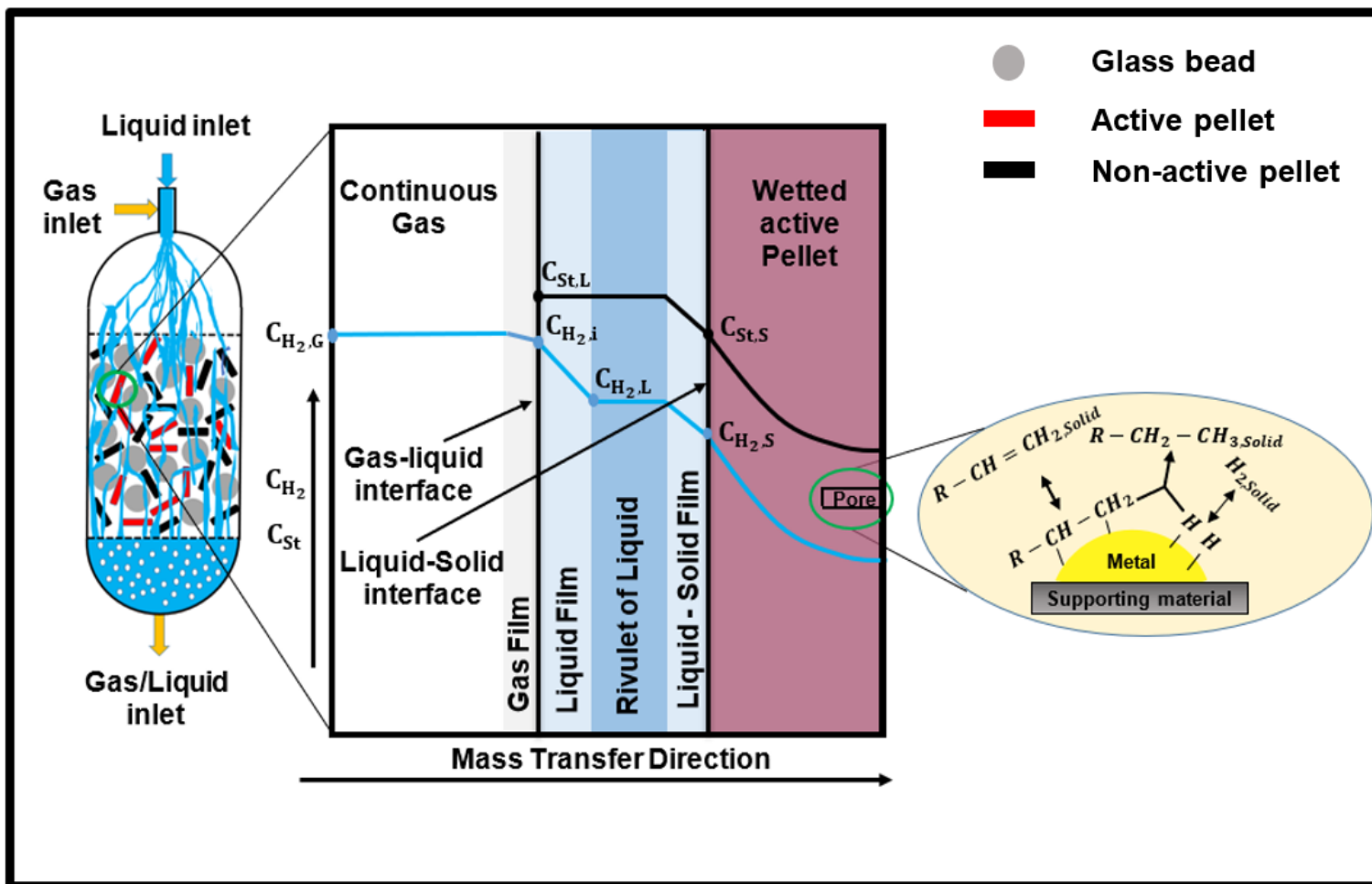
Figure 3.3: Concentration profiles of hydrogen and styrene along mass transfer direction in a TBR.

Table 3.4: Summary of rate expressions of hydrogen and styrene in a TBR.

Step	Mathematical expression		
Rate of hydrogen diffusion from gas phase to gas-liquid interface	$\text{MTR}_{\text{H}_2,\text{G}-\text{i}}^{\text{TBR}} = k_\text{G} \cdot \alpha_\text{bed} \cdot H_\text{E} \cdot \left[\dfrac{P_{\text{H}_2,\text{G}}}{H_\text{E}} - \dfrac{P_{\text{H}_2,\text{i}}}{H_\text{E}}\right]$	Equation 3.14	HYDROGEN
Rate of hydrogen diffusion from gas-liquid interface to bulk liquid	$\text{MTR}_{\text{H}_2,\text{i}-\text{L}}^{\text{TBR}} = k_\text{L} \cdot \alpha_\text{bed} \cdot f \cdot (C_{\text{H}_2,\text{i}} - C_{\text{H}_2,\text{L}})$	Equation 3.15	
Rate of hydrogen diffusion from bulk liquid to catalyst surface	$\text{MTR}_{\text{H}_2,\text{L}-\text{S}}^{\text{TBR}} = k_{\text{s},\text{H}_2} \cdot \alpha_{\text{act.pel}}^{'\text{Pd}} \cdot f \cdot \dfrac{W_\text{Pd}}{V_\text{L}} \cdot (C_{\text{H}_2,\text{L}} - C_{\text{H}_2,\text{S}})$	Equation 3.16	
Rate of hydrogen diffusion through the catalyst pore structure and reaction on catalyst active sites	$\text{MTR}_{\text{H}_2,\text{R}}^{\text{TBR}} = \varepsilon \cdot f \cdot \dfrac{W_\text{Pd}}{V_\text{L}} \cdot k_{\text{obs},1^{st}\text{order}}^{'\text{Pd}} \cdot C_{\text{H}_2,\text{S}}$	Equation 3.17	
Rate of styrene diffusion from bulk liquid to catalyst surface	$\text{MTR}_{\text{St},\text{L}-\text{S}}^{\text{TBR}} = k_{\text{s},\text{St}} \cdot \alpha_{\text{act.pel}}^{'\text{Pd}} \cdot f \cdot \dfrac{W_\text{Pd}}{V_\text{L}} \cdot \left(C_{\text{St}_,\text{L}} - C_{\text{St}_,\text{s}}\right)$	Equation 3.18	STYRENE
Rate of styrene diffusion through the catalyst pore structure and reaction on catalyst active sites	$\text{MTR}_{\text{St},\text{R}}^{\text{TBR}} = \varepsilon \cdot f \cdot \dfrac{W_\text{Pd}}{V_\text{L}} \cdot k_{\text{obs},1^{st}\text{order}}^{'\text{St},\text{Pd}} \cdot C_{\text{St},\text{S}}$	Equation 3.19	

Global mass transfer rate of hydrogen

Assuming that the steady state of the three-phase reaction is reached quickly, comparing to the overall reaction time, the mass transfer and the chemical reaction take place under the same rate.

$$\text{MTR}_{H_2,G-i}^{TBR} = \text{MTR}_{H_2,i-L}^{TBR} = \text{MTR}_{H_2,L-S}^{TBR} = \text{MTR}_{H_2,R}^{TBR} = \text{MTR}_{H_2}^{TBR} \qquad \text{Equation 3.20}$$

Following the same procedure as in the case of stirred tank reactors, the overall mass transfer rate and overall mass transfer resistance of hydrogen in trickle bed reactors are defined by Equation 3.21 and Equation 3.22, respectively.

The denominator of Equation 3.21 describes the overall mass transfer resistance of hydrogen which consists of three components (Equation 3.22). The first component is related to the mass transfer resistance because of the film which is developed between the gas and liquid phases. The second term is related to the mass transfer resistance because of the film which is developed around the catalytic pellet between the liquid and solid phases and the third component is related to the mass transfer resistance because of the pore diffusion and the chemical reaction kinetics.

$$\text{MTR}_{H_2}^{TBR} =$$

$$= \frac{P_{H_2}/H_E}{\left[\dfrac{1}{k_L \cdot \alpha_{bed} \cdot f} + \dfrac{1}{k_{s,H_2} \cdot \alpha_{act.pel}^{\prime Pd} \cdot f} \cdot \dfrac{V_L}{W_{Pd}} + \dfrac{1}{\varepsilon \cdot f \cdot k_{obs,1^{st}order}^{\prime Pd}} \cdot \dfrac{V_L}{W_{Pd}} \right]} \qquad \text{Equation 3.21}$$

$$\Omega_{H_2,tot}^{TBR} = \frac{P_{H_2}/H_E}{\text{MTR}_{H_2}^{TBR}} =$$

$$= \frac{1}{k_L \cdot \alpha_{bed} \cdot f} + \frac{1}{k_{s,H_2} \cdot \alpha_{act.pel}^{\prime Pd} \cdot f} \cdot \frac{V_L}{W_{Pd}} + \frac{1}{\varepsilon \cdot f \cdot k_{obs,1^{st}order}^{\prime Pd}} \cdot \frac{V_L}{W_{Pd}} \qquad \text{Equation 3.22}$$

Where, $MTR_{H_2}^{TBR}$ = Mass transfer rate of hydrogen, $[mol/m^3 liquid \cdot s]$

k_L = Specific gas-liquid mass transfer coefficient related to liquid side film, $[m/s]$

k_{s,H_2} = Specific liquid-solid mass transfer coefficient of hydrogen, $[m/s]$

$k'^{Pd}_{obs,1^{st}order}$ = Observed rate constant for 1st-order reaction based on unit Pd weight in the bed, $[m^3 liquid/g\,Pd \cdot s]$

H_E = Henry constant, $[Pa \cdot m^3/mol]$

f = Overall wetting efficiency of the bed, [-]

P_{H_2} = Partial pressure of hydrogen, $[Pa]$

V_L = Volume of liquid phase in the reactor, $[m^3]$

W_{Pd} = Weight of palladium in the bed, $[g]$

α_{bed} = External mass transfer area of the bed per unit volume of bed, $[m^2 bed/m^3\,bed]$

$\alpha'^{Pd}_{act.pel}$ = Overall external mass transfer area of active pellets per unit weight of palladium in the bed, $[m^2/g\,Pd]$

ε = Effectiveness factor, [-]

$\Omega_{H_2,tot}^{TBR}$ = Overall mass transfer resistance of hydrogen, $[s]$

Table 3.5: Summary of mass transfer resistances of hydrogen TBR.

	Description	Expression	Definition
External mass transfer resistances	Resistance of gas-liquid interface	$\Omega^{TBR}_{H_2,i-L}$	$\dfrac{1}{k_L \cdot \alpha_{bed} \cdot f}$
	Resistance of liquid - solid interface	$\Omega^{TBR}_{H_2,L-S}$	$\dfrac{1}{k_{s,H_2} \cdot \alpha'^{Pd}_{act.pel} \cdot f} \cdot \dfrac{V_L}{W_{Pd}}$
Resistance of internal catalyst pore structure and surface chemical reaction		$\Omega^{TBR}_{H_2,R}$	$\dfrac{1}{\varepsilon \cdot f \cdot k'_{obs,1^{st}order}} \cdot \dfrac{V_L}{W_{Pd}}$

Global mass transfer rate of substrate

In a same manner as in hydrogen case, assuming that the steady state of the three-phase reaction is reached quickly, comparing to the overall reaction time, the mass transfer and the chemical reaction take place under the same rate.

$$MTR^{TBR}_{St,L-S} = MTR^{TBR}_{St,R} = MTR^{TBR}_{St} \qquad \text{Equation 3.23}$$

Following the same procedure as we have shown in the case of hydrogen, the expressions of the overall mass transfer rate and overall mass transfer resistance of substrate are given by Equation 3.24 and Equation 3.25.

$$MTR^{TBR}_{St} = \dfrac{1}{\dfrac{1}{k_{s,St} \cdot \alpha'^{Pd}_{act.pel} \cdot f} \cdot \dfrac{V_L}{W_{Pd}} + \dfrac{1}{\varepsilon \cdot f \cdot k'^{St\,Pd}_{obs,1^{st}order}} \dfrac{V_L}{W_{Pd}}} \cdot C_{St,L} \qquad \text{Equation 3.24}$$

Where, $\text{MTR}_{\text{St}}^{\text{TBR}}$ = Mass transfer rate of styrene, [mol/m³liquid · s]

$k_{\text{s,St}}$ = Specific liquid-solid mass transfer coefficient of styrene, [m/s]

$k_{\text{obs,1}^{\text{st}}\text{order}}^{'\text{St,Pd}}$ = Observed rate constant of styrene for 1st-order reaction

based on unit Pd weight in the bed, [m³liquid/g Pd · s]

$C_{\text{St,L}}$ = Concentration of styrene in liquid phase, [mol/m³liquid]

The two components at the denominator of Equation 3.24 act as barriers to the mass transfer rate, the higher they are the slower the rate.

The denominator of Equation 3.24 describes the overall mass transfer resistance of styrene which consists of two components (Equation 3.25). The first is related to the mass transfer resistance because of the film which is developed around the catalyst particle. The second component is related to the resistance because of the pore diffusion and the chemical reaction kinetics.

$$\Omega_{\text{St,tot}}^{\text{TBR}} = \frac{C_{\text{St,L}}}{\text{MTR}_{\text{H}_2}}$$

$$= \frac{1}{k_{\text{s,St}} \cdot \alpha_{\text{act.pel}}^{'\text{Pd}} \cdot f} \cdot \frac{V_{\text{L}}}{W_{\text{Pd}}} + \frac{1}{\varepsilon \cdot f \cdot k_{\text{obs,1}^{\text{st}}\text{order}}^{'\text{St}}} \frac{V_{\text{L}}}{W_{Pd}} \qquad \text{Equation 3.25}$$

Where, $\Omega_{\text{St,tot}}^{\text{TBR}}$ = Mass transfer resistance of styrene, [s]

Table 3.6: Summary of mass transfer resistances of styrene in the TBR.

Description	Expression	Definition
Resistance of liquid-solid interface	$\Omega_{\text{St,L-S}}^{\text{TBR}}$	$\dfrac{1}{k_{\text{s,St}} \cdot \alpha_{\text{act.pel}}^{'\text{Pd}} \cdot f} \cdot \dfrac{V_{\text{L}}}{W_{\text{Pd}}}$
Resistance of internal catalyst pore structure and surface chemical reaction	$\Omega_{\text{St,R}}^{\text{TBR}}$	$\dfrac{1}{\varepsilon \cdot f \cdot k_{\text{obs,1}^{\text{st}}\text{order}}^{'\text{St}}} \dfrac{V_{\text{L}}}{W_{Pd}}$

3.2. Surface model of styrene hydrogenation

To describe mathematically the mechanism of the surface reaction between the styrene and hydrogen, based on the experimental data obtained in the course of this work (Figure 3.4), the competitive adsorption of Langmuir-Hinshelwood model was adopted. Due to the use of palladium catalyst which is a transition metal, the hydrogen is considered to be dissociatively chemisorbed onto active sites of catalyst [64-68]. The mechanism is described by the elementary steps which are presented in the Table 3.7, ($\square$ represents active catalyst sites).

Table 3.7: Elementary steps of styrene hydrogenation over Pd/C.

$\mathbf{St_S} + \square$ $\xleftrightarrow{K_{St}}$ $\mathbf{St} - \square$		$K_{St} = \dfrac{\theta_{St}}{\theta_{\square} \cdot C_{St,S}}$	(s1)
$\mathbf{H_{2,S}} + \square \ \square$ $\xleftrightarrow{K_{H_2}}$ $2 \cdot \mathbf{H} - \square$		$K_{H_2} = \dfrac{\theta_H^2}{\theta_{\square}^2 \cdot C_{H_2,S}}$	(s2)
$\mathbf{St_S} - \square \ + \ \mathbf{H} - \square$ $\xrightarrow{k'_1}$ $\mathbf{I} - \square \ + \ \square$		$r' = k'_1 \cdot \theta_{St} \cdot \theta_H$	(s3)
$\mathbf{I} - \square \ + \ \mathbf{H} - \square$ $\xleftrightarrow{K_1}$ $\mathbf{Eth} - \square \ + \ \square$		$K_1 = \dfrac{\theta_{Eth} \cdot \theta_{\square}}{\theta_R \cdot \theta_H}$	(s4)
$\mathbf{Eth_S} \ + \ \square$ $\xleftrightarrow{K_{Eth}}$ $\mathbf{Eth} - \square$		$K_{Etn,s} = \dfrac{\theta_{Eth}}{\theta_{\square} \cdot C_{Eth,S}}$	(s5)
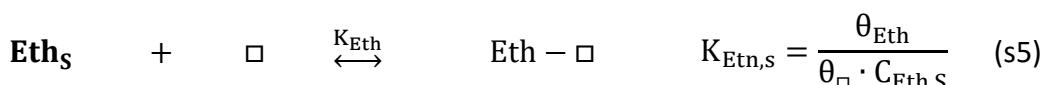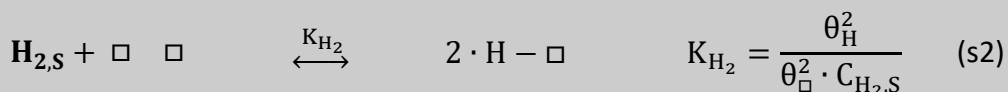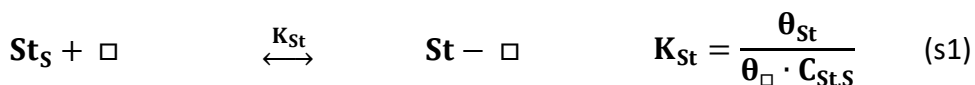
Steps s1 and s5 describe the adsorption/desorption of styrene and ethylbenzene, respectively, while step s2 represents the dissociative adsorption of hydrogen. In steps s3 and s4, it is assumed that the styrene is consecutively hydrogenated by two different hydrogen atoms, which have

been dissociated on active sites of catalyst. The first adsorbed hydrogen atom is added to the adsorbed styrene molecule in step s3 producing the semi-hydrogenated intermediate, I, which afterwards reacts with the second adsorbed hydrogen to produce an adsorbed ethylbenzene molecule (s4). In addition, it is assumed that the first hydrogen addition (step s3) is non-reversible.

Table 3.8: Summary of styrene hydrogenation model assumptions.

Both reactants chemisorbed onto catalyst active sites based on Langmuir-Hinshelwood model
Hydrogen is dissociatively chemisorbed
Styrene and hydrogen compete for the same sites
Styrene is consecutively hydrogenated by two different hydrogen atoms
The first hydrogen addition is non-reversible

Based on the assumptions which are summarised in Table 3.8, the surface reaction rate, R', is given by Equation 3.26.

$$R' = k_1' \cdot \theta_{St} \cdot \theta_H$$
<div align="right">Equation 3.26</div>

To eliminate the fractional surface coverages of styrene and hydrogen from Equation 3.26, θ_{St} and θ_H, the expressions of equilibrium constants and the mass balance of the active sites are used in the same manner as in section 2.4.3.1. The fractional surface coverage of the semi-hydrogenated intermediate, θ_I, is assumed negligible compared to the surface coverages of hydrogen, styrene and ethylbenzene. Finally, the surface reaction of styrene hydrogenation is described by Equation 3.29.

$$\theta_{St} + \theta_H + \theta_{Eth} + \theta_\square = 1 \qquad\qquad \text{Equation 3.27}$$

$$\theta_\square = \frac{1}{K_{St} \cdot C_{St,S} + \sqrt{K_{H_2} \cdot C_{H_2,S}} + K_{Eth} \cdot C_{Eth,S} + 1} \qquad\qquad \text{Equation 3.28}$$

$$R' = k_1' \cdot \frac{K_{St} \cdot C_{St,S} \cdot \sqrt{K_{H_2} \cdot C_{H_2,S}}}{\left[K_{St} \cdot C_{St,S} + \sqrt{K_{H_2} \cdot C_{H_2,S}} + K_{Eth} \cdot C_{Eth,S} + 1 \right]^2} \qquad\qquad \text{Equation 3.29}$$

$$R' = k_1' \cdot \frac{\sqrt{K_{H_2}}}{K_{St}} \cdot \frac{1}{C_{St,S}} \cdot \sqrt{C_{H_2,S}} \qquad \text{Styrene in excess} \qquad \text{Equation 3.30}$$

Figure 3.4a illustrates experimentally the competitive behaviour of hydrogen and styrene adsorption onto catalyst active sites. Initially, the styrene is in excess and the reaction rate depends inversely on its concentration (slope of green solid line in the subplot b equals -0.0071 1/min). However, after a threshold value of about 0.20 mol/L styrene, the styrene reaction order changes resulting in the reaction rate decrease with styrene concentration.
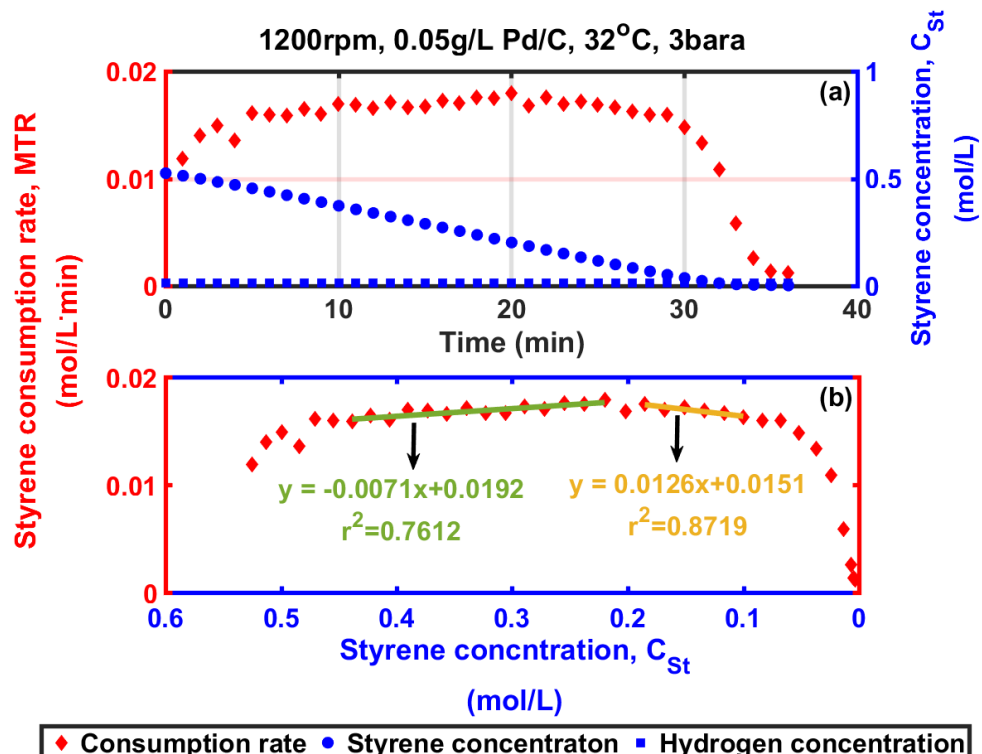
Figure 3.4: (a) Styrene and hydrogen concentration profiles; and consumption rate over time; (b) consumption rate against styrene concentration, for the styrene hydrogenation in the semi-batch STR.

3.3.   Mathematical description of reactors models

3.3.1.   Semi-batch stirred tank reactor

The semi-batch reactor operates in the dead-end mode, this means that hydrogen was supplied continuously in the reactor in an appropriate flow rate, which keeps constant the reactor pressure, while, there was not any inlet and outlet of styrene and ethylbenzene.

The material balances of the species in the three different phases have been written by assuming that any amount of styrene, which adsorbs onto catalyst particle, reacts with hydrogen producing ethylbenzene. Hydrogen is present in gas phase, in bulk liquid phase, where it is dissolved, and at the developed film between the liquid phase and the external catalyst surface. The concentration of hydrogen at the outer surface of the catalyst particle, $C_{H_2,S}$, is in equilibrium with the amount of hydrogen which is dissociatively adsorbed onto catalyst active sites.

On the other hand, styrene and ethylbenzene are present in liquid phase and at the outer surface of the catalyst particle. The concentration of styrene at the outer surface of the catalyst particle, $C_{St,S}$, is in equilibrium with the amount of styrene which is adsorbed onto catalyst active sites, while, the same stands for the concentration of ethylbenzene at the outer surface of the catalyst particle, $C_{Eth,S}$.

The material balance of one species in the reactor is given by summing the equations which describe the material balance of this species in each phase. Table 3.9 outlines the material balances of each species in each phase for the semi-batch reactor. The surface reaction rate and its mechanism has been discussed in section 3.2.

Table 3.9: Material balances for each species in each phase for the 3-phase semi-batch STR.

Hydrogen	**GAS**	$\dfrac{dC_{H_2,i}}{dt} = 0$ (constant pressure)	Equation 3.31
	LIQUID	$\dfrac{dC_{H_2,L}}{dt} = k_L \cdot \alpha \cdot (C_{H_2,i} - C_{H_2,L}) - k_{S,H_2} \cdot \alpha_S \cdot \dfrac{W_c}{V_L}(C_{H_2,L} - C_{H_2,S})$	Equation 3.32
	SOLID	$\dfrac{dC_{H_2,S}}{dt} = k_{S,H_2} \cdot \alpha_S \cdot \dfrac{W_c}{V_L}(C_{H_2,L} - C_{H_2,S}) - \dfrac{W_c}{V_L} \cdot R'$	Equation 3.33
	REACTOR	$\dfrac{dC_{H_2,R}}{dt} = k_L \cdot \alpha \cdot (C_{H_2,i} - C_{H_2,L}) - \dfrac{W_c}{V_L} \cdot R'$	Equation 3.34
Styrene	**LIQUID**	$\dfrac{dC_{St,L}}{dt} = -k_{S,St} \cdot \alpha_S \cdot \dfrac{W_c}{V_L}(C_{St,L} - C_{St,S})$	Equation 3.35
	SOLID	$\dfrac{dC_{St,S}}{dt} = k_{S,St} \cdot \alpha_S \cdot \dfrac{W_c}{V_L}(C_{St,L} - C_{St,S}) - \dfrac{W_c}{V_L} \cdot R'$	Equation 3.36
	REACTOR	$\dfrac{dC_{St,R}}{dt} = -\dfrac{W_c}{V_L} \cdot R'$	Equation 3.37
Ethylbenzene	**LIQUID**	$\dfrac{dC_{Eth,L}}{dt} = k_{S,Eth} \cdot \alpha_S \cdot \dfrac{W_c}{V_L}(C_{Eth,S} - C_{Eth,L})$	Equation 3.38
	SOLID	$\dfrac{dC_{Eth,S}}{dt} = -k_{S,Eth} \cdot \alpha_S \cdot \dfrac{W_c}{V_L}(C_{Eth,S} - C_{Eth,L}) + \dfrac{W_c}{V_L} \cdot R'$	Equation 3.39
	REACTOR	$\dfrac{dC_{Eth,R}}{dt} = \dfrac{W_c}{V_L} \cdot R'$	Equation 3.40

3.3.2. Continuous Stirred Tank Reactor, CSTR

As the semi-batch reactor, the three-phase continuous stirred tank reactor operates in dead-end mode. Styrene solution is fed into the reactor and product solution is pumped out in specific flow rates which determine the residence time in the reactor. The experimental setup does not allow the pumping of any slurry, therefore, there is not any catalyst renewal for the course of one experiment.

The material balances of the species in the three different phases have been written in the same manner as in section 3.3.1 assuming that any amount of styrene, which adsorbs onto catalyst particle, reacts with hydrogen producing ethylbenzene. We assume that the reactor outlet stream does not contain any hydrogen.

Hydrogen is present in gas phase, in bulk liquid phase, where it is dissolved, and at the developed film between the liquid phase and the external catalyst surface. The concentration of hydrogen at the outer surface of the catalyst particle, $C_{H_2,S}$, is in equilibrium with the amount of hydrogen which is dissociatively adsorbed onto catalyst active sites.

On the other hand, styrene is fed continuously into the reactor in a concentration, $C_{St,in}$, however, the feed solution does not contain any ethylbenzene. Styrene and ethylbenzene are present in liquid phase and at the outer surface of the catalyst particle. The concentration of styrene at the outer surface of the catalyst particle, $C_{St,S}$, is in equilibrium with the amount of styrene which is adsorbed onto catalyst active sites, while, the same stands for the concentration of ethylbenzene at the outer surface of the catalyst particle, $C_{Eth,S}$.

The material balance of one species in the reactor is given by summing the equations which describe the material balance of this species in each phase. Table 3.10 outlines the material balances of each species in each phase for the three-phase CSTR. The surface reaction rate and its mechanism has been discussed in section 3.2.

Table 3.10: Material balances for each species in each phase for the 3-phase CSTR.

Hydrogen	**GAS**	$\dfrac{dC_{H2,i}}{dt} = 0$	Equation 3.41
	LIQUID	$\dfrac{dC_{H2,L}}{dt} = k_L \cdot \alpha \cdot (C_{H2,i} - C_{H2,L}) - k_{S,H_2} \cdot \alpha_S \cdot \dfrac{W_C}{V_L}(C_{H2,L} - C_{H2,S})$	Equation 3.42
	SOLID	$\dfrac{dC_{H2,S}}{dt} = k_{S,H_2} \cdot \alpha_S \cdot \dfrac{W_C}{V_L}(C_{H2,L} - C_{H2,S}) - \dfrac{W_C}{V_L} \cdot R'$	Equation 3.43
	REACTOR	$\dfrac{dC_{H2,R}}{dt} = k_L \cdot \alpha \cdot (C_{H2,i} - C_{H2,L}) - \dfrac{W_C}{V_L} \cdot R'$	Equation 3.44
Styrene	**LIQUID**	$\dfrac{dC_{St,L}}{dt} = \dfrac{C_{St,in}}{\tau} - \dfrac{C_{St,R}}{\tau} - k_{S,St} \cdot \alpha_S \cdot \dfrac{W_C}{V_L}(C_{St,L} - C_{St,S})$	Equation 3.45
	SOLID	$\dfrac{dC_{St,S}}{dt} = k_{S,St} \cdot \alpha_S \cdot \dfrac{W_C}{V_L}(C_{St,L} - C_{St,S}) - \dfrac{W_C}{V_L} \cdot R'$	Equation 3.46
	REACTOR	$\dfrac{dC_{St,R}}{dt} = \dfrac{C_{St,in}}{\tau} - \dfrac{C_{St,R}}{\tau} - \dfrac{W_C}{V_L} \cdot R'$	Equation 3.47
Ethylbenzene	**LIQUID**	$\dfrac{dC_{Eth,L}}{dt} = \dfrac{C_{Eth,in}}{\tau} - \dfrac{C_{Eth,R}}{\tau} + k_{S,Eth} \cdot \alpha_S \cdot \dfrac{W_C}{V_L}(C_{Eth,S} - C_{Eth,L})$	Equation 3.48
	SOLID	$\dfrac{dC_{Eth,S}}{dt} = -k_{S,Eth} \cdot \alpha_S \cdot \dfrac{W_C}{V_L}(C_{Eth,S} - C_{Eth,L}) + \dfrac{W_C}{V_L} \cdot R'$	Equation 3.49
	REACTOR	$\dfrac{dC_{Eth,R}}{dt} = \dfrac{C_{Eth,in}}{\tau} - \dfrac{C_{Eth,R}}{\tau} + \dfrac{W_C}{V_L} \cdot R'$	Equation 3.50

3.3.3. Trickle Bed Reactor, TBR

To reduce the complexity of simulating the axial dispersion of the liquid phase in the trickle bed reactor, the one-parameter Tank-In-Series model (Figure 3.5) was chosen. Based on this model the trickle bed reactor is divided to N_T number of equally sized sections. Each section constitutes a vessel reactor which operates as an ideal Continues Stirred Tank Reactor, CSTR. The vessel reactors are identical and they operate in series. As the number of equally sized sections increases the model approaches the ideal performance of the plug flow reactor of no axial dispersion. On the other hand, if N_T is one, the model describes the perfect mixing of an ideal CSTR.
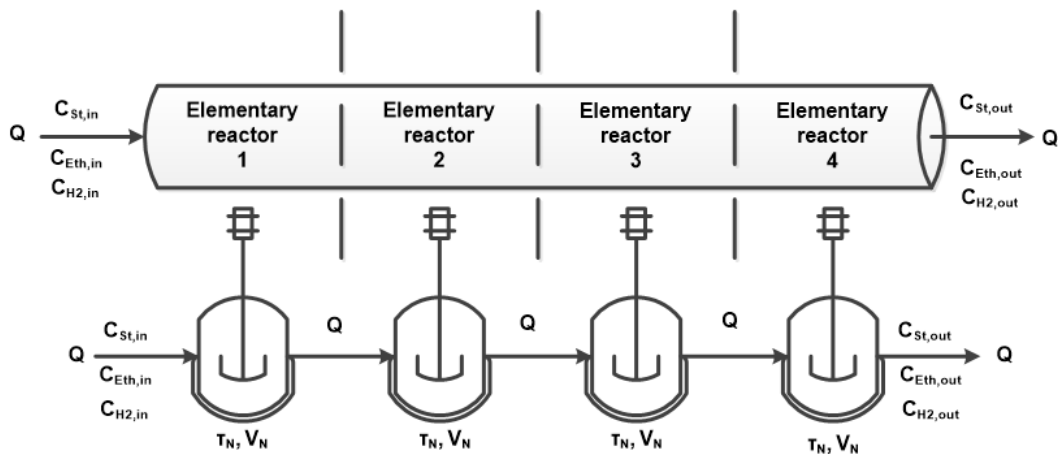
Figure 3.5: Schematic representation of rank in series model.

CSTR model

Regarding the CSRT, the material balances of the species, in the three different phases are presented in Table 3.11 assuming that any amount of styrene, which adsorbs onto catalyst particle, reacts with hydrogen producing ethylbenzene. In addition, it has been assumed that the reactor outlet stream does not contain any hydrogen.

Hydrogen is present in gas phase, in bulk liquid phase, where it is dissolved, and at the external catalyst surface. The concentration of hydrogen at the outer surface of the pellet, $C_{H_2,S}$, is in equilibrium with the amount of hydrogen which is dissociatively adsorbed onto active sites of catalyst.

On the other hand, styrene is fed continuously into the reactor, in a concentration, $C_{St,in}$, while the feed solution does not contain any ethylbenzene. Styrene and ethylbenzene are present in liquid phase and at the outer surface of the pellet. The concentration of styrene at the outer surface of the pellet, $C_{St,S}$, is in equilibrium with the amount of styrene which is adsorbed onto active sites of catalyst, while, the same stands for the concentration of ethylbenzene at the outer surface of the pellet, $C_{Eth,S}$.

The surface reaction rate and its mechanism has been discussed in section 3.2 but here the intrinsic reaction rate constant is expressed per weight of palladium and it is presented in Equation 3.51.

$$R'^{Pd} = k_1'^{Pd} \cdot \frac{K_{St} \cdot C_{St,S} \cdot \sqrt{K_{H_2} \cdot C_{H_2,S}}}{\left[K_{St} \cdot C_{St,S} + \sqrt{K_{H_2} \cdot C_{H_2,S}} + K_{Eth} \cdot C_{Eth,S} + 1\right]^2} \qquad \text{Equation 3.51}$$

Since all the CSTRs are equally sized and the volumetric flow rate is constant, the residence time in any CSTR, τ_N, is equal to the residence time of the trickle bed reactor divided by the number of the CSTRs is series, N_T.

The trickle bed reactor was operated under constant pressure and temperature; any pressure-drop and temperature gradients were assumed negligible. Therefore, all the CSTRs operate under the same pressure and temperature. At t=0, all the CSTRs have the same concentration of hydrogen, styrene and ethylbenzene. The first CSTR is fed from the feed vessel and

once it has reached steady state conditions, it feeds the second reactor. The same stands the rest of the following reactors; each reactor feeds its following reactor once it has reached steady state conditions.

It has been assumed that the mass transfer coefficients are the same among the CSTRs and they are equal to the coefficients of the trickle bed reactor. In addition, the active pellets have been added in the trickle bed reactor in such a way that the palladium concentration along the bed does not present any gradient (see section 6.2.2). Therefore, the CSTRs operate under the same palladium concentration which is equal to the palladium concentration of the trickle bed reactor reduced by a factor equal to the wetting efficiency of the trickle bed reactor.

Table 3.11: Material balances for each species in each phase for the vessel reactor.

Hydrogen	**GAS**	$$\frac{dC_{H_2,i}}{dt} = 0$$	Equation 3.52
	LIQUID	$$\frac{dC_{H_2,L}}{dt} = k_L \cdot \alpha_{bed} \cdot f \cdot (C_{H_2,i} - C_{H_2,L}) - k_{S,H_2} \cdot \alpha_{act.pel}^{'Pd} \cdot \frac{W_{Pd}}{V_L} \cdot (C_{H_2,L} - C_{H_2,S})$$	Equation 3.53
	SOLID	$$\frac{dC_{H_2,S}}{dt} = k_{S,H_2} \cdot \alpha_{act.pel}^{'Pd} \cdot f \cdot \frac{W_{Pd}}{V_L} (C_{H_2,L} - C_{H_2,S}) - \frac{W_{Pd}}{V_L} \cdot R^{'Pd}$$	Equation 3.54
	REACTOR	$$\frac{dC_{H_2,R}}{dt} = k_L \cdot \alpha_{bed} \cdot f \cdot (C_{H_2,i} - C_{H_2,L}) - \frac{W_{Pd}}{V_L} \cdot f \cdot R^{'Pd}$$	Equation 3.55
Styrene	**LIQUID**	$$\frac{dC_{St,L}}{dt} = \frac{C_{St,in}}{\tau_N} - \frac{C_{St,R}}{\tau_N} - k_{S,St} \cdot \alpha_{act.pel}^{'Pd} \cdot f \cdot \frac{W_{Pd}}{V_L} \cdot (C_{St,L} - C_{St,S})$$	Equation 3.56
	SOLID	$$\frac{dC_{St,S}}{dt} = k_{S,St} \cdot \alpha_{act.pel}^{'Pd} \cdot f \cdot \frac{W_{Pd}}{V_L} \cdot (C_{St,L} - C_{St,S}) - \frac{W_{Pd}}{V_L} \cdot f \cdot R^{'Pd}$$	Equation 3.57
	REACTOR	$$\frac{dC_{St,R}}{dt} = \frac{C_{St,in}}{\tau_N} - \frac{C_{St,R}}{\tau_N} - \frac{W_{Pd}}{V_L} \cdot f \cdot R^{'Pd}$$	Equation 3.58
Ethylbenzene	**LIQUID**	$$\frac{dC_{Eth,L}}{dt} = \frac{C_{Eth,in}}{\tau_N} - \frac{C_{Eth,R}}{\tau_N} + k_{S,Eth} \cdot \alpha_{act.pel}^{'Pd} \cdot f \cdot \frac{W_{Pd}}{V_L} \cdot (C_{Eth,S} - C_{Eth,L})$$	Equation 3.59
	SOLID	$$\frac{dC_{Eth,S}}{dt} = -k_{S,Eth} \cdot \alpha_{act.pel}^{'Pd} \cdot f \cdot \frac{W_{Pd}}{V_L} \cdot (C_{Eth,S} - C_{Eth,L}) + \frac{W_{Pd}}{V_L} \cdot f \cdot R^{'Pd}$$	Equation 3.60
	REACTOR	$$\frac{dC_{Eth,R}}{dt} = \frac{C_{Eth,in}}{\tau_N} - \frac{C_{Eth,R}}{\tau_N} + \frac{W_{Pd}}{V_L} \cdot f \cdot R^{'Pd}$$	Equation 3.61

Chapter 4

4.   Three-phase semi-batch Stirred Tank Reactor, STR

4.1.   Introduction

This chapter is dedicated to the three-phase semi-batch stirred tank reactors. It is structured in three different subsections, namely; (a) materials and methods, (b) experimental determination of mass transfer resistances and (c) modelling of the heterogeneously catalysed styrene hydrogenation.

Firstly, the methodologies, by which experimental investigations into mass transfer of three-phase stirred tank reactors were conducted, are presented. The details of the design and construction of two different semi-batch reactors are included. The experimental procedure is described also in detail for both reactors. Briefly, the main differences of the two reactor setups are a) the reactor volume which is 0.6 L and 0.3 L; and b) the type of the agitator. The reactor of 0.6 L was equipped with a two-turbine impeller, while in the reactor of 0.3 L a gas entrainment impeller was used. The first reactor was located at the University of Leeds while the second was located in Syngenta's Laboratory. The technical details of both reactors are presented in Table 4.1.

The section 4.3 is dedicated to critically presenting the experimental results for the determination of mass transfer resistances. The external mass transfer resistances might follow a level off trend leading to a plateau. In this case the differentiation between the external mass transfer regime and reaction rate regime is not feasible by observing the global mass transfer rate of hydrogen in different agitation speeds. For this reason, a new methodology is introduced

for determining the mass transfer resistances a) under the reaction conditions, b) without changing the size of the catalyst, c) under conditions which do not allow to neglect any of the rates and d) without needing to use low substrate concentration. Once the mass transfer resistances have been determined, the limiting regime is defined by highest resistance. The gas-liquid and liquid-solid mass transfer resistances were correlated to Reynolds and Sherwood number and they compared to the literature.

In section 4.4, the three-phase styrene hydrogenation in the semi-batch stirred tank reactor A was simulated by using the mathematical model introduced in section 3.3.1. The mass transfer coefficients which were used in the model had been calculated by implementing the methodology which is introduced in sections 4.2.2.2 and 4.2.2.3. The adsorption constants of styrene, hydrogen and ethylbenzene; and the intrinsic reaction rate constant were approximated by applying curve fitting of experimental styrene concentration profile and using the Global Search in-built MATLAB algorithm. After approximating the constants, the model was validated against experimental styrene concentration profiles which were not used in the curve fitting procedure.

4.2. Materials and methods

4.2.1. Design and assembly

4.2.1.1. Reactor A-0.6 L & 2-turbine impeller

The layout of the reactor setup is depicted in Figure 4.1. An autoclave Parr Instrument 0.6 L stirred tank reactor was used. The reactor vessel was made from stainless steel (316SS) and it was equipped with two 45° pitched turbine type impellers. The first was positioned near the bottom of the vessel to keep the solids suspended, while the second was positioned near the surface of the

liquid to pull reactant gas down to the liquid phase. The diameter of the vessel was 0.065 m and the diameter of the impellers was 0.035 m.

Stirrer speed

A motor connected to a belt was used to drive the autoclave agitator shaft, via a magnetic drive, which allowed continuously variable speed transmission. The rotational speed of the agitator shaft was varying between 0-1700 rpm and it was controlled using the autoclave motor-speed controller.

Temperature

Temperature control of the reactor was attained by using cooling and heating automated control loops. A Type J thermocouple was used to monitor the temperature. The cooling was provided by an automated on/off valve which was regulating the flow rate of tap water, while, the heating was provided by a heating isomantle. Both, on/off valve and heating isomantle were manipulated by a PID controller which was regulating isomantle temperature and valve's opening frequency to maintain temperature to the set-point.

Pressure

The pressure of the reactor was maintained by using an automated control loop consisted of a pressure transducer, for pressure monitoring, and a mass flow controller connected to the hydrogen inlet stream. Due to the non-use of any inert gas and taking into account the solvent vapours built-up, hydrogen partial pressure constituted the 93% of the total reactor pressure at 32°C.

The process variables were monitored, manipulated and recorded using the SpecView software which was connected to the Parr Instrument 4871 process controller.

4.2.1.2. Reactor B-0.3 L & gas entrainment impeller

The layout of the reactor setup is depicted in Figure 4.2. An autoclave Parr Instrument 0.3 L stirred reactor was used. The reactor vessel was made from stainless steel (316SS) and it was equipped with a gas entrainment impeller, which was consisted of four blades, each blade had holes at the tip. Because of the lower pressure conditions which are developed behind of the blades, the gas enters the liquid from the shaft hole which is near the top of the vessel. The diameter of the vessel is 0.065 m and the diameter of the impellers is 0.035 m.

Stirrer speed

A motor connected to a belt was used to drive the autoclave agitator shaft, via a magnetic drive, which allowed continuously variable speed transmission. The rotational speed of the agitator shaft was varying between 0-1000 rpm and it was controlled using the autoclave motor-speed controller.

Temperature

Temperature control of the reactor was attained by using a cooling and a heating automated control. A Type J thermocouple was used to monitor the temperature. The heating was provided by a heating isomantle which was manipulated by a PID controller. The cooling was provided by a Julabo refrigerated circulator which was connected to the reactor cooling coil. Depending on the process temperature, which was monitored by the Type J thermocouple, the temperature of the cooling medium was manually regulated.

Pressure

The pressure of the reactor was controlled by using a pressure regulator at the hydrogen inlet stream and it was monitored by using a pressure transducer. Due to the non-use of any inert gas, the hydrogen pressure constituted the total reactor pressure.

The process variables were monitored, manipulated and recorded using the in-front panel of the Parr Instrument 4848 reactor controller.

Table 4.1: Summary of reactors' design characteristics.

Reactor characteristics	Reactor A	Reactor B
Reactor diameter, d_r [m]	$6.5 \cdot 10^{-2}$	$6.5 \cdot 10^{-2}$
Reactor volume, V_r [m^3]	$6 \cdot 10^{-4}$	$3 \cdot 10^{-4}$
Impeller diameter, D_{im} [m]	$3.5 \cdot 10^{-2}$	$3.5 \cdot 10^{-2}$
Number of impeller blades	4	4
Impeller type	45º pitched turbine	Gas entrainment
Height of the blade, H [m]	$8 \cdot 10^{-3}$	$8 \cdot 10^{-3}$
Number of impellers	2	1
Impellers distances from the vessel bottom, [m]	$3 \cdot 10^{-3}$ and $5.4 \cdot 10^{-2}$	$3 \cdot 10^{-3}$
Ratio of liquid to gas volume	½	2
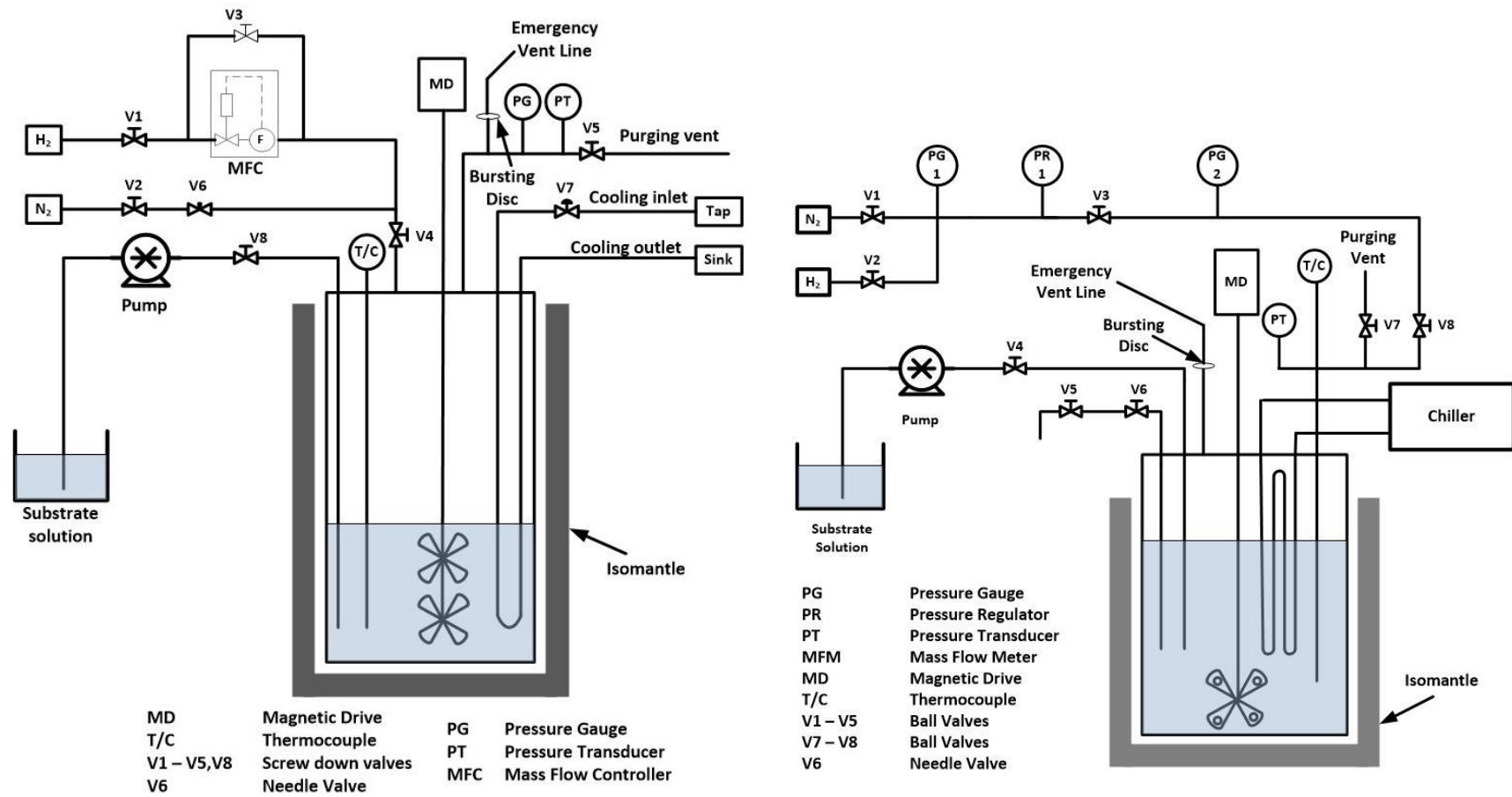
Figure 4.1: Layout of semi-batch reactor A.

Figure 4.2: Layout of semi-batch reactor B.

4.2.2. Experimental procedure

The hydrogenation of styrene was chosen as case study to investigate the mass transfer in three-phase semi-batch STRs. This is because the hydrogenation of styrene presents fast intrinsic reaction rate which allows the mass transfer rates to be the limiting regime even if intensive mixing conditions occur. Figure 4.3 presents the reaction scheme of styrene hydrogenation. All the experiments took place using methanol 99.9% (HPLC grade) as solvent, styrene 99% (without stabiliser) and decane 99% as internal standard and they were purchased from Sigma Aldrich. Compressed pure hydrogen (UN: 1049) was purchased from BOC and Pd/C (Type 87L) was purchased from Johnson Matthey. The catalyst's palladium content was approximated at 4.63% using ICP-MS. Table 4.2 summarises the physical properties of liquid and solid phase.

Table 4.2: Summary of physical properties of liquid and solid phase.

Physical property	Value
CH$_3$OH density [71], $\rho_L[kg/m^3]$ (P=0.3 MPa to 1.1 MPa)	776.9
CH$_3$OH dynamic viscosity [72], μ_L, [kg/m · s], (T=32°C)	$4.98 \cdot 10^{-4}$
Diffusion coefficient of H$_2$ – CH$_3$OH system [73] , $\mathfrak{D}$ [m^2/s]	$1.017 \cdot 10^{-8}$
Particle density, ρ_p [kg/m^3]	2100
Particle diameter, d_p [m]	$18 \cdot 10^{-6}$
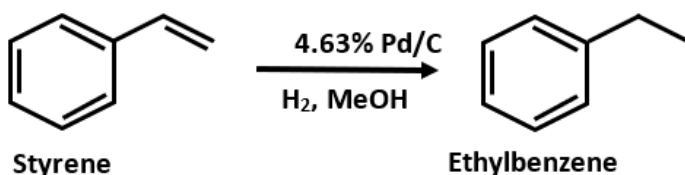
Figure 4.3: Chemical reaction scheme of styrene hydrogenation.

4.2.2.1. Start-up

The reactor vessel was filled with the catalyst and the solution. The reaction volume was 0.2 L. For safety reasons and to eliminate any likelihood of fire due to the use of pyrophoric catalyst, a transparent beaker was used to make up the slurry. First the intended for the experiment amount of catalyst was added. Then, 0.05 L of methanol was added slowly for making up a slurry. The reactor vessel was filled with the prepared slurry and an additional 0.1 L of methanol. So, the reactor vessel contained 0.15 L of methanol and the intended for the experiment amount of catalyst. The vessel was assembled to the reactor.

Once the reactor vessel had been assembled to the reactor head, it was purged with nitrogen 5 times to ensure that oxygen had been removed from the reactor vessel and the slurry. The reactor was leak tested by pressurising it and monitoring the pressure for 30 minutes; any pressure-drop indicates leakage.

Then, the reactor was purged with hydrogen 5 times to remove any nitrogen. Finally, the reactor was pressurised under 3 bara of hydrogen and the agitation was initiated. The slurry was being stirred under 3 bara of hydrogen for 30 minutes to activate the catalyst.

So far, the same procedure was applied in both reactors; reactor A and reactor B. The procedure differentiated at the heating/cooling. In reactor A, after

switching on the agitation, the setpoint of temperature was set at 32°C using the SpecView software and the controller started regulating both, the heating and the cooling, in such a way to maintain the reactor temperature at the setpoint. On the other hand, in the case of reactor B, the temperature setpoint was set at 32°C using the controller of the isomantle which started regulating only the heating. For the cooling, it was necessary to set the setpoint of the coolant of the Julabo refrigerated circulator lower than the 32°C.

After the catalyst activation, the agitation stopped. A solution of the intended amount of styrene, in 0.05 L of methanol, had been prepared. The pump was used to add the substrate solution into the reactor while the reactor was under 3 bara of hydrogen. Therefore, after that, the reactor contained 0.2 L of methanol and the intended for the experiment amounts of catalyst and substrate. The reactor pressure was checked and was increased/decreased as needed.

Once (a) the reactor had reached the 32°C, (b) the substrate solution had been added into the reactor and (c) the reactor was under the intended for the experiment pressure, the reaction was initiated by switching on the agitation.

4.2.2.2. Operation

During the reaction, the process variables were monitored. In the case of the reactor A, the SpecView software were used to monitor and record the reactor temperature, the agitation speed, the hydrogen flow rate and the reactor pressure. The agitation speed and the reactor temperature were also manipulated using the SpecView software. Regarding the hydrogen flow, it was regulated from the mass flow controller in such a way to maintain the reactor pressure at the setpoint. As it will be discussed later at the section

4.3.1, this function of the mass flow controller gives the chance to monitor the reaction rate in real time. Something that is not feasible by sampling and using off-line analytical techniques.

Regarding the reactor B, the in-front panel of the controller was used to monitor the reactor temperature, the agitation speed and the reactor pressure. The agitation speed and the reactor temperature were manipulated using the controller's in-front panel while the pressure was regulated by using the pressure regulator. According to this experimental setup, it was necessary to take samples from the reactor for analysing them to calculate the reaction rate. Sampling frequency depended on the reaction rate, one sample per minute used to be taken.

4.2.2.3. Shut-down

When ready to shut down the reactor, the agitation and the heating were switched off and the isomantle was removed while the cooling remained switched on. The gas inlet valve was closed and the purging vent valve was opened to depressurise the reactor. Then, purging with nitrogen for 5 times was applied, to remove any remaining hydrogen from the reactor and from the slurry.

After checking that the reactor was under atmospheric pressure, the reactor vessel was removed. Regarding reactor A, it was sampled in order to use gas chromatography to identify the composition of the reaction mixture at the end of the reaction. For safety reasons and to eliminate any likelihood the pyrophoric catalyst to get dried, water was added to the slurry and it was disposed. The reactor vessel and the lines of the pump were cleaned with methanol.

Start-up

Catalyst slurry make up
Use a transparent beaker to make up the catalyst slurry
Add the intended for the experiment amount of catalyst
Add slowly 0.05 L methanol
Fill the reactor vessel with the slurry
Add 0.1 L of methanol to reactor vessel
Assemble vessel to the reactor

Purging and leak test
Purge the reactor with nitrogen to ensure that oxygen has been removed
Pressurise the reactor with nitrogen & monitor the pressure for leak checking
Purge the reactor with hydrogen to ensure that any nitrogen has been removed

Catalyst activation
Pressurise reactor at 2barg with hydrogen
Set temperature setpoint at 32°C
Switch on agitation at 1200 rpm for 30 minutes

Add substrate in the reactor & Reaction initiation
Prepare the substrate solution of the intended amount of styrene in 0.05 L of methanol
After catalyst activation, switch off the agitation
Pump in the substrate solution
Switch on the agitation

Operation

Monitor process variables & sampling reactor
Monitor temperature, pressure, agitation speed and hydrogen flow
Sample reactor, if it is needed

Shut-down

Switch off agitation and the heating, remove isomantle
Depressurise the reactor
Purge with nitrogen
Once the reactor is under atmospheric pressure, remove reactor vessel
Add water to the reactor vessel and dispose of
Clean reactor vessel and tubing

Figure 4.4: Block diagram of the standard operating procedure of the semi-batch STR.

4.3. Experimental determination of the mass transfer resistances

As it has been discussed in section 2.2.3 under the title "Process scheme of heterogeneous hydrogenation-Slurry reactors" during the three-phase reactions a number of mass transfer processes need to take place before the surface catalytic reaction, these are: a) gas – liquid mass transfer, b) liquid – solid mass transfer and c) the combined internal pore diffusion and the surface chemical reaction. Each of the mass transfer processes and the intrinsic reaction rate affect the overall process rate in different extent [15, 16]. The design of three phase reactors requires the determination of the mass transfer coefficients and the reaction rate constant. The determination of mass transfer coefficients becomes even more important when the reaction rate constant and external mass transfer is of comparable magnitude. This happens in the case of fast chemical reactions. By fast chemical reactions, it is meant that even if intense mixing conditions take place, the external mass transfer processes are not faster than the surface chemical reaction and the Damk*ö*hler number (Da=mixing time/reaction time) is higher than unity, Da>1 (handbook of industrial mixing industrial mixing).

4.3.1. Experimental evaluation of the global mass transfer resistance

In this section, a typical experiment to obtain the mass transfer rate and the global mass transfer resistance of the styrene hydrogenation is presented. The hydrogenation of styrene has been chosen because it presents fast intrinsic reaction rate which allows the mass transfer rates to be the limiting regime even if intensive mixing conditions occur.

The global mass transfer resistance of hydrogen and substrate have been defined in section 3.1.1 by Equation 3.10 and Equation 3.13, respectively. To

choose which definition should be used, the limiting reactant is necessary to be defined. If hydrogen is the limiting reactant, the global mass transfer resistance is calculated by Equation 3.10, otherwise, Equation 3.13 should be used.

To determine the mass transfer resistances of hydrogen, the global mass transfer resistance must be expressed by Equation 3.10. For this reason, the global mass transfer resistance is calculated using the mass transfer rate which corresponds to the part of the reaction in which styrene is considered in excess, and the reaction is under hydrogen regime.

For reader's ease, Equation 3.10 is rewritten below,

$$\Omega_{H_2,tot}^{STR} = \frac{C_{H_2,i}}{MTR_{H_2}^{STR}}$$

Experimentally, the mass transfer rate of hydrogen is calculated based on hydrogen/styrene consumption rate. While, the concentration of hydrogen in gas-liquid interface is calculated based on Henry's law which is recalled from section 3.1.1,

Henry's law: $\qquad\qquad P_{H_2} = H_E \cdot C_{H_2,i}$

In the range of pressure and temperature which was used in the experiments, the Henry constant, H_E, was calculated by the correlation which is described by Equation 4.1 where H_E in Mpa, T in K and P_{H_2} in Pa [74].

$$Ln(H_E) = 122.3 - \frac{4815.6}{T} - 17.5 \cdot Ln(T) + 1.4 \cdot 10^{-7} \cdot P_{H_2} \qquad \text{Equation 4.1}$$

Regarding the mass transfer rate of hydrogen, there are two ways of measuring it. First, a real time measurement based on inlet mass flow of hydrogen can be applied. In this case, a mass flow controller is installed in the

inlet of hydrogen. Then, the hydrogen inlet flow is regulated from the mass flow controller in such a way to maintain the reactor pressure at the setpoint. Assuming that there is not any accumulation of hydrogen during reaction time and as long as the reactor pressure is constant, the mass flow controller measurements can be used to calculate the mass transfer rate of the hydrogen. Figure 4.5 illustrates a typical accumulative consumption and flow rate of hydrogen during the hydrogenation of styrene in reactor A.

Writing the molecular balance of the reactor with respect to hydrogen, in the case of no hydrogen accumulation, the mass transfer rate of hydrogen is defined by Equation 4.2.

$$\text{MTR}_{H_2}^{STR} = \frac{dn_{H_2,in}}{dt} \cdot \frac{1}{V_L} = \frac{P}{R \cdot T} \cdot \frac{dV_{H_2}}{dt} \cdot \frac{1}{V_L} = \frac{P}{R \cdot T} \cdot \frac{F_{H_2}}{V_L} \qquad \text{Equation 4.2}$$
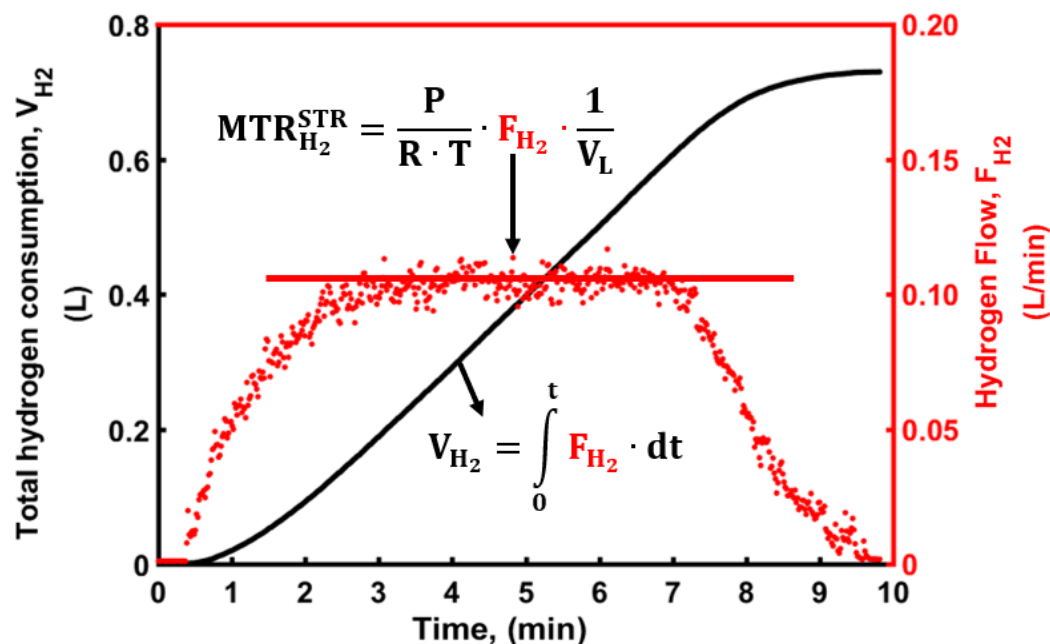
Figure 4.5: Typical hydrogen accumulative consumption and hydrogen flow rate curves.

The second way of measuring the mass transfer rate of hydrogen is by sampling the reactor and analysing the samples using gas chromatography in order to construct the styrene concentration profile. From reaction

stoichiometry and the styrene concentration profile the mass transfer rate of hydrogen is calculated.

To validate that both ways give the same results, the mass transfer rate and the styrene concentration for one experiment were calculated using both ways. Figure 4.6 is a parity plot between the styrene molar amount calculated based on gas chromatography and on mass flow controller data. There is a negative bias of maximum 1.5 mmole against the molecular amount calculated from gas chromatography. This might be due to any experimental error of the sampling and/or preparation of the reaction mixture.
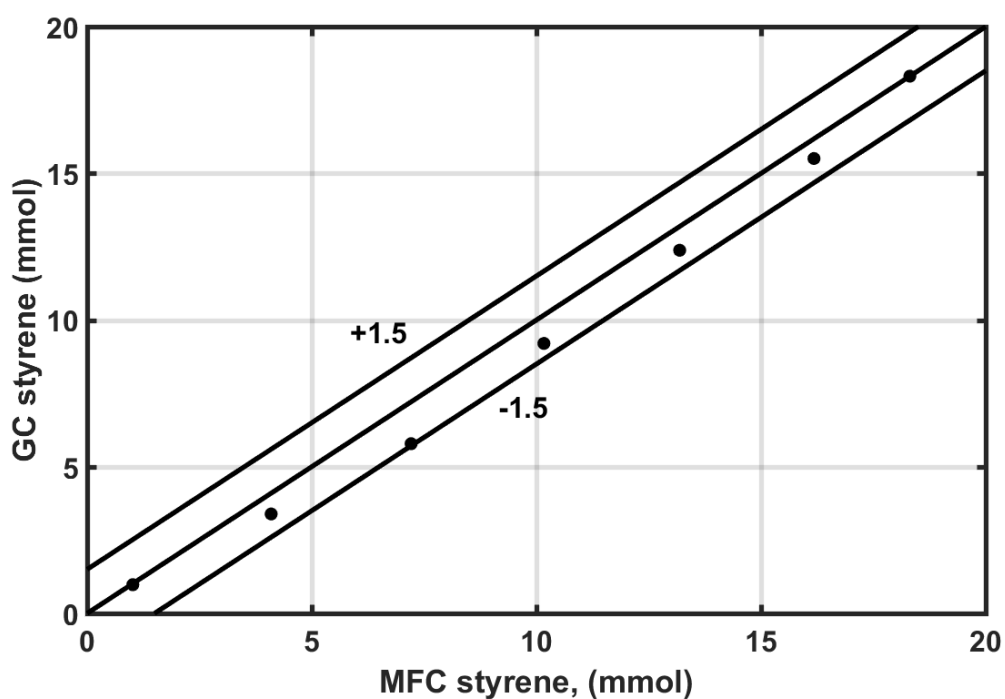
Figure 4.6: Parity plot of styrene calculated from GC against styrene calculated from MFC data.

In addition, Figure 4.7 presents the styrene concentration profile which has been calculated from samples' gas-chromatography analysis and the accumulative consumption of hydrogen from mass flow controller for the same experiment. The slopes of the two experimental data sets give the mass

transfer rate of the process, calculated by following the two different methods which have been described above. The difference of the mass transfer rate values between the GC and MFC methods is less than 1% and it is considered negligible.
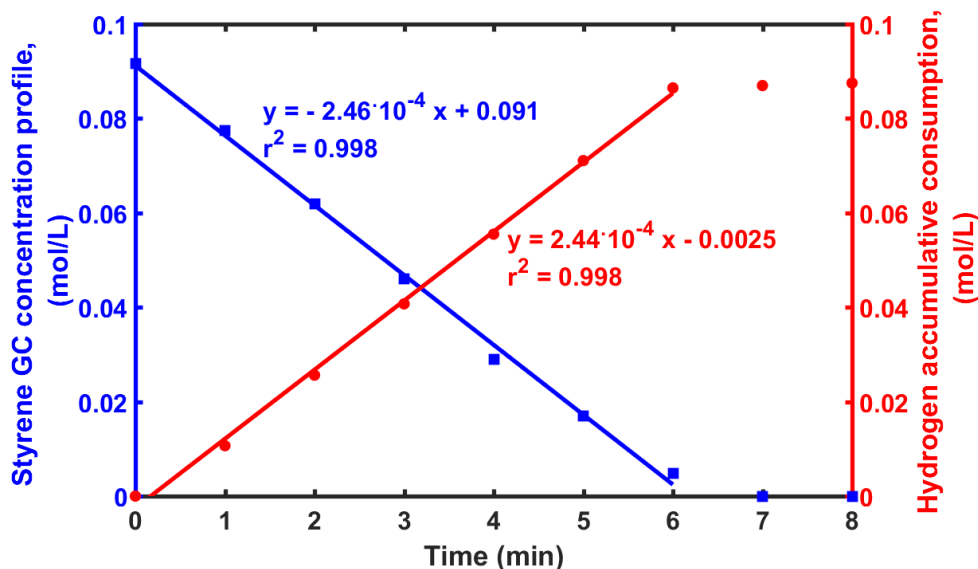
Figure 4.7: Styrene concentration profile calculated from samples GC analysis (blue) and hydrogen accumulative consumption calculated from MFC data (red); Mass transfer rates are presented as the slope of the blue and red solid lines.

Once the mass flow controller method, for calculating the mass transfer rate, has been validated, it is preferable because it provides a quick and real time mass transfer rate measurement. The mass transfer rate of hydrogen, for the experiments at the reactor A, was calculated based on the mass flow controller while the product mixture after reaction completion was always analysed in gas chromatography resulting practically always in 100% conversion to ethylbenzene.

On the other hand, in the case of reactor B, the mass flow controller method for calculating the mass transfer rate is not feasible due to the use of a different

way to maintain the pressure at the setpoint. Therefore, the gas chromatography method was used for calculating the mass transfer rate.

Figure 4.8 illustrates the molar concentration of styrene and ethylbenzene at the left-hand side axis and the accumulative consumption of hydrogen at the right-hand side axis during a typical reaction. The molecular amounts of styrene and ethylbenzene are calculated based on gas chromatography method. This plot leads to the conclusion of molar conservation as one mole of styrene reacts with one mole of hydrogen producing one mole of ethylbenzene.
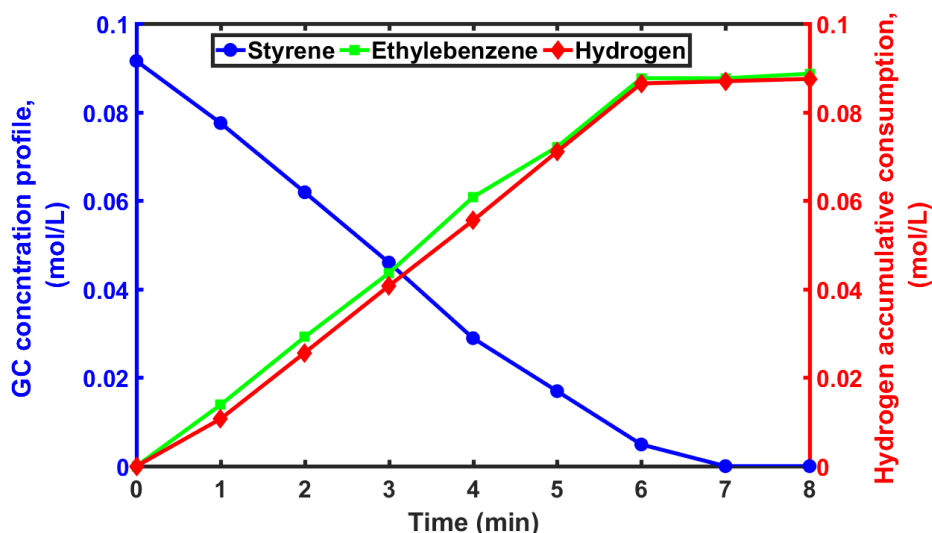
Figure 4.8: Styrene and ethylbenzene molar concentration and hydrogen accumulative molar consumption during a typical experiment.

4.3.2. Determination of gas-liquid mass transfer resistance

The expression of global mass transfer resistance of hydrogen which has been given in section 3.1.1 is rewritten below.

$$\Omega_{H_2,tot}^{STR} = \frac{C_{H_2,i}}{MTR_{H_2}^{STR}} = \frac{1}{k_L \cdot \alpha} + \left[\frac{1}{k_{s,H_2} \cdot \alpha_s} + \frac{1}{\varepsilon \cdot k'_{obs,1^{st}order}} \right] \cdot \frac{V_L}{W_C}$$

If one observes the $MTR_{H_2}^{STR}$, while styrene is in excess, at different catalyst loading, W_c, keeping same the rest of the variables (N, $C_{H_2,i}$ and T) and plots

$\Omega^{SR}_{H_2,tot}$ vs V_L/W_c, then the intercept of the graph will be equal to the $1/(k_L \cdot \alpha)$. Repeating the same procedure at different agitation speeds, the $1/(k_L \cdot \alpha)$ was calculated for several agitation speeds (Figure 4.9). Each subgraph corresponds to a set of different experiments under the same stirrer speed. In each subgraph, the reaction temperature and the concentration of hydrogen in gas-liquid interface were kept constant.

The catalyst concentration was varying from 0.05 g cat/L solvent to 1.5 g cat/L solvent while each experiment was repeated three times. The correlation coefficient, r, was calculated in order to measure the linear association between the experimental data of $\Omega^{STR}_{H_2,tot}$ and V_L/W_c at each agitation speed. The model residuals analysis showed lack of any particular pattern. The confidence intervals for the models' parameters were also calculated and they are presented in Table 4.4.

Table 4.3: Experimental conditions for determining the gas-liquid mass transfer resistances.

Variable	Value	
	Reactor A	Reactor B
Temperature, ºC	32	32
Agitation speed, rpm	200 – 1200	1000
Pressure, bara	3	3
Catalyst concentration, g/L	0.05 – 1.5	0.075 – 0.275
Ratio of liquid to gas volume	1/2	2

Figure 4.16 summarises the results for each resistance from 200 – 1200 rpm in a bar chart form. The most significant effect of agitation speed on $\Omega_{H_2,i-L}^{STR}$ is observed between 200 and 500 rpm. From 500 rpm up to 900 rpm the agitation speed affects $\Omega_{H_2,i-L}^{STR}$ less. Taking into account the 95% confidence intervals of the calculated parameters, a plateau is developed at agitation speed higher than 800 rpm. The plateau could be reached because of the impeller's overloading which affects its ability to disperse all the gas supplied.

Table 4.4: Linear regression results of global mass transfer resistance of hydrogen against the reciprocal of catalyst concentration (reactor A).

Intercept $= \Omega_{H_2,i-L}^{STR}$ Slope $= \left(\Omega_{H_2,L-S}^{STR} + \Omega_{H_2,R}^{STR} \right) \cdot W_C/V_L$			95% Confidence interval	
N (rpm)	Intercept (min)	Slope (min·g/L)	Intercept (min)	Slope (min·g/L)
200	1.3581	0.0776	± 0.0277	±0.0098
300	0.9072	0.0717	± 0.0887	±0.0181
400	0.5581	0.0334	± 0.0081	±0.0033
500	0.2986	0.0265	± 0.0110	±0.0035
600	0.2635	0.0246	± 0.0173	±0.0075
700	0.2348	0.0356	± 0.0166	±0.0059
800	0.1566	0.0409	± 0.0207	±0.0031
900	0.1133	0.0436	± 0.0142	±0.0022
1000	0.1523	0.0255	± 0.0138	±0.0024
1200	0.1909	0.0218	± 0.0472	±0.0076
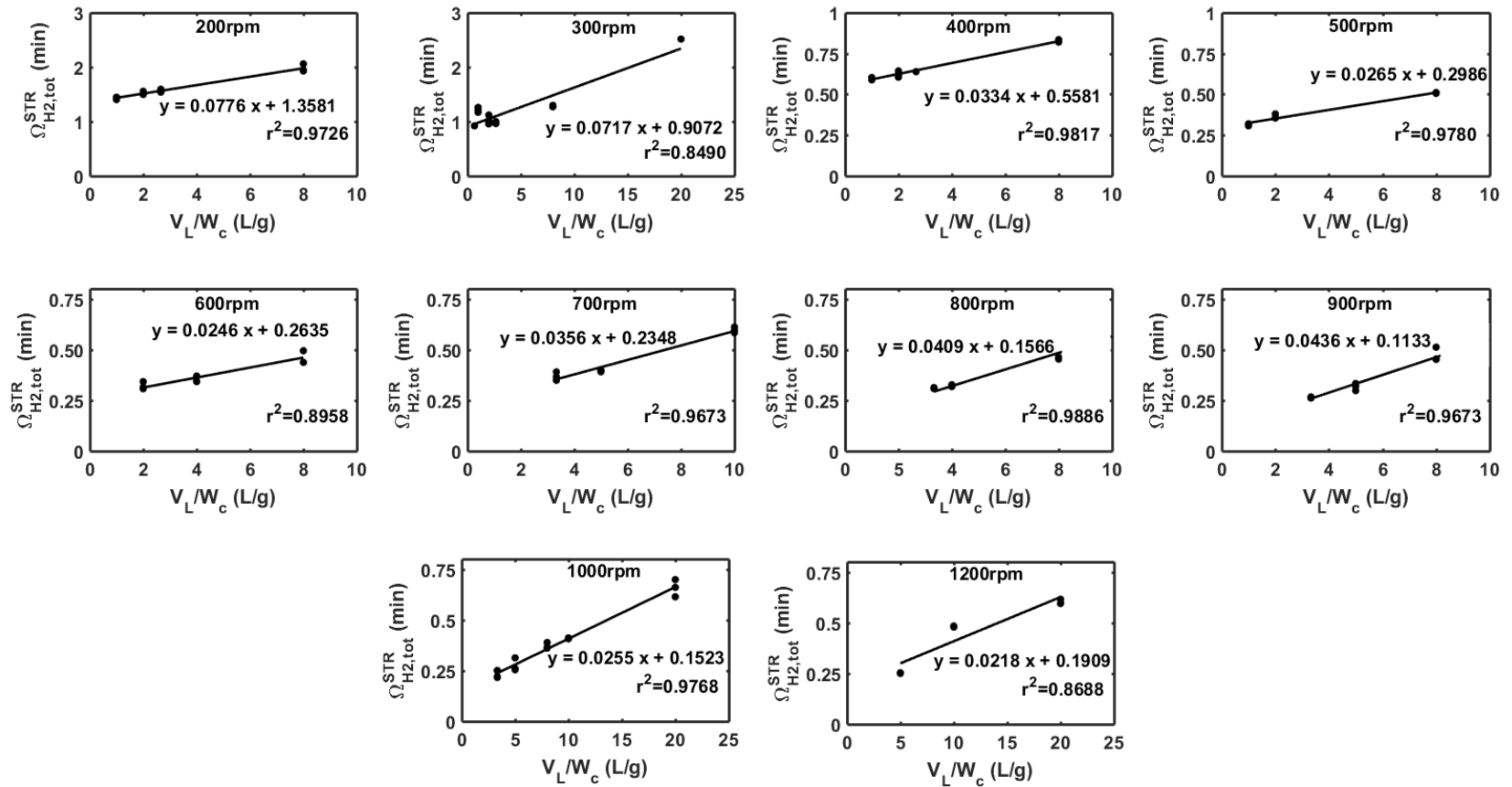
Figure 4.9: Global mass transfer resistance of hydrogen against catalyst concentration reciprocal at several agitation speeds (reactor A).

In the case of reactor B, the same procedure was followed in one single agitation speed to determine the gas-liquid mass transfer resistance in a smaller vessel equipped with a gas entrainment impeller.

The catalyst concentration was varying from 0.1 g cat/L solvent to 0.3 g cat/L solvent while each experiment was repeated twice. But, when the global mass transfer rate was plotted against the catalyst loading in the reactor vessel, the linear regression model did not pass through zero. Instead, extrapolating backwards the linear regression model, it intersects the x axis in a positive value (Figure 4.10, a).
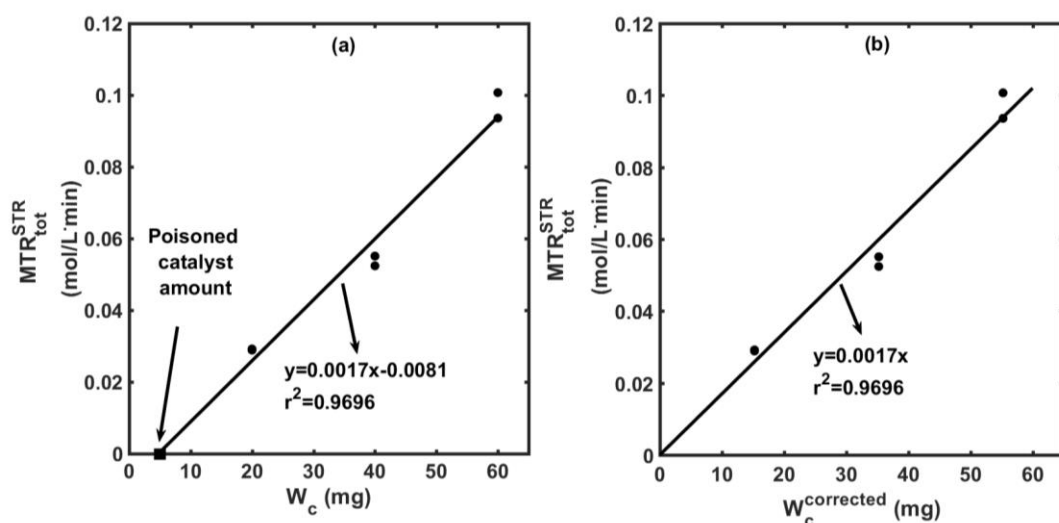
Figure 4.10: Global mass transfer rate of hydrogen against catalyst loading before and after correction for poisoning, a and b, respectively.

This is an indication that the catalyst amount which was actually used for reaction was lower than the one it had been presumed that had been added into reaction mixture. After ensuring that the balance for catalyst weighing was calibrated, this issue was considered as a poisoning of the catalyst due to any contamination of the reactor vessel and/or piping of the experimental apparatus.

The poisoned amount of catalyst was given by the intersection point between x axis and linear regression model in the plot of mass transfer rate versus catalyst loading and it was equal to 4.75 mg.

Therefore, to calculate the gas-liquid mass transfer resistance the global mass transfer resistance of hydrogen was plotted against the reciprocal of corrected concentration of catalyst (Figure 4.11). The corrected catalyst concentration was varying from 0.075 g cat/L solvent to 0.275 g cat/L solvent while each experiment was repeated twice. To check if the linear regression models fits the data, the coefficient of determination, r^2, was calculated. The model residuals analysis showed lack of any particular pattern. The confidence intervals for the model parameters were also calculated and they are presented in Table 4.5. The experimental process conditions are detailed in Table 4.3.
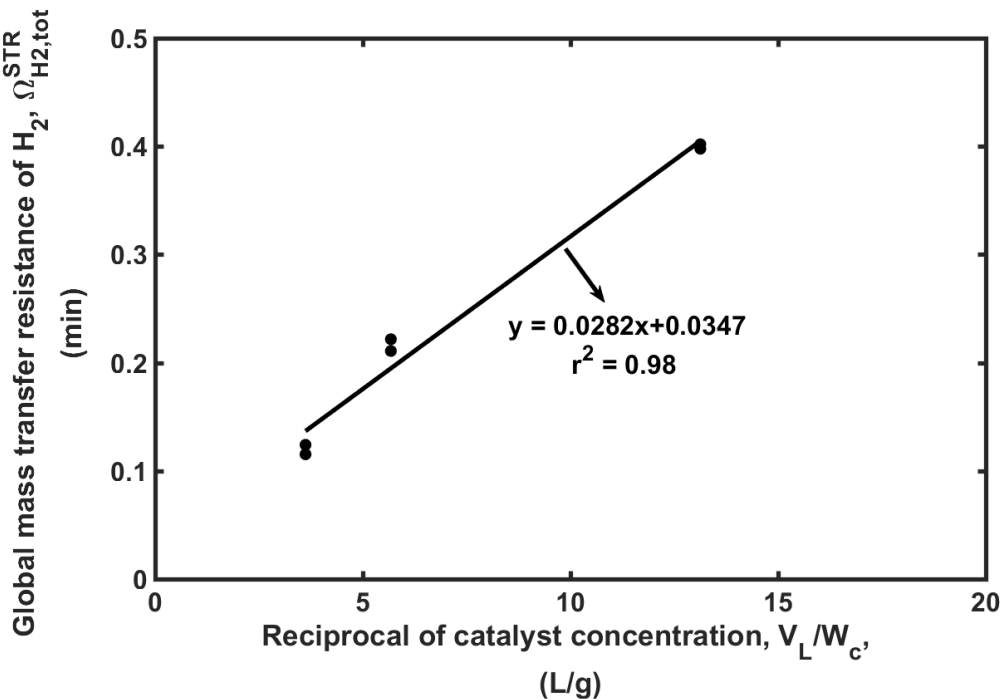
Figure 4.11: Global mass transfer resistance of hydrogen against catalyst concentration reciprocal (reactor B).

Table 4.5: Linear regression results of global mass transfer resistance of hydrogen against the reciprocal of catalyst concentration (reactor B).

Intercept $= \Omega^{STR}_{H_2,i-L}$			95% Confidence interval	
Slope $= \left(\Omega^{STR}_{H_2,L-S} + \Omega^{STR}_{H_2,R}\right) \cdot W_C/V_L$				
N	Intercept	Slope	Intercept	Slope
(rpm)	(min)	(min·g/L)	(min)	(min·g/L)
1000	0.0347	0.0282	± 0.0231	±0.0057

4.3.3. Determination of chemical reaction resistance

The expression of the global mass transfer resistance in section 2.4.4.1 has been extracted by assuming a first-order with respect to hydrogen and zero-order with respect to substrate surface chemical reaction. This has been done

in order to combine the chemical step with the mass transfer steps, a manipulation inspired by Levenspiel [59]. However, it is necessary, now, to use the model which is described by Equation 3.29 in section 3.2.

Equation 3.29: $\quad R' = k_1' \cdot \dfrac{K_{St} \cdot C_{St,S} \cdot \sqrt{K_{H_2} \cdot C_{H_2,S}}}{\left[K_{St} \cdot C_{St,S} + \sqrt{K_{H_2} \cdot C_{H_2,S}} + K_{Eth} \cdot C_{Eth,S} + 1\right]^2}$

The calculation of the global mass transfer resistance is based on the mass transfer rate of hydrogen where the styrene is in excess. Therefore, the surface chemical reaction rate is expressed by Equation 3.30.

Equation 3.30: $\quad R' = k_1' \cdot \dfrac{\sqrt{K_{H_2}}}{K_{St}} \cdot \dfrac{1}{C_{St,S}} \cdot \sqrt{C_{H_2,S}} = k_{obs}' \cdot \sqrt{C_{H_2,S}}$

To encounter the hydrogen first-order and styrene zero-order assumption of the surface chemical reaction, the observed chemical reaction constant for the assumed 1st-order reaction with respect to hydrogen was expressed by Equation 4.3.

- $MTR_{H_2,R}^{STR} \cdot V_L = \varepsilon \cdot W_C \cdot k_{obs,1^{st}order}' \cdot C_{H_2,S}$

- $R' \cdot W_C = \varepsilon \cdot W_C \cdot k_{obs}' \cdot \sqrt{C_{H_2,S}}$

- $MTR_{H_2,R}^{STR} \cdot V_L = R' \cdot W_C$

$k_{obs,1^{st}order}' = k_{obs}' \cdot \dfrac{1}{\sqrt{C_{H_2,S}}}$ $\qquad$ Equation 4.3

The concentration of hydrogen at catalyst surface cannot be measured by the experimental setup which was used. Therefore, it is needed to express this concentration in terms of a measurable concentration and this is none other than the gas-liquid interfacial hydrogen concentration given by Henry's law.

The two concentrations are given by Equation 4.4 and Equation 4.5, respectively.

$$C_{H_2,i} = MTR_{H_2}^{STR} \cdot \left[\frac{1}{k_L \alpha} + \frac{1}{k_{s,H_2} \cdot \alpha_s \cdot \frac{W_C}{V_L}} + \frac{1}{\varepsilon \cdot k'_{obs,1^{st}order} \cdot \frac{W_C}{V_L}} \right]$$

Equation 4.4

$$C_{H_2,S} = MTR_{H_2}^{STR} \cdot \frac{1}{\varepsilon \cdot k'_{obs,1^{st}order} \cdot \frac{W_C}{V_L}}$$

Equation 4.5

So, the concentration of hydrogen at catalyst surface is expressed as function of gas-liquid interfacial hydrogen concentration as Equation 4.6 describes.

$$C_{H_2,S} = \beta \cdot C_{H_2,i}$$

Equation 4.6

$$\beta = \Omega_{H_2,R}^{STR} / \Omega_{H_2,tot}^{STR}$$

Equation 4.7

$$\sqrt{\beta} = \frac{\frac{1}{\varepsilon \cdot k'_{obs} \cdot \frac{W_C}{V_L}} \cdot \sqrt{C_{H_2,i}}}{\Omega_{H_2,tot}^{STR}}$$

Equation 4.8

Substituting the expressions of $k'_{obs,1^{st}order}$ and $C_{H_2,S}$ to, Equation 3.10, the global mass transfer resistance of hydrogen is given by Equation 4.9 .

$$\Omega_{H_2,tot}^{STR} = \frac{C_{H_2,i}}{MTR_{H_2}^{STR}}$$

$$= \frac{1}{k_L \alpha} + \frac{1}{k_{s,H_2} \cdot \alpha_s \cdot \frac{W_C}{V_L}} + \frac{1}{\varepsilon \cdot k'_{obs} \cdot \frac{1}{\sqrt{\beta}} \cdot \frac{W_C}{V_L}} \cdot \sqrt{C_{H_2,i}}$$

Equation 4.9

Changing the hydrogen pressure in the reactor, one is able to manipulate the concentration of hydrogen in gas-liquid interface, $C_{H_2,i}$. We conducted experiments at several hydrogen pressures observing the initial $MTR_{H_2}^{STR}$. Each

experiment took place under same a) stirrer speed, b) temperature and c) catalyst concentration. It should be noticed that the experiments took place under conditions which ensured that $\Omega_{H_2,R}^{STR} > \Omega_{H_2,i-L}^{STR}$ and $\Omega_{H_2,R}^{STR} > \Omega_{H_2,L-S}^{STR}$.

Table 4.6: Experimental conditions for determining the chemical reaction resistance.

Variable	Value	
	Reactor A	Reactor B
Temperature, ºC	32	32
Agitation speed, rpm	900 & 1200	1000
Pressure, bara	3 - 11	3 - 15
Catalyst concentration, g/L	0.05 & 0.125	0.086
Ratio of liquid to gas volume	1/2	2

This is because the chemical reaction needs to be the limiting regime. Otherwise gas to liquid or liquid to solid mass transfer is the limiting regime of the process, resulting in the $\Omega_{H_2,tot}^{STR}$ independence of $\sqrt{C_{H_2,i}}$. This independence does not allow the calculation of the factor of $\sqrt{C_{H_2,i}}$ in Equation 4.9. This is depicted in Figure 4.12a, where the global mass transfer resistance of hydrogen has been plotted against the square root of gas-liquid interfacial concentration of hydrogen while the process is not under chemical reaction regime.
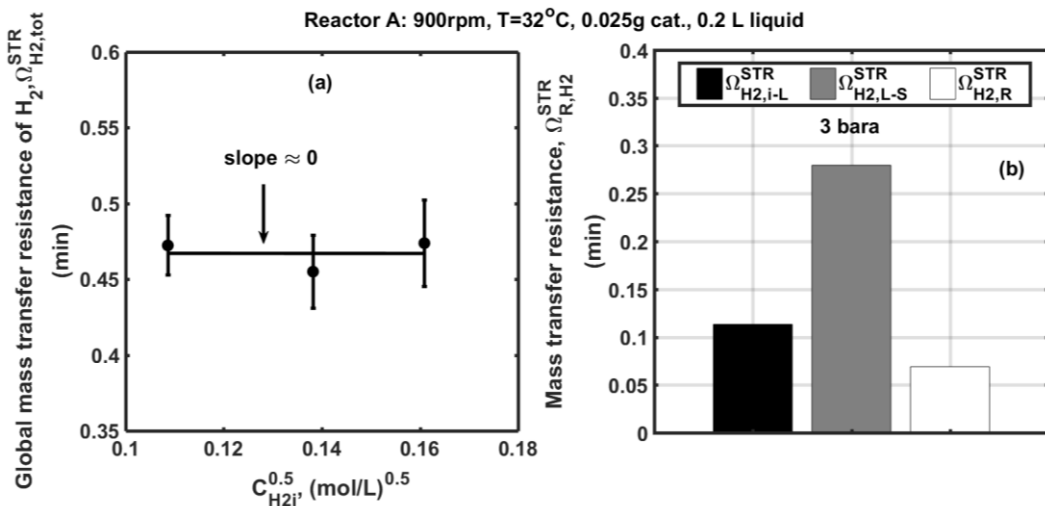
Figure 4.12: (a) Global mass transfer resistance of hydrogen against square root of gas-liquid interfacial hydrogen concentration under external mass transfer resistance regime, (b) the separated resistances, liquid-solid the highest resistance.

In Figure 4.13a and Figure 4.14a (reactor A and reactor B, respectively), the global mass transfer resistance of hydrogen has been plotted against the square root of gas-liquid interfacial concentration of hydrogen, while the process is under chemical reaction regime.

In the case of reactor A, once the $\Omega_{H_2,R}^{STR}/\sqrt{C_{H_2,i}}$ term had been approximated by the linear regression, the $\Omega_{H_2,R}^{STR}$ at 3 bara, 1200 rpm and 0.05 g catalyst/ L solvent was calculated. Given the calculated $\Omega_{H_2,R}^{STR}$ and the value of $\Omega_{H_2,tot}^{STR}$ under the same conditions (3 bara, 1200rpm and 0.05 g catalyst/ L solvent), the factor β was calculated.
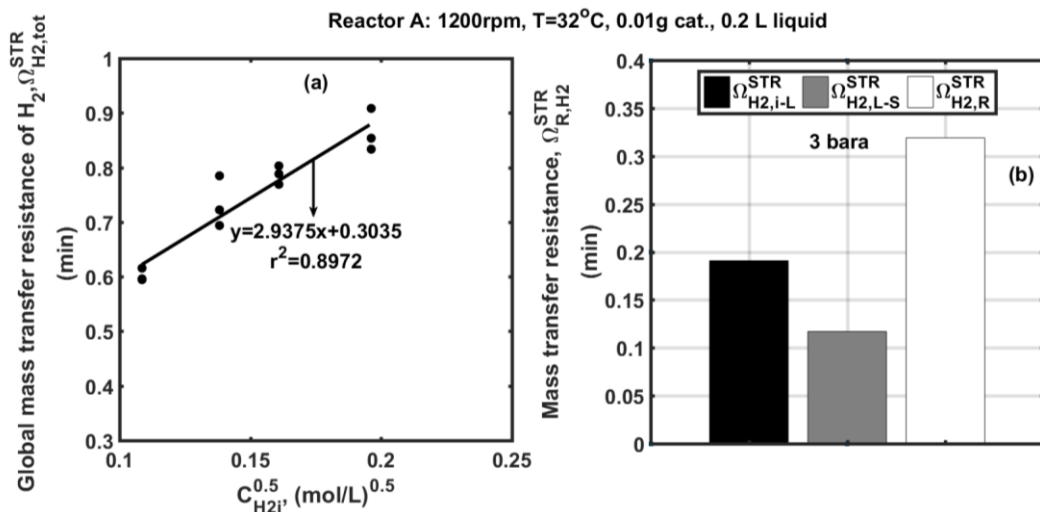
Figure 4.13: (a) Global mass transfer resistance of hydrogen against square root of gas-liquid interfacial hydrogen concentration under chemical reaction regime, (b) the separated resistances, chemical reaction the highest resistance (reactor A).
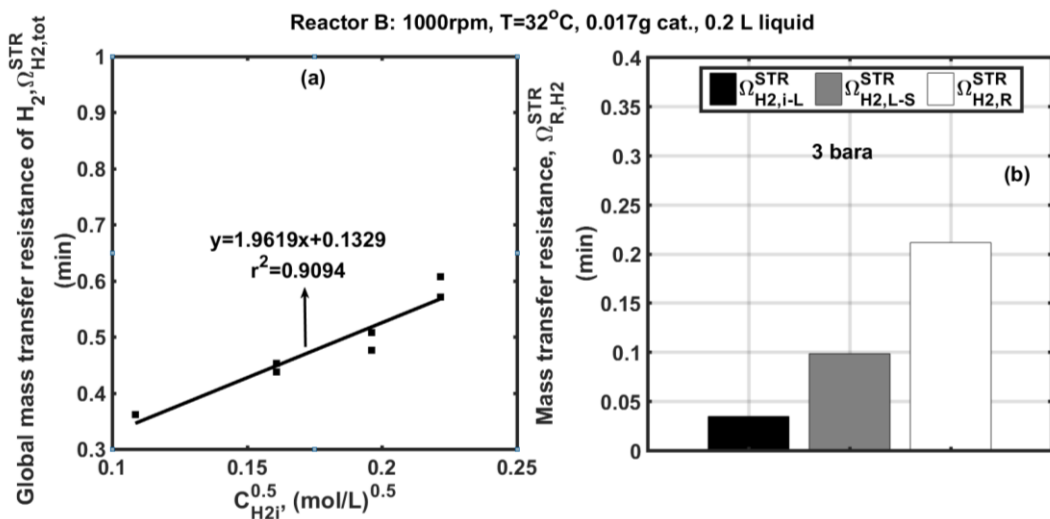
Figure 4.14: Global mass transfer resistance of hydrogen against square root of gas-liquid interfacial hydrogen concentration under chemical reaction regime, (b) the separated resistances, chemical reaction the highest resistance (reactor B).

Table 4.7: Linear regression results of global mass transfer resistance of hydrogenagainst the reciprocal of catalyst concentration.

Intercept $= \Omega^{STR}_{H_2,i-S} + \Omega^{STR}_{H_2,L-S}$ Slope $= \Omega^{STR}_{H_2,R}/\sqrt{C_{H_2,i}}$		Reactor A	Reactor B
Intercept (min)		0.3035	0.1329
Slope (min $\sqrt{L}/\sqrt{mol}$)		2.9375	1.9619
95% Confidence interval	Intercept (min)	±0.0224	±0.0267
	Slope (min $\sqrt{L}/\sqrt{mol}$)	±0.7005	±0.7119

From the values of the factor β and the $\Omega^{STR}_{H_2,R}$ at 3 bara, 1200rpm and 0.05 g catalyst/ L solvent, the term $\sqrt{C_{H_2,i}}/\varepsilon \cdot k'_{obs}$ was calculated. The term $\sqrt{C_{H_2,i}}/\varepsilon \cdot k'_{obs}$ is independent of agitation speed in contrast to the factor β. Using Equation 4.7 and the value of the term $\sqrt{C_{H_2,i}}/\varepsilon \cdot k'_{obs}$, the square root of factor β was calculated at agitation speeds from 200-1200 rpm (Reactor A) and in given catalyst concentration. Once the factor β was available, the $\Omega^{STR}_{H_2,R}$ was calculated at any agitation speed. The resistance of liquid-solid interface, $\Omega^{STR}_{H_2,L-S}$, was calculated by subtracting $\Omega^{STR}_{H_2,i-L}$ and $\Omega^{STR}_{H_2,R}$ from $\Omega^{STR}_{H_2,tot}$. Figure 4.15 illustrates the steps of the procedure of calculations.

In the case of reactor B, the same procedure was followed and once the $\Omega^{STR}_{H_2,R}/\sqrt{C_{H_2,i}}$ term had been approximated by the linear regression, the $\Omega^{STR}_{H_2,R}$ at 3 bara, 1000rpm and 0.086 g catalyst/ L solvent was calculated. Given the calculated $\Omega^{STR}_{H_2,R}$ and the value of $\Omega^{STR}_{H_2,tot}$under the same conditions (3 bara, 1000rpm and 0.086 g catalyst/ L solvent), the factor β was calculated.
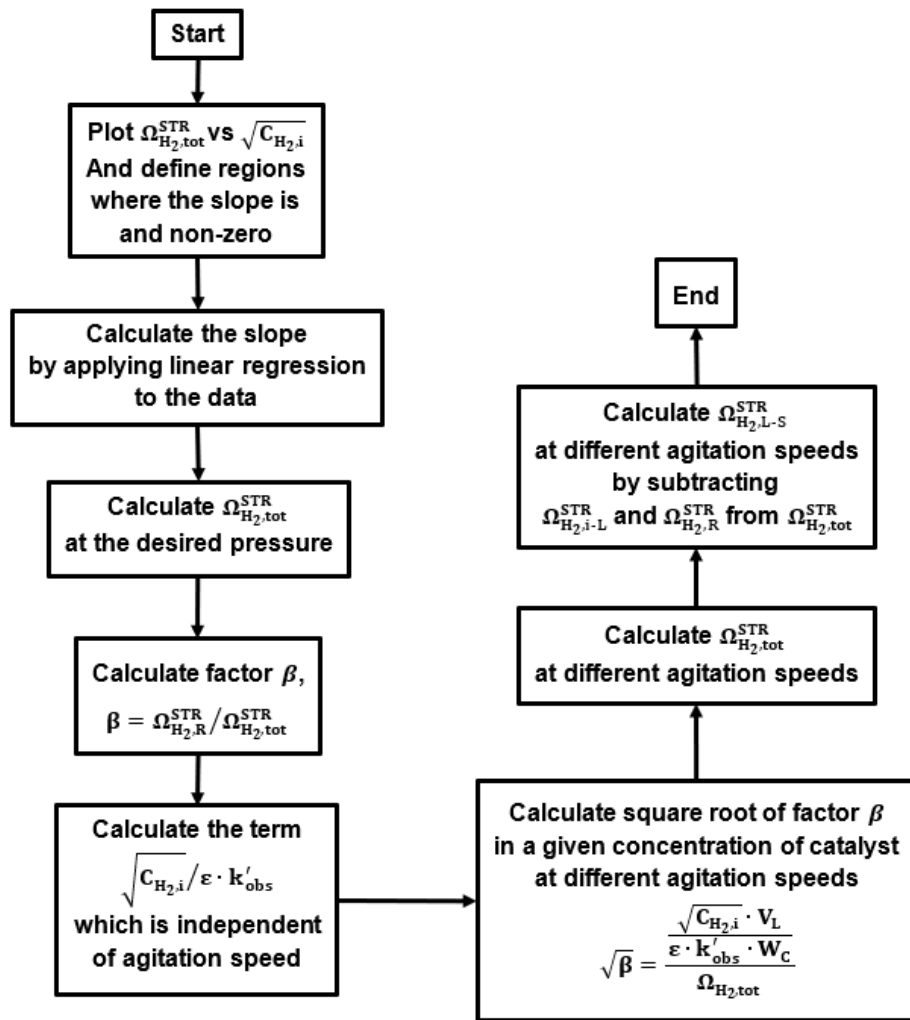
Figure 4.15: Steps for $\Omega_{H_2,R}^{STR}$ and $\Omega_{H_2,L-S}^{STR}$ calculation.

Summary of the separated mass transfer resistances

Figure 4.16 summarises the separated mass transfer resistances with respect to agitation speed in the case of reactor A. $\Omega_{H_2,L-S}^{STR}$ presents the most significant decrease between 300 and 400 rpm indicating that the suspension speed lies on that range. A bump of $\Omega_{H_2,L-S}^{STR}$ takes place between 700 and 900 rpm. This may happen because at 700 rpm the stirrer starts pumping large gas volumes which make the density of the gas-liquid mixture to decrease and to cause the formation of gas cavities behind the stirrer blades. This decrease of density and the formation of gas cavities lead to a decrease of the power

input with respect to the power input into a pure liquid at the same agitation speed [75-78]. In other words, the gassed system needs higher agitation speed in order to have the same power input as the ungassed. Apart from the bump, the $\Omega_{H_2,L-S}^{STR}$ shows the same trend as $\Omega_{H_2,i-L}^{STR}$, reaching a plateau.
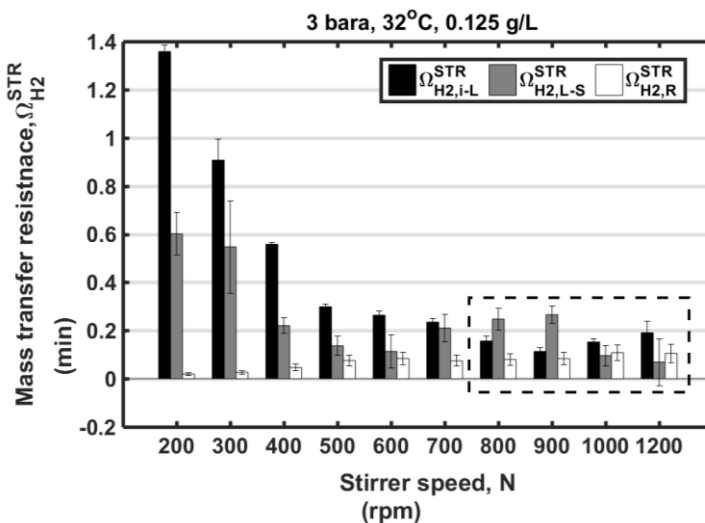
Figure 4.16: Mass transfer resistances against agitation speed; dashed rectangular indicates the developed plateau (reactor A).

Consequently, the mass transfer resistances are independent of agitation speed after a critical value of agitation speed. Therefore, the limiting regime of fast three-phase reactions cannot be ensured just by observing the plateau of mass transfer rate against agitation speed plots. This is because the plateau can be due to either the external mass transfer resistances or chemical reaction rate. On the other hand, the chemical reaction rate regime is ensured if we calculate each resistance and we ascertain that the highest resistance is $\Omega_{H_2,R}^{STR}$.

Observed chemical reaction rate constant approximation

Once the slopes and the factors β had been determined, one is able to calculate the observed chemical reaction constant assuming a unity effectiveness factor due to the use of fine particle catalyst. The procedure of

determining the absence of internal pore diffusion limitations and supporting the assumption of unity effectiveness factor is presented in Appendix D, where the Thiele modulus is estimated. The observed chemical reaction constant is given by Equation 4.10.

$$k'_{obs} = \frac{1}{slope_{\left(\Omega^{STR}_{H_2,tot} \; vs \sqrt{C_{H_2,i}}\right)}} \cdot \sqrt{\beta} \cdot \frac{V_L}{W_c} \qquad \text{Equation 4.10}$$

Where $\quad k'_{obs} = k'_1 \cdot \frac{\sqrt{K_{H_2}}}{K_{St}} \cdot \frac{1}{C_{St,S}}$

Table 4.8 summarises the results for the observed chemical reaction constant calculation from the two different reactors applying the same methodology. From both reactors, the same value for the observed chemical reaction constant were calculated. The observed chemical reaction constant is a function of (a) adsorption constants of hydrogen and styrene on catalyst active sites, (b) the intrinsic reaction rate constant and (c) the concentration of styrene.

Table 4.8: Observed chemical reaction rate constant calculated based on the experimental results of both reactors.

	Reactor A	Reactor B
$k'_{obs} \left(\sqrt{mol \cdot L \; liquid}/g \; cat \cdot min\right)$	4.86	4.68
95% Confidence interval of k'_{obs}	±1.32	±1.98

Therefore, using the same catalyst and under excessive styrene concentration the observed chemical reaction constant should depend only on temperature and it should be independent of the reactor and the mixing conditions. This happened in the case of the two different experimental setups

(reactor A and reactor B) showing that (a) the suggested methodology for determining the mass transfer resistances in three-phase semi-batch stirred tank reactors is reactor case independent and (b) the term of $k_1' \cdot \sqrt{K_{H_2}}/K_{St}$ is independent of reactor setup as long as the chemical reaction takes place over the same active phase of catalyst, under the same temperature and using the same solvent.

4.3.4. Correlations of external mass transfer coefficients

4.3.4.1. Gas-liquid mass transfer coefficient

Several correlations have been developed for the calculation of the gas-liquid mass transfer coefficient. In this work, the classical correlation (Equation 4.11) based on the theory of isotropic turbulence using the power consumption per liquid volume and the superficial gas velocity was used [76, 79-84].

$$k_L \cdot \alpha = B_1 \cdot \left(\frac{P}{V_L}\right)^{x_1} \cdot U_G^{b_1} \qquad \text{Equation 4.11}$$

The power consumption in an ungassed vessel was calculated by using the power number, N_P, and the impeller Reynolds number, $Re_{im} = N \cdot D_{im}^2 \cdot \rho_L/\mu_L$, [76, 85] (Equation 4.12).

$$N_P = \frac{P}{\rho_L \cdot N^3 \cdot D_{im}^5} \qquad \text{Equation 4.12}$$

Once the impeller Reynolds number had been calculated in different agitation speeds, N, the power number was approximated by the graph which is developed by Bates et al. [86] between the N_P and Re_{im}. In the case of 45° pitched turbine type of impellers, the power number is constant for impeller Reynolds number higher than 10^3. The impeller's Reynolds number of reactor A was ranged from 6405 to 38433, so we considered the power number

constant in this application. The power number when more than one impellers are used can be approximated as the power number of single impeller multiplied by the number of impellers ($N_{P,n} = N_{im} \cdot N_{P,1}$) [87] .

Rearranging Equation 4.12 with respect to power consumption and dividing by the liquid volume V_L, we conclude to Equation 4.13.

$$\frac{P}{V_L} = \frac{N_{im} \cdot N_{P,1} \cdot \rho_L \cdot D_{im}^5}{V_L} \cdot N^3 \qquad \text{Equation 4.13}$$

Using one vessel, one agitation system and constant volume of liquid, the $N_{im} \cdot N_{P,1} \cdot \rho_L \cdot D_{im}^5 / V_L$ term can be considered constant.

During the experiments the superficial velocity of hydrogen was being determined by the consumption rate of hydrogen because of the dead-end operation of the reactor. The superficial velocity was varied between 0.01 and 0.05 mL/min and was considered practically constant.

Substituting Equation 4.13 to Equation 4.11 and taking into account that the superficial velocity of hydrogen is constant, the gas-liquid mass transfer coefficient and the gas-liquid mass transfer resistance are given by Equation 4.14 and Equation 4.15.

$$k_L \cdot \alpha = B_2 \cdot N^{3 \cdot x_1} \qquad \text{Equation 4.14}$$

$$\frac{1}{k_L \cdot \alpha} = \frac{1}{B_2} \cdot N^{-3 \cdot x_1} \qquad \text{Equation 4.15}$$

where, $B_2 = B_1 \cdot U_G^{b_1} \cdot \left(N_{im} \cdot N_{P,1} \cdot \rho_L \cdot D_{im}^5 / V_L \right)^{x_1}$

By applying nonlinear regression analysis, the exponent x_1 and the constant term B_2 were approximated. Figure 4.17 summarises the results. The exponent x_1 was calculated equal to 0.47. Several researchers have reported

the exponent x_1 for their systems to be between 0.3-0.65, Table 4.9. This means that the behaviour of our system, with respect to $k_L \cdot \alpha$, agrees with the results presented in the literature, justifying the proposed methodology to calculate the $k_L \cdot \alpha$.
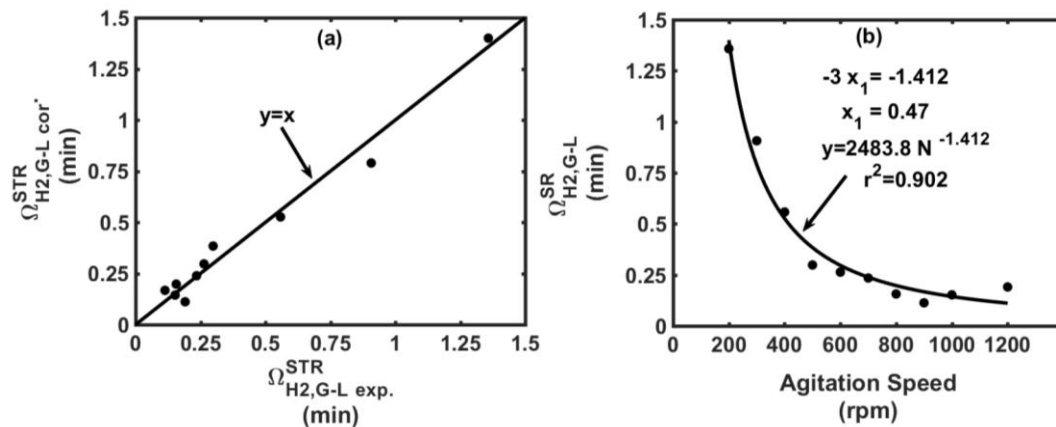
Figure 4.17: Summary of gas-liquid mass transfer resistance correlation results.

Table 4.9: Values of exponent x_1 proposed by different workers.

Reference	x_1	Reference	x_1
Robinson and Wilke [88]	0.40	Karimi et al. [82]	0.6
Linek et al. [89]	0.65	Yawalkar et al. [90]	0.47, 0.4, 0.54
Linek et al. [91]	0.59	Figueiredo and Calderbank [84]	0.3-0.6
Chandrasekharan and Calderbank [92]	0.56	R. V. Chaudhari [93]	0.63
Riet [94]	0.4		

4.3.4.2. Liquid-solid mass transfer coefficient

In the case of liquid-solid mass transfer coefficient the well-known correlation of the Sherwood number with Reynolds and Schmidt numbers for forced-convection mass transfer from single spheres, which is given by Equation 4.16 was used [95, 96].

$$Sh = 2 + A \cdot \left(Re_p\right)^m \cdot Sc^n \qquad \text{Equation 4.16}$$

The expression of the Reynolds number is based on the Kolmogoroff's theory of isotropic turbulence which suggests that the turbulent velocities are a function of only (a) the rate of energy dissipation and (b) the kinematic viscosity of the fluid [97].

The Reynolds number of particle, Re_p, is defined as,

$$Re_p = \epsilon \cdot \frac{d_p^4}{v_L^3} = \epsilon \cdot \frac{d_p^4 \cdot \rho_L^3}{\mu_L^3} \qquad \text{Equation 4.17}$$

The average energy dissipation rate per unit mass in the stirred tank is given by Equation 4.18 [76].

$$\epsilon \approx \epsilon_{aver} = \frac{P}{\rho_L \cdot (\pi/4) \cdot D_{im}^2 \cdot H} \qquad \text{Equation 4.18}$$

Substituting the expression of power input, P, which is given by Equation 4.13 to Equation 4.13, the average energy dissipation is described by Equation 4.19.

$$\epsilon \approx \epsilon_{aver} = \frac{N_{im} \cdot N_{P,1} \cdot \rho_L \cdot D_{im}^5}{\rho_L \cdot (\pi/4) \cdot D_{im}^2 \cdot H} \cdot N^3 \qquad \text{Equation 4.19}$$

Therefore, the Reynolds number of particle, Re_p, is expressed by Equation 4.20.

$$\text{Re}_p = \epsilon \cdot \frac{d_p^4 \cdot \rho_L^3}{\mu_L^3} = \frac{N_{im} \cdot N_{P,1} \cdot D_{im}^3}{(\pi/4) \cdot H} \cdot \frac{d_p^4 \cdot \rho_L^3}{\mu_L^3} \cdot N^3 \qquad\qquad \text{Equation 4.20}$$

To approximate the exponent of particle Reynolds number, the exponent of the Schmidt number was set to 1/3 as this is the most frequent value in the literature [56].

It has been already mentioned that the gassed system needs higher agitation speed in order to have the same power input as the ungassed. The reactor A can be considered as ungassed up to 600 rpm and gassed for agitation speeds higher than 600 rpm. If one observes the $\Omega_{H_2,L-S}^{STR}$ vs N, it is clear that the $\Omega_{H_2,L-S}^{STR}$ at 600 rpm and 1000 rpm is almost the same. Because of that, it has been assumed that the power input at 600 rpm and 1000 rpm is the same. In other words, the higher agitation speed has compensated the effect of gassing. Therefore, the interval from 700 rpm to 900 rpm have not been taken into account at the correlations.

By applying nonlinear regression analysis to $(Sh - 2)/Sc^{1/3}$ versus Re_p, the exponent m and the constant term A were approximated. Figure 4.18 summarises the results.
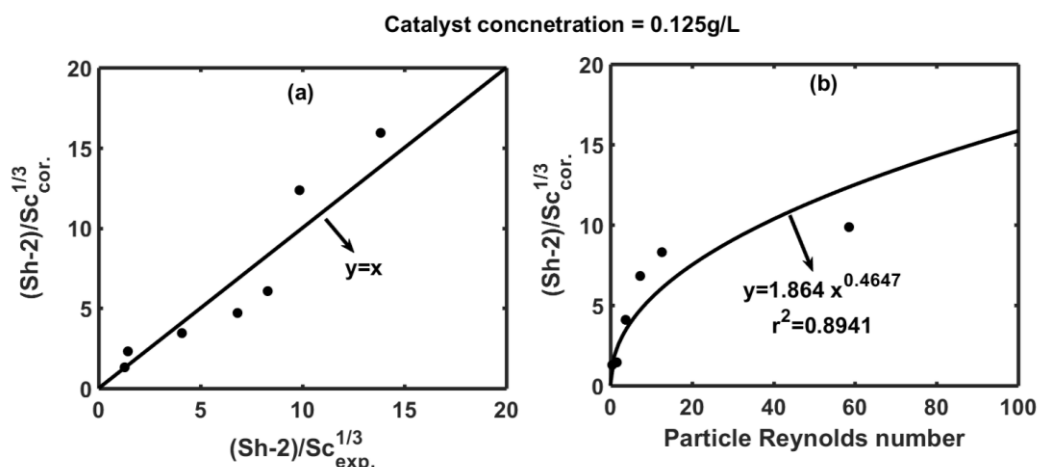
Figure 4.18: Summary of $k_{s,H_2} \cdot a_s$ correlation results.

The exponent m which was calculated from our data is equal to 0.46. That value agrees well with the classical Frössling equation [59, 98, 99] in which the exponent of particle Reynolds number is 1/2. Gholap et al. [100] and Ohashi [95] have reported a lower exponent of particle Reynolds number equal to 0.41 while Sano et al. [101] reported an exponent of particle Reynolds number equal to 0.25 for agitated vessels and bubble columns. In the system of the presented work the constant term A equals 1.86. In the case of steady state diffusion in a stagnant fluid, the Sherwood number equals 2. High values of A indicates high contribution of forced convection to the mass transfer. Miller [102] has reported the A equals 1.1 for mass transfer from fixed solid spheres in agitated vessels. This agrees with our results if one thinks that the contribution of forced convection in a system of free moved objects should be higher than the contribution in the case of fixed objects. This means that the behaviour of our system, with respect to $k_{s,H_2} \cdot \alpha_s$, agrees with the results presented in the literature, justifying the methodology which was implemented in order to calculate the $k_{s,H_2} \cdot \alpha_s$.

4.4. Modelling of heterogeneously catalysed styrene hydrogenation

4.4.1. Adsorption constants curve fitting approximation

The semi-batch reactor model has been presented in section 3.3.1 and it consists of ten differential equations, each one gives the molar balance of hydrogen, styrene and ethylbenzene in the gas, liquid and solid phase (Table 3.9). As it has been already described, the sum of material balance of each species in each phase gives the material balance for the species in the reactor.

The model contains eight different coefficients; four are related to the external mass transfer, three are related to the adsorption/desorption of the molecules to the catalyst active sites, and one is related to the intrinsic chemical reaction kinetics.

The mass transfer coefficients of hydrogen were experimentally calculated following the suggested methodology of section 4.2.2.2 and 4.2.2.3, while the liquid-solid mass transfer coefficient of styrene and ethylbenzene were correlated to the liquid-solid mass transfer coefficient of hydrogen based on their values of diffusion coefficients in methanol and they are presented in Table 4.10.

Table 4.10: Mass transfer coefficients used in the model for curve fitting approximation of the surface chemical reaction constants.

Coefficient	$k_L \cdot \alpha$	$k_{S,H_2} \cdot \alpha_S$	$k_{S,St} \cdot \alpha_S$	$k_{S,Eth} \cdot \alpha_S$
	$1/s$	$L/s \cdot g$	$L/s \cdot g$	$L/s \cdot g$
Value	0.0873	2.85	1.14	1.20
95% Confidence interval	±0.0216	±1.95	±0.78	±0.82

The experimental data which was used for the curve fitting approximation of the surface chemical reaction constants has been obtained in the reactor A under the experimental conditions which are outlined in Table 4.11. The styrene concentration profile was calculated by using the accumulative consumption curve of hydrogen and it is given by Equation 4.21.

$$C_{St,R}^{Exp}(t) = C_{St,R}^{Exp}(0) - \frac{P}{R \cdot T} \cdot \frac{1}{V_L} \cdot \int_0^t F_{H_2} \cdot dt$$

Equation 4.21

Where, $C_{St,R}^{Exp}$ = Experimental concentration of styrene in the reactor, [mole/L]

Table 4.11: Experimental conditions for the experiment which used for the curve fitting approximation of the surface chemical reaction constants.

Variable	Value
Temperature, °C	32
Agitation speed, rpm	1200
Pressure, bara	3
Catalyst concentration, g/L	0.05

Objective function and constrains

The objective function which should be minimised is the sum of squared errors between the experimental and simulated concentration of styrene, $C_{St,R}^{Exp}$ and $C_{St,R}^{Sim}$, respectively, and it is described by Equation 4.22.

$$\mathcal{F}_{obj} = \min \left[\sum_0^t \left(C_{St,R}^{Exp}(t) - C_{St,R}^{Sim}(t) \right)^2 \right]$$

Equation 4.22

Regarding the constraints which the optimum solution needs not to violate, they came from the observed chemical reaction constant and its 95% confidence intervals which have been calculated in section 3.2.2.3 based on the experimental results. Therefore, taking into account the definition of the observed chemical reaction constant and its 95% confidence intervals, the constraints are given by Equation 4.23.

$$0.059 \frac{\sqrt{\text{mole} \cdot \text{L}}}{\text{g} \cdot \text{s}} < \frac{k_1' \cdot \sqrt{K_{H_2}}}{K_{St} \cdot C_{St,S}} < 0.103 \frac{\sqrt{\text{mole} \cdot \text{L}}}{\text{g} \cdot \text{s}} \qquad \text{Equation 4.23}$$

The GlobalSearch in-built MATLAB algorithm was used for the minimisation of objective function which is given by Equation 4.22. The algorithm needs an initial guess for the independent variables and the bounds of each variable. The bounds specify the search space. Due to the lack of any sense about where the constants might lie, the algorithm run with several different initial guesses and different bounds. Table 4.12 and Table 4.13 summarise the initial guesses and the bounds which were used in seven different runs.

Table 4.12: Initial guess of each constant.

Case	$K_{H_2}(\text{L/mole})$	$K_{St}(\text{L/mole})$	$K_{Eth}(\text{L/mole})$	$k_1'(\text{mole/g} \cdot \text{s})$
1	100	100	100	0.01
2-7	100	100	5	0.01

Initially, the algorithm searches for the optimum combinaton of constants which minimises the objective function in a broad search space while the initial guesses of the adsorption constants have the same value, case 1. In case 2 of searching, an investigation of the initial guess effect on the objective function and on the optimum solution was carried out. In this case, the initial guess of ethylbenzene adsorption constant is changed to be near the optimum solution of case 1. The algorithm converges to a different optimum solution which improves the minimum of objective function.

Table 4.13: Lower and upper bound of each constant, LB and UB, respectively.

Case	K_{H_2}(L/mol)		K_{St}(L/mol)		K_{Eth}(L/mol)		k'_1(mol/g·s)	
	LB	UB	LB	UB	LB	UB	LB	UB
1	10^{-4}	10^3	10^{-4}	10^3	10^{-4}	10^3	10^{-4}	10^3
2	10^{-4}	10^3	10^{-4}	10^3	10^{-4}	10^3	10^{-4}	10^3
3	1	10^3	1	10^3	10^{-1}	10^2	10^{-3}	1
4	10	$1.5 \cdot 10^3$	10	$5 \cdot 10^2$	10^{-1}	10	10^{-3}	1
5	10^2	$1.5 \cdot 10^3$	10	$5 \cdot 10^2$	10^{-1}	10	10^{-3}	1
6	$5 \cdot 10^2$	$1.5 \cdot 10^3$	10	$3 \cdot 10^2$	10^{-1}	10	$5 \cdot 10^{-3}$	10^{-1}
7	$7 \cdot 10^2$	$1.5 \cdot 10^3$	10	$3 \cdot 10^2$	10^{-1}	8	$5 \cdot 10^{-3}$	10^{-1}

From case 3 to case 7, an investigation of the search space effect on the objective function and on the optimum solution was carried out. Although the search space shrinks around the optimum solution, the mimimum of the objective function did not improve sensibly. Table 4.14 summarises the optimum solutions and the minimum values of objective function for each case, the lowest value among the minimums has been highlighed with red colour. The results of cases 3 to 7 indicate that active sites adsorb preferably hydrogen against styrene and ethylbenzene while styrene is more preferable than ethylbenzene.

Table 4.14: Summary of GlobalSearch algorithm results for each case.

	Obj. function minimum x10⁻⁴	Optimum solution							
		$K_{H_2}(L/mol)$		$K_{St}(L/mol)$		$K_{Eth}(L/mol)$		$k'_1(mol/g \cdot s)$	
		Value	95% C.I	Value	95% C.I	Value	95% C.I	Value	95% C.I
Case 1	1.4848	577.84	$\pm$3425.65	232.48	±758.02	55.31	±207.58	0.0548	±0.0229
Case 2	0.4881	100.32	±214.02	100.40	±122.91	12.98	±29.27	0.0624	±0.0170
Case 3	0.4397	845.81	±708.49	118.08	±53.14	2.53	±6.85	0.0310	±0.0026
Case 4	0.4363	1288.90	±1152.5	133.03	±64.05	1.38	±7.03	0.0287	±0.0023
Case 5	0.4531	358.73	±287.08	99.99	±41.79	5.56	±7.14	0.0380	±0.0044
Case 6	0.4346	1198.22	±1034.38	126.50	±58.76	0.50	±6.42	0.0287	±0.0022
Case 7	0.4361	1314.30	±1179.5	133.82	±64.24	1.32	±7	0.0287	±0.0021

Figure 4.19a depicts the experimental and simulated concentration profile of styrene by substituting the mean values of mass transfer coefficients which are presented in Table 4.10. The ±95% confidence bounds of the concentration profile were simulated using the ±95% confidence intervals of the adsorption and intrinsic chemical reaction constants, which correspond to the lowest objective function value (case 6), Table 4.14.

Figure 4.19b depicts the experimental and simulated concentration profile of styrene by substituting the mean values of optimum solution which correspond to the lowest objective function value (case 5). The ±95% confidence bounds of the concentration profile were simulated using the ±95% confidence intervals of the mass transfer coefficients which are given in Table 4.10. When the lower 95% confidence intervals of the mass transfer coefficients are used, the three-phase reaction becomes slower due to the higher mass transfer resistance. On the other hand, when the upper 95% confidence intervals of the mass transfer coefficients are used, the three-phase reaction cannot be evolved faster because it is limited by the intrinsic chemical reaction kinetics. This explains why the simulated concentration is not in the middle of the ±95% confidence bounds in Figure 4.19b.
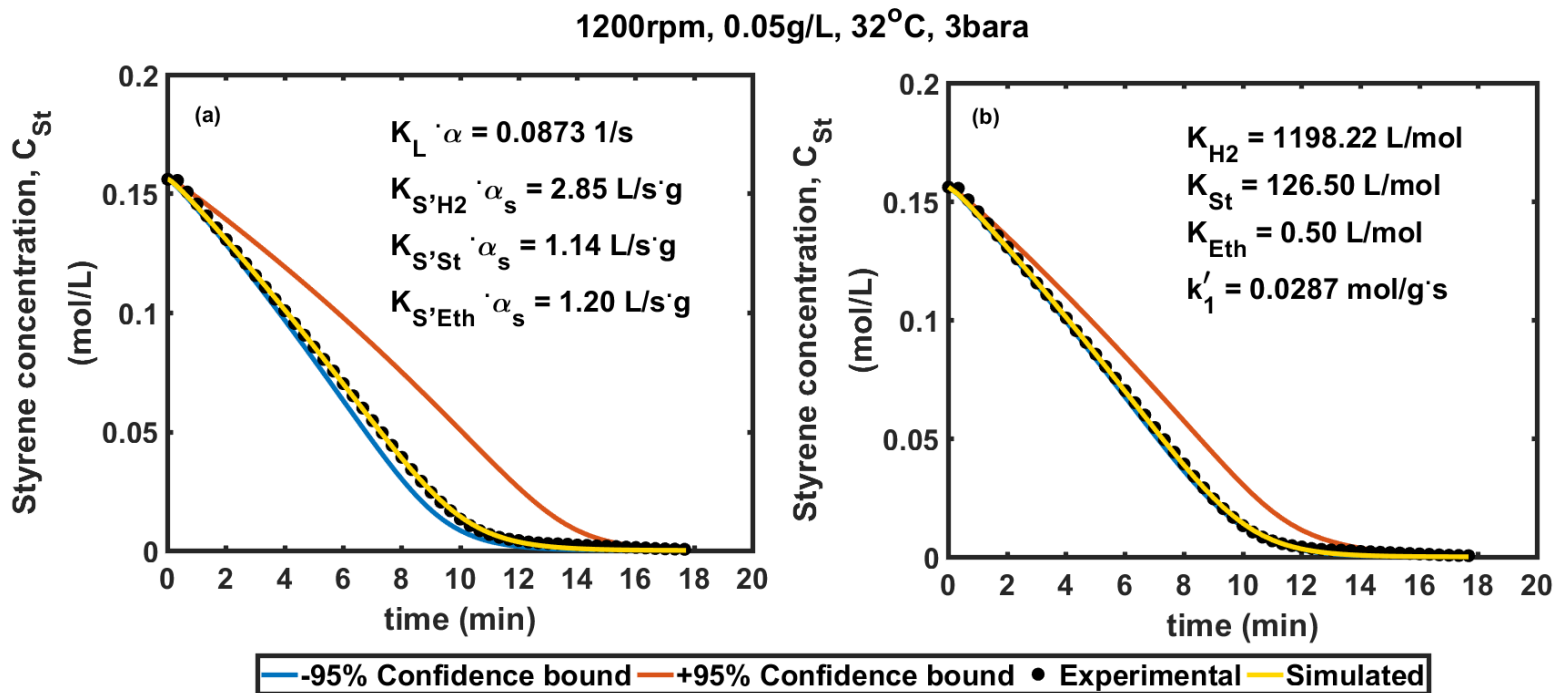
Figure 4.19: (a) Experimental and simulated styrene concentration profiles using the mean of mass transfer coefficients and the confidence intervals of adsorption and intrinsic chemical reaction constant; (b) experimental and simulated styrene concentration profiles using the mean of case 6 optimum solution and the confidence intervals of mass transfer coefficients.

Sensitivity analysis

To evaluate the sensitivity of the model to the parameters of the surface chemical reaction kinetics (i.e. adsorption constant of hydrogen, K_{H_2}, styrene, K_{St}, ethylbenzene, K_{Eth} and intrinsic chemical reaction rate constant, k_1'), the styrene's concentration profile was simulated by perturbating the parameters ±10%, ±20%, ±30%, ±40%, ±50% from their nominal values; and the deviation from the nominal simulated styrene's profile were calculated $\left(|dY| = |Y_{per} - Y_{nom}|\right)$. The nominal simulated styrene's profile refers to the model output when all parameters used are at their nominal values. Each time one parameter was perturbated while the rest were at their nominal values.

Perturbation $\qquad \delta\% = \dfrac{X_{perturbated} - X_{nominal}}{X_{nominal}} \cdot 100\% \qquad$ Equation 4.24

Where, $X = K_{H_2}, K_{St}, K_{Eth}, k_1'$

Figure 4.20 and Figure 4.21 summarise the sensitivity analysis results. In the subplots of the first the simulated styrene concentration profiles with one perturbated parameter are presented. Figure 4.20a summarises the deviations from the nominal simulated styrene's profile, when a -10% perturbation has been introduced in each parameter each time (subplots b, c and d referred to +10%, -50% and +50% perturbation, respectively). From Figure 4.20c and Figure 4.21 one ascertains that the model's output sensitivity on adsorption constant of ethylbenzene, K_{Eth}, is negligible and the constant can be removed from the model. Figure 4.22 presents the simulated concentration profiles of styrene. The blue curve represents the profile using all the parameters of case 6 optimum solution while in red curve the K_{Eth} has been neglected.
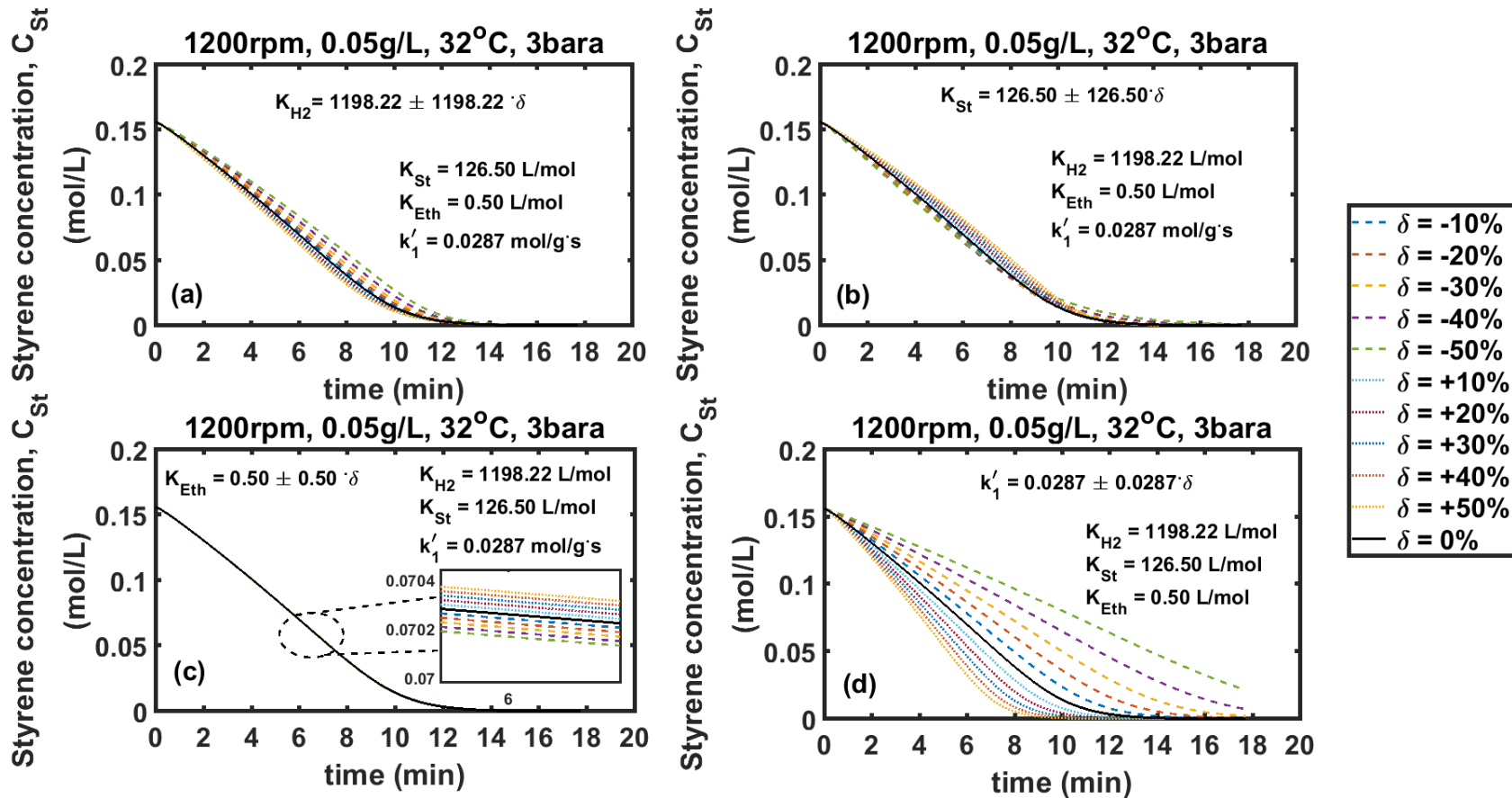
Figure 4.20: Simulated styrene concentration profiles with perturbated surface chemical reaction parameters; in subplot a K_{H_2} perturbated ±10%, ±20%, ±30%, ±40%, ±50% from its nominal value while the rest of the parameters are at their nominal values, the same stands for K_{St}, K_{Eth}, k'_1 in subplots b, c and d, respectively.
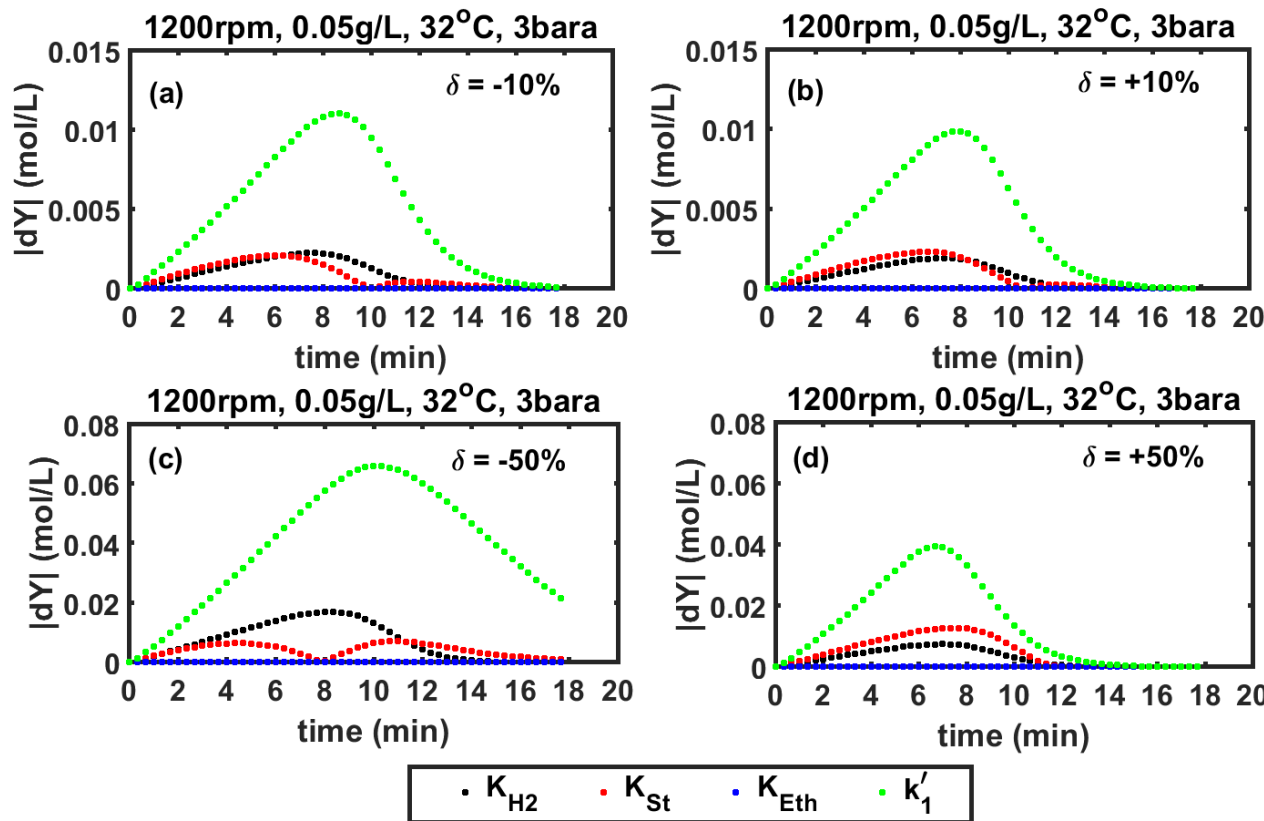
Figure 4.21: Deviation of simulated styrene concentration profiles, when perturbated surface chemical reaction parameters used, from the nominal simulated styrene concentration profile.
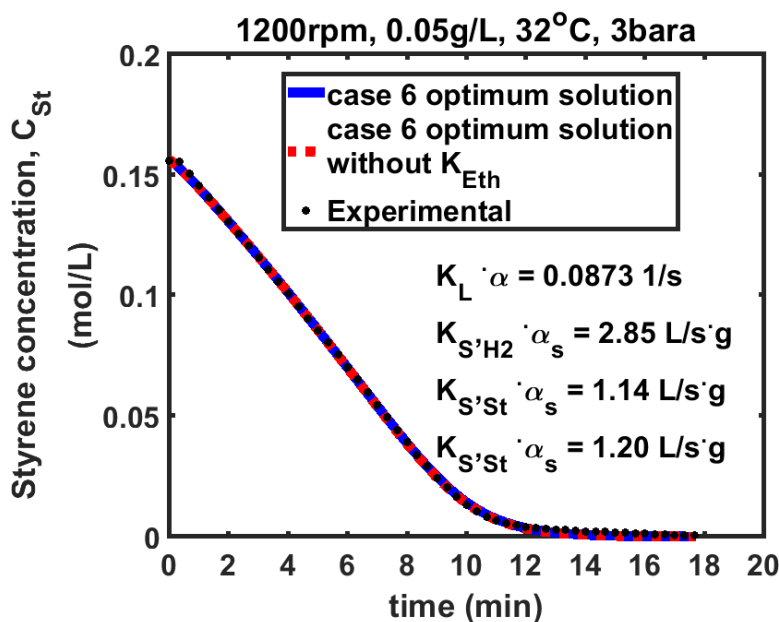
Figure 4.22: Simulated styrene concentration profile using case 6 optimum solution with (blue) and without (red) adsorption constant of Ethylbenzene, K_{Eth}; and experimental styrene concentration profile.

4.4.2. Model validation

The model was validated against experimental data which was not used in the curve fitting approximation of the adsorption and intrinsic chemical reaction constants.

The adsorption and intrinsic chemical reaction constants which were used in the model validation came from case 6 optimum solution. For any of the experiments which is used in model validation, the mass transfer coefficients of hydrogen and their ±95% confidence intervals were calculated by applying the suggested methodology of section 4.2.2.2 and 4.2.2.3. The liquid-solid mass transfer coefficient of styrene and ethylbenzene were correlated to the liquid-solid mass transfer coefficient of hydrogen based on their values of diffusion coefficients in methanol (Appendix C).

Table 4.15 outlines the mass transfer coefficients and their ±95% confidence intervals which were used in the model to simulate each experimental styrene concentration profile.

The ±95% confidence bounds of the concentration profiles are generated using the ±95% confidence intervals of the mass transfer coefficients.

Figure 4.23 shows the experimental and simulated concentration profiles of styrene for each of the four different cases of experimental conditions. For all cases, the experimental data lies inside the 95% confidence bounds of the simulated concentration profile. The confidence bounds of the simulated concentration profiles are calculated based on the linear regression models between $\Omega_{H_2,tot}^{STR}$ vs V_L/W_c and $\Omega_{H_2,tot}^{STR}$ vs $\sqrt{C_{H_2,i}}$. Therefore, the broadness of the confidence bounds is a result of the mean of squared errors or the coefficient of determination. Higher the coefficient of determination, narrower the confidence bounds.

Table 4.15: Summary of mass transfer coefficients and their 95% confidence intervals for the experiments which are used in model validation, all the experiments are performed at 32°C and 3 bara.

		400rpm 0.125g/L	600rpm 0.125g/L	600rpm 0.5g/L	900rpm 0.3g/L
$k_L \cdot \alpha$ (s^{-1})	Value	0.02986	0.06325	0.06325	0.1471
	95% Confidence interval	±0.00043	±0.00415	±0.00415	±0.0184
$k_{S,H_2} \cdot \alpha_S$ $(L/s \cdot g)$	Value	0.5837	1.0475	0.7787	0.4485
	95% Confidence interval	±0.0838	±0.5862	±0.5243	±0.0837
$k_{S,St} \cdot \alpha_S$ $(L/s \cdot g)$	Value	0.2335	0.419	0.3115	0.1794
	95% Confidence interval	±0.0335	±0.2345	±0.2097	±0.0335
$k_{S,Eth} \cdot \alpha_S$ $(L/s \cdot g)$	Value	0.2452	0.4400	0.3271	0.1884
	95% Confidence interval	±0.0352	±0.2462	±0.2202	±0.0352
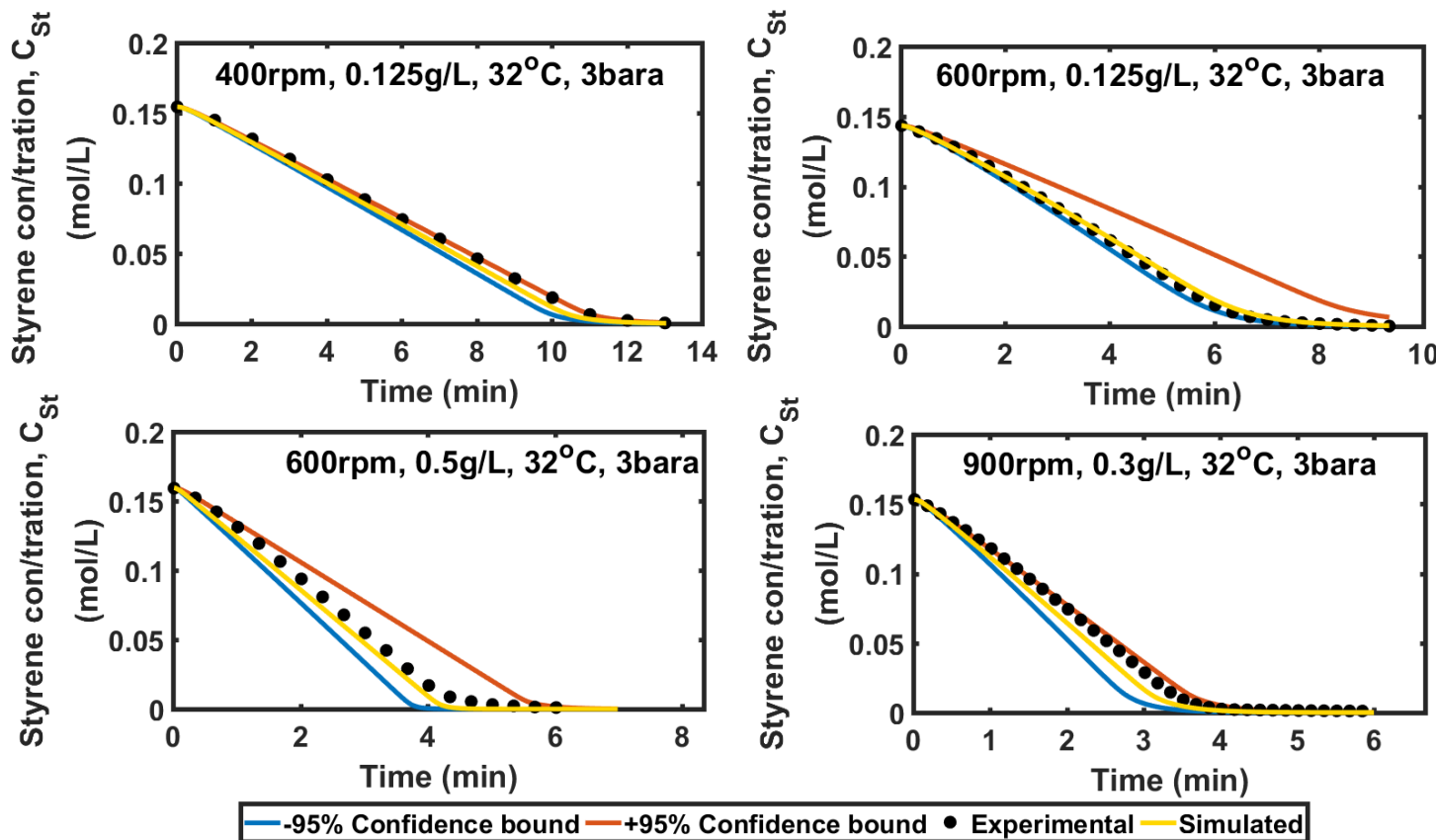
Figure 4.23: Experimental and simulated concentration profiles of styrene for different experimental conditions validating the 3-phase reactor model.

4.5.   Conclusions

The mass transfer resistances in a three-phase semi-batch stirred tank reactor were calculated by changing catalyst loading and the pressure of hydrogen. This allows to avoid the use of different catalyst particles and give the chance to calculate the mass transfer resistances without caring about the type of catalyst.

So far, an established practice to ensure that a three-phase reaction is limited by reaction kinetics and not by the external mass transfer processes is the observation of the global mass transfer rate of hydrogen in different agitation speeds. According to this practice, If the global mass transfer rate of hydrogen does not increase with the agitation speed, the process is said to be reaction limited.

However, as it was showed in Figure 4.16, both of the external mass transfer resistances might follow a level off trend leading to a plateau. Therefore, the plateau at mass transfer rate against agitation speed plots is not enough to ensure that the process is limited by either chemical reaction or external mass transfer. On the other hand, the calculation of each mass transfer resistance provides more reliable conclusions about the limiting regime as Figure 4.12, Figure 4.13 and Figure 4.14 showed.

The proposed methodology to determine the limiting regime is appropriate to be used even if none of the mass transfer rates can be neglected. The values of gas-liquid and liquid-solid mass transfer resistances, which obtained by implementing the proposed methodology, were correlated to Reynolds and Sherwood number. The correlations were found in agreement with the literature.

The styrene hydrogenation in three-phase semi-batch stirred tank reactor was simulated by having assumed that the surface chemical reaction follows the Langmuir-Hinshelwood model, the hydrogen is dissociatively chemisorbed onto palladium active sites, the styrene and hydrogen compete for the same sites and that the styrene is hydrogenated in two consecutive steps. It was also assumed that any amount of styrene which adsorbs onto catalyst particle reacts with hydrogen producing ethylbenzene and that any hydrogen passing through the mass flow controller is being consumed by the reaction.

The adsorption constants and the intrinsic reaction rate constant which were used in the surface reaction model were not approximated experimentally. Instead, a curve fitting approach using the GlobalSearch in-built MATLAB algorithm was used to approximate them. The model after the curve fitting approximation was validated against experimental data which had not been used in curve fitting. Taking into account that the simulated profiles lie inside the confidence bounds, the results of validation indicated that the model describes adequately the three-phase semi-batch hydrogenation of styrene in the stirred tank reactor.

Chapter 5

5.   Three-phase Continues Stirred Tank Reactor, CSTR

5.1.   Introduction

This chapter is dedicated to the three-phase continuous stirred tank reactor. It is structured in three different subsections, namely; (a) materials and methods, (b) experimental heterogeneous catalysed styrene hydrogenation and (c) modelling of the heterogeneous catalysed styrene hydrogenation.

Firstly, the methodologies, by which the experimental investigations into the styrene hydrogenation over Pd/C catalyst in CSTR were conducted, are presented. Including the details of the design and construction of the CSTR. The experimental procedure is also described in detail.

In section 5.3, the hypothesis that the gas-liquid and the liquid-solid mass transfer coefficients of the same stirred tank reactor equipped by the same agitator are independent of the operation mode of the reactor- semi-batch or continuous flow-is tested. For this reason, initially, experiments were conducted to create the appropriate data of concentration profiles. In addition, the mass transfer coefficients, which were used in the continuous flow reactor model which has been introduced in section 3.3.2, were not experimentally estimated under continuous flow reactor mode. Instead, they have been calculated, in the semi-batch reactor mode, following the developed methodology described in section 4.3 related to the semi-batch reactor.

5.2.   Materials and methods

5.3.   Design and assembly

The setup of the three-phase stirred tank continuous flow reactor is based on the setup of the semi-batch stirred tank reactor A, which was transformed in a continuous flow reactor by adding a dip-leg, an HPLC pump and a back-pressure regulator at the reactor outlet stream. The experimental setup of the three-phase stirred tank continuous flow reactor is shown in Figure 5.1.

The monitoring and the control of the agitation speed, temperature and pressure are the same as they have been described in section 4.2.1.1 under the title "Reactor A-0.6 L & 2-turbine impeller". Details on reactor characteristics can be found in Table 4.1.

Liquid volume

The volume of liquid in the reactor vessel was monitored by using a balance on which the feed and the product vessel were placed and it was regulated manually by using the outlet pump. As far as the reading of the balance was being maintained constant the liquid volume in the reactor was constant as well.

The substrate solution did not contain any catalyst. The catalyst was charged into reactor vessel and it was kept in there using a 2 µm filter at the end of the dip-leg.
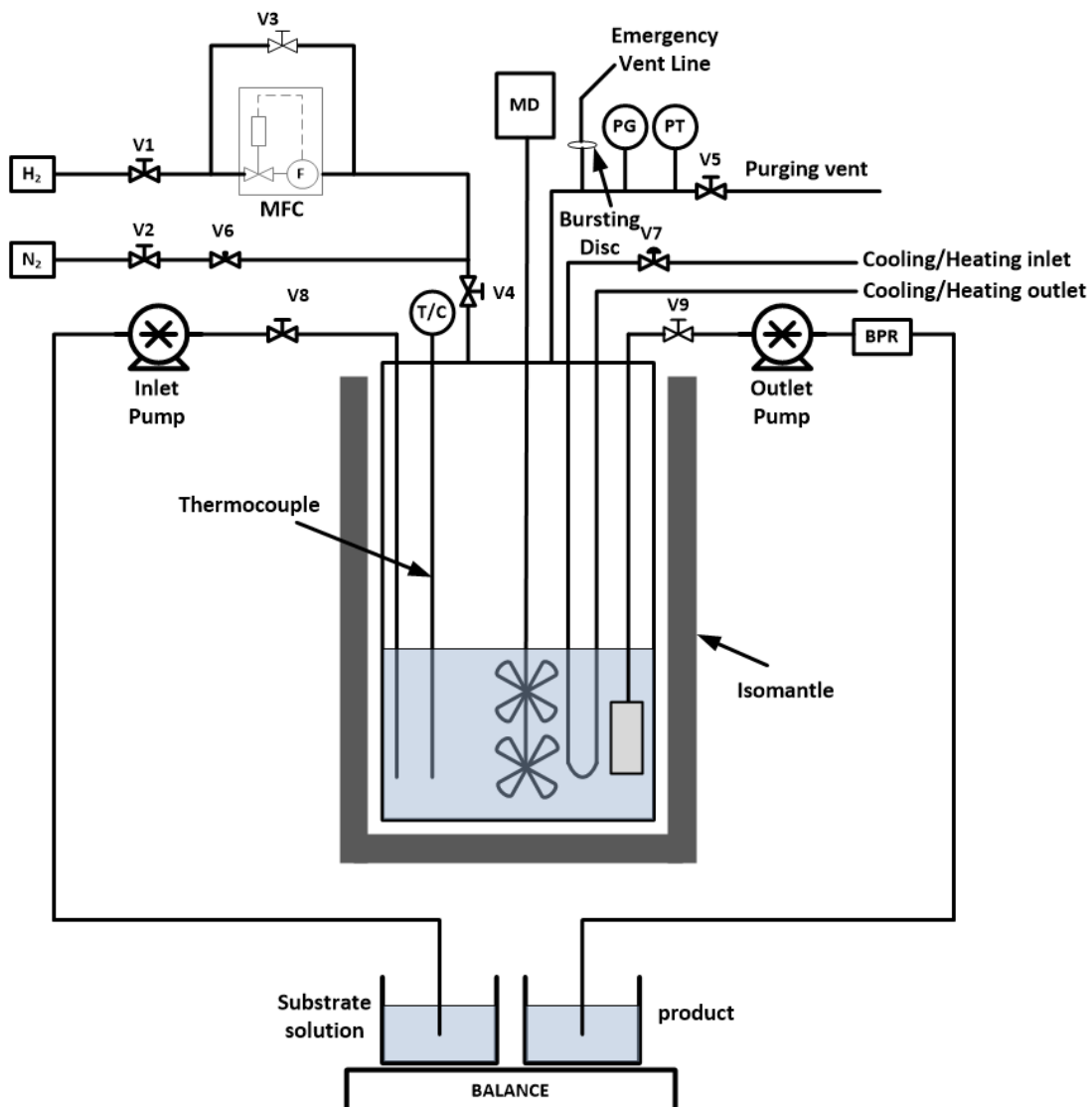
Figure 5.1: Experimental setup of the three-phase CSTR.

5.3.1. Experimental procedure

The hydrogenation of styrene was chosen as case study to investigate the mass transfer in trickle bed reactors, because of two reasons; firstly, the hydrogenation of styrene presents fast intrinsic reaction rate which allows the mass transfer rates to be the limiting regime even if intensive mixing conditions occur. Secondly, the same reaction has been studied in the semi-batch stirred tank reactor, so the results of the two reactors can be compared and a methodology for transferring the process from the semi-batch stirred tank reactor to the CSTR can be built.

Figure 4.3 presents the reaction scheme of styrene hydrogenation. All the experiments took place using methanol 99.9% (HPLC grade) as solvent, styrene 99% (without stabiliser) and decane 99% as internal standard and they were purchased from Sigma Aldrich. Compressed pure hydrogen (UN: 1049) was purchased from BOC and 4.63% palladium on activated carbon (Type 87L) was purchased from Johnson Matthey. Table 4.2 summarises the physical properties of liquid and solid phase.

5.3.1.1. Start-up

The same procedure for starting-up the reaction in the continuous stirred tank reactor as in the case of the experiments on semi-batch stirred tank reactor A was followed (section 4.2.2.1).

Once (a) the reactor was under the intended for the experiment temperature and pressure (32°C and 3 bara, respectively), (b) the substrate solution had been added into the reactor, (c) the feed solution had been prepared and (d) the feed and product vessels had been placed on the balance, the agitation and the pumps were switched on simultaneously in order to initiate the reaction and to keep the liquid volume constant.

It is worth mentioning that at time zero (t=0) the reactor vessel and the feed vessel had the same styrene concentration.

5.3.1.2. Operation

During the reaction, the SpecView software was used to monitor and record the reactor temperature, the agitation speed, the hydrogen flow rate and the reactor pressure. The agitation speed and the reactor temperature were manipulated using the SpecView software. Regarding the hydrogen flow, it

was regulated from the mass flow controller in such a way to maintain the reactor pressure at the desired setpoint.

As it has been already mentioned the liquid volume in the reactor vessel was monitored by the means of the balance and it was regulated by changing appropriately the outlet flow using the outlet pump.

The reactor was sampled from the outlet stream and the samples were used for off-line concentration analysis using the same gas chromatography as the one which was used for the semi-batch styrene hydrogenation and it is described in section 4.2.3.

5.3.1.3. Shut-down

The same procedure for shutting-down the reaction in the continuous flow reactor as in the case of the experiments on semi-batch reactor A was followed (section 4.2.2.3).

5.4.   Modelling of heterogeneously catalysed styrene hydrogenation

This section is dedicated to critically presenting the mathematical model of the three-phase styrene hydrogenation in the continuous stirred tank reactor. The mass transfer coefficients which were used in the continuous flow reactor model were not experimentally calculated under continuous flow reactor mode. Instead, the mass transfer coefficients which have been calculated in the semi-batch reactor were used.

Under turbulent mixing conditions the gas-liquid mass transfer depends on (a) the power consumption per liquid volume which is correlated to the impeller Reynolds number and (b) the superficial gas velocity (Equation 4.12). In addition, the liquid-solid mass transfer coefficient is usually correlated by using Sherwood, Reynolds and Schmidt numbers as Equation 4.17 suggests. The

Reynolds number of the particle in a stirred tank depends on the technical characteristics of the agitation system, on agitation speed and on the physical characteristics of the liquid. Therefore, as long as one reaction proceeds under the same agitation speed, in the same vessel equipped by the same agitation system, using the same solvent and catalyst and under the same temperature and pressure, the gas-liquid and liquid-solid mass transfer coefficient should be independent of the operation mode of the reactor; semi-batch or continuous flow.

The adsorption constants of styrene, hydrogen and ethylbenzene; and the intrinsic reaction rate constant was showed to be independent of the reactor setup in section 4.3.3. Therefore, in the model of the CSTR the same constants with those of the model of the semi-batch stirred tank reactor were used.

5.4.1. Generation of experimental concentration profiles

The three-phase continues stirred tank reactor operated in dead-end mode, this means that hydrogen was supplied continuously in the reactor in an appropriate flow rate which was keeping the reactor pressure constant while styrene solution was fed into the reactor and product solution was pumped out in specific flow rates which determined the residence time of liquid in the reactor. The experimental setup did not allow the pumping of any slurry, therefore, there was not any catalyst renewal for the course of each experiment.

The experimental conditions of each experiment are summarised in Table 5.1. The reaction was performed in three different liquid residence times under the same pressure, temperature and agitation speed. In addition, the reaction in

the residence time of 6 min was performed in two different catalyst concentrations.

Table 5.1: Summary of experimental conditions.

Exp.	N (rpm)	P (bara)	T (°C)	$C_{cat.}$ (g/L)	τ (min)
1	1200	3	32	0.1	6
2	1200	3	32	0.05	6
3	1200	3	32	0.05	8
4	1200	3	32	0.05	10

As it has been described in "Materials and methods" section 5.2, temperature, pressure and agitation speed were automatedly controlled by the means of a PID controller.

On the other hand, the liquid volume was controlled manually by changing the outlet flow rate appropriately in such a way to keep the balance reading constant. Although the liquid volume was manually controlled, it was adequately maintained close to the initial value. The maximum deviation of the liquid volume from its initial value is 2%, 0.92%, 1.26% and 0.77%, for the experiments 1, 2, 3 and 4, respectively.

The reactor was sampled from the outlet stream every residence time for either eight or nine residence times and the samples were used for off-line concentration analysis using gas chromatography. The concentration profiles of styrene and ethylbenzene based on the gas chromatography analysis are presented in Figure 5.3.

Styrene and ethylbenzene profiles indicate that the conversion decreases with time. Taking into account that the flow rate and the concentration of the feed were kept constant, there might be any catalyst deactivation resulting in conversion decrease.

Catalyst deactivation might occur for several reasons which are avoided when the reactor operates in semi-batch mode:

- Catalyst deactivation might be caused by any poisoning from the substrate and/or any impurity which was present in the feed vessel in traces and it cannot be detected by gas chromatography. Although the same substrate was used when the reactor was operated in the semi-batch mode, the poisoning effect was not observed. This might occur because in this case the catalyst was being exposed to much less amount of substrate and/or impurity in the course of one reaction while in CSTR because the catalyst was not renewed, the effect of any poisoning was accumulative.

- Sintering – At the end of each experiment, catalyst cake formation is observed (Figure 5.2) around the 2 µm filter of the dip-leg. Because the inside of the cake is not well mixed and the solids concentration is high, a temperature increase is likely to occur which favours the growth of crystal size resulting in sintering of catalyst particles. The sintering results in the loss of the available surface area for mass transfer which making the reaction slower.

- Leaching of the active metal sites from the support into the solution, reducing catalyst activity. In this case, the 2 µm filter at the end of the dip-leg is not small enough to keep the nanoparticles of active metal in

the reactor. Leaching of solid catalysts in liquid media has been reviewed by Sádaba et al. [103].
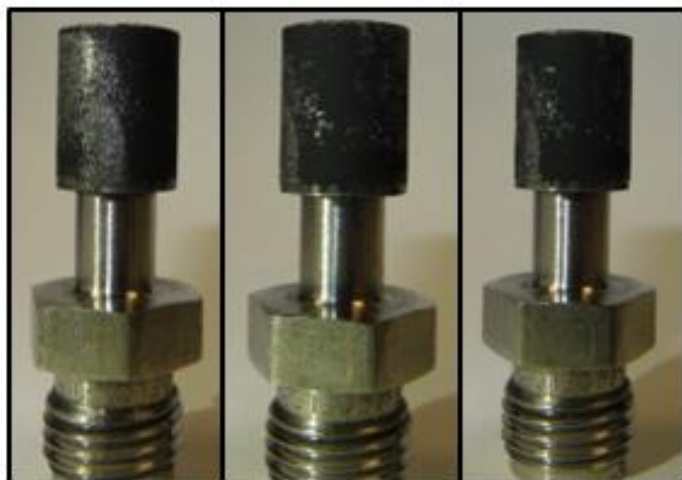
Figure 5.2: Catalyst cake formation around the 2 μm filter.
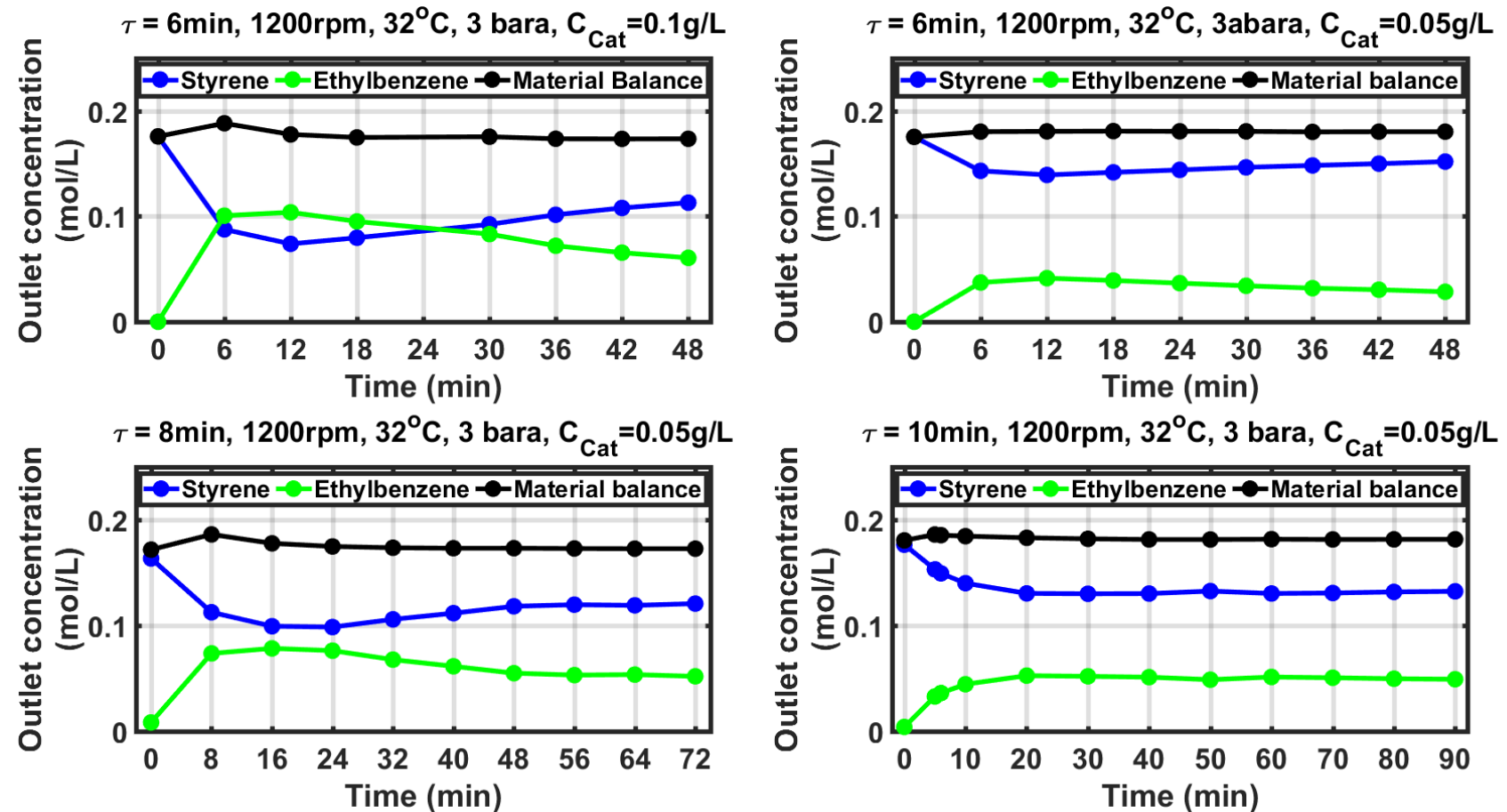
Figure 5.3: Concentration profiles of styrene and ethylbenzene; and material balance between styrene and ethylbenzene.

5.4.2. Catalyst decay empirical model and CSTR simulation

Because the reason of styrene conversion decrease over time remains experimentally unclarified, this decrease was simulated as a catalyst loss by an empirical model of catalyst loading decay, W_C, with respect to time. The empirical model is given by Equation 5.1.

$$W_C = W_{c,0} \cdot \left(\sum_1^i e^{-t/m_i} \right) / i \qquad \text{Equation 5.1}$$

Where, $W_{c,0}$= Initial catalyst loading, [g]

$\quad$ t = Reaction time, [s]

$\quad$ m_i = Exponential factor, [s^{-1}]

To approximate the catalyst decay exponential factors, m_i, a curve fitting procedure was implemented between the experimental and simulated concentration profiles of styrene. The simulated concentration profiles of styrene are given by the reactor model described in section 3.3.2 (Table 4.2), substituting the respective mass transfer coefficients given in Table 5.2. For the curve fitting the GlobalSearch in-built MATLAB algorithm was used.

The objective function which was minimised is the sum of squared errors between the experimental and simulated concentration of styrene, $C_{St,R}^{Exp}$ and $C_{St,R}^{Sim}$, respectively, and it is described by Equation 5.2.

$$\mathcal{F}_{obj} = \min \left[\sum_0^t \left(C_{St,R}^{Exp}(t) - C_{St,R}^{Sim}(t) \right)^2 \right] \qquad \text{Equation 5.2}$$

Mass transfer coefficients and adsorption constants

The continuous flow reactor model consists of ten differential equations, each one gives the molecular balance of hydrogen, styrene and ethylbenzene in the gas, liquid and solid phase.

The model contains eight different coefficients; four are related to the external mass transfer, three are related to the adsorption/desorption of the molecules to the catalyst active sites, and one is related to the intrinsic chemical reaction kinetics.

The mass transfer coefficients of hydrogen have been calculated in the semi-batch reactor mode conducting the same reaction under the experimental conditions of pressure, temperature, agitation speed and catalyst concentration of experiments 1 to 4 (Table 5.1). The liquid-solid mass transfer coefficient of styrene and ethylbenzene are correlated to the liquid-solid mass transfer coefficient of hydrogen based on their values of diffusion coefficients in methanol. Table 5.2 summarises the mass transfer coefficients used in the model of three-phase CSTR.

The methodology for calculating the mass transfer coefficients in three-phase stirred tank reactors is described in section 4.3.

The adsorption constants of styrene, hydrogen and ethylbenzene; and the intrinsic reaction rate constant which were used in the model of the mechanically agitated continuous flow reactor are the same with those which were used in the model of the semi-batch stirred tank reactor A and they are depicted in Table 4.15 (case 5).

Table 5.2: Summary of mass transfer coefficients used in the model of three-phase CSTR.

Exp.	N (rpm)	C_{cat} (g/L)	$k_L \cdot \alpha$ (1/s)	$k_{S,H_2} \cdot \alpha_S$ (L/s·g)	$k_{S,St} \cdot \alpha_S$ (L/s·g)	$K_{S,Eth} \cdot \alpha_S$ (L/s·g)
1	1200	0.1	0.0873	1.74	32	0.1
2	1200	0.05	0.0873	2.85	32	0.05
3	1200	0.05	0.0873	2.85	32	0.05
4	1200	0.05	0.0873	2.85	32	0.05

The algorithm needs an initial guess for the exponetial factors of the catalyst decay empirical model and the bounds of each factor which specify the search space. The initial guess for the exponetial factor were chosen randomly as long as the objective function could be determined at the initial point. Due to the lack of any sense about where the factors might lie, the algorithm runs with broad enough bounds. Table 5.2 and Table 5.3 summarise the initial guesses and the bounds which were used for the approximation of the exponential factors in each case.

Table 5.3: Initial guess of exponential factors.

Exp	$x_1, (1/s)$	$x_2, (1/s)$	$x_3, (1/s)$	$x_4, (1/s)$
1	2000	2	2	-
2	2000	2	2	2
3	2000	2	2	-
4	2000	2	2	-

Table 5.4: Lower and upper bound of each constant, LB and UB, respectively.

Exp	x_1, s^{-1}		x_2, s^{-1}		x_3, s^{-1}		x_4, s^{-1}	
	LB	UB	LB	UB	LB	UB	LB	UB
1	10^{-3}	10^4	10^{-3}	10^5	10^{-3}	10^5	-	-
2	10^{-1}	10^4	10^{-1}	10^4	10^{-1}	10^5	10^{-3}	10^5
3	10^{-3}	10^4	10^{-3}	10^6	10^{-3}	10^6	-	-
4	10^{-3}	10^6	10^{-3}	10^6	10^{-3}	10^6	-	-

Table 5.5: Summary of GlobalSearch algorithm results for each experiment.

Exp.	Obj. function minimum	Optimum solution			
	$x10^{-5}$	x_1, s^{-1}	x_2, s^{-1}	x_3, s^{-1}	x_4, s^{-1}
1	5.8058	980.57	83013.94	574.56	-
2	3.2542	43.95	669.56	523.54	99999
3	4.8906	1394.45	163807.56	318.78	-
4	7.0055	197.87	83248.19	2.78	-

After applying the GlobalSearch in-built algorithm in MATLAB with the mentioned inputs of (a) initial guesses and (b) bounds of exponential factors, the optimum solution of the exponential factors which minimise the objective

function was approximated. Table 5.5 reveals the optimum solution for each experiment.

The exponential factors of the catalyst decay empirical model were substituted in the reactor model and it run for the different conditions, which are described in Table 5.1, to simulate the concentration profiles of styrene. Figure 5.4 illustrates the simulated and experimental concentration profiles of styrene for the four different experiments. The catalyst simulated loading is presented as well.
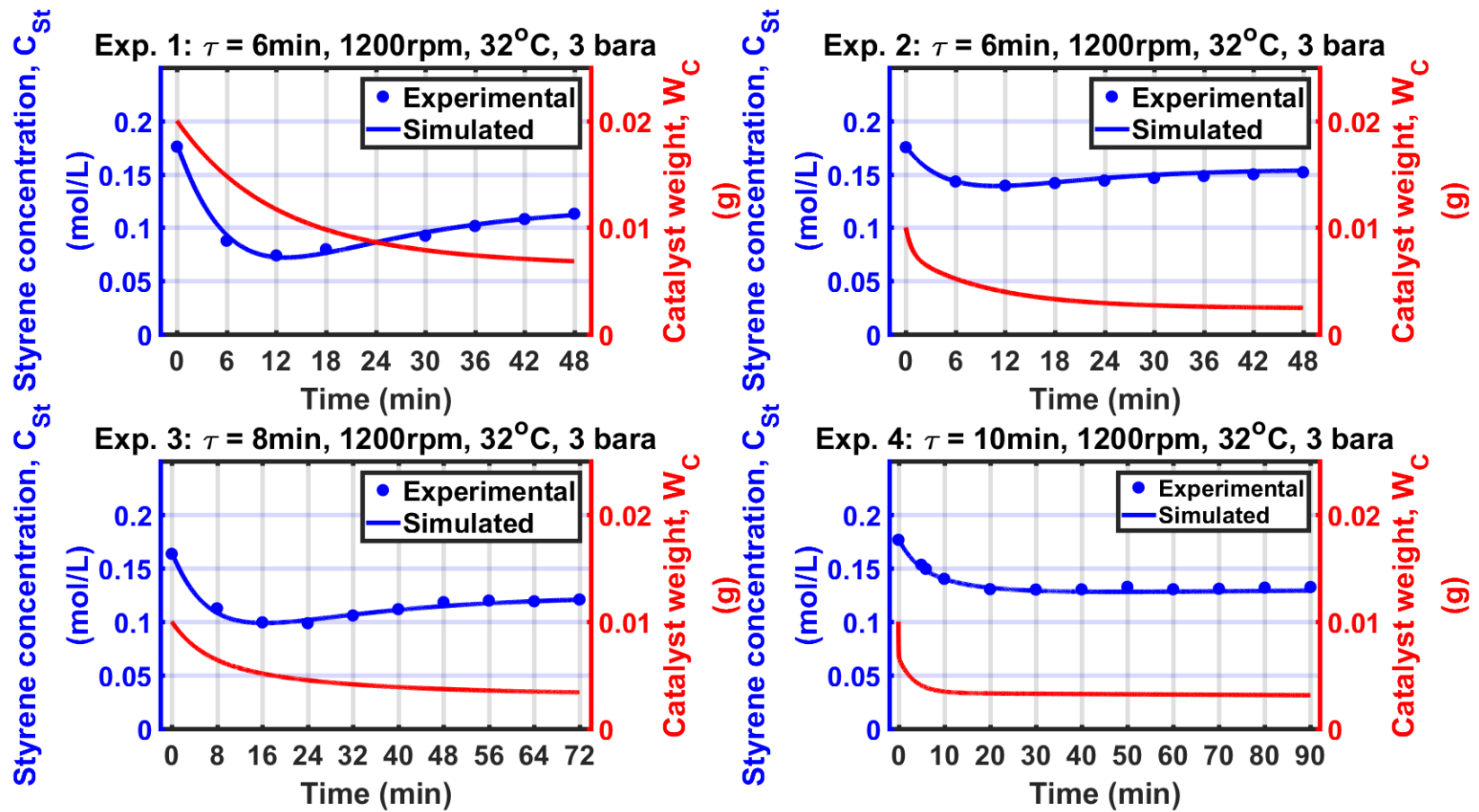
Figure 5.4: Experimental and simulated concentration profiles of styrene in the 3-phase CSTR; and simulated catalyst loading.

5.4.3. Determination of gas-liquid mass transfer resistance

The mass transfer coefficients which were used for simulating the styrene concentration profiles in continuous flow were assumed to be the same with those which have been calculated under the same experimental conditions in the semi-batch reactor A. To provide more evidence and support this assumption, the gas-liquid mass transfer resistance was calculated by following the suggested methodology, described in section 4.3.2. The catalyst weight was calculated by using the empirical model, described in Equation 5.1. Then, the gas-liquid mass transfer resistance was compared to the gas-liquid mass transfer resistance of the semi-batch reactor which was used in the simulation.

To follow the methodology, described in section 4.3.2, for calculating the gas-liquid mass transfer resistance, the global mass transfer resistance of hydrogen, $\Omega_{H_2,tot}^{STR}$, needs to be calculated for different catalyst loadings. The global mass transfer resistance was defined as the ratio between the gas-liquid interfacial concentration of hydrogen, $C_{H_2,i}$, and the mass transfer rate of hydrogen, $MTR_{H_2}^{STR}$. For the continuous flow experiments, the latter was calculated by the difference of styrene concentration between the feed and the outlet and by dividing this value by the residence time. The catalyst loading is calculated using the empirical model for the corresponding time. For instance, for the experiment 1 and after 36 minutes of reactor operation the final concentration of styrene is 0.1075 mole/L and the catalyst loading is 0.0074g.

As the described methodology of section 4.3.2 suggests, the global mass transfer resistance is plotted against the reciprocal of the catalyst

concentration in Figure 5.5. The intercept of the linear regression model of the plotted data defines the gas-liquid mass transfer resistance, $\Omega_{H_2,i-L}^{STR}$. Table 5.6 summarises the results.

Table 5.6: Linear regression results of global mass transfer resistance of hydrogen against the reciprocal of catalyst concentration.

Intercept $= \Omega_{H_2,i-L}^{STR}$		95% Confidence interval	
Slope $= \left(\Omega_{H_2,L-S}^{STR} + \Omega_{H_2,R}^{STR}\right) \cdot W_C/V_L$			
N	Intercept	Slope	Intercept	Slope
(rpm)	(min)	(min·g/L)	(min)	(min·g/L)
1200	0.1652	0.0331	± 0.0848	±0.0045
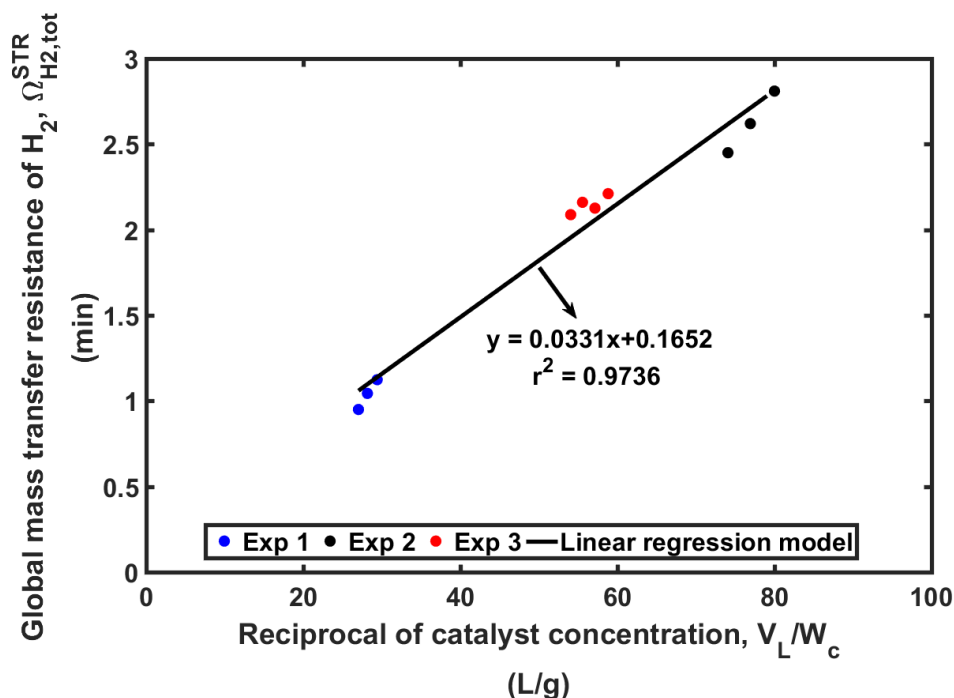
Figure 5.5: Global mass transfer resistance of hydrogen against catalyst concentration reciprocal for the CSTR.

The results of the linear regression model of the continuous flow reactor are compared to the linear regression model of the semi-batch reactor A in Figure

5.6. In both cases, the agitation speed, the pressure and the temperature were 1200 rpm, 3 bara and 32°C, respectively. The 95% confidence intervals for each model variable are presented in the same figure in the form of error bars.
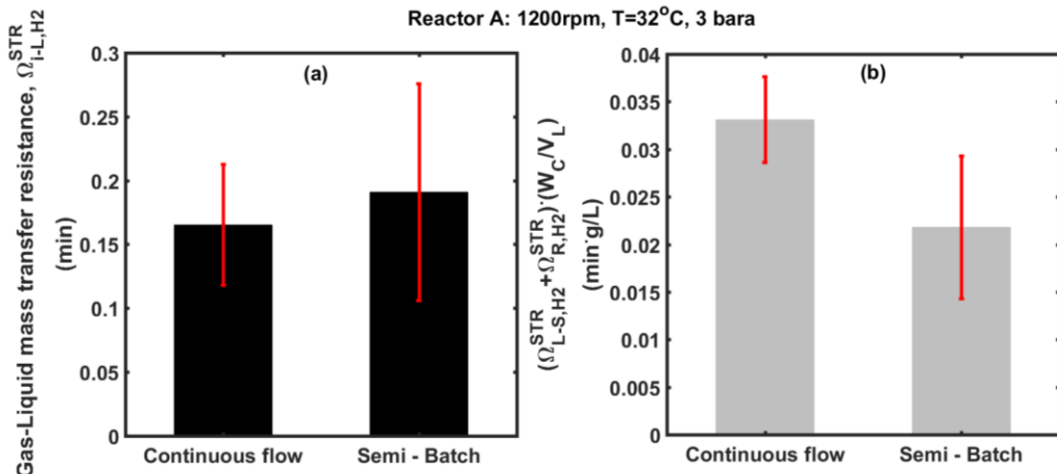
Figure 5.6: Comparison of the gas-liquid mass transfer resistances in figure a and of the slopes in figure b of the linear regression models calculated in the semi-batch and continuous flow reactor.

The gas-liquid mass transfer resistances are close enough to each other for accepting the assumption that the gas-liquid mass transfer is independent of the operation mode of the reactor; semi-batch or continuous flow. Moreover, taking into account the 95% confidence intervals there is an overlap between them. Bearing in mind that the linear regression model of the continuous flow reactor was based on the values of the empirical model of catalyst loading, the difference regarding the gas-liquid mass transfer resistances is considered negligible.

Regarding the slopes, although there is higher difference between the calculated value in the CSTR and the one calculated in the semi-batch reactor A, there is an overlap when the 95% confidence intervals are taken into account. The slope of the regression model describes the sum of liquid-solid

mass transfer resistance and the resistance due to the chemical reaction kinetics multiplied by the catalyst concentration. From its definition, the slope is subject to higher complexity which combines the physical and chemical experimental variables. The calculation of the slope comes from data of three different experiments with varying residence time and in extension with varying liquid flow rate. This flow rate variation might change the flow patterns in the vessel of the continuous flow reactor affecting the distribution of catalyst fine particles and the liquid-solid mass transfer.

The results of the gas-liquid mass transfer resistance and the slope encourage the assumption of external mass transfer independency of reactor operation mode as long as the reaction proceeds under the same agitation speed, in the same vessel equipped by the same agitator, using the same liquid volume of the same solvent and under the same temperature and pressure.

5.5. Conclusions

The mathematical model of the styrene hydrogenation in the three-phase continuous stirred tank reactor was developed and tested against experimental data. The decreasing styrene conversion over time shown experimentally was taken into account in the model by introducing an exponential catalyst loading decay model. The mass transfer coefficients which were used in the continuous flow reactor model were not experimentally calculated under continuous flow reactor mode.

Instead, the mass transfer coefficients which have been calculated in the semi-batch reactor were used by assuming that as long as one reaction proceeds under the same agitation speed, in the same vessel equipped by the same agitator, using the same solvent, the same catalyst and under the

same temperature and pressure, the external mass transfer coefficients should be independent of the operation mode of the reactor; semi-batch or continuous flow.

Evidence to support this assumption was provided by calculating the gas-liquid mass transfer resistance and the combination of the liquid-solid mass transfer resistance and the resistance due to the chemical reaction kinetics based on the simulated catalyst loading and the experimental styrene conversion. The gas-liquid mass transfer resistance in the continuous flow reactor is close enough to the corresponding resistance in the semi-batch reactor for accepting the assumption. On the other hand, regarding the sum of liquid-solid mass transfer resistance and the resistance due to the chemical reaction kinetics multiplied by the catalyst concentration, there is a higher difference between the calculated value in the CSTR and the one calculated in the semi-batch reactor A but they overlap each other when the 95% confidence intervals are taken into account. This difference might be caused by the flow rate variation which is likely to change the flow patterns in the vessel of the continuous flow reactor affecting the distribution of catalyst fine particles.

Chapter 6

6.   Trickle bed reactor, TBR

6.1.   Introduction

This chapter is dedicated to the three-phase semi-batch stirred tank reactors. It is structured in three different subsections, namely; (a) materials and methods, (b) experimental determination of mass transfer resistances and liquid hold-up and (c) modelling of the heterogeneous catalysed styrene hydrogenation.

The section 6.2 offers insights into the methodologies by which the experimental investigations, for revealing the mass transfer behaviour of trickle bed reactor, were conducted. Including the details of the design and construction of the trickle bed reactor. The experimental procedure is also described in detail.

Then, in section 6.3, the experimental results for the determination of mass transfer resistances in trickle bed reactor are critically presented once the liquid hold-up and the liquid residence time have been approximated. A new methodology, for transferring predictively the heterogeneous catalysed styrene hydrogenation from the semi-batch stirred tank reactor to the trickle bed reactor respecting the reactant regimes, is introduced. The mass transfer resistances were determined by (a) varying the palladium content of the bed and (b) using the adsorption and intrinsic reaction rate constant of the surface reaction which have been approximated in the semi-batch stirred tank reactor

(section 4.4.1). The wetting efficiency of the bed and the film thickness were also approximated.

The section 6.4 is dedicated to critically presenting the simulation of the heterogeneous hydrogenation of styrene in the TBR. As it has been mentioned in section 3.3.3, to reduce the complexity of simulating the axial dispersion of the liquid phase in the trickle bed reactor, the one-parameter Tank-In-Series model was chosen. To approximate the number of CSTRs, N, in series which simulates better the trickle bed reactor, curve fitting between the experimental and simulated concentration profiles of styrene for eight different experiments were applied and the Bodenstein number was calculated for comparison to the literature.

6.2.   Materials and methods

6.2.1.   Design and assembly of the trickle bed reactor

The trickle bed reactor system comprises the Trickle Bed Reactor (TBR) module and the gas supply/control module. Figure 6.2 depicts the layout of the trickle bed reactor system setup.

The trickle bed reactor system has been designed for performing continuous hydrogenations by flowing gas and liquid phase through the immobile solid phase. The maximum temperature in which the system operates reaches 50°C while the maximum pressure reaches 17 bars.

Reactor column

The core of the trickle bed reactor system is the stainless steel (316SS) reactor column which withstands pressure up to 137 bar and temperature up to 150°C. The column accommodates the immobile solid phase through which the gas and the liquid phase flow.

The column consists of two concentric cylinders; the inner accommodates the catalyst while the outer is the heating/cooling jacket of the reactor. Within the jacket there is a welded spiral to create rotational flow around the inner cylinder. Along the linear length of the cylinders and between the gaps which are created by spiral path there are six ports which allow the passage of thermocouples.

The top end of the reactor is equipped with two ports; the one is used as the liquid inlet and the other as the gas inlet. The bottom end is equipped with one port through which gas and liquid flow out. The catalyst is kept in place by using two removable 5 μm frit plates; one at the top, one at the bottom.

Figure 6.1 depicts a technical drawing of the reactor column given by Parr Instrument.

Liquid phase

The reactor is fed from the top with the liquid phase using an HPLC pump (R-Pump 1). There is a three-way valve which switches between the pure solvent and the substrate solution. This gives the chance for an easy and quick switching when it is needed. The liquid phase is collected in the vessel R-T3 while there are three drain points which can be used to by-pass blockages in the rig. The reactor can operate in recycle mode due to the existence of the valves R-V12 and R-V8.

The level of the trickle bed reactor is maintained by observing the level indicator and using the HPLC pump which is attached in the outlet of the reactor (R-Pump 2). The back-pressure regulator R-BPR is attached at the outlet of the HPLC pump (R-Pump 2) to ensure the system pressure does not push material through the pump. During the steady state operation, the bed

of the reactor should not be submerged in the liquid phase, consequently, the level of the liquid in the reactor column should not be higher than 9 cm from the bottom of the reactor.

The flood of the reactor is prevented by three ways:

1. The use of R-BPR

    Higher liquid level in the reactor leads to pressure increase which results in higher outflow for a set pressure at the R-BPR because the R-BPR will open to maintain the set upstream pressure.

2. The existence of the R-V6, F14 & Tank 3

    The F14 acts as an overflow which leads the liquid to the 500 ml pressurised tank 3.

3. The maximum pressure of R-Pump 1

    Setting maximum pressure of R-Pump 1 4 times the operating pressure, the pump will stop pumping liquid once the level of liquid in the reactor vessel has reached the 3/4 of the vessel height.

Gas phase

Supply and control of nitrogen and hydrogen gases is attained due to the use of the gas supply/control panel which is described later.

Hydrogen Flow

Hydrogen is supplied only at the top of the reactor (Line F6) from the gas supply/control panel. The flow of hydrogen is controlled by using the Bronkhorst mass flow controller which is located at the gas supply/control panel. The maximum flow rate through the mass flow controller is 2 nL/min.

Reverse flow of hydrogen is prevented by using check valve CV6 between MFC and V19.

The system is designed to operate as "Dead End" reactor. This means that there should be no hydrogen after the end of reactor bed. Hydrogen is flowing in a nitrogen atmosphere.

Nitrogen Flow

Nitrogen is supplied from the gas supply/control panel either at the bottom of the FBR (Lines F14 & F7) or at the top of the FBR (Line F6) passing through the MFC.

In the case of reverse flow of nitrogen in F14, nitrogen is exhausted through vent pipe in gas supply/control panel passing through the condenser and the BPR.

Temperature

The reactor temperature is maintained by using a Huber Unistat 705 air-cooled heat exchanger. The temperature is monitored by using 5 K-type thermocouples and 1 Pt100 sensor along the length of the reactor bed. The Pt100 sensor is connected to Julabo heat exchanger.

Pressure

The pressure of the trickle bed reactor system is maintained by using the back-pressure regulator (R-BPR) installed after the R-Pump 2 and the back-pressure regulator (BPR) installed in the Gas /pressure control panel. The maximum pressure of the first is 17.2 bar and this of the latter is 51 bars. Due to the use of the R-BPR the pressure of the system does not exceed 17.2 bar.

The pressure of the reactor is monitored by using the pressure transducer, R-PT1, and the pressure gauge, R-PG1.

Gas supply/control panel

The gas supply/control module supplies and controls nitrogen and hydrogen gases. Nitrogen is used for purging and pressurising the processing volumes. Hydrogen gas flowrate is controlled by using a mass flow controller, MFC. The gas supply/control module is equipped with four safety relief valves, rated at 45 bar; two connected to nitrogen stream and two connected to hydrogen stream. There are also two pressure gauges which are used for the nitrogen and hydrogen stream pressure. A flame arrestor is connected to hydrogen stream to prevent any flame propagation. The use of the back-pressure regulator, BPR, allows the regulation of the pressure to the reactor module. The pressure transduces, PT3, is used to monitor the pressure upstream the back-pressure regulator, BPR.
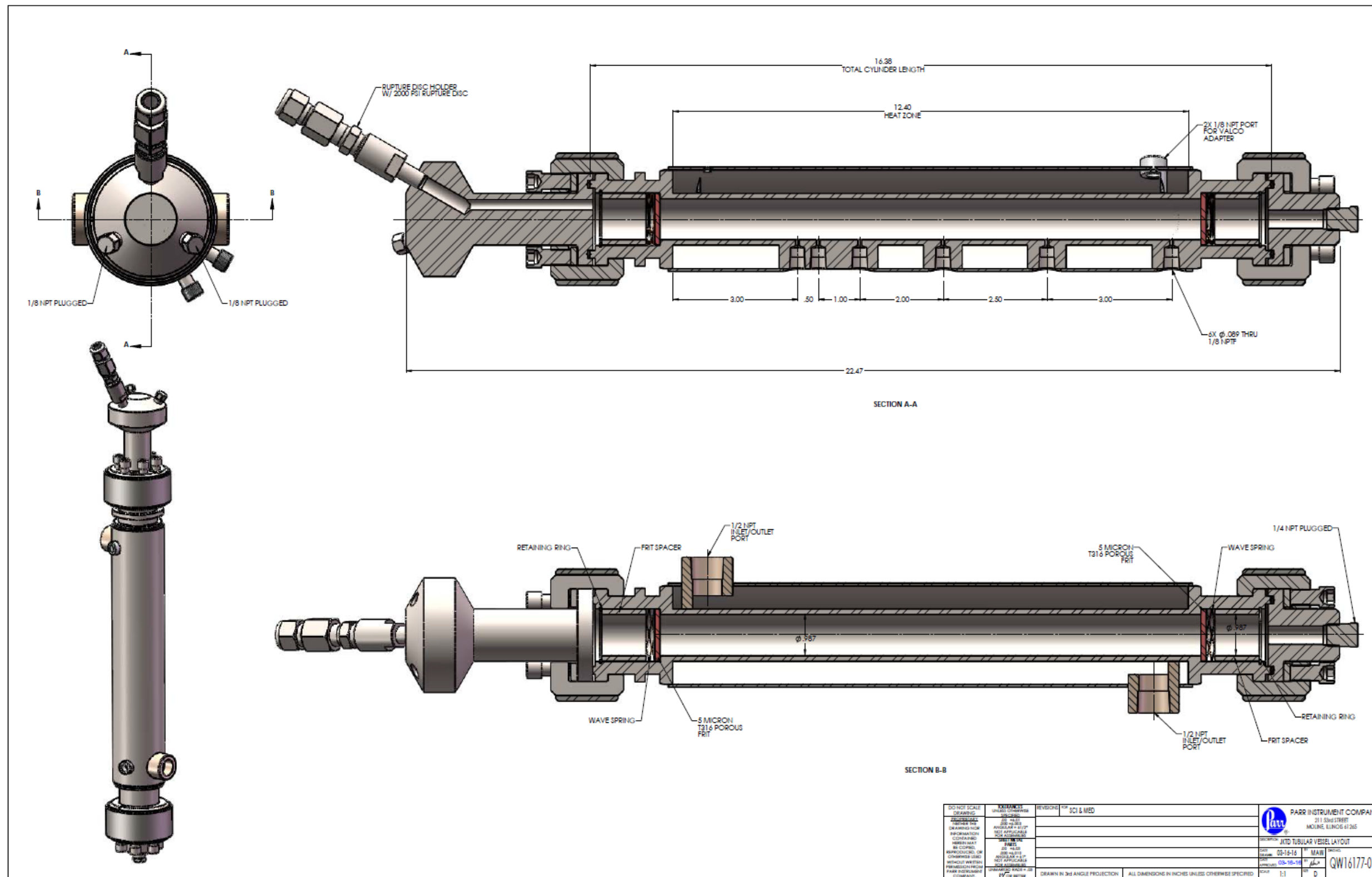
Figure 6.1: Technical drawing of the reactor column.
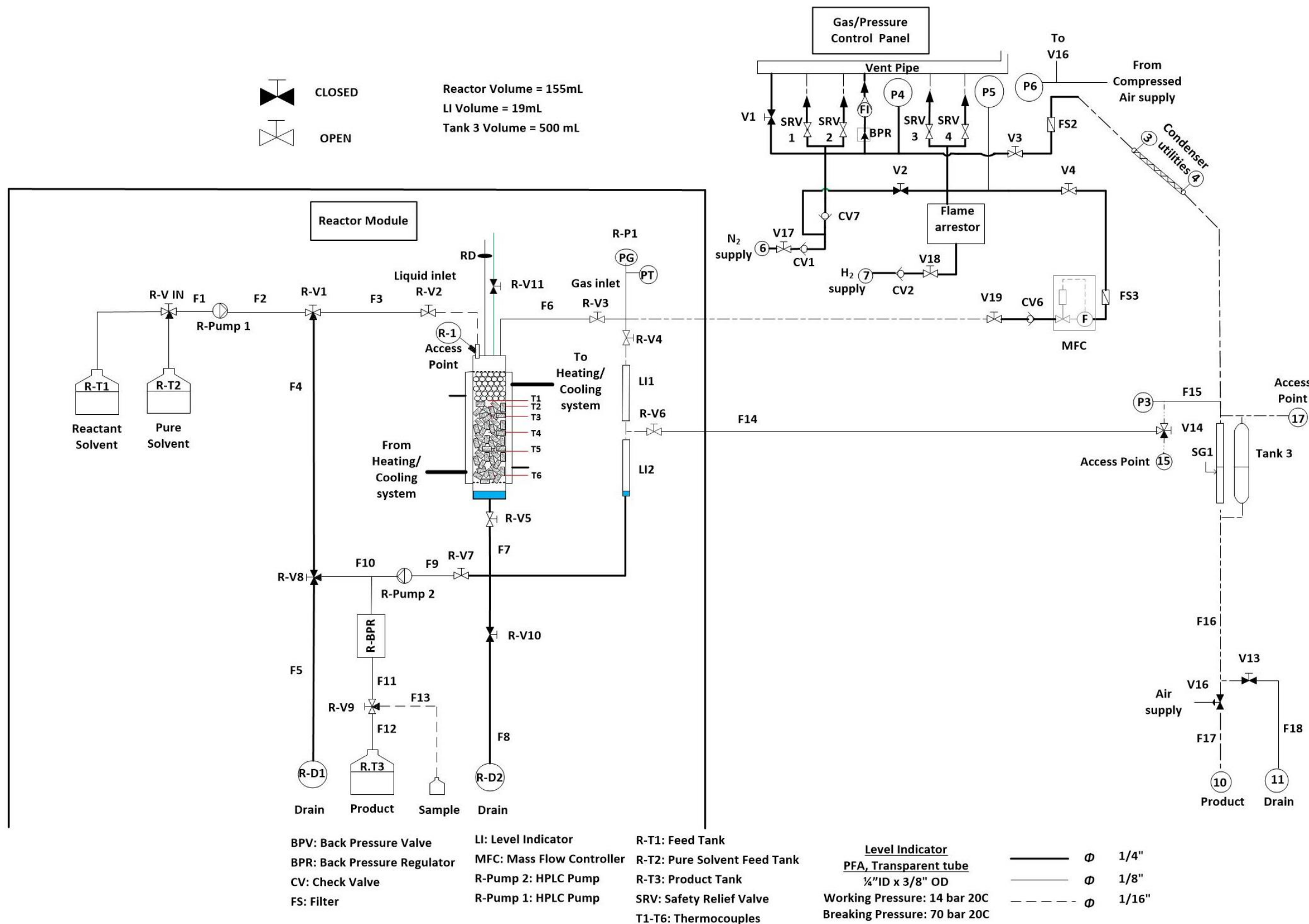
Figure 6.2: Line diagram of the trickle bed reactor rig.
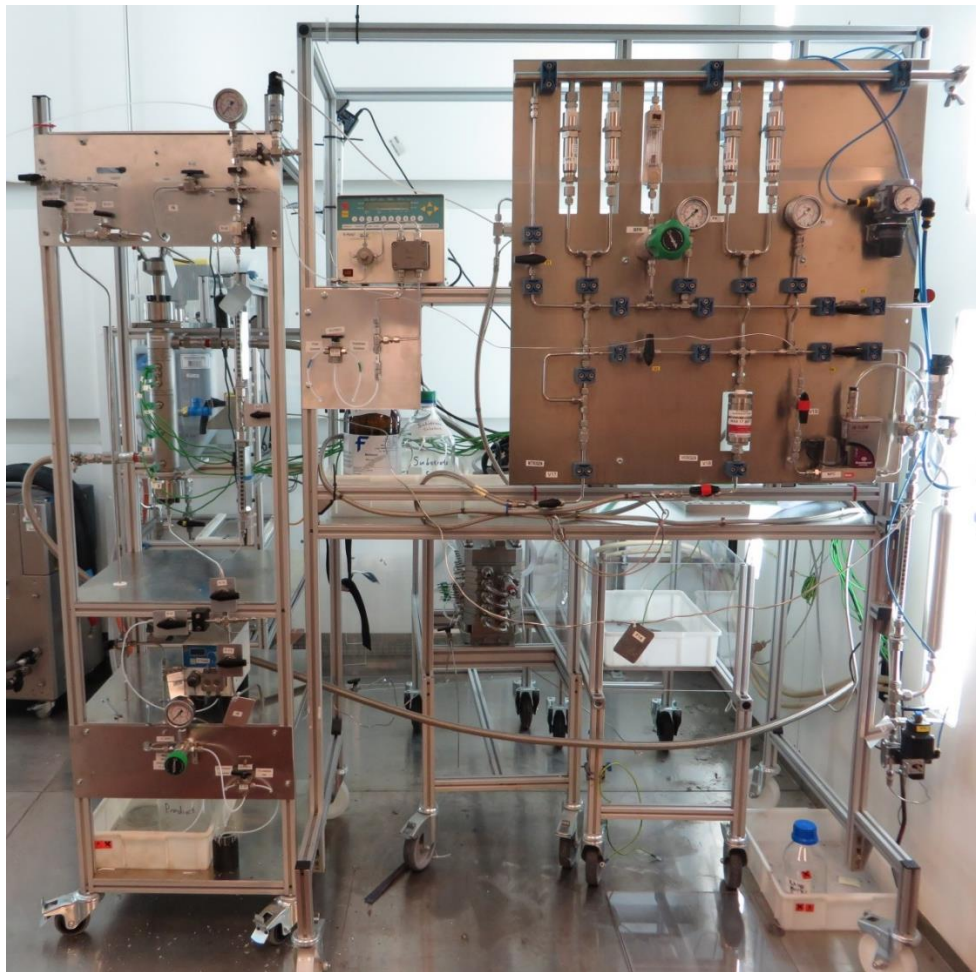
Figure 6.3: Picture of the trickle bed reactor rig.

Figure 6.4: Trickle bed reactor vessel.

6.2.2. Experimental procedure of styrene hydrogenation in the TBR

The hydrogenation of styrene was chosen as case study to investigate the mass transfer in trickle bed reactors, because of two reasons; firstly, the hydrogenation of styrene presents fast intrinsic reaction rate which allows the mass transfer to be the limiting regime even if intensive mixing conditions occur. Secondly, the same reaction was studied in the semi-batch three-phase stirred tank reactors, so the results can be compared and a methodology for transferring the process from the semi-batch stirred tank reactor to the trickle bed reactor can be developed.

Figure 4.3 presents the reaction scheme of styrene hydrogenation. All the experiments take place using methanol 99.9% (HPLC grade) as solvent, styrene 99% (without stabiliser) and decane 99% as internal standard; all of which are purchased from Sigma Aldrich. Compressed pure hydrogen (UN: 1049) is purchased from BOC, Pd/C extrudates and activated carbon supporting material are purchased from Johnson Matthey. The catalyst's palladium content was approximated at 1.25% using ICP-MS. Ballotini solid soda glass beads (diameter 2.85-3.3mm) are purchased from Sigmund Lindner GMBH. Physical properties of methanol are found in Table 4.2.

6.2.2.1. Start-up

Bed preparation-Reactor column filling

The bed of the reactor consists of (a) non-active glass beads, (b) activated carbon pellets bare of palladium and (c) 1% palladium on activated carbon pellets. For the course of this work the pellets which are coated with palladium are called "active" and the bare pellets are called "non-active".

The reactor was filled with 232g of glass beads and 2g of pellets, the ratio of active and non-active pellets (active/non-active) ranged between 3.9%-33.3%. The height of the bed was 32cm.

To achieve a well-distributed bed lengthwise the reactor column, the bed was added incrementally into the reactor column. First, 232g of glass beads and the intended for the experiment amount of active and non-active pellets were weighed. Then, the 232g of glass beads was separated to 5 equal parts. The same was done for the amounts of active and non-active pellets. Afterwards, 5 different mixtures of the same amounts of glass beads, active and non-active pellets were made and poured into the reactor column.

Once the reactor column has been filled with the glass beads, active and non-active pellets mixture, the reactor is placed at the rig.

Rig preparation-Reaction start

Once the reactor had been placed appropriately at the rig, the preparation of the rig starts following the steps:

- Nitrogen purging

  First, to ensure all air has been removed from the rig before flowing hydrogen, the system was purged with nitrogen for 5 times at 6 bara.

- Solvent flushing

  Then, while the system was under pressure (6 bara N_2), the rig was flushed with solvent, to avoid any contamination of residuals of past experiments.

- Liquid flow establishment-Cooling/heating system initialisation

  The intended for the experiment liquid flow was set in the inlet pump using pure solvent. The outlet flow and the liquid height of the reactor

column was regulated using the outlet pump. The outlet flow was measured regularly by the means of a volumetric cylinder and a stopwatch. The temperature setpoint was set and the heat exchanger was initiated.

- Hydrogen flow establishment

The mass flow controller was set at 60ml/min and the valve R-V4 was closed to constrain hydrogen to flow through the bed. Once the hydrogen had started flowing through the bed, bubbles appear in the level indicator. In this point, it is worth mentioning that the cross connection downstream the reactor had been placed in a slope which allowed gas-liquid separation; gas was flowing to stream F14 through the level indicator while liquid was flowing to product vessel forced by the outlet pump.

- Reaction initialisation

Once the temperature had been raised to 32^oC, the gas and liquid flows had been established and the catalyst had been activated by flowing hydrogen for 30 minutes, valve R-V.IN is switched to substrate solution and the valve R-V4 was opened. After that the reaction was on and the supply of hydrogen to the reactor bed is regulated by the mass transfer rate of the reaction; in other words, the reactor is operated in dead-end mode.

6.2.2.2. Operation

The followings were monitored:

- Liquid level

The liquid level in the reactor column using the level indicator.

- Pressure

  The pressure of the rig was monitored using the pressure transducers R-P1 and P3, the readings of which were recorded by LabView.

- Temperature

  Temperature monitoring was achieved by using six thermocouples installed lengthwise the reactor column. One was connected to heat exchanger and five were connected to the picometer device which had been connected to the PC. The temperature of the thermocouples connected to the picometer device were recorded in the PC.

- Concentration

  The reactor was sampled from the stream F12. Concentration monitoring was achieved off-line by analysing the samples using gas-chromatography.

6.2.2.3. Shut-down

To stop the reaction, hydrogen supply was turned off and the pure solvent was supplied by switching appropriately the valve R-V.IN. Purge with nitrogen took place to ensure the system was free of hydrogen. The system was depressurised and the reactor column was dissembled from the rig. The glass beads were separated from the pellets using appropriate sieves. The glass beads were washed and reused while the active and non-active pellets were disposed of.

A detailed SOP of the Trickle Bed Reactor is found in Appendix E.

6.2.3. Experimental procedure for the liquid hold-up determination

The draining method was used for determining the liquid hold-up in the reactor column. Briefly, according to this method, liquid should flow through the bed

and suddenly the inlet and outlet valves should be closed simultaneously. Then, the outlet valve opens and the draining liquid is collected and weighed. From this value the free-draining hold up is calculated. To calculate the stagnant hold-up due to the residual liquid in the reactor column, the column should be weighed before flowing liquid, as dry column, and after the draining. The difference between the weight of dry and wet column is used to calculate the stagnant hold-up.

To eliminate any dead time and experimental error to the determination of the liquid hold-up, related to the pipe network, the apparatus downstream the valve R-V5 was not used. For the experimental determination of the liquid hold-up, pure methanol was used. To imitate the reaction flow conditions and eliminate the risks associated with the hydrogen and pyrophoric catalyst, nitrogen, glass beads and non-active pellets were used.

The experimental procedure is described from the following steps:

1. The column was filled with 232g glass beads and 2g of non-active pellets. This constituted the dry column.

2. The dry column was weighed and the value of W_{Dry} was kept.

3. To ensure that the bed was completely wet, pure methanol was poured to the column from its top of the column until the bed was submerged to pure methanol. The bed was left in methanol for 30 minutes.

4. After 30 minutes, the column was drained. The inlet pump R-Pump 1 was initiated at 5 mL/min and valve R-V2 opened.

5. The mass flow controller was switched on, nitrogen flow was set at 60 mL/min and valve R-V3 opened.

6. Methanol and nitrogen were left to flow through the bed for 60 minutes.

7. After 60 minutes, the gas and liquid inlets valves, R-V2 and R-V3 respectively, and the outlet valve R-V5 closed simultaneously. The inlet pump and the mass flow controller were switched off.

8. The outlet valve opened again and remained open until no liquid flow was present, the draining liquid was collected and weighed. The amount of the draining liquid was used to calculate the free-draining liquid hold-up.

9. The outlet valve closes, the column was dissembled from the rig and it was weighed. The reading of the balance was the weight of the wet column, W_{wet}.

10. The difference between the weight of the wet column and the dry column was used to calculate the stagnant liquid hold-up.

The procedure was repeated twice for liquid flow rates of 5 mL/min, 10 mL/min and 20 mL/min.

6.3. Experimental determination of mass transfer resistances and liquid hold-up in TBR

6.3.1. Determination of liquid hold-up and liquid residence time

The calculation of the global mass transfer resistance requires the mass transfer rate to be known. For this reason, the calculation of the liquid phase residence time is necessary. From its definition the residence time is the time which a liquid volume spends in the reactor. For an empty column, this is calculated by dividing the volume by the flow rate. In contrast, for a column packed with porous and non-porous material the calculation of the residence becomes more complicated since the approximation of liquid volume in the reactor is not such straightforward; and it depends on the physical characteristics of the bed, the physical characteristics of the liquid and gas

phase and on the liquid and gas flow rates. For calculating the residence time by using the Equation 6.1, the liquid hold-up and the bed void need to be defined [104].

$$\tau = \frac{\varphi_b \cdot (HL_{fd} + HL_{st})}{Q_L} \cdot L_b \cdot \mathcal{S}$$ Equation 6.1

Where, τ = Residence time, [s]

φ_b = Bed void, [-]

HL_{fd}, HL_{st} = Free draining and stagnant liquid holdup, [m^3liquid/ m^3voids]

Q_L = Volumetric flow rate of liquid, [m^3liquid/s]

L_b = Length of reactor bed, [m]

$\mathcal{S}$ = Cross sectional area of the reactor, [m^2]

To define the liquid hold-up the liquid in the reactor must have been approximated experimentally by implementing the draining method which is described in section 6.2.3. To approximate the liquid in the reactor as closer as possible to the reaction conditions and in the same time to eliminate the risks associated with the hydrogen and pyrophoric catalyst, nitrogen, glass beads and non-active pellets were used. The reactions were conducted under 6 bara but the experiments for the liquid approximation in the reactor were conducted at atmospheric pressure. In this pressure range the density and viscosity of the liquid phase is considered practically constant [15].

The experimental approximation of the liquid in the reactor is conducted in three different liquid phase flow rates while the rest of experimental conditions

are the same. Specifically, temperature is 32°C, atmospheric pressure and 60 mL/min nitrogen flow.

To calculate the voids in the reactor, the volume which is occupied by the solids (i.e. volume of the bed) in the reactor needs to be calculated. This was calculated by measuring the volume displacement of a liquid when the bed is submerged in the liquid. The total weight of the active and non-active pellets was keeping constant through the experiments and because the active and non-active pellets have the same physical properties, the volume of the bed was calculated only for 232g of glass beads and 2g of non-active pellets.

Therefore, for calculating experimentally the volume of the bed, a glass volumetric cylinder was filled with methanol and the bed was poured into the same glass volumetric cylinder where it was left for 60 min. The liquid volume which was displaced was 0.095L. The volume of the bed voids was calculated by subtracting the volume of the bed from the volume of the reactor. The ratio between the volume of the bed voids and the volume of the reactor column constitutes the bed void.

The liquid hold-up and the residence time have been plotted against the liquid flow rate and the liquid in the reactor in Figure 6.5. The upper x axis which corresponds to the volume of the liquid in the reactor has been scaled taking into account its dependence on the liquid flow rate. Therefore, one can read the corresponding volume of liquid in the reactor for a certain liquid flow rate.
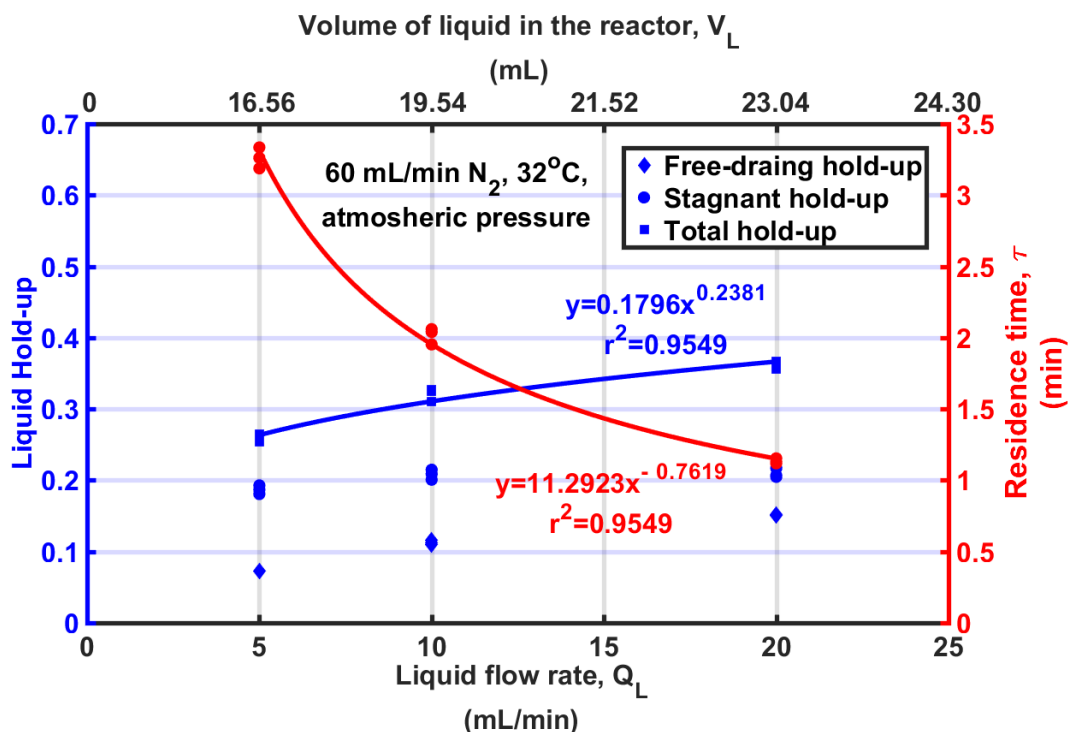
Figure 6.5: Liquid hold-up and residence time against liquid flow rate.

Table 6.1: Technical characteristics of the reactor bed for calculating the liquid hold-up.

Bed void, ϕ_b	Bed length, L_b	Bed cross-sectional area, $\mathcal{S}$
(-)	(m)	(m^2)
0.4	0.32	$4.9\cdot10^{-4}$

6.3.2. Transferring the styrene hydrogenation from the semi-batch STR to the TBR

The aim of this section is to investigate the variables which define the limiting reactant of the three-phase hydrogenation of styrene and to build a methodology for predictively transferring the three-phase reaction from the mechanically agitated reactor to the trickle bed reactor respecting the reactant regimes.

Bearing in mind the concentration profile of styrene in the semi-batch mechanically agitated reactor, it is distinguished in two different regions. In Figure 6.6 the styrene concentration in liquid (blue dots), the concentration of hydrogen in gas-liquid interface (blue squares) and the consumption rate of styrene and hydrogen (red rhombus) have been plotted with respect to time for a reaction in which the chemical reaction kinetics resistance, Ω_{R,H_2}^{STR}, is the highest. Initially, the concentration of styrene decreases linearly with respect to time. This linear behaviour indicates that the rate is independent of styrene concentration. But, after a threshold value of styrene concentration, a second region is developed where the styrene consumption rate decreases with time. Taking into account that hydrogen concentration is kept constant during the reaction, this indicates that the reaction order of styrene changes from zero to first order.
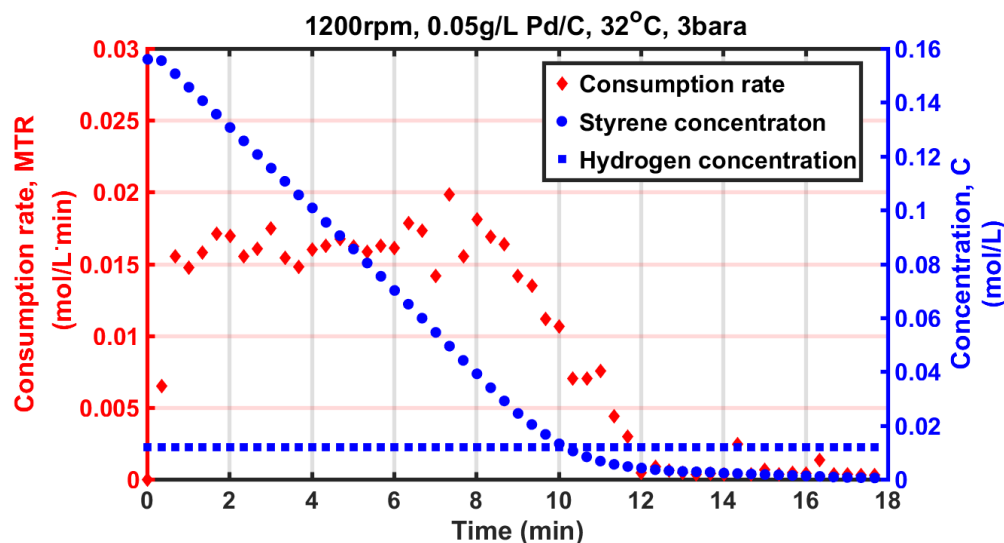
Figure 6.6: Styrene concentration profile and styrene consumption rate over reaction time.

This behaviour is explained by the Langmuir-Hinshelwood surface reaction model which has been introduced in section 2.4.3.1 and 3.2 and it is described by Equation 3.29 which is recalled bellow.

Equation 3.29:
$$R' = k_1' \cdot \frac{K_{St} \cdot C_{St,S} \cdot \sqrt{K_{H_2} \cdot C_{H_2,S}}}{\left[K_{St} \cdot C_{St,S} + \sqrt{K_{H_2} \cdot C_{H_2,S}} + K_{Eth} \cdot C_{Eth,S} + 1\right]^2}$$

According to the surface reaction model, if the styrene is in excess, the terms related to the hydrogen and ethylbenzene in the denominator become negligible. The concentration of styrene at the outer surface of the catalyst is considered constant and equal to the mean value between the initial and final concentration of the linear part of the styrene concentration profile. Practically, in this case, the surface reaction is expressed by Equation 3.30 which is recalled from section 3.2. Based on Equation 3.30, the reaction rate depends linearly on the square root of hydrogen concentration and reversely on the styrene concentration.

Equation 3.3:
$$R' = k_1' \cdot \frac{\sqrt{K_{H_2}}}{K_{St} \cdot \overline{C_{St,S}}} \cdot \sqrt{C_{H_2,S}} = k_{obs}' \cdot \sqrt{C_{H_2,S}}$$

$$k_{obs}' = k_1' \cdot \frac{\sqrt{K_{H_2}}}{K_{St} \cdot \overline{C_{St,S}}}$$

Styrene stops being considered in excess as soon as its term in the denominator of the surface reaction model becomes lower than the hydrogen's term. The adsorption constants of hydrogen and styrene have been defined in section 4.4.1, and they are equal to 1198.22 L/mole and 126.50 L/mole, respectively. Therefore, the threshold value of styrene concentration in the liquid phase was approximated to 0.024 mole/L. The same value was graphically approximated, as the initial concentration of styrene at the curvy part of the its concentration profile in Figure 6.6.

As far as the $K_{St} \cdot C_{St,S}$ is higher than the $\sqrt{K_{H_2} \cdot C_{H_2,S}}$, the surface reaction is independent of styrene concentration and it is limited by hydrogen. On the

other hand, in the region where the $K_{St} \cdot C_{St, S}$ is lower than the $\sqrt{K_{H_2} \cdot C_{H_2, S}}$, the styrene affects the rate of the surface reaction and it becomes the limited reactant.

The hydrogenation of styrene in the trickle bed reactor was conducted by using the same catalyst as the one which was used in the mechanically agitated semi-batch reactor but on a different type of carrier. More specifically, palladium on fine particles of activated carbon was used in the mechanically agitated semi-batch reactor, while palladium on extrudates of activated carbon was used in the trickle bed reactor. Details on the catalysts characteristics are available in Appendix A.

As the same system of adsorbate and adsorbents was used in both reactors and the reactions took place under the same temperature, the adsorption constants K_{St} and K_{H_2} were assumed to be the same between the two different reactors. Therefore, if the critical variable which defines the regimes of the reaction rate is the relationship between the $K_{St} \cdot C_{St, S}$ and the $\sqrt{K_{H_2} \cdot C_{H_2, S}}$ and if the styrene concentration along the trickle bed reactor is higher than the threshold value of 0.0265 mole/L, the styrene consumption rate should be independent of the styrene concentration.

To evaluate the validity of this assumption, styrene hydrogenation was conducted in the trickle bed reactor varying the inlet concentration of styrene. Figure 6.7 presents the concentration profiles of six experiments in which the concentration of styrene along the reactor bed never decreased lower than the threshold value of 0.0265 mole/L which means that the $K_{St} \cdot C_{St, S}$ was always higher than the $\sqrt{K_{H_2} \cdot C_{H_2, S}}$.
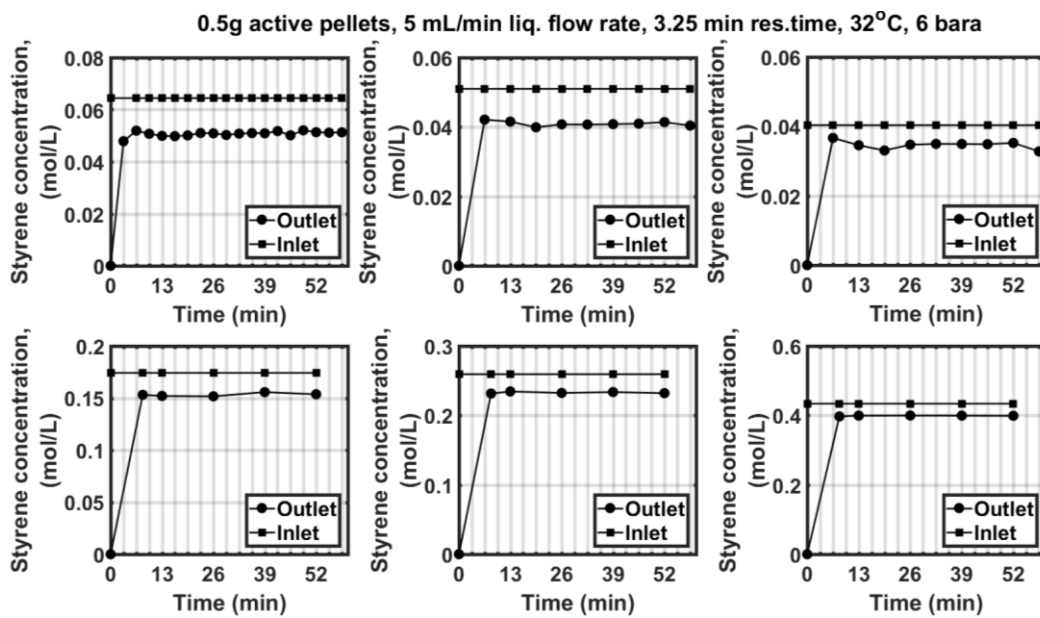
Figure 6.7: Styrene concentration profiles for six different experiments; styrene concentration higher than the threshold value of 0.023 mole/L.
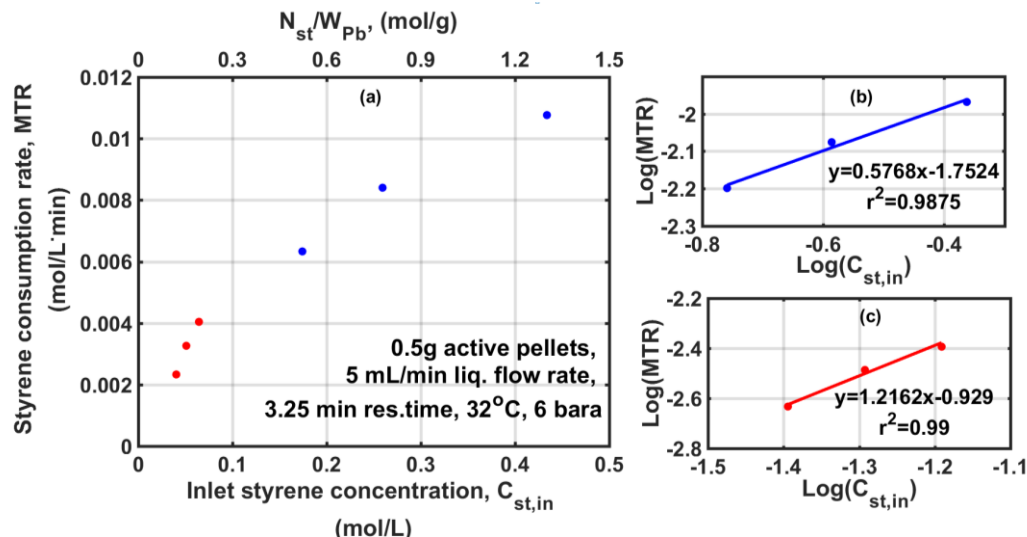
Figure 6.8: (a) Styrene consumption rate against the inlet concentration of styrene; (b) and (c) decadic logarithm of styrene consumption rate against the inlet concentration of styrene for calculating the styrene's reaction order.

The styrene consumption rates for the above six experiments have been calculated and they are presented against the initial styrene concentration in the Figure 6.8. From this figure one ascertains that the consumption rate depends on the initial concentration of styrene, although it is higher than the threshold value. To calculate the reaction order of styrene, the decadic

logarithm of the consumption rate and the initial styrene concentration were calculated; and linear regression on the data was applied. The trend between the consumption rate of styrene and its initial concentration in Figure 6.8a indicates that the reaction order changes. For this reason, the data was separated into two sets. The results of the linear regression of each data set are presented in plots b and c of Figure 6.8. The slopes of the models correspond to the reaction order of styrene.

To summarise, the assumption that the relationship between the $K_{St} \cdot C_{St,s}$ and the $\sqrt{K_{H_2} \cdot C_{H_2,s}}$ is the critical variable which defines the regimes of the reaction is invalid, since the initial concentration of styrene affects the consumption rate, although, the $K_{St} \cdot C_{St,s}$ is kept higher than the $\sqrt{K_{H_2} \cdot C_{H_2,s}}$ along the reactor bed.

The consumption rate of styrene of the same reaction which has been presented in Figure 6.6 is plotted against the styrene concentration with respect to the palladium content, N_{st}/W_{Pd}, in Figure 6.9. The content of palladium in the reactor is constant for the course of one reaction, so the higher ratios correspond to the beginning of the reaction when the molar amount of styrene is higher. As it is expected, the consumption rate is constant as far as the ratio, N_{st}/W_{Pd}, is higher than a threshold value. For values lower than 12.65 mole styrene/ g Pd, the consumption rate of styrene starts being affected of N_{st}/W_{Pd}.
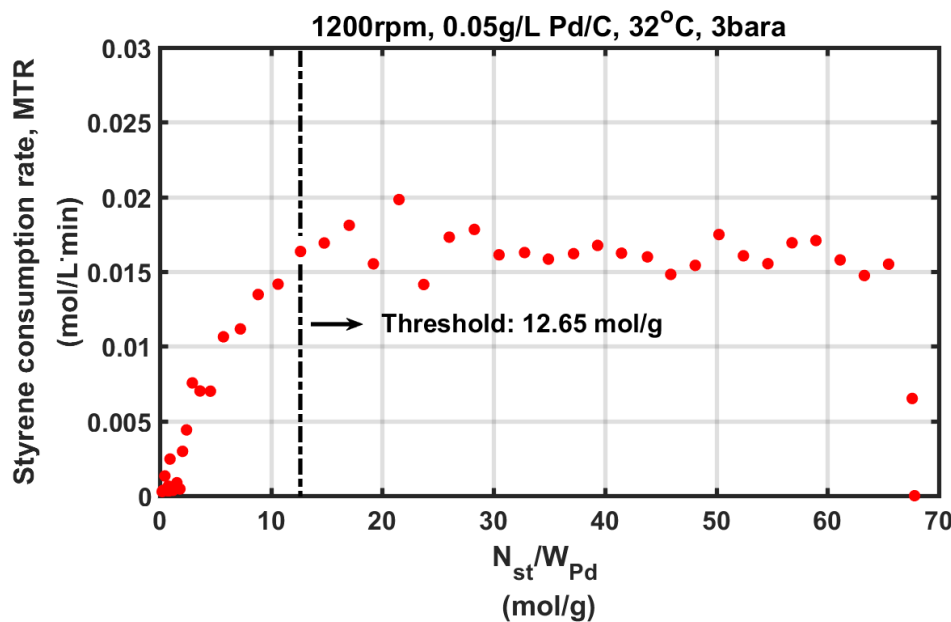
Figure 6.9: Styrene consumption rate in the semi-batch STR against the molar amount of styrene per mass of catalyst active phase, N_{st}/W_{Pd}.

The significance of the styrene concentration with respect to the palladium content, N_{st}/W_{Pd}, on defining the limiting reactant regime was investigated by hydrogenating styrene in the trickle bed reactor in regions lower and higher than the threshold value of N_{st}/W_{Pd}.

In detail, the reactor column was filled with 232g of glass beads, 0.125g of active pellets and 1.875g of non-active pellets. The most convenient and less time-consuming way to vary the ratio N_{st}/W_{Pd} is to change the inlet concentration of styrene without changing bed composition. This is done by injecting a known amount of styrene in the feed vessel while the reactor is under operation, creating a step change to the inlet styrene concentration. This procedure was followed two more times with different bed compositions, more specifically, by using 232g of glass beads, 0.225g of active pellets and 1.775g of non-active pellets 232g of glass beads, 0.075g of active pellets and 1.925g of non-active pellets. Figure 6.10 illustrates the concentration profile of styrene at the outlet of the reactor for the three different bed compositions.
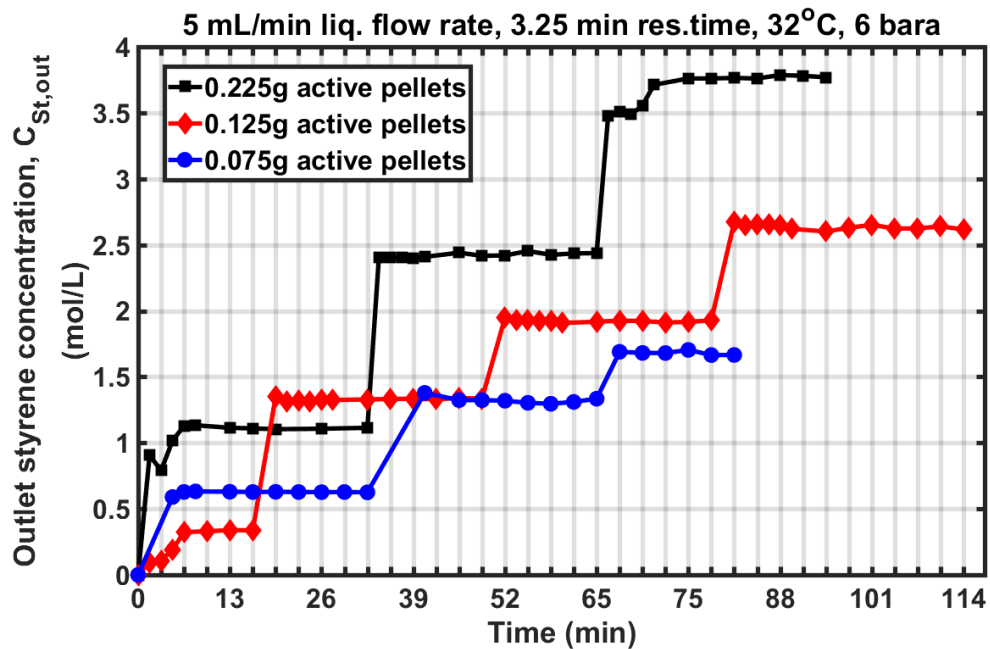
Figure 6.10: Styrene concentration at the outlet of the reactor for three different reactor bed compositions.

Then, the consumption rate and the specific consumption rates of styrene were calculated for the different inlet styrene concentrations and plotted against the styrene concentration with respect to the palladium content, N_{st}/W_{Pd}, in Figure 6.11 and Figure 6.12, respectively.

Figure 6.11 and Figure 6.12 reveal that the consumption rate of styrene reaches a plateau for all bed compositions when the N_{st}/W_{Pd} ratio is higher than the threshold value. As it has been already mentioned, the experimental procedure which was followed allowed to keep the content of palladium in the bed constant. Therefore, the consumption rate is independent of the styrene concentration and the reaction is under hydrogen regime when styrene concentration with respect to the palladium content is higher than 12.65 mole/g.
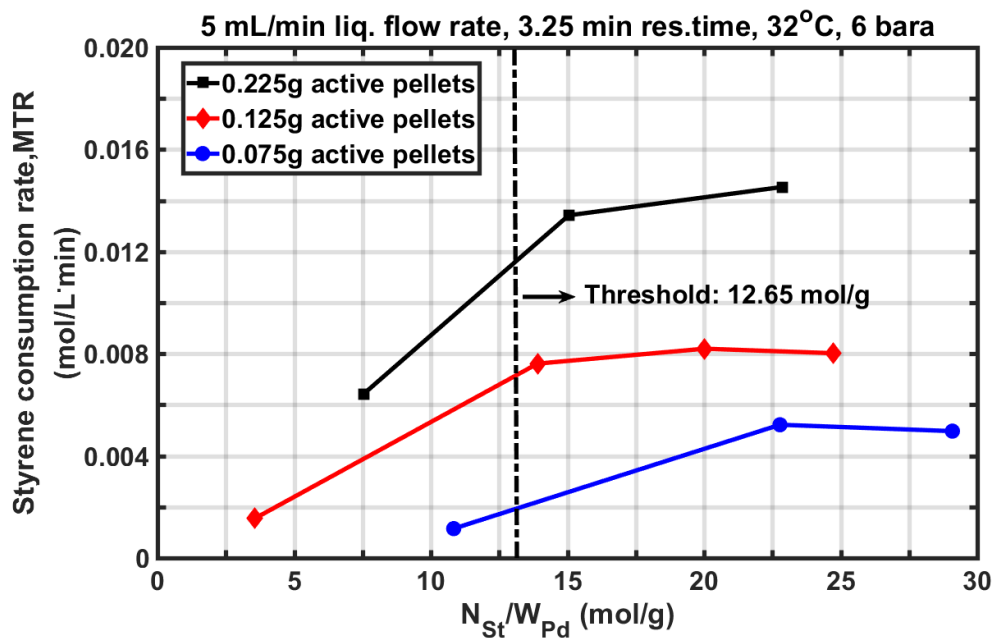
Figure 6.11: Styrene consumption rate in the trickle bed reactor against the concentration of styrene with respect to the palladium content in the reactor bed, N_{st}/W_{Pd}.
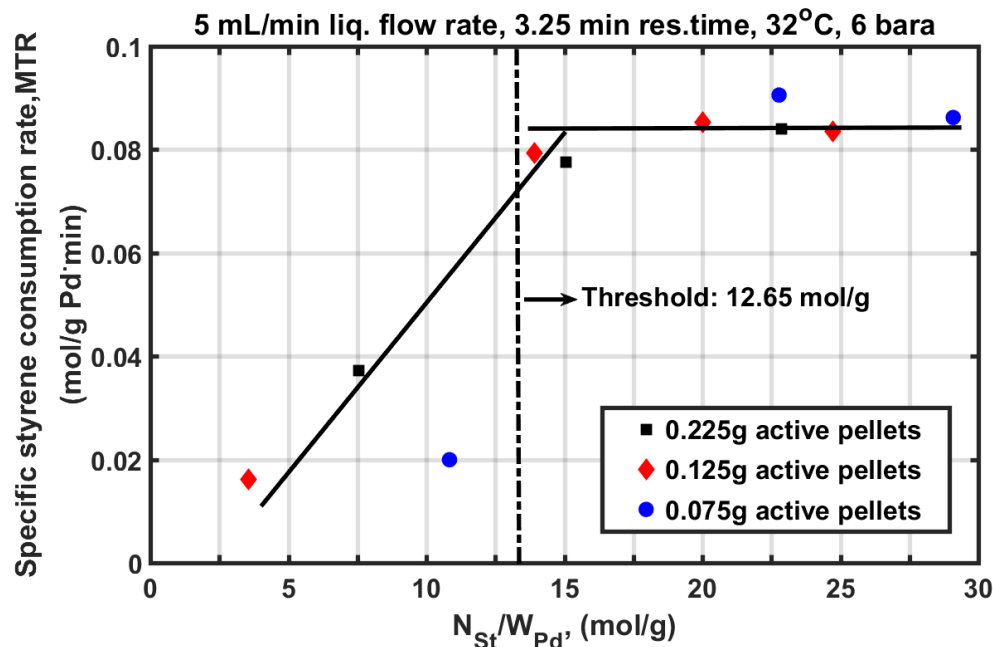
Figure 6.12: Hydrogen and styrene consumption rate per mass of palladium.against the styrene concentration with respect to palladium content.

To summarise, the physical variable which allowed to predictively transfer the

three-phase reaction from the semi-batch mechanically agitated reactor to the

trickle bed reactor conserving the reactant regimes is the concentration of styrene with respect to the palladium content. The three-phase reaction was found to be under hydrogen regime when the concentration of styrene with respect to the palladium content is higher than the threshold value of Nst/WPd independently of which reactor is used. So, if the reactant regimes have been defined in the mechanically agitated semi-batch reactor and the threshold value of styrene concentration with respect to the palladium content has been calculated, the three-phase styrene hydrogenation can be predictively transferred to the trickle bed reactor respecting the reactant regimes.

6.3.3. Determination of gas-liquid mass transfer resistance

The aim of this section is to critically present an in-situ methodology for determining the gas-liquid mass transfer resistance and the gas-liquid mass transfer coefficient in the three-phase styrene hydrogenation in the trickle bed reactor. It is an in-situ methodology because the gas-liquid mass transfer resistance is determined on the reactive system.

The global mass transfer resistance of hydrogen and substrate have been defined in section 3.1.2 and they are given by Equation 3.22 and 3.25, respectively. To determine the gas-liquid mass transfer resistance, the reaction needs to be limited by hydrogen, so the global mass transfer resistance is expressed by Equation 3.22.

To calculate experimentally the global mass transfer resistance the first expression of Equation 3.22 should be recalled.

$$\Omega_{H_2,tot}^{TBR} = \frac{C_{H_2,i}}{MTR_{H_2}^{TBR}}$$

Experimentally, the mass transfer rate of hydrogen is calculated based on styrene consumption rate which is defined by Equation 6.2.

$$MTR_{H_2}^{TBR} = MTR_{St}^{TBR} = \frac{C_{St,out} - C_{St,in}}{\tau}$$

Equation 6.2

Regarding the concentration of hydrogen, it is expressed as the molar amount of hydrogen dissolved in methanol per volume of liquid in the bed. The Henry's constant, which was calculated from Equation 4.2, was used to approximate the dissolved molar amount of hydrogen in methanol. The amount of liquid in the reactor varies with the liquid flow rate and it has been experimentally approximated in section 6.2.2.1, presented in Figure 6.5.

Under the range of pressure and temperature under which the experiments were conducted, the Henry constant, H_E, is calculated by the correlation which is described by Equation 4.2 and it is rewritten for reader ease below [74].

$$Ln(H_E) = 122.3 - \frac{4815.6}{T} - 17.5 \cdot Ln(T) + 1.4 \cdot 10^{-7} \cdot P_{H_2}$$

The global mass transfer resistance of hydrogen consists of three different components: (a) the gas-liquid mass transfer resistance, (b) the liquid-solid mass transfer resistance and (c) the resistance related to the intrinsic chemical reaction kinetics. Taking into account the expression of each component, the global mass transfer resistance is given from the extension of Equation 3.22 which have been interpreted in section 3.1.2 and it is rewritten below.

$$\Omega_{H_2,tot}^{TBR} = \frac{C_{H_2,i}}{MTR_{H_2}^{TBR}} = \frac{1}{k_L \cdot \alpha_{bed} \cdot f} + \left[\frac{1}{k_{s,H_2} \cdot \alpha_{act.pel}'^{Pd} \cdot f} + \frac{1}{\varepsilon \cdot k_{obs,1^{st}order}' \cdot f} \right] \cdot \frac{V_L}{W_{Pd}}$$

The weight of the bed, W_{bed}, is comprised of the weight of (a) the glass beads, (b) the active pellets and (c) the non-active pellets. The use of active and non-active pellets with the same physical characteristics allowed the change the palladium content of the bed while the rest of the bed characteristics were kept the same. This is important because the constant overall volume and weight of the bed gave the opportunity to keep the liquid flow rate constant for all the experiments for obtaining the same residence time. Taking into account that the gas-liquid mass transfer resistance depends on the mixing conditions and on flow patterns which are strongly affected by the liquid flow rate, the use of one liquid flow rate and the unchanged bed physical characteristics become crucial for the determination of the gas-liquid mass transfer resistance.

Table 6.2: Summary of the bed characteristics.

Bed Composition			Palladium content, W_{Pd} (g Pd)
Glass beads, (g)	Active pellets, (g)	Non-active pellets, (g)	
232	0.075	1.925	$0.94 \cdot 10^{-3}$
232	0.125	1.875	$1.56 \cdot 10^{-3}$
232	0.225	1.775	$2.81 \cdot 10^{-3}$

To change the palladium content in the bed, W_{Pd}, the ratio between active and non-active pellets was varying while their total weight was keeping constant. The compositions of the bed, the volume of the bed and the bed activities which were used at the experiments for determining the gas-liquid mass

transfer resistance are presented in Table 6.2Table 6.2: Summary of the bed characteristics..

To evaluate the dependence of reaction rate on the catalyst loading, the consumption rates corresponded to the hydrogen's reaction regime have been plotted in Figure 6.14 against (i) the palladium content of the bed and (ii) the weight of active pellets in the bed. At the left y axis, the consumption rate is expressed in molar amount per minute while at the right axis of the same figure the consumption rate has been divided by the total weight of the bed. As it was expected, the reaction rate depends linearly on the catalyst loading.
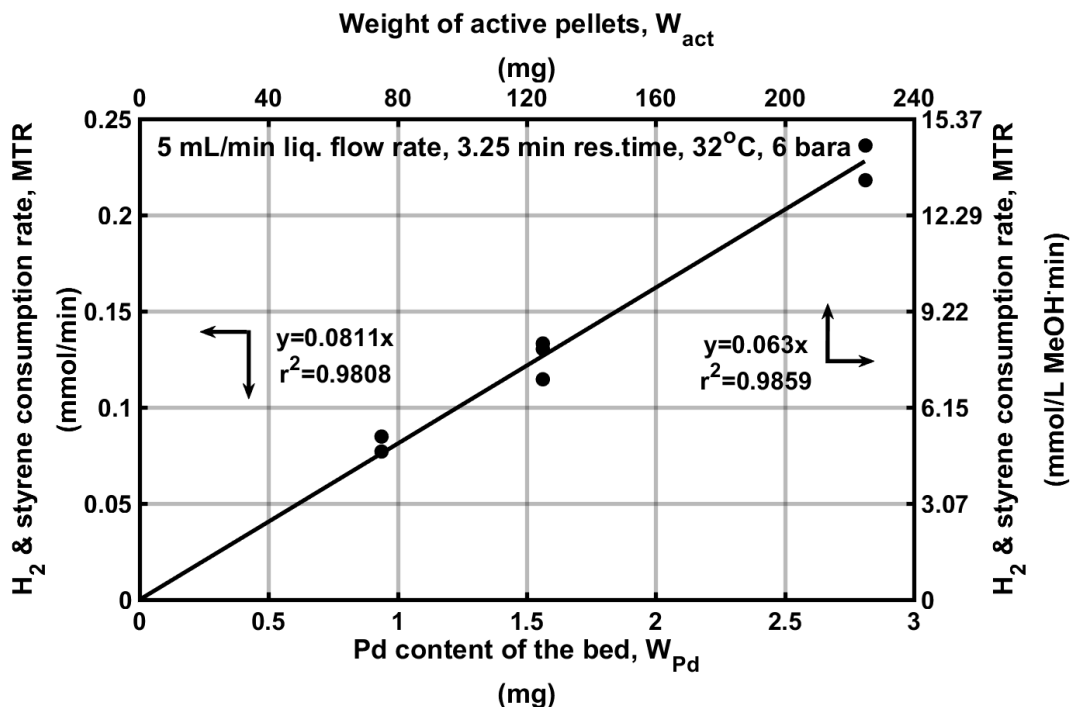
Figure 6.13: Consumption rate under hydrogen's reaction regime against the weight of the active pellets and palladium content of the bed.

If one observes the mass transfer rate of hydrogen, $\mathrm{MTR}_{\mathrm{H_2}}^{\mathrm{TBR}}$, using different palladium content in the bed, W_{Pd}, but under the same liquid flow rate, pressure, temperature and overall bed weight; and plots the $\Omega_{\mathrm{H_2,tot}}^{\mathrm{TBR}}$ against $V_{\mathrm{L}}/W_{\mathrm{Pd}}$, then the intercept of the plot is equal to the $1/K_{\mathrm{L}} \cdot \alpha_{\mathrm{p}} \cdot f$. Table 6.3

summarises the experimental conditions for determining the gas-liquid mass transfer resistance.

Table 6.3: Experimental conditions for determining the gas-liquid mass transfer resistance.

Variable	Value
Liquid flow rate, (L/min)	$5 \cdot 10^{-3}$
Residence time, (min)	3.25
Liquid in the reactor, (L)	$16.27 \cdot 10^{-3}$
Pressure, (bara)	6
Temperature, (°C)	32
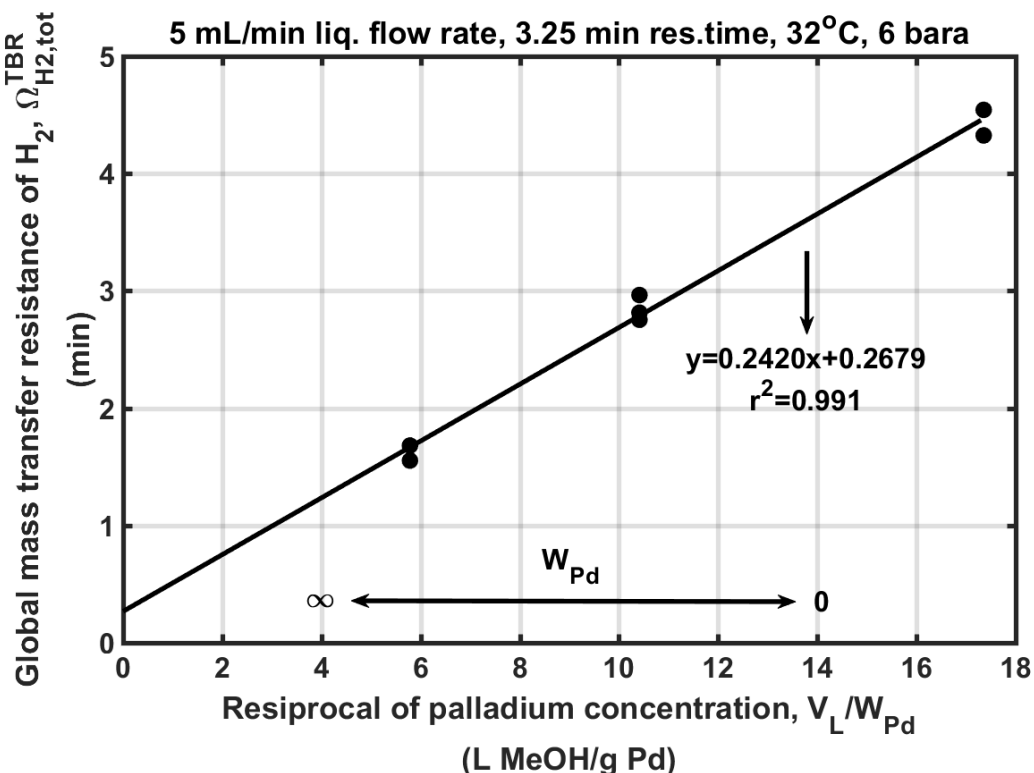
Figure 6.14: Global mass transfer resistance of hydrogen in the TBR against the reciprocal of palladium concentration.

Figure 6.14 illustrates the plot of the global mass transfer resistance of hydrogen against the reciprocal of the palladium concentration. After applying linear regression on the data, the intercept, the slope and their 95% confidence intervals have been calculated and presented in Table 6.4.

Table 6.4: Summary of linear regression model between $\Omega_{H_2,tot}^{TBR}$ and V_L/W_{Pd}.

Intercept		Slope	
(**min**)		(**min·g Pd/L MeOH**)	
$\Omega_{H_2,i-L}^{TBR} = \dfrac{1}{k_L \cdot \alpha_{bed} \cdot f}$		$\dfrac{1}{k_{s,H_2} \cdot \alpha_{Act.pel}'^{Pd} \cdot f} + \dfrac{1}{\varepsilon \cdot k_{obs,1^{st}order}'^{Pd} \cdot f}$	
Value	**95% confidence interval**	**Value**	**95% confidence interval**
0.2679	±0.1169	0.2420	±0.0265

Specific effective gas-liquid mass transfer coefficient calculation

The external surface area of the bed per volume of the bed, α_{bed}, was approximated as it is necessary to calculate the specific gas-liquid mass transfer coefficient, k_L, from the value of the intercept. The external surface area of the bed corresponds to the external surface area created by the glass beads.

The proportion of pellets to glass beads in the bed is about 4%. This means that methanol and hydrogen meet four pellets every hundred glass beads, therefore, it is likely the solvent to have been saturated with hydrogen before they come in contact on the pellets. Consequently, the gas-liquid mass transfer was assumed that took place on the interfacial area developed by the

glass beads and the external surface area created by the pellets did not contribute in the interfacial area for gas-liquid mass transfer.

Table 6.5: Characteristics of the glass beads and pellets in the bed, (r=radius and L=length); external surface area of the pellets without considering the pores.

	Glass bead	Pellet
Shape	Sphere	Cylinder
Dimensions, (m)	$r=3.075 \cdot 10^{-3}$	$r=1.98 \cdot 10^{-3}$ $L=3.20 \cdot 10^{-3}$
External surface area, (m²)	$2.971 \cdot 10^{-5}$	$2.976 \cdot 10^{-5}$
Number in the bed	6517	276
Average weight, (g)	0.0356	0.00725

First, the external surface area of one glass bead was calculated and it was multiplied by the total number of glass beads in the bed. The number of the glass beads in the bed was approximated by dividing the total weight of the glass beads in the bed by the average weight of a single glass bead. The number of the pellets in the column was also approximated by following the same procedure.

Since, the external surface area of the pellets did not contribute to the gas-liquid mass transfer, the gas-liquid mass transfer coefficient was calculated by taking into account only the external surface area developed by the glass beads. Table 6.6 summarises the calculated values of the gas-liquid mass

transfer coefficient and the external surface area of the bed per unit volume of the bed which contributes to the gas-liquid mass transfer.

Table 6.6: External surface area of the bed and experimental gas-liquid mass transfer coefficient.

External surface area of the bed, α_{bed} $\left(\dfrac{m^2 bed}{m^3 bed}\right)$	Specific effective gas-liquid mass transfer coefficient, $k_L \cdot f$ (m/s)
2038	$3 \cdot 10^{-5}$

Comparison to the literature

Gas-liquid mass transfer coefficients of trickle bed reactors, calculated by different researchers, using different fluids and beds were found in the literature. Due the variety of experimental conditions and technical characteristics among the found works, the mass transfer coefficients were compared by means of the Reynolds number. For this reason, the liquid Reynolds number of each was calculated and found to be between 0.46 and 23.89. Details of the experimental conditions of each work are summarised in Table 6.7. Then, all the available values of the gas-liquid mass transfer coefficient including the one of this work were plotted against the Reynolds number (Figure 6.15). The calculated value of our work fits well to the others' data. The gas-liquid mass transfer coefficient depends linearly on the $Re^{-0.5942}$ which is very close to the well-known correlation (Equation 6.3) of Gupta and Thodos [105] for the heat and mass transfer in beds of spheres with a bed porosity between 0.444 and 0.778.

$$\phi_b \cdot Sh_L = \phi_b \cdot \frac{k_L \cdot d_p}{D} = 2.05 \cdot Re^{-0.575} \qquad \text{Equation 6.3}$$

$$Re_L^{GB} = \frac{d_p \cdot U_L}{\mu_L} \qquad \text{Equation 6.4}$$
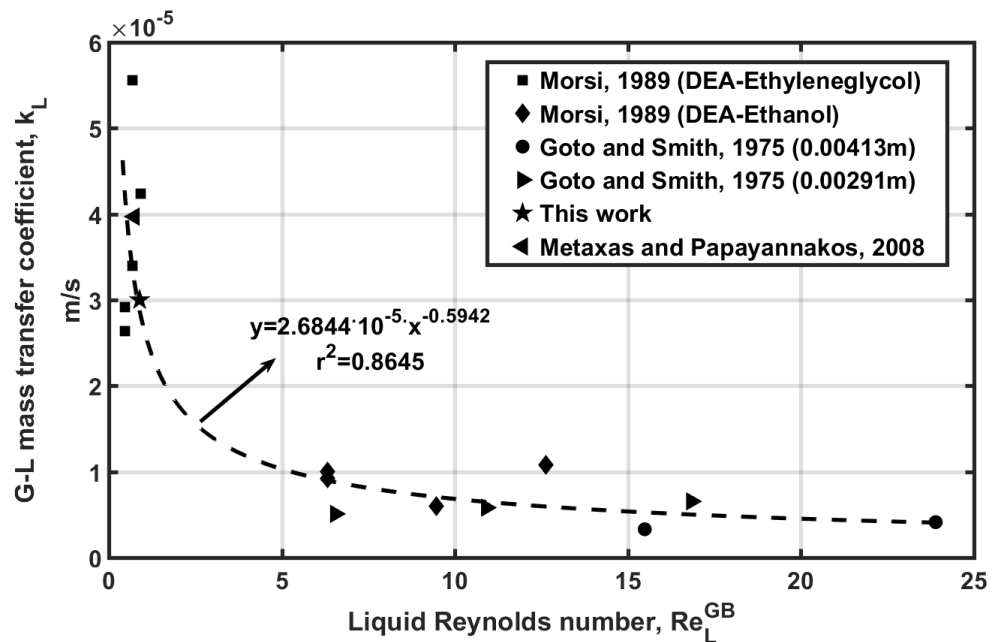
Figure 6.15: Gas-liquid mass transfer coefficient against liquid Reynolds number for different works.

Table 6.7: Summary of experimental conditions and characteristics of the beds of different works on k_L approximation.

	Liquid	Gas	Packing	Superficial liquid velocity	Bed technical characteristics	Technique
				m/s		
Morsi [106]	DEA-ETH DEA-ETG	CO_2	d_p = 0.0024m spherical Co/Mo/Al$_2$O$_3$	$(3.7 - 9.93) \cdot 10^{-3}$	d_R = 0.05m L_R = 0.49m ϕ_b = 0.385	Absorption in combination with fast chemical reaction
Goto and Smith [107]	Water	O_2	d_p = 0.00413m (glass beads) d_p = 0.00291m (CuO·ZnO)	$(2 - 5.17) \cdot 10^{-3}$	d_R = 0.0258m L_R = 0.152m ϕ_b = 0.371 ϕ_b = 0.441	Absorption and desorption of O_2 in water
Metaxas and Papayannakos [108]	n-hexane	H_2	d_p = 0.00238m (silicon carbide)	$0.09 \cdot 10^{-3}$	d_R = 0.0254m L_R = 0.16m	Curve fitting between experimental data and reactor model
This work	Methanol	H_2	d_p = 0.003085m (glass beads)	$0.169 \cdot 10^{-3}$	d_R = 0.025m L_R = 0.32m ϕ_b = 0.4	Variation of Pd content of the bed

6.3.4. Wetting efficiency and film thickness approximation

The specific gas-liquid mass transfer coefficient was calculated by adopting the concept of the film theory which has been presented in section 2.4.1.1. Therefore, it is defined by Equation 6.5 as the ratio between the diffusion coefficient and the thickness of the stagnant film through which the mass transfer occurs.

$$k_L = \frac{\mathfrak{D}}{\delta}$$

Equation 6.5

The film thickness was estimated as the ratio between the overall liquid hold-up and the external surface area of the bed per unit volume of the bed, α_p''' [109]. If the bed is not completely wetted, the liquid is distributed in a smaller surface area resulting in thicker film. The film thickness for a completely wetted bed is given by Equation 6.6.

Table 6.8 outlines the diffusion coefficient of hydrogen in methanol, the external surface area of the bed per unit volume of the bed, the liquid hold-up and the calculated values of the film thickness and the mass transfer coefficient.

$$\delta = \frac{HL_{fd} + HL_{st}}{\alpha_{bed}}$$

Equation 6.6

Table 6.8: Summary of gas-liquid mass transfer coefficient theoretical calculation

Diffusion coefficient, [73], $\mathfrak{D}$	Overall liquid hold-up, $HL_{fd}+HL_{st}$	External surface area per volume, α_{bed}	Film thickness (f=1),δ	G-L mass transfer coefficient, k_L
(m^2/s)	$\left(\dfrac{m^3\ liquid}{m^3\ bed\ voids}\right)$	$\left(\dfrac{m^2\ bed}{m^3\ bed}\right)$	(m)	(m/s)
$1.017{\cdot}10^{-8}$	0.259	2038	$0.163{\cdot}10^{-3}$	$6.24{\cdot}10^{-5}$

The theoretically calculated gas-liquid mass transfer coefficient is higher than the one which was calculated from the experimental methodology described in section 6.3.3. This indicates that the bed had not been fully wetted during the reactor operation. The wetting efficiency, f, was estimated at 48% by dividing the effective value of gas-liquid mass transfer coefficient by the theoretical one. Therefore, the actual thickness of the film at the gas-liquid interface is 48% thicker and equal to $0.339{\cdot}10^{-3}$m, since the liquid volume was distributed in a smaller surface area. The film thickness is about the 11% of the characteristic length of the glass beads.

Table 6.9: Wetting efficiency and film thickness considering the wetting efficiency.

Wetting Efficiency, f	Actual film thickness, δ_{actual}
(-)	(m)
48%	$0.339{\cdot}10^{-3}$

Comparison to the literature

To compare the calculated value of the wetting efficiency, the work of Julcour-Lebigue et al. [110] was adopted. They implemented the step injection of a coloured liquid at the inlet of a bed of adsorbing particles in combination with image processing to calculate the wetting efficiency of systems with different characteristics and under several experimental conditions. Then, they calculated the dimensionless numbers of Reynolds, Weber, Stokes, Morton, Froude and Galileo for the different conditions and they fitted their experimental data to Equation 6.7, where N is the dimensionless number. They found that using more than 3 dimensionless numbers in the correlation does not improve the optimization criteria which they used. The exponents, x_i, for different combinations of dimensionless numbers and the predicted value of the wetting efficiency of our work are presented in Table 6.10.

The lowest relative difference between the experimental and predicted wetting efficiency is 8.6% (overestimation) and it given when the Weber and Stokes numbers are used in Equation 6.7. All the combinations of dimensionless numbers overestimate the wetting efficiency, this may happen because the effect of gas velocity has not been taken into account.

$$f = 1 - \exp\left[-N_0 \cdot \Phi_b^{x_b} \cdot \prod_{i=1}^{n} N_i^{x_i}\right]$$

Equation 6.7

Table 6.10: Exponential factors of dimensional numbers taken from Julcour-Lebigue et al. [110] and predicted wetting efficiency.

N_0	x_b	Re_L	We_L	Stk_L	Mo_L	Fr_L	Ga_L	f (%)
1.581	-2.269	-0.181	0.224	0	0	0	0	54.1
0.580	-2.976	0.228	0	0	0.100	0	0	56.7
2.252	-1.583	0	0.086	0.107	0	0	0	53
0.862	-2.632	0	0.128	0	0.038	0	0	54.9
2.256	-1.777	0	0.138	0	0	0	-0.072	53.6
4.059	0.095	0	0	0.219	-0.066	0	0	58
1.986	-1.552	0	0	0	0.020	0.139	0	92.1

6.3.5. Determination of chemical reaction resistance

The resistance related to the intrinsic chemical reaction kinetics in the trickle bed reactor, Ω_{R,H_2}^{TBR} is defined by Equation 6.8.

$$\Omega_{R,H_2}^{TBR} = \frac{V_L}{W_{Pd}} \cdot \frac{1}{\varepsilon \cdot k_{obs,\,1^{st}order}^{\prime Pd} \cdot f}$$

Equation 6.8

The observed chemical reaction constant, $k_{obs,\,1^{st}order}^{\prime Pd}$, is given by the Equation 6.9 while the factor β is defined following the same manner as in section 4.3.3 and it is given by Equation 6.11 and Equation 6.12.

$$k_{obs,1^{st}order}^{\prime Pd} = k_1^{\prime Pd} \cdot \frac{\sqrt{K_{H_2}}}{K_{St} \cdot C_{St,S}} \cdot \frac{1}{\sqrt{C_{H_2\,S}}}$$

Equation 6.9

$$C_{H_2,s} = \beta_{H_2} \cdot C_{H_2,i} \qquad\qquad \text{Equation 6.10}$$

$$\beta_{H_2} = \Omega_{H_2,R}^{TBR} / \Omega_{H_2,tot}^{TBR} \qquad\qquad \text{Equation 6.11}$$

$$\sqrt{\beta_{H_2}^{TBR}} = \frac{\dfrac{1}{\varepsilon \cdot k_{obs,\,1^{st}order}^{\prime Pd} \cdot f} \cdot \dfrac{V_L}{W_{Pd}} \cdot \sqrt{C_{H_2,i}}}{\Omega_{H_2,tot}^{TBR}} \qquad\qquad \text{Equation 6.12}$$

$$k_1^{\prime Pd} = \frac{k_1'}{\begin{bmatrix} \text{Catalyst palladium content} \\ \text{in semi} - \text{batch experiments,} \\ (\text{g Pd/g cat}) \end{bmatrix}} \qquad\qquad \text{Equation 6.13}$$

The intrinsic chemical reaction constant, k_1', is independent of the physical characteristics of the system which means that it is not affected by the reactor type, as far as the chemical system is the same. Palladium on fine particles of activated carbon was used in the mechanically agitated semi-batch reactor for hydrogenating styrene, while palladium on extrudates of activated carbon was used in the trickle bed reactor for hydrogenating the same molecule. The palladium nanoparticles in both catalyst types (fine particle and extrudate) are of the same size, with a number average of 4.5 nm (Appendix A, Figure 9.8). Therefore, the intrinsic chemical reaction constant should be the same between both reactor set-ups.

Furthermore, as the same system of adsorbate and adsorbents was used in both reactors and the reactions took place under the same temperature, the adsorption constants K_{St} and K_{H_2} were assumed to be the same between the two different reactors. The intrinsic chemical reaction constant and the two adsorption constants have been approximated in section 4.4.1 and they are

presented in Table 6.11. The two adsorption constants are expressed in volume of liquid phase per mole.

The catalyst which was used in the trickle bed reactor is an eggshell type, which means that the extrudates have been coated with palladium only on their outer surface. This eliminates any resistance owing to the pore diffusion, therefore, the effectiveness factor, ε, is considered equal to unity.

Table 6.11: Summary of adsorption and intrinsic reaction constants approximated in section 3.3.2.2

K_{H_2}	K_{St}	$k_1^{'}$	$k_1^{'Pd}$
$\left(\dfrac{\text{L MeOH}}{\text{mol}}\right)$	$\left(\dfrac{\text{L MeOH}}{\text{mol}}\right)$	$\left(\dfrac{\text{mol}}{\text{g cat·s}}\right)$	$\left(\dfrac{\text{mol}}{\text{g Pd·s}}\right)$
1198.28	126.5	0.0287	0.62

To calculate the observed chemical reaction constant, k'_{obs}, the concentration of styrene at the outer catalyst surface, $C_{St,S}$, is necessary. This concentration was not feasible to be measured, so it was calculated based on the styrene concentration in the liquid phase, $C_{St,L}$, and on the factor β of styrene which is defined by Equation 6.15. The concentration of styrene at the outer surface of the catalyst is given also by solving Equation 2.60 for $C_{St,S}$ (Equation 6.17).

$$C_{St,S} = \beta_{St}^{TBR} \cdot C_{St,L}$$

Equation 6.14

$$\beta_{St}^{TBR} = \Omega_{St,R}^{TBR} / \Omega_{St,tot}^{TBR}$$

Equation 6.15

$$\Omega_{St,R}^{TBR} = \frac{V_L}{W_{Pd}} \cdot \frac{1}{\dfrac{k_1^{'Pd} \cdot \sqrt{K_{H_2}}}{K_{St}} \cdot f} \cdot \frac{C_{St,S}^2}{\sqrt{C_{H_2,S}}}$$

Equation 6.16

$$C_{St,S} = C_{St,L} - MTR_{St,L-S}^{TBR} \cdot \frac{1}{k_{S,St} \cdot \alpha'^{Pd}_{act.pel}} \cdot \frac{V_L}{W_{Pd}}$$

Equation 6.17

From Equation 6.15, Equation 6.16 and Equation 6.17 one ascertains that for high liquid concentrations of styrene, the resistance of styrene related to the intrinsic reaction kinetics is high, resulting in unity value of β factor which makes the concentration of styrene at the outer surface of the catalyst equal to its concentration in the liquid phase.

Figure 6.16 illustrates the conversion of styrene against its initial concentration in the liquid phase. The conversion for all the experiments, is lower than 2%. Consequently, the concentration of styrene in the liquid phase is assumed to be constant along the reactor bed and equal to its inlet concentration.

Table 6.12 summarises all the variables for calculating the Ω_{R,H_2}^{TBR} for each experiment.
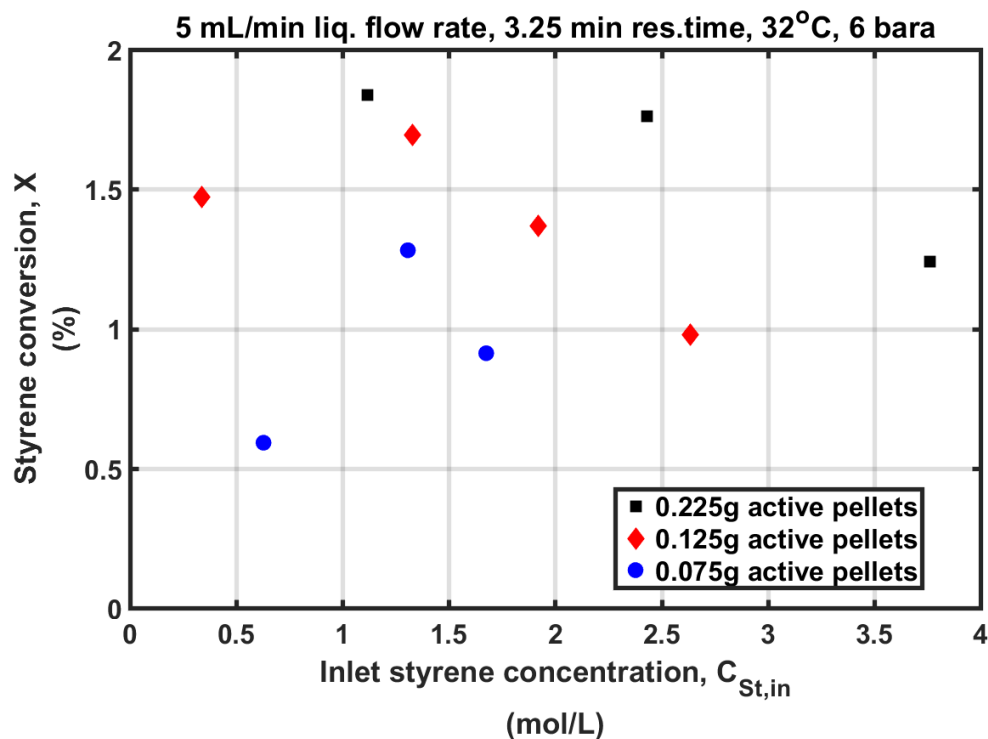
Figure 6.16: Styrene conversion against inlet styrene concentration.

Table 6.12: Summary of variables for calculating the Ω_{R,H_2}^{TBR}.

$\dfrac{V_L}{W_{Pd}}$	$C_{St,\,S}$	$C_{H_2,\,i}$	$k_{obs,\,1^{st}order}^{'Pd}$	$\sqrt{\beta_{H_2}^{TBR}}$	Ω_{R,H_2}^{TBR}
(g/L)	$\left(\dfrac{mol}{L\ Liquid}\right)$	$\left(\dfrac{mol}{L\ Liquid}\right)$	$\left(\dfrac{L\ Liquid}{g\ Pd\cdot s}\right)$	(-)	(min)
0.058	1.3248	0.0225	0.3854	0.1605	0.1125
0.058	1.6925	0.0225	0.5991	0.1953	0.1836
0.096	1.3535	0.0225	0.3522	0.1436	0.0677
0.096	1.9479	0.0225	0.7857	0.2225	0.1403
0.096	2.6605	0.0225	1.4356	0.2975	0.2620
0.173	2.4759	0.0225	1.1559	0.2574	0.1171
0.173	3.8098	0.0225	2.9632	0.4289	0.2772

Figure 6.17 depicts the chemical reaction resistance against the inlet concentration of styrene for three different palladium concentrations. Due to the competitive absorption of styrene and hydrogen on catalyst active sites, the increase of styrene concentration makes the surface reaction slower and the chemical reaction resistance higher. Experimentally, this is shown in section 3.2 in Figure 3.4. On the other hand, for similar initial concentrations of styrene, the chemical reaction resistance decreases inversely with palladium concentration since reactor bed becomes richer in active sites.
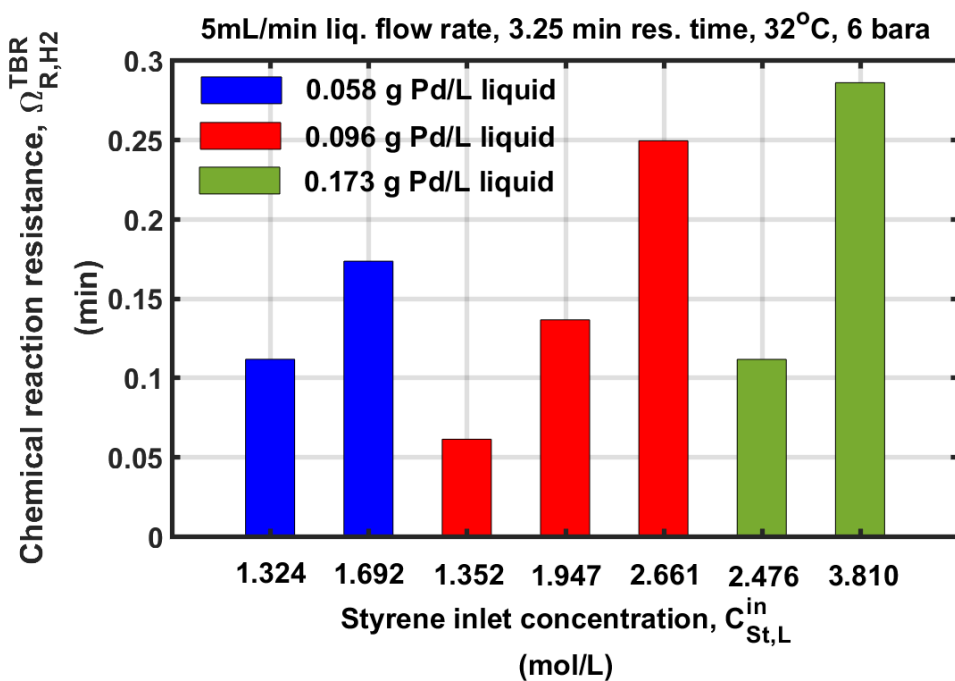
Figure 6.17: Chemical reaction resistance against the inlet concentration of styrene for different palladium concentrations.

6.3.6. Determination of liquid-solid mass transfer resistance

The liquid-solid mass transfer resistance is given by Equation 6.18 and its determination is based on (a) the gas-liquid mass transfer resistance, which has been calculated as the intercept of linear regression model between the global mass transfer resistance, Ω_{i-L,H_2}^{TBR}, and the reciprocal of the palladium concentration and (b) the chemical reaction resistance, Ω_{R,H_2}^{TBR}, which was calculated in the section 6.3.5.

$$\Omega_{L-S,H_2}^{TBR} = \Omega_{tot,H_2}^{TBR} - \Omega_{i-L,H_2}^{TBR} - \Omega_{R,H_2}^{TBR} \qquad \text{Equation 6.18}$$

Table 6.13 outlines the results of the resistances for different experimental conditions.

Table 6.13: Summary of mass transfer resistances for different experimental conditions.

$\dfrac{W_{Pd}}{V_L}$	$C_{St,\,s}$	$C_{H_2,\,i}$	$\Omega_{H_2,tot}$	$\Omega_{H_2,i\text{-}L}$	$\Omega_{H_2,R}$	$\Omega_{H_2,L\text{-}S}$
(g/L)	$\left(\dfrac{mol}{L\ Liquid}\right)$	$\left(\dfrac{mol}{L\ Liquid}\right)$	(min)	(min)	(min)	(min)
0.058	1.3248	0.0225	4.3254	0.2682	0.1125	3.9457
0.058	1.6925	0.0225	4.5433	0.2682	0.1836	4.1017
0.096	1.3535	0.0225	2.9646	0.2682	0.0677	2.6352
0.096	1.9479	0.0225	2.7536	0.2682	0.1403	2.3490
0.096	2.6605	0.0225	2.8143	0.2682	0.2620	2.2969
0.173	2.4759	0.0225	1.6816	0.2682	0.1171	1.3019
0.173	3.8098	0.0225	1.5532	0.2682	0.2772	0.9993

Specific effective liquid-solid mass transfer coefficient calculation

The external surface area of the active pellets per weight of palladium, $\alpha'^{Pd}_{act.pel}$, was approximated as it is necessary to calculate the specific liquid-solid mass transfer coefficient, k_{s,H_2}, from the value of the liquid-solid mass transfer resistance. The external surface area of one active pellet was calculated and it was multiplied by the total number of active pellets in the bed. The number of the active pellets in the bed was approximated by dividing the total weight of the active pellets in the bed by the average weight of a single active pellet. The external surface available for liquid-solid mass transfer resistance was

varying due to the need of change the palladium content in the bed by changing the weight of active pellets. Table 6.14 introduces the external surfaces area and the mean experimental liquid-solid mass transfer coefficient considering the wetting efficiency which has been estimated in section 6.3.4.

Table 6.14: External surface area of active pellets in different expressions and the mean experimental liquid-solid mass transfer coefficient.

External surface area of active pellets, $\alpha_{act.pel}$				Mean experimental liquid-solid mass transfer coefficient, k_S
Per weight of palladium	Per active pellet	Per weight of pellet	Per volume of bed	
$\left(\dfrac{m^2act.pel}{g\ Pd}\right)$	$\left(\dfrac{m^2act.pel}{act.pel}\right)$	$\left(\dfrac{m^2act.pel}{g\ act.pel}\right)$	$\left(\dfrac{m^2act.pel}{m^3bed}\right)$	(m/s)
0.3284	$2.976 \cdot 10^{-5}$	$4.1045 \cdot 10^{-3}$	3.24	$(4.72 \pm 0.56) \cdot 10^{-4}$

Correlation of liquid-solid mass transfer coefficient

To compare the obtained value of the liquid-solid mass transfer coefficient, K_s, to those available in literature, the dimensionless Sherwood, Schmidt and Reynolds numbers, Sh, Sc and Re respectively, were employed. For encountering the non-spherical shape of the pellets, the shape factor, γ, were used in the calculation of the Sherwood and Reynolds numbers. Taking into account the bed void, their expressions for a packed bed, are given by Equation 6.20, Equation 6.21 and Equation 6.22, respectively [111]. The bed void, the pellet diameter and the diffusion coefficient are referred in Table 6.1, Table 6.5 and Table 6.8, respectively. The rest of the system variables, necessary for calculating the dimensionless numbers are summarised in Table 6.15.

The Sherwood number is an indicator of the relative contribution of the convective and diffusive mass transfer. In the case of the studied system, the Sherwood number is high enough to allow the omission of the diffusive mass transfer contribution. Consequently, the most common function found in the literature to correlate the liquid-solid mass transfer coefficient, is according to Equation 5.17.

$$\frac{Sh}{Sc^{1/3}}=B \cdot Re_L^m \qquad \qquad \text{Equation 6.19}$$

$$Sh=\frac{K_s \cdot d_p}{D} \cdot \left(\frac{\phi_b}{1-\phi_b}\right) \cdot \frac{1}{\gamma} \qquad \qquad \text{Equation 6.20}$$

$$Sc=\frac{\mu_L}{\rho_L \cdot D} \qquad \qquad \text{Equation 6.21}$$

$$Re_L^p=\frac{d_p \cdot U_{sL}}{\mu_L} \cdot \left(\frac{1}{1-\phi_b}\right) \cdot \frac{1}{\gamma} \qquad \qquad \text{Equation 6.22}$$

Table 6.15: System variables for calculating Sh, Sc and Re numbers.

Shape factor, γ	Liquid		
	Dynamic viscosity [72], μ_L	Density [71], ρ_L	superficial velocity, U_L
(-)	$\left(\frac{Kg}{m \cdot s}\right)$	$\left(\frac{Kg}{m^3}\right)$	$\left(\frac{Kg}{m^2 \cdot s}\right)$
2.417	$4.98 \cdot 10^{-4}$	776.9	0.131

Table 6.16: Summary of the dimensionless numbers.

Sh	Sc	Re_L^p
(-)	(-)	(-)
24.54	63.03	0.36

To identify the factors B and m, several experimental values of liquid-solid mass transfer coefficients in a range of Reynolds number are necessary. Because in the present study, the liquid-solid mass transfer coefficient was calculated in a single Reynolds number, this is infeasible. Therefore, several correlations with different factors, reported in the literature, were tried. The one which predicts better the experimental liquid-solid mass transfer coefficient is given by Satterfield et al. [112] who studied the liquid-solid mass transfer in packed beds with downward concurrent gas-liquid flow and they reported factors B and m equal to 8.18 and 0.26, respectively. The latter agrees with Miyashita et al. [113], who studied the transport phenomena in low Reynolds numbers (<550) and reported value of exponent of Reynolds number, m, in the range between 0.11 and 0.33.

6.3.7. Summary of mass transfer resistances determination

Figure 6.18 illustrates the separated mass transfer resistances in bar chart form for different inlet styrene and palladium concentrations. The addition of active pellets in the bed benefits both; the liquid-solid mass transfer and the chemical reaction. The mass transfer of hydrogen and styrene from the liquid phase to the external surface of the catalyst takes place on the film which is developed around the active pellets. Therefore, by adding more active pellets

to increase the palladium content of the bed, the external surface area for liquid-solid mass transfer increases, resulting in lower liquid-solid mass transfer resistance. Moreover, the active pellets are carriers of palladium active sites on which the reaction occurs. Therefore, the addition of active pellets means more active sites available for being occupied by hydrogen and styrene. This makes the chemical reaction to proceed faster and the resistance related to the chemical reaction lower.
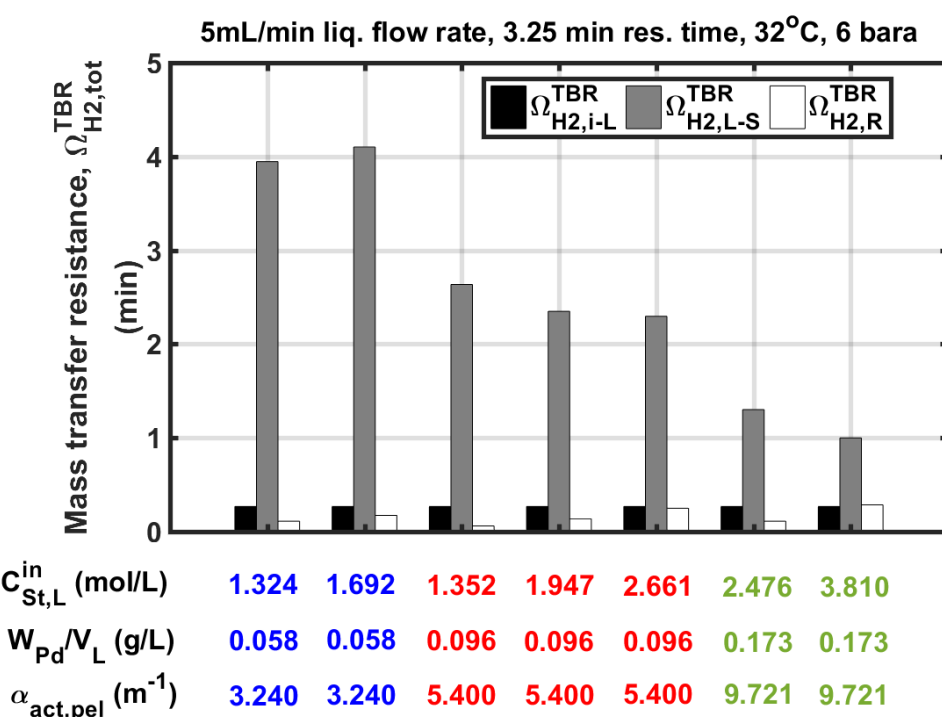
Figure 6.18: Bar chart of the mass transfer resistances for different inlet styrene concentration, palladium concentration and external surface of active pellets per volume of bed.

This becomes more coherent if the liquid to solid and the chemical reaction resistances are expressed in terms of unit pellet. Regarding the first, this is done by multiplying the reciprocals of the mean liquid-solid mass transfer coefficient and the external surface area of active pellet per active pellet (Table 6.14). To express the chemical reaction resistance in terms of unit

pellet, the reciprocal of Equation 6.9 should be used, while, the intrinsic chemical reaction rate constant, expressed per weight of palladium, needs to be substituted by the intrinsic chemical reaction rate constant, expressed per unit pellet. The chemical reaction resistance depends linearly on the inlet styrene concentration; therefore, the highest resistance corresponds to the highest inlet styrene concentration.
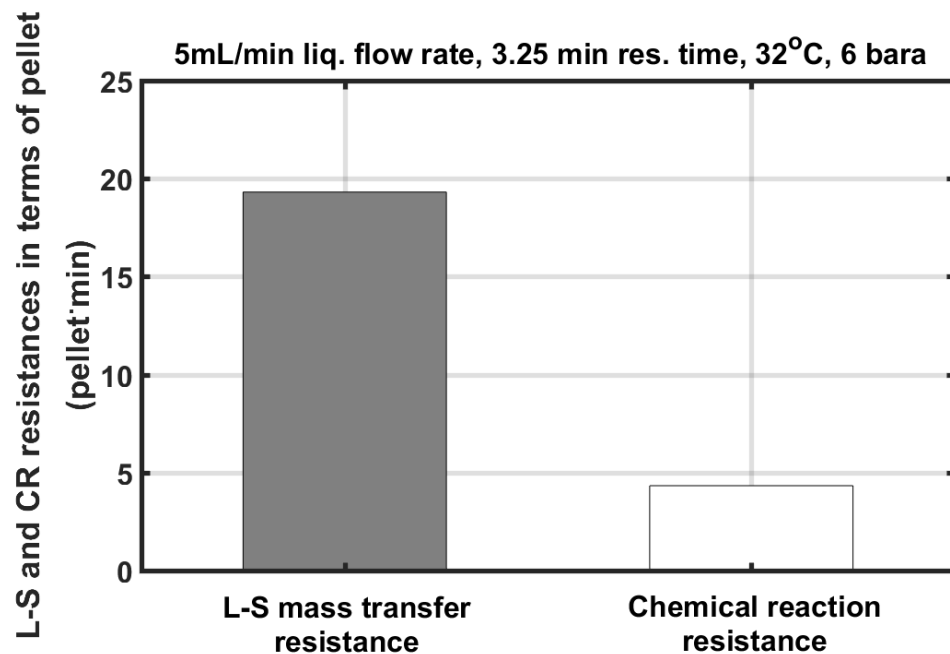

Figure 6.19: Bar chart of liquid-solid (L-S) and chemical reaction (CR) resistances expressed in terms of pellet.

Figure 6.19 presents the liquid-solid and the chemical reaction resistances in terms of unit fully wetted pellet. Even though the chemical reaction resistance has been calculated using the highest styrene inlet concentration, it is lower than the liquid-solid mass transfer resistance. Figure 6.19 indicates that one pellet provides almost 20 min resistance to the liquid-solid mass transfer while it delays less than 5 min the chemical reaction. By adding more pellets in the bed, they will reduce the corresponding resistances by their total number. For instance, if the bed contains 5 pellets the resistance to the liquid-solid mass

transfer will reduce at 4 min while the resistance to the chemical reaction will be less than 1 min.

Back again to Figure 6.18, from which one ascertains that the highest resistance of the three-phase reaction arises from the liquid-solid mass transfer. Consequently, the trickle bed reactor operated under liquid-solid mass transfer regime in all cases. To operate the reactor in the chemical reaction regime the chemical reaction resistance needs to be increased selectively. This can be achieved by employing active pellets with lower palladium content. In this case, the addition of active pellets in the bed will increase the external surface available for liquid-solid mass transfer, so its resistance will decrease. In the same time, the number of active sites in the bed will increase less comparing to their increase when higher palladium content is used. The liquid-solid mass transfer resistance could selectively decrease if the external surface area available for liquid-solid mass transfer increases by using smaller pellets. In this case, special care should be taken regarding the pressure drop rise along the bed which might lead to column flood. Finally, the chemical reaction resistance could selectively increase by increasing the reactants concentration.

6.4. Modelling of heterogeneously catalysed styrene hydrogenation

The trickle bed reactor model has been presented in section 3.3.3 and it consists of ten differential equations, each one gives the molecular balance of hydrogen, styrene and ethylbenzene in the gas, liquid and solid phase (Table 3.11). As it has been already described, the sum of material balance of each species in each phase gives the material balance for the species in the reactor. To reduce the complexity of simulating the axial dispersion of the

liquid phase in the trickle bed reactor, the one-parameter Tank-In-Series model was chosen.

The mass transfer coefficients which are used in the model have been calculated by implementing the methodology which is introduced in section 6.2. The adsorption constants of styrene, hydrogen and ethylbenzene; and the intrinsic chemical reaction rate constant which are used in the model of the TBR are the same with those which are used in the model of the semi-batch STR and they have been approximated by applying curve fitting of experimental styrene concentration profile in section 4.4.1.

Approximation of CSTRs number, N_T

To approximate the number of CSTRs, N_T, in series which simulates better the trickle bed reactor, curve fitting between the experimental and simulated concentration profiles of styrene for eight different experiments were applied. The curve fitting problem took place in the discretised search space between one and twenty CSTRs in series; and the optimum number of CSTRs in series was found to be three. The objective function is given by Equation 6.23. Figure 6.20 presents the experimental and simulated styrene concentration profiles at the trickle bed reactor outlet while the trickle reactor has been simulated by using three CSTRs in series.

$$\mathcal{F}_{obj}(N_T) = \min\left[\sum_0^t \left(C_{St,R}^{Exp}(t) - C_{St,R}^{Sim}(t)\right)^2\right] \qquad \text{Equation 6.23}$$

Where, $N_T = (1,2,3,\ldots20)$

Comparison to the literature

The trickle bed reactor performs as a sequel of three CSTRs in which perfect mixing conditions occur. To compare this finding, the number of equally sized CSTRs was calculated by Equation 6.24 using the Bodenstein number, Bo, which is the parameter of the axial dispersion model [111]. The Bodenstein number is a dimensionless number and it gives the ratio between the mass transfer due to the motion of bulk liquid, which is a result of the velocity gradients and the mass transfer due to the axial dispersion; it has been also correlated to the Reynolds number by several researchers. Given the liquid Reynolds number of the trickle bed reactor based on the glass bead diameter, which has been calculated, in section 6.3.3 by Equation 6.4, equal to 0.809, the Bodenstein number is found in the literature to range between 0.015 and 0.06 [114]. For these values of Bodenstein number, the number of CSTRs in series, N_T, is equal to two, which is not far from the approximated value from the curve fitting.

$$n = \frac{Bo^2}{2} \cdot \frac{1}{Bo - 1 + e^{-Bo}}$$
<div align="right">Equation 6.24</div>

$$Bo = \frac{U_L \cdot d_{GB}}{D_{ax}}$$
<div align="right">Equation 6.25</div>
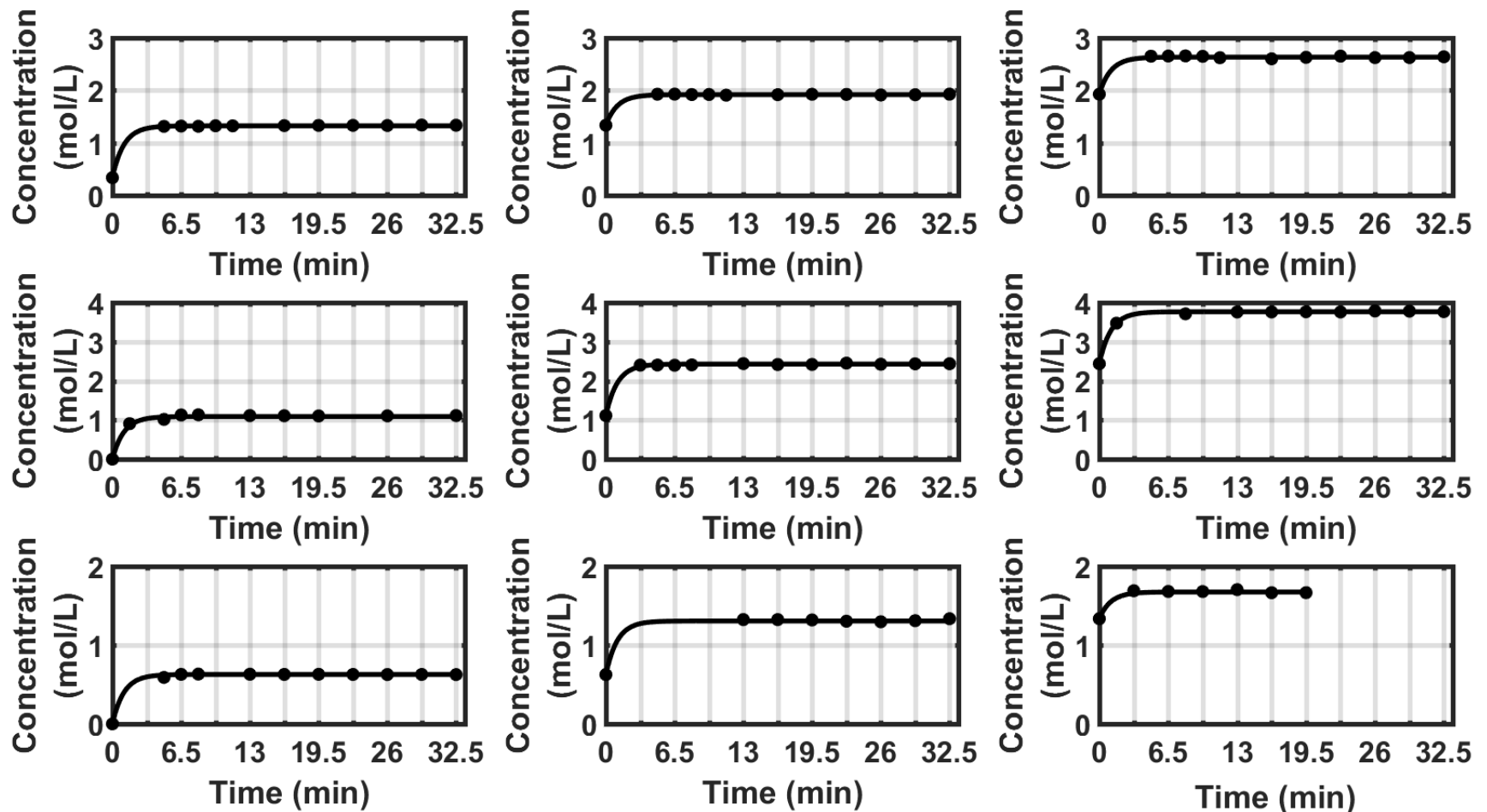
Figure 6.20: Experimental (dots) and simulated (line) styrene concentration at the TBR outlet; 5ml/min liquid flow rate, 3.25min residence time, 30°C and 6bara.

6.5.   Conclusions

The liquid hold-up and the liquid residence time were experimentally approximated using the draining method for three different liquid flow rates. The approximated value of the residence time was used for calculating the global mass transfer rate of the three-phase styrene hydrogenation in the trickle bed reactor; and the volume of the liquid in the reactor was used for calculating the reactants concentrations.

The critical variable for transferring predictively the three-phase reaction from the semi-batch stirred tank reactor to the trickle bed reactor respecting the reactant regimes was found to be the concentration of styrene with respect to the palladium content. In other words, if the reactant regimes have been defined in the mechanically agitated semi-batch reactor; and the threshold value of styrene concentration with respect to the palladium content has been calculated, the three-phase styrene hydrogenation can be predictively transferred to the trickle bed reactor respecting the reactant regimes.

The determination of the gas-liquid mass transfer resistance was based on the intercept of the plot of the global mass transfer resistance against the reciprocal of palladium concentration in the bed. To develop such a plot different bed weights of active pellets was necessary to be used without changing the mixing conditions and the flow patterns in the bed. This was achieved by (a) using active and non-active pellets with the same physical characteristics and (b) keeping their overall weight in the bed constant. The palladium content in the bed was feasible to vary by changing the ratio between the active and non-active pellets.

The specific effective gas-liquid mass transfer was calculated from the experimental value of the gas-liquid mass transfer resistance while the theoretical specific gas-liquid mass transfer coefficient was calculated based on the concept of the stagnant film theory. The theoretical value was found higher than the effective one, therefore, the wetting efficiency was considered their ratio. The thickness of the liquid film was approximated as the ratio between the overall liquid hold-up and the external surface area of the bed per unit volume.

The intrinsic chemical reaction constant and the adsorption constants was assumed to be the same as those in the semi-batch mechanically agitated reactor because the same chemical system was used in both reactor setups. Based on this assumption the chemical reaction resistance was calculated using the values of the intrinsic chemical reaction constant and the adsorption constants which had been approximated in section 4.4.1.

The liquid-solid mass transfer resistance was calculated by subtracting the gas-liquid and the chemical reaction resistances from the global mass transfer resistance. In addition, the specific liquid-solid mass transfer coefficient was calculated.

The specific effective gas-liquid mass transfer coefficient, the wetting efficiency and the specific effective liquid-solid mass transfer coefficient were found to be in agreement with some values available in the literature. This indicates that the suggested methodology for determining the mass transfer resistances of three-phase reaction in a trickle bed reactor and the wetting efficiency of the reactor bed is robust.

Chapter 7

7. Design of continuous three-phase hydrogenators

7.1. Introduction

In this chapter, an effort, to consolidate the findings of batch experimentation and those related to the continuous flow reactors (CSTR and TBR) in a methodology for designing the continuous three-phase hydrogenation, is made.

7.2. Semi-batch stirred tank reactor experimentation

The three-phase catalysed reactions present a complicated behaviour, which emanates from the combination of the physical and chemical processes which they imply. Regarding the physical processes, a three-phase reaction involves mass transfer from gas to liquid phase, from liquid to solid phase and within solid phase [15, 16]. The chemical reaction takes place on catalyst surface and involves interactions of the gas and liquid reactants with the active sites of catalyst.

As it has been shown in section 4.3.3, the term of $k_1' \cdot \sqrt{K_{H_2}}/K_{St}$ is independent of reactor setup as long as the chemical reaction takes place over the same active phase of catalyst, under the same temperature and using the same solvent. Therefore, since the semi-batch stirred tank reactor provides time-effective operation, it can be used for reaction screening and for defining this term. Once this term has been calculated in the semi-batch reactor mode, it can be used in the design equation of the continuous flow reactors; CSTR or TBR.

To calculate the term of $k_1' \cdot \sqrt{K_{H_2}}/K_{St}$ in the semi-batch stirred tank reactor, the unravelling of the effect of each individual process on the overall mass transfer rate is necessary.

First, a set of experiments under high agitation, providing intensive mixing conditions, in which the hydrogenation is performed in different catalyst concentrations, needs to be carried out. Then, the global mass transfer resistance of hydrogen, $\Omega_{H_2,tot}^{STR}$, is calculated and plotted against the reciprocal of the catalyst concentration, V_L/W_C.

For example, in Figure 7.1, the styrene hydrogenation over fine particles of Pd/C has been performed in three different catalyst concentrations, at 900 rpm, 32°C and 3 bara; and the global mass transfer resistance of hydrogen was plotted against catalyst concentration reciprocal.

Bearing in mind the expression of global mass transfer resistance of hydrogen, which has been given in section 3.1.1- rewritten below- and using the linear regression model parameters, the ratio between (a) the gas-liquid mass transfer resistance and (b) the sum of the liquid-solid and chemical reaction resistances should be calculated, as Equation 7.1 shows. To ensure the gas-liquid mass transfer resistance is not the limiting step, the $\Omega_{H_2,RATIO}^{STR}$ should be higher than unity. For the example described above, this implies that the catalyst concentration should be lower than 0.38 g/L.

$$\Omega_{H_2,tot}^{STR} = \frac{C_{H_2,i}}{MTR_{H_2}^{SR}} = \frac{1}{k_L \cdot \alpha} + \left[\frac{1}{k_{s,H_2} \cdot \alpha_s} + \frac{1}{\varepsilon \cdot k_{obs,1^{st}order}'} \right] \cdot \frac{V_L}{W_C}$$

$$\Omega_{H_2,RATIO}^{STR} = \frac{\Omega_{H_2,L-S}^{STR} + \Omega_{H_2,R}^{STR}}{\Omega_{H_2,i-L}^{STR}} = \frac{slope_{\left(\Omega_{H_2,tot}^{STR} \, vs \, V_L/W_C\right)} \cdot V_L/W_C}{Intercept_{\left(\Omega_{H_2,tot}^{STR} \, vs \, V_L/W_C\right)}} \qquad \text{Equation 7.1}$$
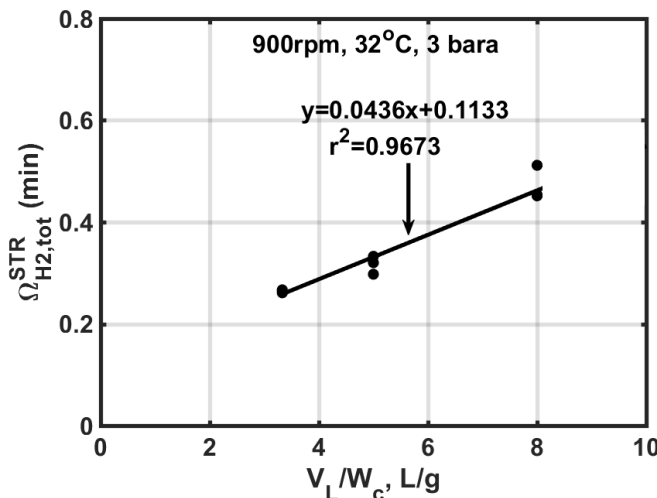
Figure 7.1: Global mass transfer resistance against the reciprocal of catalyst concentration in the semi-batch STR.

Under the same agitation speed as the one which was used in the experiments for developing Figure 7.1 and using catalyst concentration which ensures that the gas-liquid mass transfer is not the limiting step, the hydrogenation needs to be performed under different hydrogen concentrations.
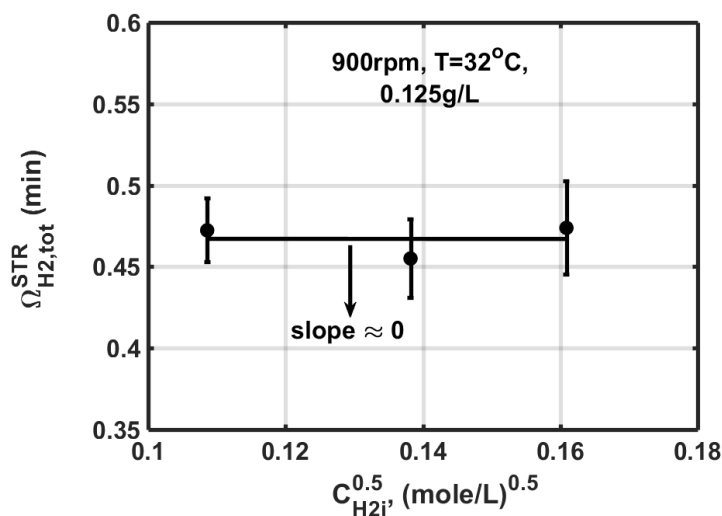

Figure 7.2: Global mass transfer resistance against the square root of hydrogen concentration in the semi-batch STR.

If the global mass transfer resistance is independent of the square root of hydrogen concentration, the liquid-solid mass transfer rate is the limiting step and the term of $k_1' \cdot \sqrt{K_{H_2}}/K_{St}$ is not possible to be calculated. This happened in the case of the example of 900 rpm, 32°C and using 0.125 g/L catalyst (Figure 7.2). In this case, the procedure needs to be repeated in a different agitation speed.

For example, in Figure 7.3, the styrene hydrogenation has been performed in three different catalyst concentrations, at 1200 rpm, 32°C and 3 bara; and the global mass transfer resistance of hydrogen was plotted against catalyst concentration reciprocal.
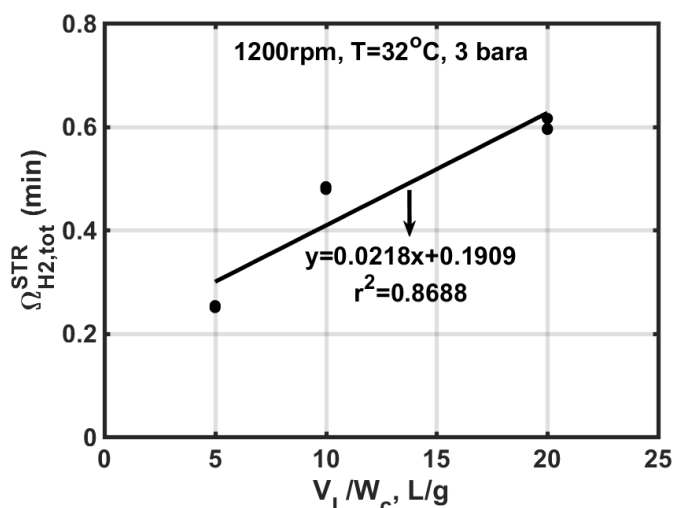

Figure 7.3: Global mass transfer resistance against the reciprocal of catalyst concentration in the semi-batch STR.

In a same manner as the example of 900 rpm, 32°C and 3 bara, to ensure the gas-liquid mass transfer resistance is not the limiting step, the $\Omega_{H_2,RATIO}^{STR}$ should be higher than unity. In the case of 1200 rpm, 32°C and 3 bara, this implies that the catalyst concentration should be lower than 0.11 g/L.

The hydrogenation of styrene was performed under different hydrogen concentrations and under 1200 rpm, 32°C using 0.05 g/L. This time, the global

mass transfer resistance depends linearly on the square root of hydrogen concentration, indicating that the chemical reaction is the limiting step and the term of $k_1' \cdot \sqrt{K_H}/K_{St}$ was calculated by Equation 7.2.

$$\frac{k_1' \cdot \sqrt{K_{H_2}}}{K_{St}} = k_{obs}' \cdot C_{St,S} = \frac{1}{slope_{\left(\Omega_{H_2,tot}^{STR} \, vs\sqrt{C_{H_2,i}}\right)}} \cdot \sqrt{\beta} \cdot \frac{V_L}{W_c} \cdot C_{St,S} \qquad \text{Equation 7.2}$$

Regarding the concentration of styrene at the outer surface of the catalyst particle, $C_{St,S}$, it was taken equal to the mean of styrene concentration in the liquid phase as far as styrene is in excess.
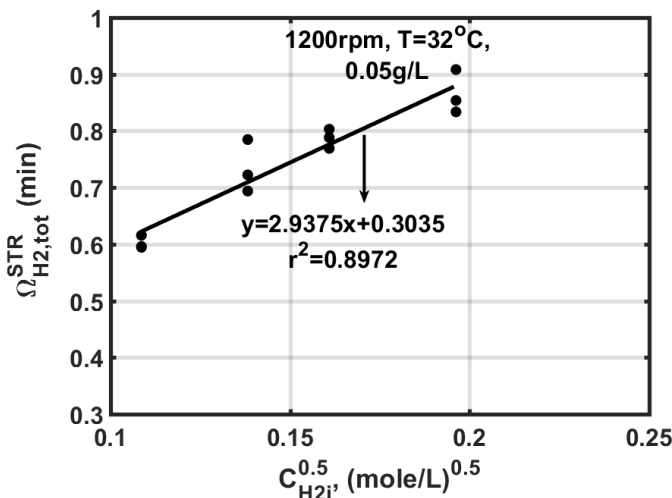

Figure 7.4: Global mass transfer resistance against the square root of hydrogen concentration under chemical reactionregime in the semi-batch STR.

7.3. Continuous flow experimentation

7.3.1. Continuous stirred tank reactor experimentation

The transfer of the heterogeneous catalysed hydrogenation in the continuous stirred tank reactor over the same catalyst and in the same solvent is somewhat straight forward procedure. In section 5.3, the hypothesis that the gas-liquid and the liquid-solid mass transfer coefficients of the same vessel

equipped by the same agitator are independent of the operation mode of the reactor- semi-batch or continuous flow- was shown true.

Therefore, once the mass transfer resistances of the three-phase hydrogenation have been determined in the semi-batch reactor, they can be used in the design equation of the continuous stirred tank reactor as long as the reaction proceeds under the same agitation speed, in the same vessel equipped by the same agitator, using the same solvent and under the same temperature and pressure.

7.3.2. Trickle bed reactor experimentation

As in the case of stirred tank reactors, hydrogen has to overcome two external mass transfer processes before the reaction to take place on catalyst active phase, however, in the trickle bed reactor gas is the continuous phase in which liquid is dispersed developing thin rivulets around the coarse particle catalyst.

This makes the mass transfer behaviour (gas-liquid and liquid-solid) of the trickle bed reactor to seem different from the mass transfer behaviour of the stirred tank reactors and so far, there has not been any developed correlation between the two. However, the chemical reaction resistance can be calculated by using the appropriate information obtained in the semi-batch stirred tank reactor.

More specifically, the intrinsic chemical reaction constant, k_1', is independent of the physical characteristics of the system which means that it is not affected by the reactor type, as far as the chemical system remains the same. The adsorption constants K_{St} and K_{H_2} depends on the characteristics adsorbate-adsorbent system and on the temperature. Therefore, if the same system of adsorbate and adsorbents is used in both reactors and the reactions takes

place under the same temperature they should be the same between the two different reactors.

Consequently, if the reaction which has been screened in section 7.2 in the semi-batch stirred tank reactor needs to be transferred to the TBR using palladium on extrudates of activated carbon and it is going to performed under the same temperature, the chemical reaction resistance in the TBR, Ω_{R,H_2}^{TBR}, is described by Equation 7.3. Because different supporting material with different palladium content is used between the two reactor setups, the term $k_1' \cdot \sqrt{K_H}/K_{St}$ needs to be expressed in terms of palladium content (Equation 7.5).

$$\Omega_{R,H_2}^{TBR} = \frac{V_L}{W_{Pd}} \cdot \frac{1}{\varepsilon \cdot k_{obs,\ 1^{st}order}^{\prime Pd} \cdot f} \qquad \text{Equation 7.3}$$

$$k_{obs,1^{st}order}^{\prime Pd} = k_1^{\prime Pd} \cdot \frac{\sqrt{K_{H_2}}}{K_{St}} \cdot \frac{1}{C_{St,S}} \cdot \frac{1}{\sqrt{C_{H_2\,S}}} \qquad \text{Equation 7.4}$$

$$k_1^{\prime Pd} \cdot \frac{\sqrt{K_{H_2}}}{K_{St}} = \frac{k_1'}{\begin{bmatrix} \text{Catalyst palladium content} \\ \text{in semi} - \text{batch experiments,} \\ \text{(g Pd/g cat)} \end{bmatrix}} \cdot \frac{\sqrt{K_{H_2}}}{K_{St}} \qquad \text{Equation 7.5}$$

The expression of global mass transfer resistance of hydrogen which has been given in section 3.1.2 is rewritten below.

$$\Omega_{H_2,tot}^{TBR} = \frac{1}{k_L \cdot \alpha_{bed} \cdot f} + \left[\frac{1}{k_{s,H_2} \cdot \alpha_{act.pel}^{\prime Pd} \cdot f} + \frac{1}{\varepsilon \cdot f \cdot k_{obs,1^{st}order}'} \right] \cdot \frac{V_L}{W_{Pd}}$$

If the reaction is performed using different palladium content in the bed, W_{Pd}, but under the same liquid flow rate, pressure, temperature and overall bed weight; and plots the $\Omega_{H_2,tot}^{TBR}$ against V_L/W_{Pd}, then the intercept of the plot is equal to the $1/K_L \cdot \alpha_p \cdot f$ which corresponds to the gas-liquid mass transfer

resistance (Equation 7.5). The liquid-solid mass transfer resistance can be calculated from the slope of the linear regression model and the chemical reaction resistance which has been calculated by using the term $k_1' \cdot \sqrt{K_{H_2}}/K_{St}$ obtained in the semi-batch stirred tank reactor.

Following this procedure, the unravelling of the effect of each individual process on the overall mass transfer rate in the trickle bed reactor is carried out.
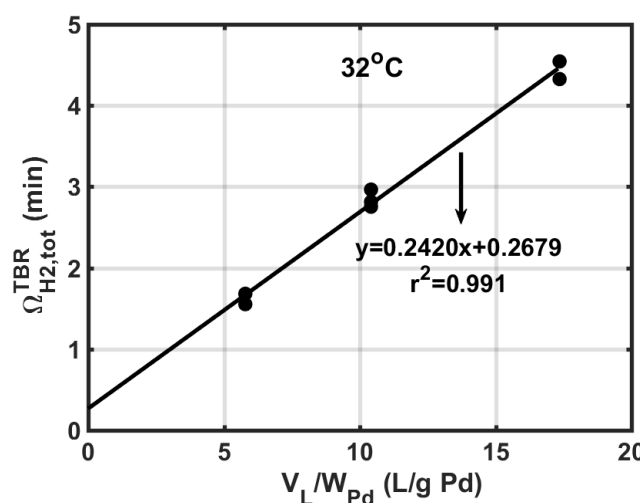

Figure 7.5: Global mass transfer resistance against the reciprocal of palladium concentration in the TBR.

7.4.   Conclusions

The information obtained from the screening of a heterogeneous catalysed reaction in a semi-batch stirred tank reactor can be used for transferring the reaction to continuous flow. The term of $k_1' \cdot \sqrt{K_{H_2}}/K_{St}$ is independent of reactor setup as long as the chemical reaction takes place over the same active phase of catalyst, under the same temperature and using the same solvent. Therefore, once this term has been calculated in the semi-batch reactor mode, it can be used in the design equation of the continuous flow reactors; CSTR or TBR.

In the case of transferring the heterogeneous catalysed reaction to continuous stirred tank reactor, the procedure is straight forward. More specifically, the gas-liquid and liquid solid mass transfer resistances, calculated in the semi-batch stirred tank reactor in a specific agitation speed, can be used in the design equation of a CSTR with the same vessel equipped by the same agitator which operates under the same agitation speed, using the same liquid volume of the same solvent as the semi-batch.

On the other hand, if the heterogeneous catalysed reaction needs to be transferred to a trickle bed reactor, the only information obtained from the semi-batch experimentation which remains the same between the two reactor setups is the term of $k_1' \cdot \sqrt{K_{H_2}}/K_{St}$. Using this term, the chemical reaction resistance of the TBR can be calculated and after appropriate experimentation the gas-liquid and liquid-solid mass transfer resistances can be determined.

Chapter 8

8.   Conclusions and future work

8.1.   Conclusions

In order to give an answer to the research question:

"What information do we need for transferring a heterogeneously catalysed

hydrogenation from batch to continuous flow?"

the styrene hydrogenation over palladium on activated carbon was performed in four different reactor setups; two semi-batch stirred tank reactors, one continuous stirred tank reactor and one trickle bed reactor. The substrate selection was based on the fast-intrinsic reaction kinetics which was likely to allow the external mass transfer to be the limiting regime despite the intensive mixing conditions. Additionally, mathematical models were developed and the heterogeneously catalysed styrene hydrogenation in the three different reactor types was simulated.

A new methodology was introduced for determining the mass transfer resistances of fast three-phase reactions a) under the reaction conditions, b) without changing the size of the catalyst, c) under conditions which do not allow to neglect any of the rate and d) without needing to use low substrate concentration. Instead, they were determined by changing the catalyst loading and the pressure of hydrogen. This allowed to avoid the use of different catalyst particles and give the chance to calculate the mass transfer resistances without caring about the type of catalyst. The gas-liquid and liquid-

solid mass transfer resistances were correlated to Reynolds and Sherwood number and found to be in agreement with the literature after comparison.

The styrene hydrogenation in three-phase semi-batch stirred tank reactor was simulated by having assumed that the surface chemical reaction follows the Langmuir-Hinshelwood model, the hydrogen is dissociatively chemisorbed onto palladium active sites, the styrene and hydrogen compete for the same sites and that the styrene is hydrogenated in two consecutive steps. It was also assumed that any amount of styrene which adsorbs onto catalyst particle reacts with hydrogen producing ethylbenzene and that any hydrogen passing through the mass flow controller is being consumed by the reaction.

The adsorption constants and the intrinsic reaction rate constant which were used in the surface reaction model were not approximated experimentally. Instead, a curve fitting approach using the GlobalSearch in-built MatLab algorithm was used to approximate them. The model after the curve fitting approximation was validated against experimental data which had not been used in curve fitting. Taking into account that the simulated profiles lay inside the confidence bounds, the results of validation indicated that the model described well the three-phase semi-batch hydrogenation of styrene in the stirred tank reactor.

The hypothesis that the gas-liquid and the liquid-solid mass transfer coefficients of the same stirred tank reactor equipped by the same agitator are independent of the operation mode of the reactor- semi-batch or continuous flow-was shown true tested.

Therefore, the transfer of the heterogeneous catalysed hydrogenation in the continuous stirred tank reactor over the same catalyst and in the same solvent

is somewhat straight forward procedure. Once the mass transfer resistances of the three-phase hydrogenation have been determined in the semi-batch reactor, they can be used in the design equation of the continuous stirred tank reactor as long as the reaction proceeds under the same agitation speed, in the same vessel equipped by the same agitator, using the same solvent and under the same temperature and pressure.

The mathematical model of the styrene hydrogenation in three-phase continuous stirred tank reactor was developed and tested against experimental data. An unforeseen decreasing styrene conversion over time shown experimentally remained unclarified, therefore, it was taken into account in the model by introducing an exponential catalyst loading decay model. The mass transfer coefficients which were used in the continuous flow reactor model were not experimentally calculated under continuous flow reactor mode. Instead, the mass transfer coefficients which have been calculated in the semi-batch reactor were used.

Regarding the trickle bed reactor, the critical variable for transferring predictively the three-phase reaction from the semi-batch stirred tank reactor to the trickle bed reactor respecting the reactant regimes was found to be the concentration of styrene with respect to the palladium content. In other words, if the reactant regimes have been defined in the semi-batch stirred tank reactor; and the threshold value of styrene concentration with respect to the palladium content has been calculated, the three-phase styrene hydrogenation can be predictively transferred to the trickle bed reactor respecting the reactant regimes.

The determination of the gas-liquid mass transfer resistance was based on intercept of the plot of the global mass transfer resistance against the reciprocal palladium concentration in the bed. To develop such a plot different bed weights of active pellets was necessary to be used without changing the mixing conditions and the flow patterns in the bed. This was achieved by (a) using active and non-active pellets with the same physical characteristics and (b) keeping their overall weight in the bed constant. The palladium content in the bed was feasible to vary by changing the ratio between the active and non-active pellets.

The thickness of the liquid film was approximated as the ratio between the overall liquid hold-up and the external surface area of the bed per unit volume. the wetting efficiency was approximated as the ratio between the specific effective gas-liquid mass transfer calculated from the experimental value of the gas-liquid mass transfer resistance and the theoretical specific gas-liquid mass transfer coefficient calculated based on the concept of the stagnant film theory.

The specific effective gas-liquid mass transfer coefficient, the wetting efficiency and the specific effective liquid-solid mass transfer coefficient were found to be in agreement with some values available in the literature. This indicates that the suggested methodology for determining the mass transfer resistances of three-phase reaction in a trickle bed reactor and the wetting efficiency of the reactor bed is robust.

Moreover, a methodology for designing the three-phase hydrogenation in the trickle bed reactor was developed. The developed methodology is based on the fact that the term of $k_1' \cdot \sqrt{K_{H_2}}/K_{St}$ is independent of reactor setup as long

as the chemical reaction takes place over the same active phase of catalyst, under the same temperature and using the same solvent. According to this methodology the semi-batch stirred tank reactor is used for defining the term of $k_1' \cdot \sqrt{K_{H_2}}/K_{St}$. The chemical reaction resistance is calculated using this term, the gas-liquid mass transfer resistance is calculated from the plot of the global mass transfer resistance against the reciprocal of palladium concentration in the bed and the liquid-solid mass transfer resistance is calculated by subtracting these two resistances from the overall mass transfer resistance. The latter is defined as the ratio between the hydrogen concentration in the gas-liquid interphase and the overall mass transfer rate of the hydrogenation.

8.2.   Future work

The developed methodology for determining the mass transfer resistances of three-phase reactions in semi-batch stirred tank reactor should be tested in different chemistries. Initially, this could be done by hydrogenating different substrates over Pd/C and then using different noble metal catalysts. This will allow to evaluate its independency of the chemical characteristics of the system.

Regarding the continuous stirred tank reactor, the decrease in conversion could be proved as catalyst deactivation result by conducting the hydrogenation in an experimental setup which will allow the continuous renewal of catalyst.

Moreover, the transfer of the three-phase styrene hydrogenation from semi-batch to continuous flow took place only in one agitation speed. This did not give the chance for developing any correlation of the gas-liquid and liquid-

solid mass transfer coefficients between the two reactor operation modes. For example, is there any particular trend between the mass transfer of the two reactor setups which could expressed from dimensionless numbers such as Reynolds and Sherwood?

Regarding the experimentation on the trickle bed reactor, the developed methodology for determining the mass transfer resistances took place only in a single liquid and gas flow rate. It would be beneficial the methodology to take place in a series of liquid and gas flow rates. This will give the chance to investigate the dependence of the external mass transfer resistances or coefficients on liquid and gas Reynolds numbers. Then correlations between the mass transfer of the semi-batch stirred tank reactor and the trickle bed reactor would be possible to be developed.

As the suggestion for the semi-batch stirred tank mass transfer characterisation, the methodology which was developed in the trickle bed could be tested in different chemistries to evaluate its independency of the chemical characteristics of the system.

9.   Appendices

9.1.   Appendix A: Catalysts and glass beads

### *Pd/C Fine particles size distribution-Number average*
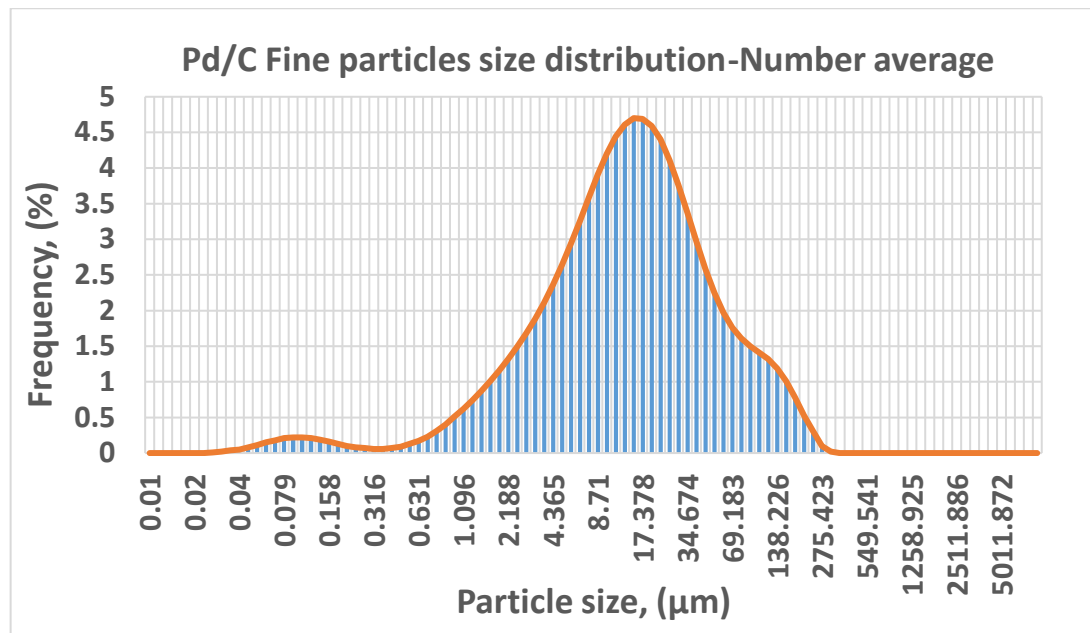
Figure 9.1: Size distribution of Pd/C fine particles used in the experiments of semi-batch (reactor A and reactor B) and continuous stirred tank reactors.
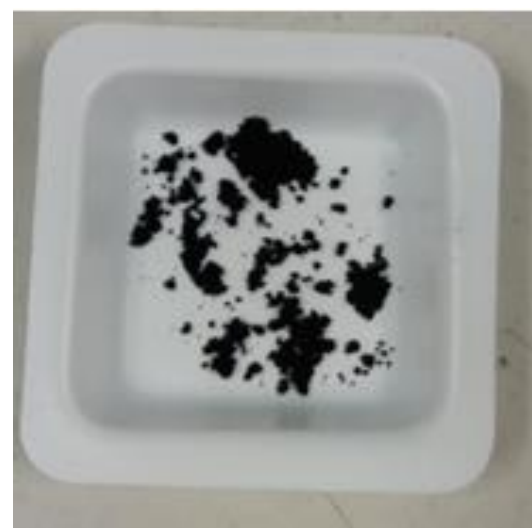

Figure 9.2: Picture of Pd/C powder.

Pellets size distribution using ImageJ software
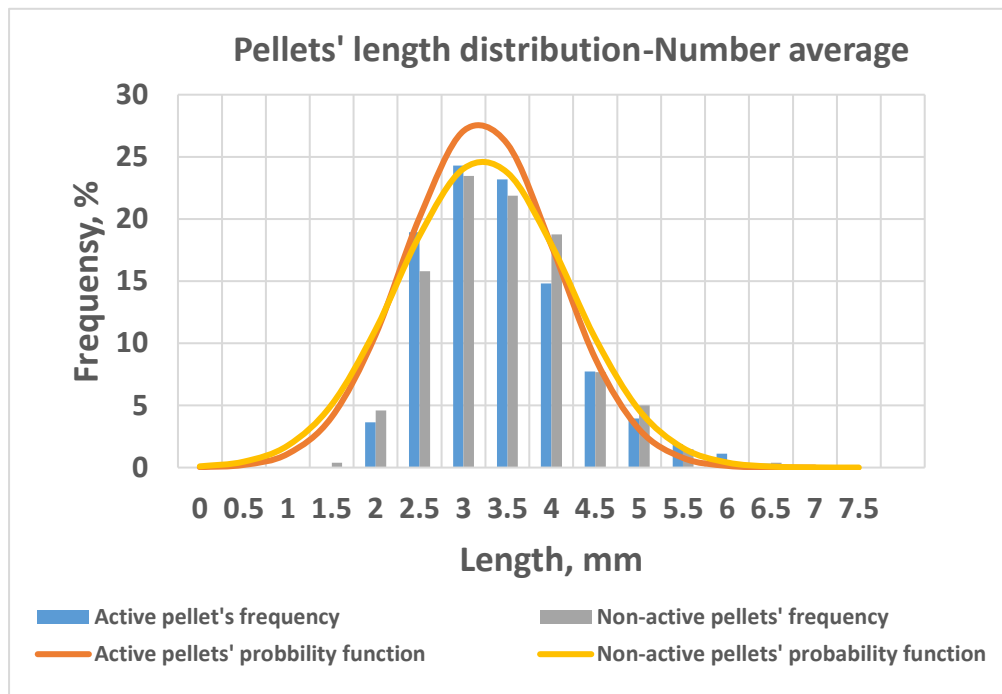
Figure 9.3: Length distribution of active and non-active pellets used in the experiments of trickle bed reactor
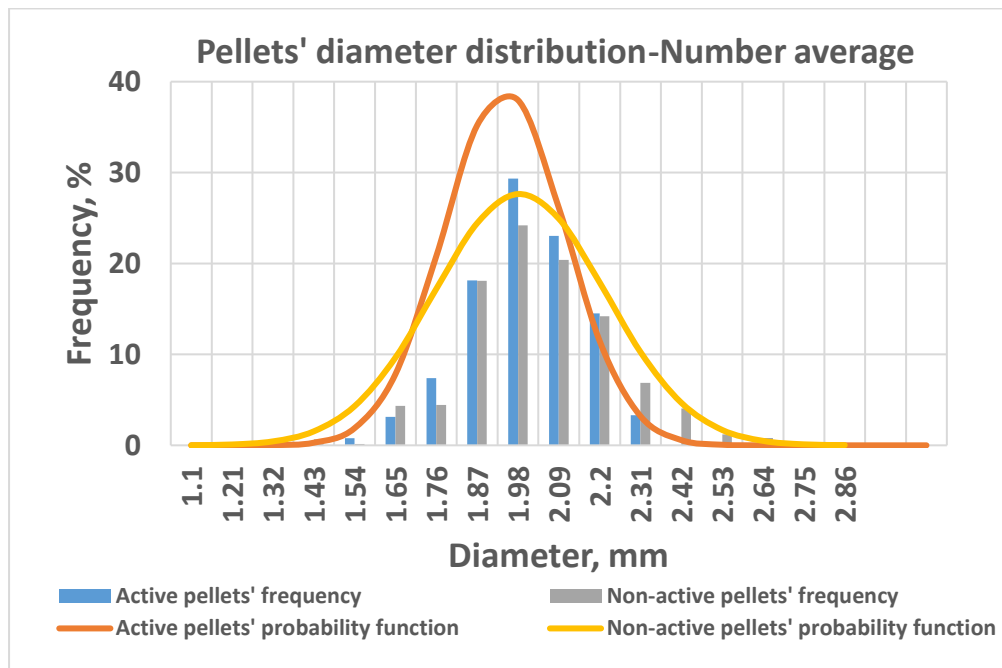

Figure 9.4: Length distribution of active and non-active pellets used in the experiments of trickle bed reactor

*Pellets and glass beads weight distribution*
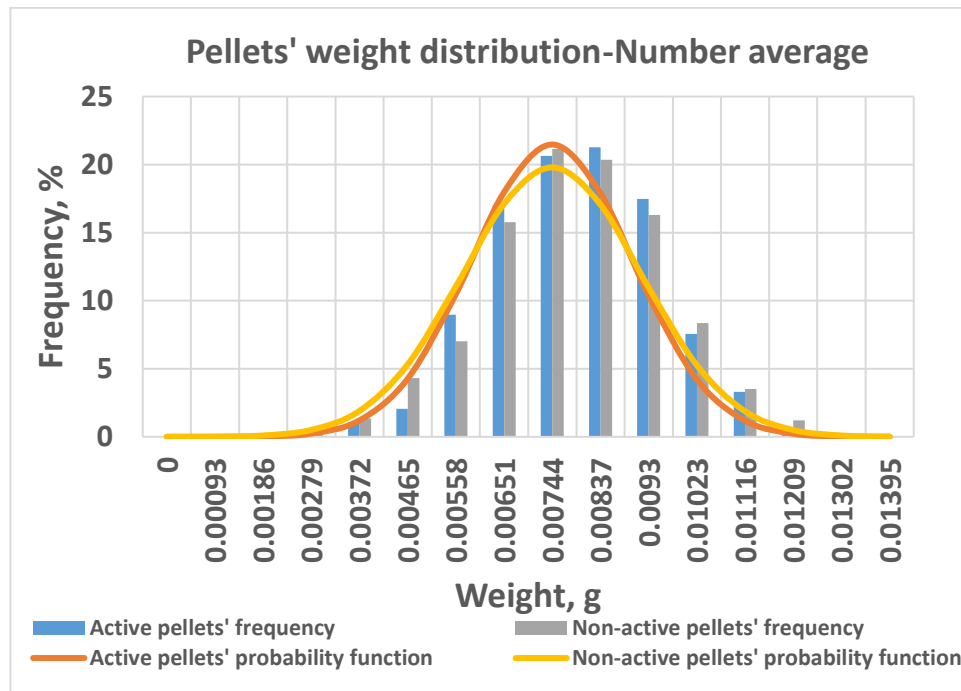
Figure 9.5: Weight distribution of active and non-active pellets used in the experiments of trickle bed reactor.
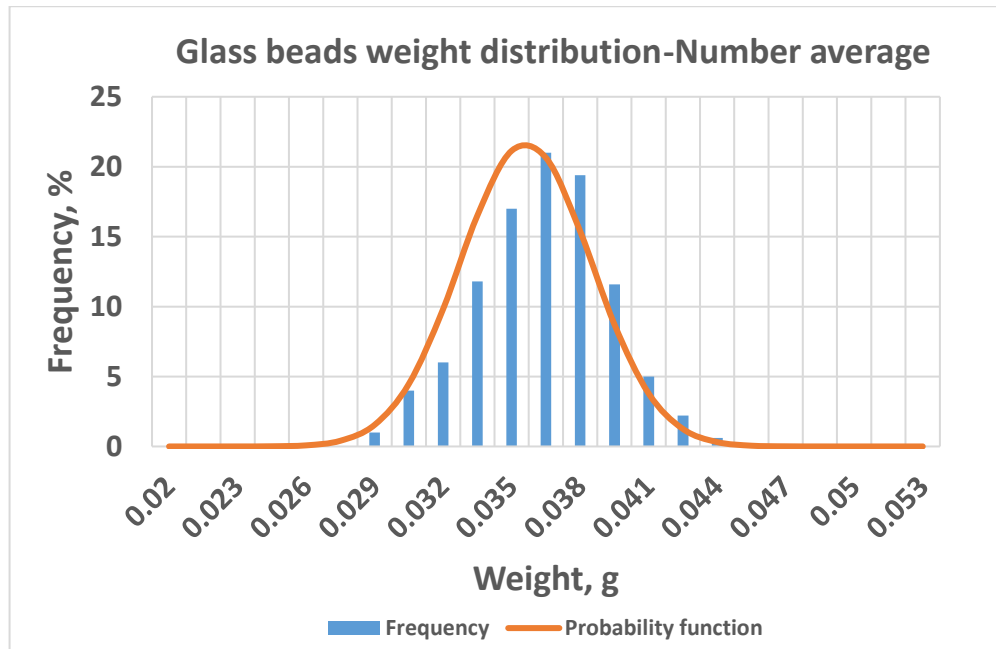

Figure 9.6: Weight distribution of glass beads used in the experiments of trickle bed reactor.

Pictures of pellets and glass beads
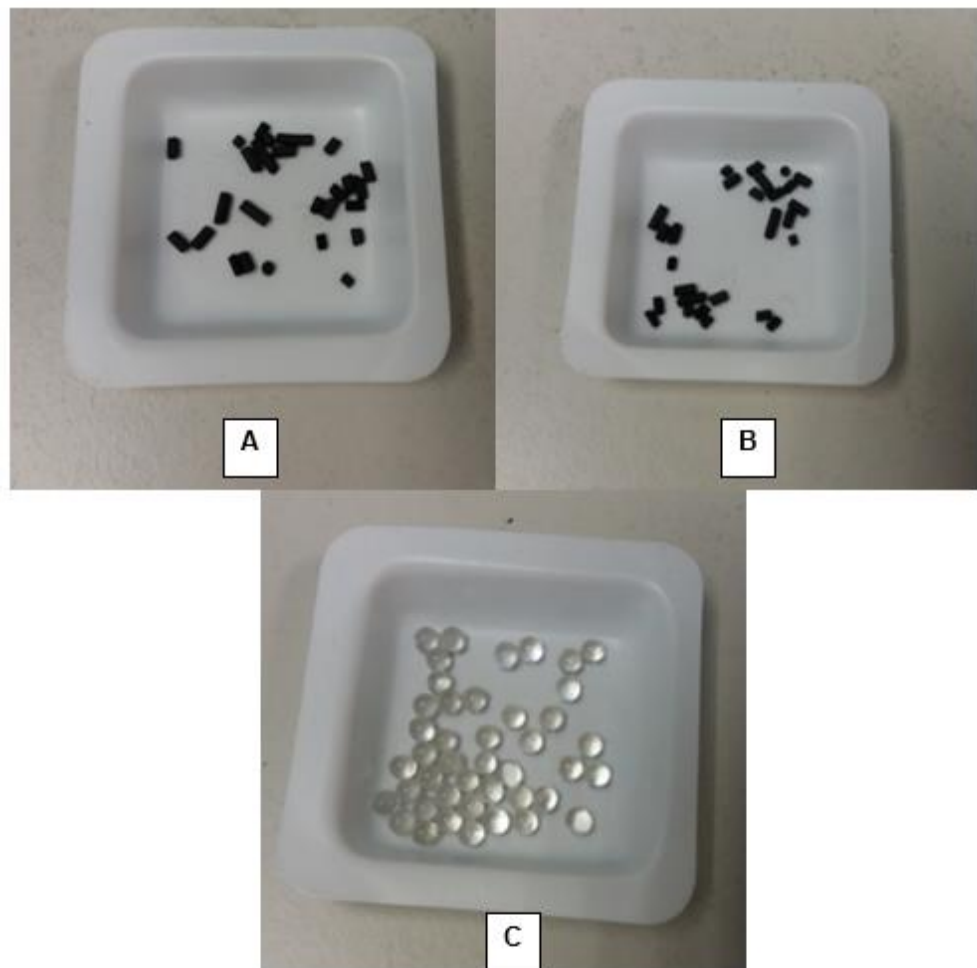
Figure 9.7: Pictures of active (A) and non-active pellets (B); and glass beads (C).

Palladium nanoparticles size distribution
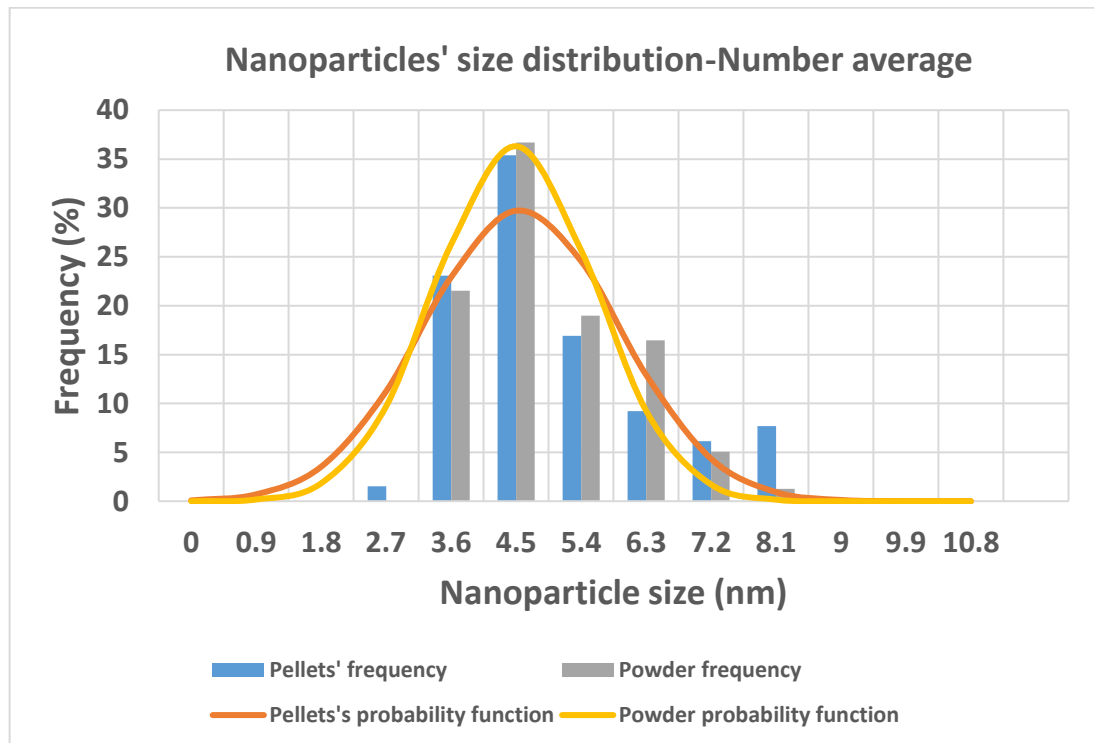
Figure 9.8: Size distribution of palladium nanoparticles of pellet powder catalyst. The average size of palladium nanoparticles is the same for both catalyst types.
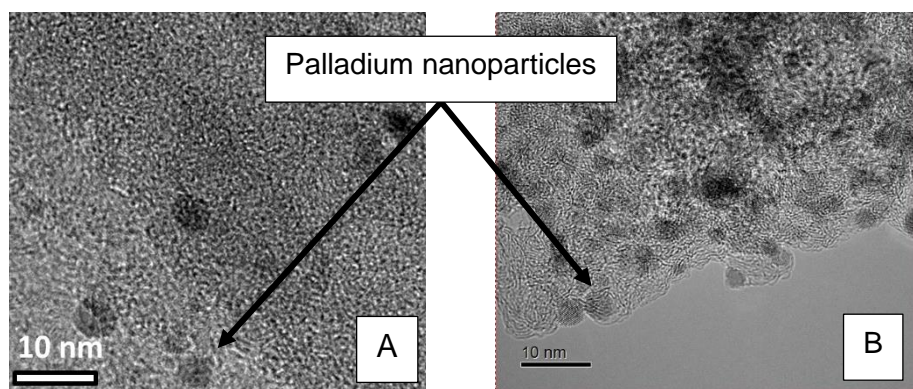

Figure 9.9: Images from TEM of pellets (A) and powder (B).

9.2.   Appendix B: Gas chromatography

Gas chromatography

The gas chromatography analytical technique was used throughout the project for the reaction samples analysis for all the reactor setups; semi-batch STR, CSTR and TBR.

Basics of gas chromatography

Gas chromatography (GC) is one of the most common methods of sample separation and identification in analytical chemistry [115]. Gas chromatography consists of the column (stationary phase), the carrier gas (mobile phase), the column oven, the sample injector and the detector. Figure 9.10 depicts a schematic representation of a gas chromatography. The column of the gas chromatography is a narrow tube which is packed with the stationery phase and it is placed in the oven. The stationary phase consists of a liquid which is adsorbed onto the surface of an inert solid.
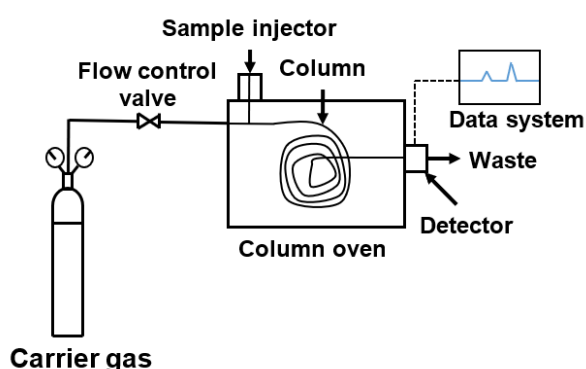
Figure 9.10: Schematic representation of gas chromatograph [115].

Analytes separation

The sample is injected into the head of the column and it is being vaporised due to the high temperature of the oven. The vapours are transported lengthwise the column due to the flow of the carrier gas. The role of the carrier

gas is only the transport of the sample's vapours. The separation of the sample to its compounds (known as solutes or analytes) is based on the different retention times which each compound spends in the column. The retention time of each compound depends on its relative vapour pressure which depends on the temperature and on its intermolecular interaction with the stationary phase.

Analytes identification

The gas chromatography is one of the most powerful techniques of sample separation, however, it is a poor method for the identification of unknown analytes. When unknown compounds are present in the sample, a combination of gas chromatography and mass spectroscopy is usually necessary for the identification of the unknown compounds.

If the sample consists of known compounds, it is easy to identify which peak corresponds to one analyte. This is attained by producing different samples; each containing only one of the analytes. Injecting in the gas chromatography one sample each time, the retention time of the analyte is defined. Repeating this procedure for each sample, the retention time of the different analytes is defined. Knowing the retention time, one can identify which peak corresponds to each analyte. If the method or the column change, the retention time changes; and the procedure needs to be repeated.

Detector

At the column outlet, there is the detector which is a concentration sensor. It provides a record of the chromatography known as chromatogram. The signal of the detector is proportional to the quantity of each analyte; this allows the

quantitative analysis of the sample. Regarding the type of the detector, the most common is the flame ionization detector, FID [116].

When a flame ionization detector is used, the column effluent is burned in an oxygen-hydrogen flame. This process produces ions which form a small current which constitutes the signal. As the function of the flame ionization detector is based on the combustion of the column effluent, compounds not containing organic carbon do not burn, and consequently, are not detected [116]. This is an advantage of the FID detectors because the signal is not affected by the presence of water, atmospheric gases and carrier gas. The sensitivity of the FID detectors is very high to most of the organic molecules; a compound is detected even if its concentration is in the scale of ppb.

The characteristics of the gas chromatography and the column which was used throughout the project are outlined in Table 9.1.

Table 9.1: Characteristics of gas chromatography used throughout the project.

Hewlett Packard HP 6890 Series	
Column characteristics	
Type	DB-624
Length (m)	30
Diameter (mm)	0.25
Film thickness (µm)	1.40

Calibration of gas chromatography

Quantitative analysis requires calibration of the detector by injecting mixtures of different but known compositions, containing an internal standard. The response factor with respect to the internal standard is then determined by plotting the ratio of the peak areas of the analyte to the internal standard against the ratio of their molar amounts. In this work, decane was used as internal standard.

$$RF = \frac{\text{Peak Area}_{AN}/\text{Peak Area}_{Dec}}{n_{AN}/n_{Decane}}$$ Equation 9.1

Where, Peak Area_{AN} and Peak Area_{Dec} the peak areas of analyte and internal standard and n_{AN} and n_{IS} the molecular amounts of analyte and internal standard.
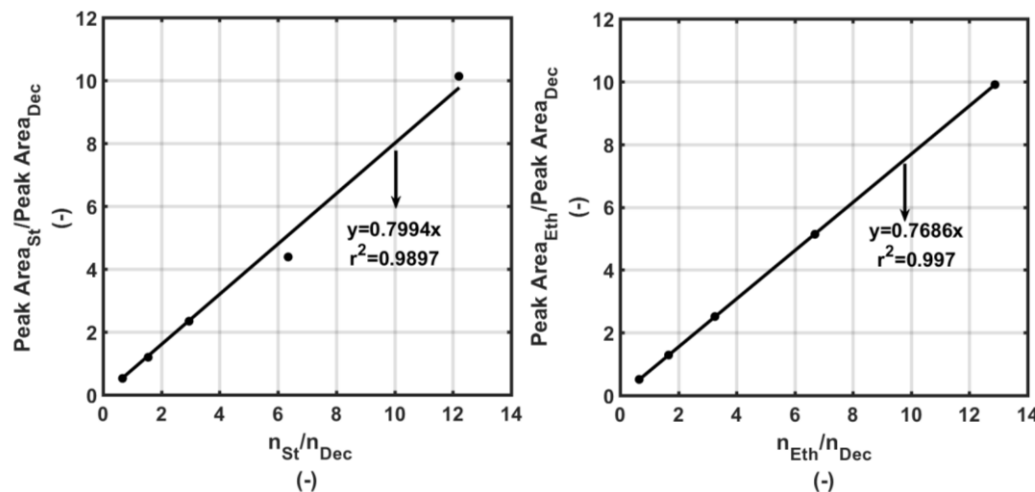

Figure 9.11: Gas chromatography calibration.

Method

Table 9.2: gas chromatography method details.

Oven			
	Rate	Temperature range	Hold time
	(ºC/min)	(ºC)	(min)
Initial		85	5
Ramp 1	1	90	2
Ramp 2	0.1	91	0
Ramp 3	50	200	5

Inlet				
Heater	**Pressure**	**Total Flow (H$_2$)**	**Mode**	**Split ratio**
300	15	35.1	Split	9.3:1

Column		
Pressure	**H$_2$ flow**	**Average velocity**
psi	**mL/min**	**cm/s**
15	2.4	64

Detector			
Heater	**Hydrogen Flow**	**Air flow**	**Makeup flow (N$_2$)**
(ºC)	**mL/min**	**mL/min**	**mL/min**
300	30	300	45

9.3.   Appendix C: L-S mass transfer coefficients of styrene and ethylbenzene

First, the molecular diffusion coefficients of styrene and ethylbenzene in water were found in the literature. Then, using twice Equation 9.2 [117], for water and methanol, respectively, the molecular diffusion coefficients of styrene and ethylbenzene in methanol were correlated to those in water from Equation 9.3.

$$\mathfrak{D}_i = 7.4 \cdot 10^{-8} \cdot x_i \cdot \frac{M_i \cdot T}{n_i \cdot V^{0.6}}$$
Equation 9.2

$$\mathfrak{D}_M = 1.83 \cdot \mathfrak{D}_W$$
Equation 9.3

Where, i = Water or methanol

x_i = Association parameter of solution i

M_i = Molecular weight of solution i, [g/mol]

T = Temperature, [K]

n_i = Viscosity of solution i at temperature T, [cp]

V = Molar volume of solute, $[ml/mole]$

Table 9.3: Molecular diffusion coefficient and values for Equation 9.2.

	Water	**Methanol**
x_i [117]	2.6	1.9
M_i, [g/mol]	18	32
n_i at 32ºC [72], [cp]	0.76	0.50
$\mathfrak{D}_{St}$ [118], $[m^2/s]$	$8.24 \cdot 10^{-10}$	$15.1 \cdot 10^{-10}$
$\mathfrak{D}_{Eth}$ [118], $[m^2/s]$	$9.16 \cdot 10^{-10}$	$16.76 \cdot 10^{-10}$

Once the molecular diffusion coefficients of styrene and ethylbenzene in methanol had been calculated, their liquid-solid mass transfer coefficients

were correlated to the liquid-solid mass transfer coefficient of hydrogen by assuming that the mass transfer coefficient are proportional to the square root of molecular diffusion coefficients, as the penetration and renewal-surface theory suggests. Therefore, the liquid-mass transfer coefficient of styrene and ethylbenzene are given by Equation 9.4 and Equation 9.5, respectively.

$$k_{S,St} = 0.4 \cdot k_{S,H_2}$$ Equation 9.4

$$k_{S,Eth} = 0.41 \cdot k_{S,H_2}$$ Equation 9.5

9.4.　　Appendix D: Thiele Modulus and effectiveness factor estimation

To evaluate the effect of pore diffusion on reaction rate, Thiele modulus, which is given by Equation 2.24 and it is rewritten below, should be estimated.

Thiele Modulus: $$m \cdot L = L \cdot \sqrt{\frac{k'''_{obs,1^{st}order}}{D_e}}$$

To estimate the effective diffusion coefficient, D_e, Equation 2.16, Equation 2.17 and Equation 2.18, which are rewritten below, were used.

$$\frac{1}{D_e} = \frac{1}{D_{m,e}} + \frac{1}{D_{k,e}}$$

$$D_{m,e} = \frac{\mathfrak{D} \cdot \Phi_p}{\tilde{\tau}}$$

$$D_{k,e} = 0.194 \cdot \frac{\Phi_p{}^2}{\tilde{\tau}} \cdot \frac{1}{S_s \cdot \rho_p} \cdot \sqrt{\frac{T}{M}}$$

Table 9.4: Values for calculating the effective diffusion coefficient.

Molecular diffusion coefficient, $[m^2/s]$	$\mathfrak{D}$	10^{-9}
Internal void of supporting material, [-]	Φ_p	0.24
Tortuosity, [-]	$\tilde{\tau}$	4
Specific surface area of supporting material, $[m^2/g]$	S_s	679.22
Density of supporting material, $[kg/m^3]$	ρ_p	725
Temperature, [K]	T	305
Molar mass of diffusing species, [g/mol]	M	12
Molecular effective diffusion coefficient, $[m^2/s]$	$D_{m,e}$	$6 \cdot 10^{-11}$
Knudsen effective diffusion coefficients, $[m^2/s]$	$D_{k,e}$	$2.85 \cdot 10^{-8}$
Effective diffusion coefficient, $[m^2/s]$	D_e	$\sim 6 \cdot 10^{-11}$

The characteristic length, L, of the catalyst is the one third of the supporting material radius, so L=R/3.

From Figure 9.1 the average particle size of supporting material is 18 μm. The observed chemical reaction constant has been calculated in section 4.3.3 and it is presented in Table 4.8. The observed chemical reaction constant for the assumed 1st-order reaction with respect to hydrogen was expressed by Equation 4.3. The observed 1st-order reaction rate expressed in 1/s is calculated by multiplying the $k'_{obs,1^{st}order}$ by catalyst concentration in the reaction mixture

Table 9.5: Observed chemical reaction rate constant.

k'_{obs}	k'_{obs}	$k'_{obs,1^{st}order}$	$k_{obs,1^{st}order}$
$\left(\dfrac{\sqrt{mol \cdot L\ liquid}}{g\ cat \cdot min}\right)$	$\left(\dfrac{\sqrt{mol \cdot L\ liquid}}{g\ cat \cdot min}\right)$	$\left(\dfrac{L\ liquid}{g\ cat \cdot min}\right)$	(1/s)
4.86	0.081	0.7459	0.037

Substituting the characteristic length, the observed chemical reaction constant for the assumed 1st-order reaction with respect to hydrogen, expressed in 1/s, and the effective diffusion coefficient to Equation 2.24, the Thiele modulus is calculated equal to 0.075. From Figure 2.15 one approximates the effectiveness factor to unity.

9.5.   Appendix E: Standard operating procedure of TBR

9.5.1.   Start-up

Prepare the rig

1	Make sure all gas supplies are turned off.	☐
2	Turn on the light behind the viewing chamber and open the picometer and pressure software on the computer.	☐
3	Check the FBR rig is earthed.	☐
4	Switch on the LED of the Level Indicator.	☐
5	Make sure rig screens are in place. Two screens are used – At the front ant at the back of the rig.	☐
6	Put all valves in their starting position. ALL CLOSED.	☐
7	Add the substrate solution into R-T1 using a funnel. Remove any flammable liquid from the area after the container has been charged.	☐
8	Add the solvent into R-T2 using a funnel. Remove any flammable liquid from the area after the container has been charged.	☐
9	Make sure that there is a vessel to collect solvent from drains R-D1, R-D2, D11 (below R-V8, R-V10 and V13 respectively), and at the product collection points, R-T3 and D10 (below V16).	☐
10	If reactor vessel is full of catalyst pellet submerged in solvent, open R-V10 and R-V5 to drain	☐

Pressurise with Nitrogen

|		
1	Check that all valves are turned off on the manifold	☐
2	Make sure H2 supply is turned off	☐
3	Start the MFC software - See MFC Start-up (page 12)	☐
4	Open the valve on the N2 bottle.	☐
5	Set the N2 regulator to approximately 5 bars.	☐
6	Open the on/off valve on the N2 regulator and open V17	☐
7	Increase pressure on the BPR until no gas is exhausted, P4 should now read 5 bars	☐
8	Open V1 slowly and purge vent pipe for 5 seconds then close V1	☐
9	Open V2, P5 should read 5 bars	☐
10	Open V3	☐
11	Open V4. Set the gas flow rate on the MFC software to 2 NL/min.	☐
12	Open V19, should see the arrow on the MFC software move up.	☐
13	Open R-V3.	☐
14	Open R-V4.	☐
15	Open R-V5	☐
16	Open V14 from F14 to F15	☐
17	Open R-V6	☐
18	R-P1 should read 8 bar, the same as P4 and P5.	☐
19	Open R-V7.	☐
20	Increase pressure on the R-BPR until no gas is exhausted, R-P2 should read 5 bars.	☐
21	Now the system between R-V2, R-BPR, R-V10, V16, V13 and V1 is pressurised with N2 (green lines in figure 9).	☐

SEE Figure 9.12, NEXT PAGE
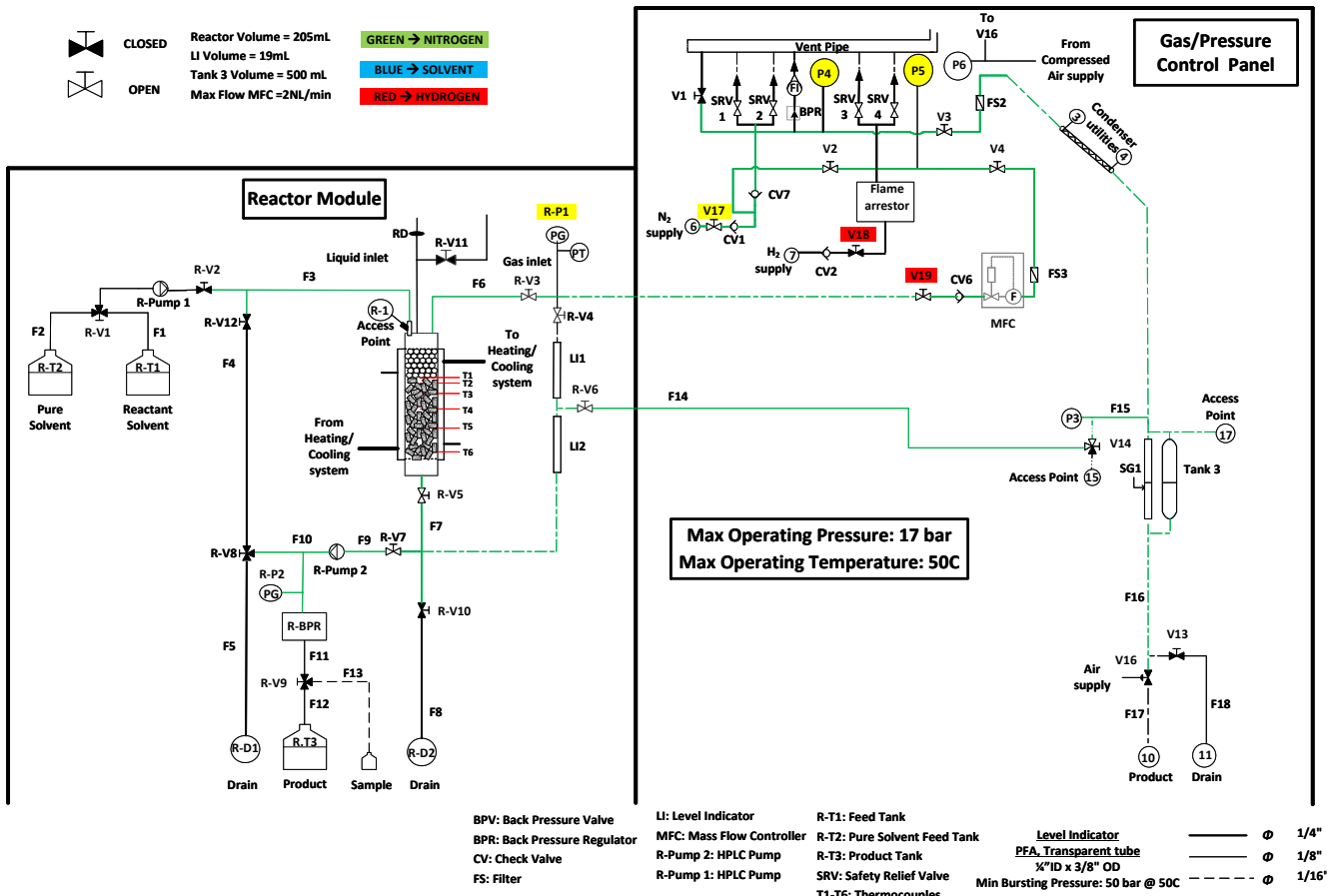
Figure 9.12: Pressurised system with Nitrogen.

Purge with Nitrogen

Once the system has been pressurised with nitrogen:

|		
1	Close V19.	☐
2	Close V14.	☐
3	Open R-V10.	☐
4	Pressurise again the system by closing R-V10 & opening V19 & V14.	☐
5	Repeat steps 1-4 for 4 times. At the last time in step 1 instead of closing V19 close V2 and before pressurise again close V19 to pressurise the system only by using line F14.	☐
6	Open R-V2.	☐
7	Leave the system under pressure for 10 min to check if there is any leak. If the pressure is kept constant there is no leak in the system.	☐
8	Close V14.	☐
9	Open R-V10 to purge for the fifth time.	☐
10	Close R-V10.	☐
11	Close R-V2.	☐
12	The system has been now • purged with nitrogen 5 times & • checked for any leak	☐
13	Go to "establish liquid flow – Clean FBR system with solvent".	☐

SEE FIGURE 9.13, NEXT PAGE
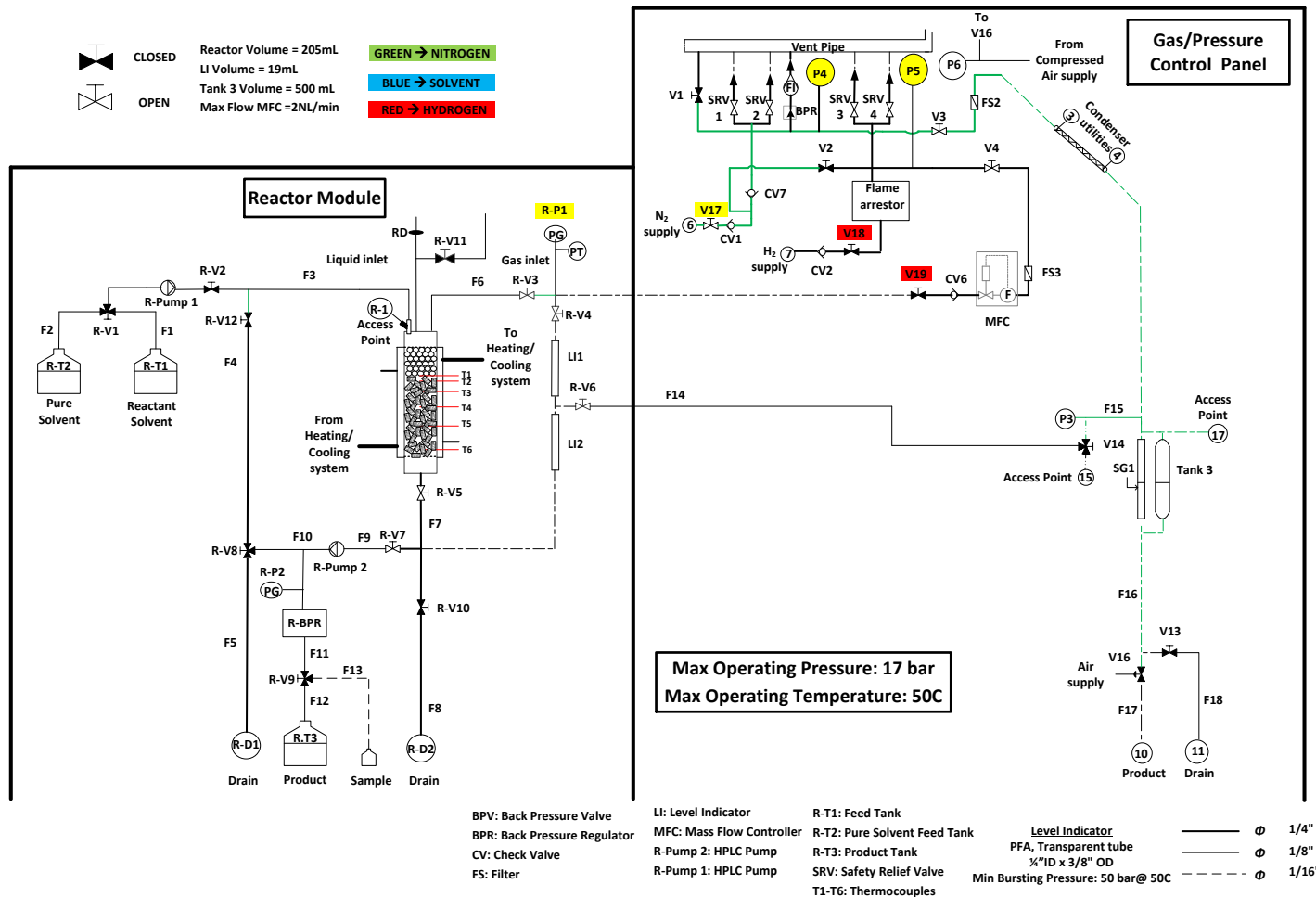
Figure 9.13: System after purging with nitrogen

Establish liquid flow – Clean with solvent

Once the system has been purged with nitrogen for 5 times and checked for any leak:

|		
1	Pressurise the system by opening V14 from F15 to F14.	☐
2	R-P1 & R-P2 should read 5 bar the same as P4.	☐
3	Open R-V9 from F11 to F12.	☐
4	Open R-V1 from F2 to F3 (pure solvent tank R-T2).	☐
5	Open R-V2.	☐
6	Turn on R-Pump 1 (feed pump) and set "pre-set maximum pressure" to 5 bars over desired operating pressure.	☐
7	Reduce the pressure on R-BPR until there is flow to R-T3.	☐
8	Let 100ml of solvent to pass through collecting in R-T3.	☐
9	Switch R-V9 to F13. Let 100ml of solvent to pass through F13.	☐
10	Switch R-V9 to F12.	☐
11	Use R-Pump 2 and the level indicator to regulate the level in the reactor column. Level must be lower that the blue line in the level indicator.	☐
12	Start heating/cooling system	☐

SEE FIGURE 9.14, NEXT PAGE
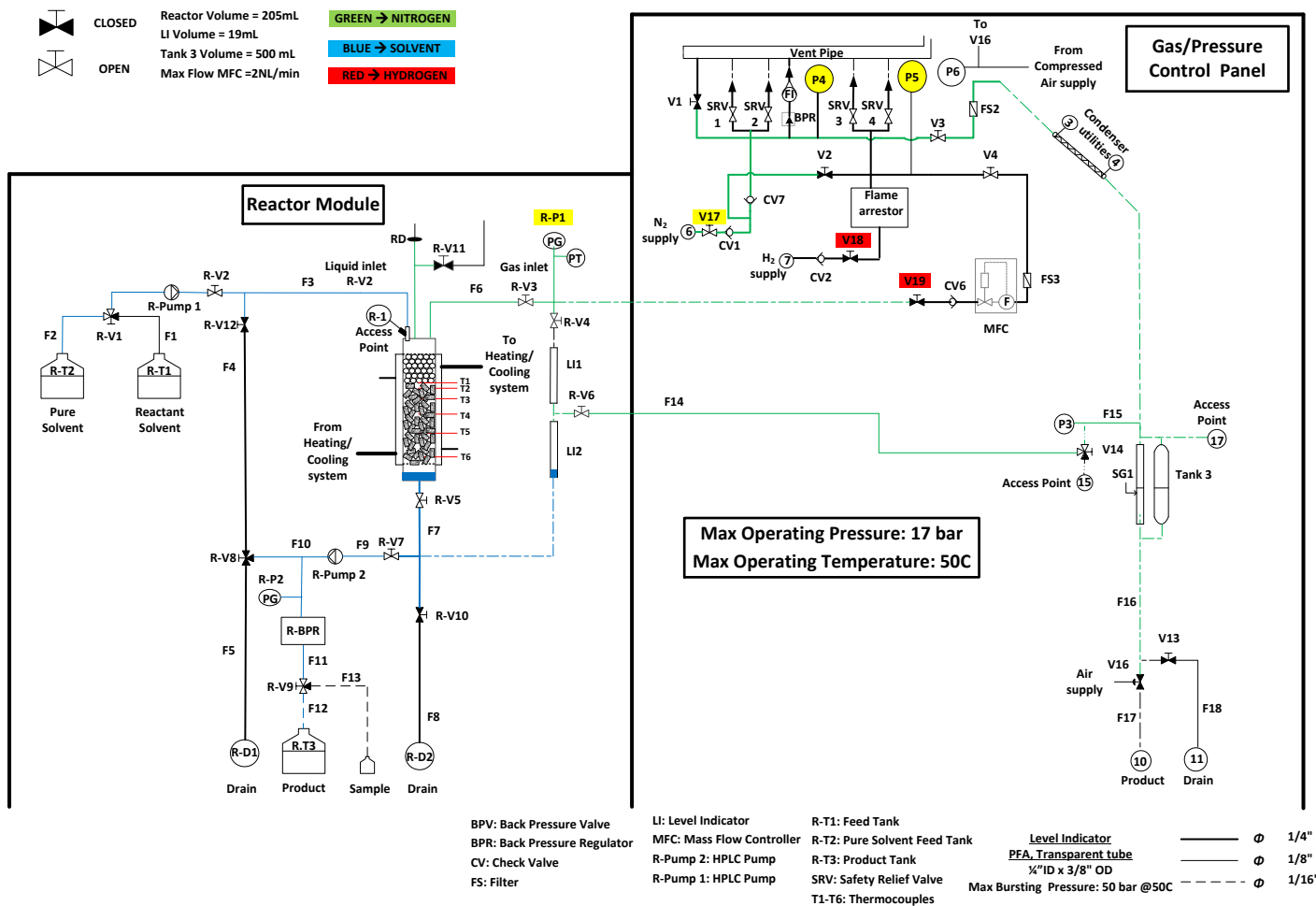
Figure 9.14: System under pressure (Nitrogen) and solvent flow established.

Establish hydrogen flow – Start reaction

1	Open valve on H2 cylinder and set the regulator to the required inlet gas pressure for reaction • Required inlet gas pressure to the MFC is 5 bars higher than the pressure indicated. • Note that the maximum working pressure of the system is limited to 17 bars.	☐
2	Open ON/OFF valve on the H2 regulator.	☐
3	Open V18.	☐
4	Check that P5 is showing the same pressure as set on the H2 regulator.	☐
5	Set the intended H2 Flow rate on the MFC software for the reaction.	☐
6	Close R-V4.	☐
7	Open V19. H2 is flowing through the reactor.	☐
8	Switch F1 from pure solvent to substrate solution.	☐
9	REACTION IS RUNNING.	☐

SEE FIGURE 9.15, NEXT PAGE
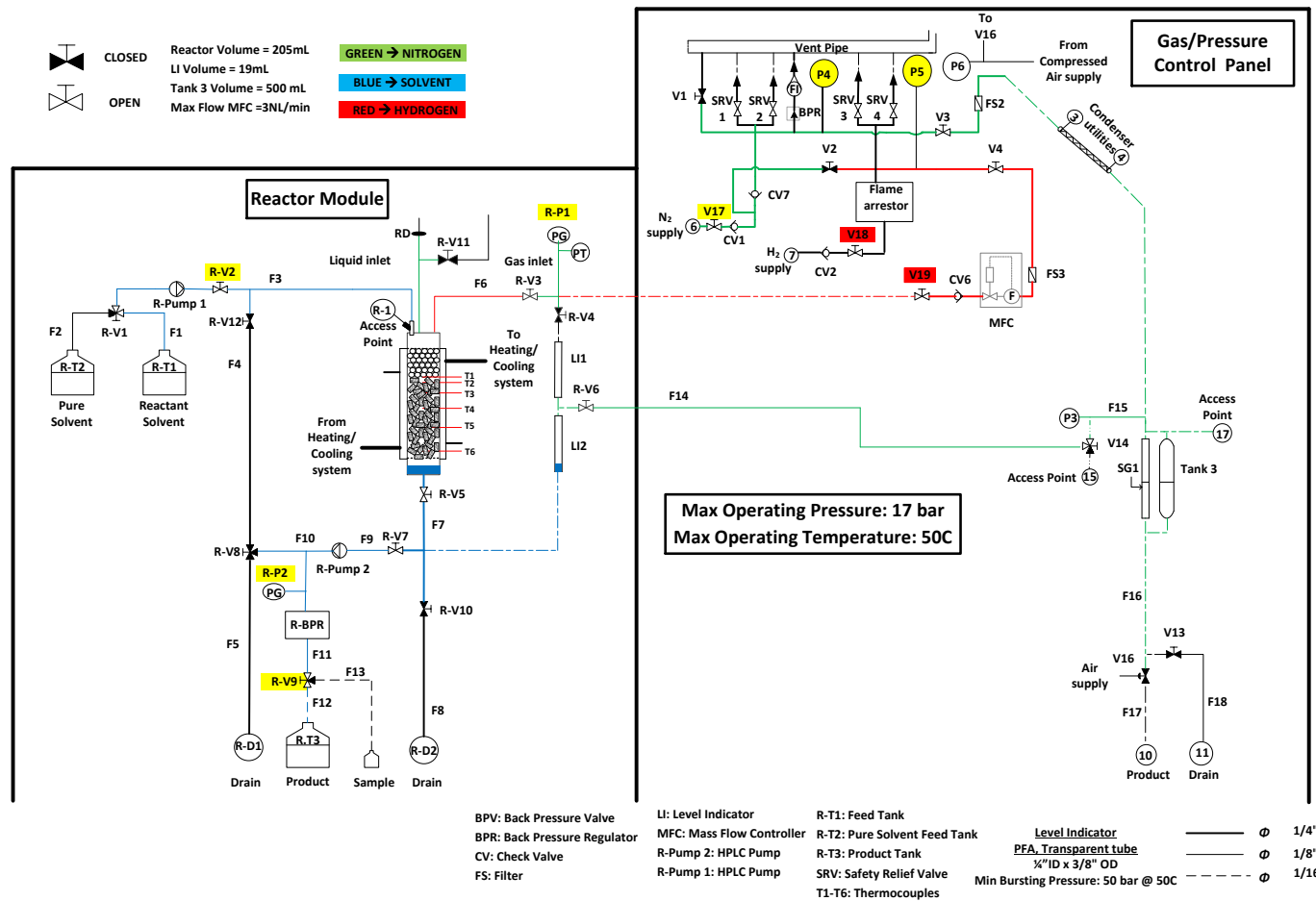
Figure 9.15: P&ID of the system showing valves position during reaction period.

9.5.2. Monitoring/ Reaction Period

Throughout the experiment, the following must be continuously checked:

1	Level of liquid in reactor column using the level indictor	☐

2	Check R-P1 and P3– P6
	
	    • R-P1 gives the pressure in the reactor
	    • P3 gives the pressure before tank 3
	    • P4 gives the pressure of the nitrogen supply
	    • P5 gives the pressure of the hydrogen supply
	    • P6 gives the pressure of the compressed air
		☐

3	Check for leaks	☐
4	Gas supply pressures	☐
5	Liquid level of R-T1	☐
6	Temperature readings of picometer.	☐
7	Check level of R-T3 (Product Tank).	☐
8	Check R-Pump 1 pressure	☐
9	Check R-Pump 2 pressure	☐
10	Check the rotameter is reading 0.5 NL/min.	☐
11	Switch R-V11 to F13, when you need to sample.	☐

9.5.3. Shutdown

When ready to shut down the rig, follow the procedures below:

Stop reaction

	1	Close V18 & V19.	☐
	2	Switch R-V1 to F1. From substrate solution to pure solvent.	☐
	3	Turn off Heating/Cooling and let the reactor to cool down to room temperature.	☐

Clean FBR system with solvent

	1	Let 200ml of pure solvent to pass through.	☐
	2	Switch off R-Pump 1.	☐
	3	Drain the system to R-T3 from liquid using R-Pump 2. Switch off R-Pump 2 when reactor is empty of liquid.	☐

Purge with Nitrogen

	1	Close V14.	☐
	2	Open R-V10 to depressurise the system.	☐
	3	Open V2.	☐
	4	Pressurise again the system by closing R-V10 & opening V19 & V14.	☐
	5	Follow steps under "Purge with Nitrogen" beginning from 1 to 4. The last time of purging do not pressurise the system.	☐
	6	Close R-V10	☐

Depressurise gas supply/control panel

|			
	1	Turn off nitrogen and hydrogen supply at their manifold.	☐
	2	Close V17.	☐
	3	Open V1 to depressurise the gas supply/control panel.	☐
	4	Close V1.	☐
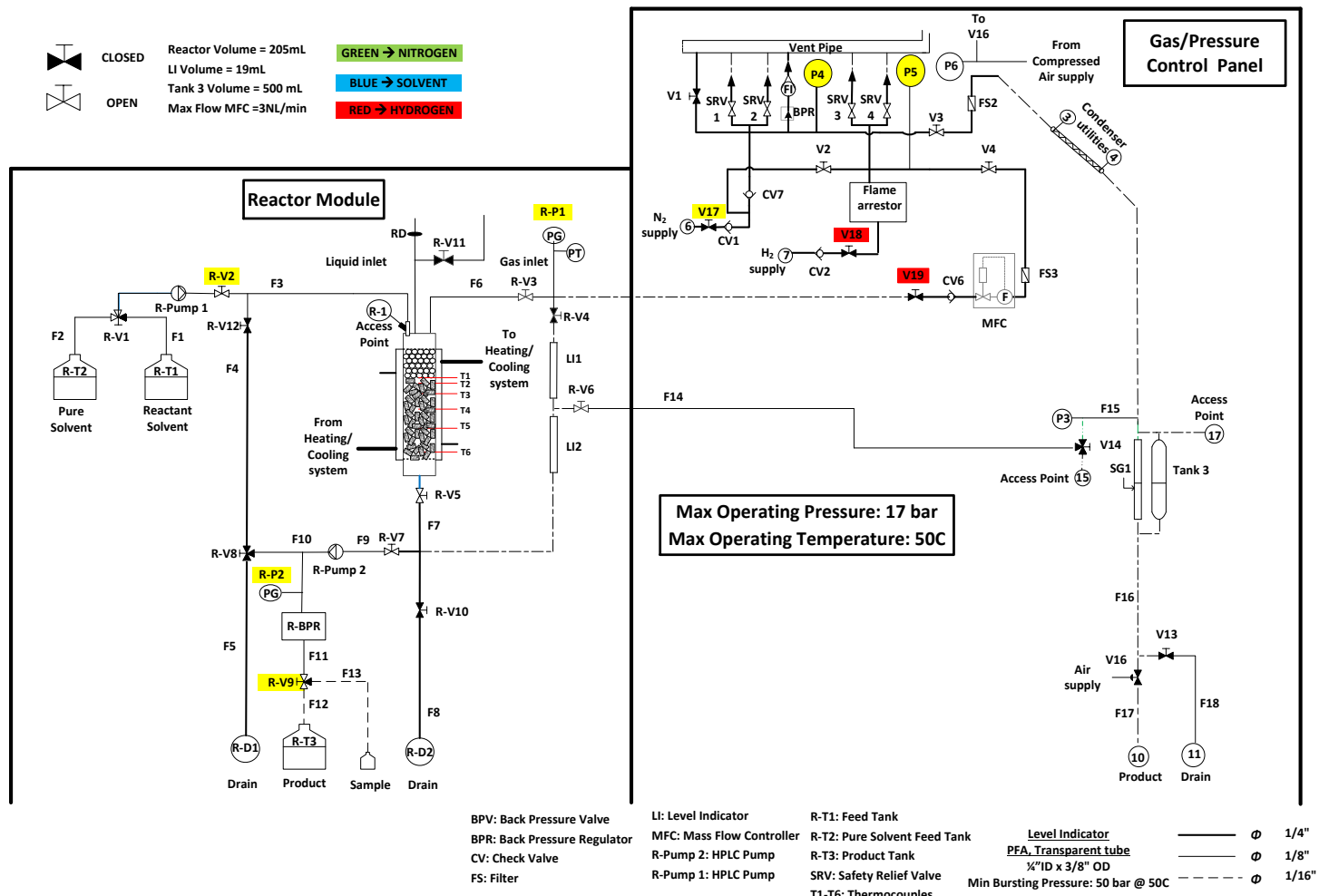
Figure 9.16: FBR system after depressurising gas supply/control panel in shut down procedure.

Catalyst keeping

- **If the reactor vessel is going to be left with catalyst pellets**

1	R-V1 must be switched to F1, pure solvent tank R-T2.	☐
2	Close R-V7.	☐
3	Close R-V6.	☐
4	Fill the reactor with solvent to cover the catalyst pellets.	☐
5	Switch off R-Pump 1.	☐
6	Close R-V1.	☐
7	Close R-V2.	☐

SEE FIGURE 14, NEXT PAGE

- **If the reactor vessel is going to be empty**

1	Ensure that the system is under atmospheric by reading R-P1. R-V3 must be open.	☐
2	Ensure that the system is empty of liquid. Open R-V10 to check.	☐
3	Close R-V2.	☐
4	Close R-V3.	☐
5	Close R-V5.	☐
6	Place a tray underneath the reactor to prevent any spillage.	☐
7	Unscrew the rings at the top and at the bottom of the reactor.	☐
8	Take out the reactor column.	☐
9	Empty the reactor from catalyst pellets.	☐

- If the used Pd/C catalyst is going to be reused, it must be collected and stored in labelled bottles with H_2O.

- If the used Pd/C catalyst is not going to be reused, it must be wasted in labelled bottles with H_2O and placed in special waste drawer in the main lab (B37) before being disposed as special waste.
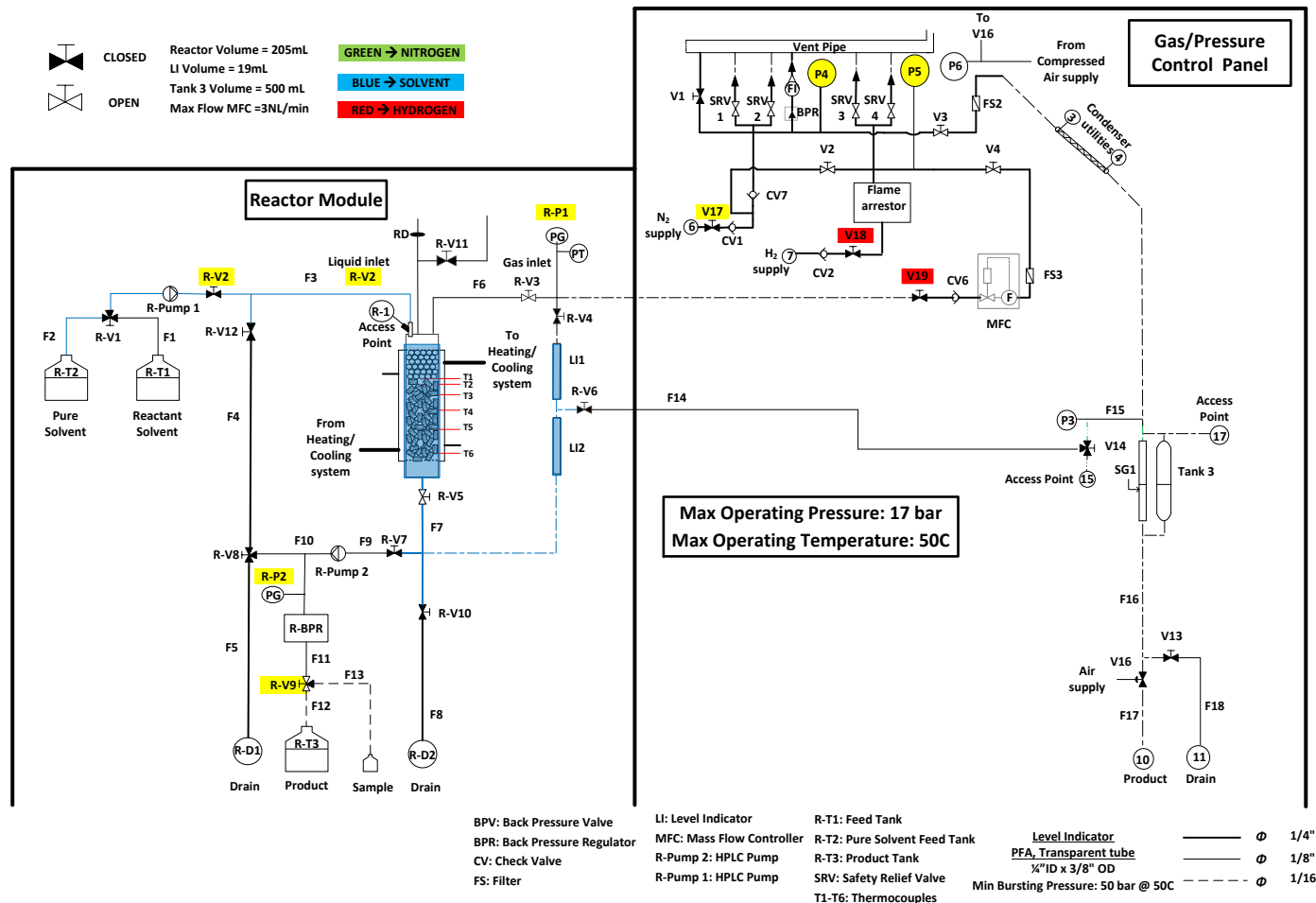
Figure 9.17: FBR system after shut down procedure in the case of leaving the catalyst pellets in the reactor vessel.

10. References

1. Berzelius, J.J., Quelques idées sur une nouvelle force agissant dans les combinaisons des corps organiques. Ann. Chim., 1836. **61**: p. 146-151.

2. Bartholomew, C.H. and R.J. Farrauto, *Fundamentals of industrial catalytic processes*. second ed. Vol. 1. 2006, New Jersey: John & Sons, Inc.

3. Somorjai, G.A. and M.W. Roberts, *Industrial developments.* Catalysis Letters, 2000. **67**(1): p. 66-72.

4. Oxford Economics, *The economic benefits of chemistry research to the UK.* 2010, EPSRC.

5. Davis, M.E. and R.J. Davis, *Fundamentals of Chemical Reaction Engineering*. 2003, New York: Mc Graw Hill.

6. Chaudhari, R.V. and P.A. Ramachandran, *Three Phase Slurry Reactors.* AIChemE Journal 1980. **26**(2): p. 177-201.

7. Rylander, P.N., *Hydrogenation methods*. 1985, Florida: Academic Press Inc Ltd.

8. Biardi, G. and G. Baldi, *Three-phase catalytic reactors.* Catalysis Today, 1999. **52**: p. 223-234.

9. Fernelius, W.C. and H. Wittcoff, *Chemical Processing-Batch or Continuous, Part I.* Journal of Chemical Education, 1982. **59**(9): p. 766-768.

10. Wiles, C. and P. Watts, *Continuous flow reactors: a perspective.* Green Chem., 2012. **14**(1): p. 38-54.

11. Wegner, J., S. Ceylan, and A. Kirschning, *Ten key issues in modern flow chemistry.* Chem Commun (Camb), 2011. **47**(16): p. 4583-92.

12. Roberge, D.M., B. Zimmermann, F. Rainone, M. Gottsponer, M. Eyholzer, and N. Kockmann, *Microreactor Technology and Continuous Processes in the Fine Chemical and Pharmaceutical Industry: Is the Revolution Underway?* Organic Process Research & Development, 2008. **12**: p. 905-910.

13. Roberge, D.M., L. Ducry, N. Bieler, P. Creton, and B. Zimmermann, *Microreactor Technology: A revolution for the Fine Chemical and Pharmaceutical Industries?* Chemical Engineering & Technology, 2005. **28**(3): p. 318-323.

14. Calabrese, G.S. and S. Pissavini, *From batch to continuous flow processing in chemicals manufacturing.* AIChE Journal, 2011. **57**(4): p. 828-834.

15. Dietrich, E., C. Mathieu, H. Delmas, and J. Jenck, *Raney-Nichkel catalyzed hydrogenations: g-l mass transfer in gas-induced stirred slurry reactors.* Chemical Engineering Science, 1992. **47**(13): p. 3597-3604.

16. Beenackers, A.A.C.M. and W.P.M.V. Swaaij, *Mass transfer in gas-liquid slurry reactors.* Chemical Engineering science, 1993. **48**(18): p. 3109-3139.

17. Murthy, A.K.S., *Design and Scaleup of Slurry Hydrogenation Systems.* Engineering Practice, 1999: p. 94-107.

18. Zhang, L., *Selective hydrogenation of a,b-unsaturarted aldehydes towards clean synthesis over noble metal catalysts in mass transfer*

efficient three phase reactors, in *School of Chemical Engineering*. 1997, The University of Birmingham.

19. Bradley, W.E., G.W. Hendricks, H.C. Huffman, and A.E. Kelley, *Hydrogenation of petroleum fractions*, in *Fifth World Petroleum Congress*. 1959, World Petroleum Congress: New York, USA.

20. Sulman, E.M., O.S. Popov, A. Yermakova, and A.A. Belyaev, *Kinetic model and mechanism for selective hydrogenation of acetylene alcohols.* React. Kinet. Catal. Lett., 1988. **36**(1): p. 59-64.

21. Klingler, F.D., *Asymmetric Hydrogenation of Prochiral Amino Ketones to Amino Alcohols for Pharmaceutical Use.* Acc. Chem. Res, 2007. **40**: p. 1367-1376.

22. Zhang, L., J.M. Winterbottom, A.P. Boyes, and S. Raymahasay, *Studies on the Hydrogenation of Cinnamaldehyde over Pd on C Catalysts.* J. Chem. Tech. Biotechnol., 1998. **72**: p. 264-272.

23. Gunstone, F.D., *VEGETABLE OILS IN FOOD TECHNOLOGY: Composition, Properties and Uses*, ed. R.J. Hamilton. 2002, Oxford: Blackwell Publishing Ltd.

24. Warner, K., W.E. Neff, G.R. Lista, and P. Pintauro, *Electrochemical Hydrogenation of Edible Oils in a Solid Polymer Elecrolyte Reactor. Sensory and Compositional Characteristics of Low Trans Soybean Oils.* J. Am. oil chem. soc, 2000. **77**(10): p. 1113-1118.

25. Visentin, F., *Kinetic Study of Hydrogenation Reactions of Aromatic Nitro Compounds Using a New Pressure Resistant Reaction Calorimeter*

Combined with a FTIR-ATR Device. 2005, Swiss Federal Institute of Technology Zurich: Zurich.

26. Gelder, E.A., S.D. Jackson, and C.M. Lok, *The hydrogenation of nitrobenzene to aniline: a new mechanism.* Chem Commun (Camb), 2005(4): p. 522-4.

27. Bruice, P.Y., *Organic Chemistry.* 3rd ed. 2001, New Jersey: Prentice-HAll, Inc.

28. Schlogl, R., *Heterogeneous catalysis.* Angew Chem Int Ed Engl, 2015. **54**(11): p. 3465-520.

29. Chaudhari, R.V., R. Jagathan, D.S. Kohle, G. Emig, and H. Hofmann, *Kinetic modelling of a complex consecutive reaction in a slurry reactor: hydrogenation of phenyl acetylene.* Chemical Engineering Science, 1986. **41**(12): p. 3073-3081.

30. Cheng, Y., J. Chang, and J. Wu, *Kinetic study of pyrolysis gasoline hydrogenation over supported palladium catalyst.* Applied Catalysis, 1986. **24**: p. 273-285.

31. Zhou, Z.M., Z.M. Cheng, Y.N. Cao, J.C. Zhang, D. Yang, and W.K. Yuan, *Kinetics of the Selective Hydrogenation of Pyrolysis Gasoline.* Chemical Engineering & Technology, 2007. **30**(1): p. 105-111.

32. Nijhuis, T.A., F.M. Dautzenberg, and J.A. Moulijn, *Modeling of monolithic and trickle-bed reactors for the hydrogenation of styrene.* Chemical Engineering Science, 2003. **58**(7): p. 1113-1124.

33. Corvaisier, F., Y. Schuurman, A. Fecant, C. Thomazeau, P. Raybaud, H. Toulhoat, and D. Farrusseng, *Periodic trends in the selective*

hydrogenation of styrene over silica supported metal catalysts. Journal of Catalysis, 2013. **307**: p. 352-361.

34. *Handbook of pharmaceutical catalysis.* 2009, Jonshon Matthey Plc.

35. Santen, R.A.v., P.W.N.M.v. Leeuwen, J.A. Moulijn, and B.A. Averill, *Preparation of catalyst supports, zeolites and mesoporous materials.* Stud. Surf. Sci. Catal., 1999. **123**: p. 3-28.

36. Bond, G.C., *Heterogeneous Catalysis: Principles and Applications.* 2nd ed. 1987, Oxford: Clarendon Press.

37. Thomas, J.M., B.F.G. Johnson, R. Raja, G. Sankar, and P.A. Midgley, *High-Performance Nanocatalysts for Single-Step Hydrogenations.* Acc. Chem. Res., 2003. **36**(1): p. 20-30.

38. Yu, W.-Y., G.M. Mullen, and C.B. Mullins, *Hydrogen Adsorption and Absorption with Pd–Au Bimetallic Surfaces.* The Journal of Physical Chemistry C, 2013. **117**(38): p. 19535-19543.

39. Edvardsson, J. and S. Irandoust, *Reactors for Hydrogenation of Edible Oils.* J. Am. oil chem. soc, 1994. **71**(3): p. 235-242.

40. Tarhan, M.O., *Catalytic Reactor Design.* 1983, New York: McGraw-Hill, Inc.

41. Nigam, K.D.P. and A. Schumpe, eds. *Three-Phase Sparged Reactors.* 1996, Gordon and Breach Publishers: Amsterdam.

42. Tsutsumi, A., Y.H. Kim, S. Togawa, and K. Yoshida, *Classification of three-phase reactors.* Sadhana, 1987. **10**(1&2): p. 247-259.

43. Kantarci, N., F. Borak, and K.O. Ulgen, *Bubble column reactors.* Process Biochemistry, 2005. **40**(7): p. 2263-2283.

44. Epstein, N., *Three-Phase Fluidization_Some Knowledge Gaps.* Can. J. Chem. Eng, 1981. **59**(6): p. 649-657.

45. Witerbottom, J.M. and M.B. King, *Reactor Design for Chemical Engineers.* 1999, Cornwall: Stanley Thornes Ltd.

46. Yong, H.Y. and D.D. Kim, *Bubble-wake model for radial velocity profiles of liquid and solid phases in three-phase fluidized beds.* Ind. Eng. Chem. Res, 2001. **40**: p. 4463-4469.

47. Haugwitz, S., *Modeling, control and optimisation of a plate reactor*, in *Department of Automatic Control* 2007, Lund University.

48. Mederos, F.S., J. Ancheyta, and J. Chen, *Review on criteria to ensure ideal behaviors in trickle-bed reactors.* Applied Catalysis A: General, 2009. **355**(1-2): p. 1-19.

49. Satterfield, C.N., *Trickle-Bed Reactors.* A.I.Ch.E Journal, 1975. **21**(2): p. 209-228.

50. Midoux, N., M. Favier, and J. Charpentir, *Flow Pattern, Pressure Loss and Liquid Holdup Data in Gas-Liquid Downflow Packed Beds with Foaming and Non-Foaming Hydrocarbons.* J. Chem. Eng. Jpn, 1976. **9**(5): p. 350-356.

51. Cheng, L., G. Ribatski, and J.R. Thome, *Two-Phase Flow Patterns and Flow-Pattern Maps: Fundamentals and Applications.* Applied Mechanics Reviews, 2008. **61**(5): p. 050802.

52. Noyes, A.A. and W.R. Whitney, *The rate of solution of solid substances in their own solutions.* J. Am. Chem. Soc, 1897. **19**(11): p. 930-934.

53. Cussler, E.L., *Diffusion Mass Transfer in Fluid Systems.* 3rd ed. 2009, New York: Cambridge University Press.

54. Bourne, J.R., *Mixing and the Selectivity of Chemical Reactions.* Organic Process Research & Development, 2003. **7**(4): p. 471-508.

55. Whitman, W.G., *The Two-Film Theory of Gas Absorption.* Chemical and Metallurgical Engineering, 1923. **29**(4): p. 146-148.

56. Skelland, A.H.P., *Diffusional Mass Transfer.* 1974, New York: John Wiley & Sons.

57. Astarita, G., *Mass Transfer with Chemical Reaction.* 1967, Amsterdam: Elsevier Publishing Company.

58. Danckwerts, P.V., *Significance of liquid-film coefficients in gas absorption.* Industrial and Engineering Chemistry, 1951. **43**(6): p. 1460-1467.

59. Levenspiel, O., *Chemical Reaction Engineering.* 3rd ed. 1999, New York: John Wiley & Sons.

60. Forni, L., *Mass and heat transfer in catalytic reactions.* Catalysis Today, 1999. **52**(2-3): p. 147-152.

61. Satterfield, C.N. and T.K. Sherwood, *The Role of Diffusion in Catalysis.* 1963, Massachusetts: ADDISON-WISLEY PUBLISHING COMPANY, INC.

62. Kumar, K.V., K. Porkodi, and F. Rocha, *Langmuir–Hinshelwood kinetics – A theoretical study.* Catalysis Communications, 2008. **9**(1): p. 82-84.

63. Baxter, R.J. and P. Hu, *Insight into why the Langmuir–Hinshelwood mechanism is generally preferred.* The Journal of Chemical Physics, 2002. **116**(11): p. 4379.

64. Ramachandran, P.A. and J.M. Smith, *Adsorption of Hydrogen Sulfide in a Slurry Reactor.* Ind. Eng. Chem. Fundam., 1978. **17**(1): p. 17-23.

65. R.J.Behm, K.Christmann, and G.Ertl, *Adsorption of hydrogen on Pd(100).* Surface Science, 1980. **99**: p. 320-340.

66. H.Conrad, G.Ertl, and E.E.Latta, *Adsorption of hydrogen on palladium single crystal surface.* Surface Science, 1974. **41**: p. 435-446.

67. Baber, A.E., H.L. Tierney, T.J. Lawton, and E.C.H. Sykes, *An atomic-scale View of palladium alloys and their ability to dissociate molecular hydrogen.* ChemCatChem, 2011. **3**(3): p. 607-614.

68. H.Okuyama, W.Siga, N.Takagi, M.Nishijima, and T.Aruga, *Path and mechanism of hydrogen absorption at Pd(100).* Surface Science, 1998. **401**: p. 344-354.

69. Červený, L., *Catalytic Hydrogenation*. 1986, Elsevier: Amsterdam.

70. Satterfield, C.N., *Heterogeneous Catalysis in Industrial Practice*. 2nd ed. 1991, New York: McGraw-Hill.

71. Machado, J.R.S. and W.B. Streett, *Equation of State and Thermodynamic Properties of Liquid Methanol from 298 to 4879 K and pressures to 1040 bar.* J. Chem. Eng. Data, 1983. **28**(2): p. 218-223.

72. Anton Paar GmbH. *Viscosity of Methanol*. 2016 [cited 2016; Available from: https://wiki.anton-paar.com/en/methanol/.

73. Koneripalli, N., Z. Tekie, and B. Morsi, *Mass transfer characteristics of gases in methanol and ethanol under elevated pressures and temperatures.* The Chemical Engineering Journal, 1994. **54**: p. 63-77.

74. Liu, Q., F. Takemura, and A. Yabe, *Solubility of hydrogen in liquid methanol and methyl formate at 20 to 140 Celcius degrees.* J. Chem. Eng. Data, 1996. **41**: p. 1141-1143.

75. Westerterp, K.R., L.L.V. Dierendonck, and J.A.D. Kraa, *Interfacial areas in agitated gas-liquid contactors.* Chemical Engineering Science, 1963. **18**: p. 157-176.

76. Garcia-Ochoa, F. and E. Gomez, *Theoretical prediction of gas–liquid mass transfer coefficient, specific area and hold-up in sparged stirred tanks.* Chemical Engineering Science, 2004. **59**(12): p. 2489-2501.

77. Vasconcelos, J.M.T., S.C.P. Orvalho, A.M.A.F.Rodrigues, and S.S.Alves, *Effect of blade shape on the performance of six-bladed disk turbine impellers.* Ind. Eng. Chem. Res, 2000. **39**(1): p. 203-213.

78. F.Kudrewizki and P.Rade, *Model of dissipation of mechanical energy in gassed stirred tanks.* Chemical Engineering Science, 1986. **41**(9): p. 2247-2252.

79. Markopoulos, J., C. Christofi, and I. Katsinaris, *Mass Transfer Coefficients in Mechanically Agitated Gas-Liquid Contactors.* Chemical Engineering & Technology, 2007. **30**(7): p. 829-834.

80. Labík, L., T. Moucha, M. Kordač, F.J. Rejl, and L. Valenz, *Gas-Liquid Mass Transfer Rates and Impeller Power Consumptions for Industrial*

Vessel Design. Chemical Engineering & Technology, 2015. **38**(9): p. 1646-1653.

81. Kapic, A. and T.J. Heindel, *Correlating Gas-Liquid Mass Transfer in a Stirred-Tank Reactor.* Chemical Engineering Research and Design, 2006. **84**(3): p. 239-245.

82. Karimi, A., F. Golbabaei, M.R. Mehrnia, M. Neghad, K. Mohammad, A. Nikpey, and M.R. Pourmand, *Oxygen mass transfer in a stirred tank bioreactor using different impeller configutions for enviromental purposes.* Iranian Journal of Enviromental Health Sciences & Engineering, 2013. **10**(6).

83. Moucha, T., V. Linek, and E. Prokopová, *Gas hold-up, mixing time and gas–liquid volumetric mass transfer coefficient of various multiple-impeller configurations: Rushton turbine, pitched blade and techmix impeller and their combinations.* Chemical Engineering Science, 2003. **58**(9): p. 1839-1846.

84. Figueiredo, M.M.L.D. and P.H. Calderbank, *The scale-up of aerated mixing vessels for specified oxygen dissolution rates.* Chemical Engineering Science, 1979. **34**: p. 1333-1338.

85. Hiraoka, S., Y. Kato, Y. Tada, N. Ozaki, Y. Murakami, and Y.S. Lee, *Power Consumption and Mixing Time in an Agitated Vessel with Double Impeller.* Chemical Engineering Research and Design, 2001. **79**(8): p. 805-810.

86. Bates, R.L., P.L. Fondy, and R.R. Corpstein, *An examination of some geometric parameters of impeller power.* I&EC Process Design and Development, 1963. **2**(4): p. 310-314.

87. Nienow, A.W. and M.D. Lilly, *Power drawn by multiple impellers in sparged agitated vessels.* Biotechnology and Bioengineering, 1979. **21**: p. 2341-2345.

88. Robinson, C.W. and C.R. Wilke, *Oxygen absorption in stiired tanks: A correlation for ionic strength effects.* Biotechnology and Bioengineering, 1973. **15**: p. 755-782.

89. Linek, V., J. Sinkule, and P. Benes, *Critical assessment of gassing-in methods for measuring kla in fermentors.* Biotechnology and Bioengineering, 1990. **38**: p. 323-330.

90. Yawalkar, A.A., A.B.M. Heesink, G.F. Versteeg, and V.G. Pangarkar, *Gas-liquid mass transfer coefficient in stirred tank reactors.* Can. J. Chem. Eng, 2002. **80**(5): p. 840-848.

91. Linek, V., V. Vacek, and P. Benes, *A critical review and experimental verification of the correct use of the dynamic method for the determination of oxygen transfer in aerated agitated vessels to water, electrolyte solutions and viscous liquids.* Chem. Eng. J., 1987. **34**: p. 11-34.

92. Chandrasekharan, K. and P.H. Calderbank, *Further observations on the scale-up of aerated mixing vessels.* Chemical Engineering Science, 1980. **36**: p. 819-823.

93. R. V. Chaudhari, R.V.G., G. Emig and H. Hofmann, *Gas Liquid Mass Trasfer in "Dead End" Autoclave Reactors.* The Canadian Journal of Chemical Engineering, 1987. **65**: p. 8.

94. Riet, K.V., *Review of measuring methods and results in nonviscous gas-liquid mass transfer in stirred vessels.* I&EC Process Design and Development, 1979. **18**(3): p. 357-364.

95. Ohashi, H.T.a.Y., *Particle to Liquid Mass Transfer in a Rotating Catalyst Basket Reactor.* Journal of Chemical Engineering of Japan, 1977. **10**(1): p. 3.

96. Hughmark, G.A., *Mass transfer for suspended solid particles in agitaed liquids.* Chemical Engineering Science, 1969. **24**: p. 291-297.

97. Brian, P.L.T., H.B. Hales, and T.K. Sherwood, *Transport of Heat and Mass Between Liquids and Spherical Particles in an Agitated Tank.* AIChemE Journal, 1969. **15**(5): p. 727-733.

98. Middleman, S., *Mass Transfer from particles in agitated systems: Application of Kolmogoroff theory.* A.I.Ch.E Journal, 1965. **11**(4): p. 750-761.

99. Rousseau, R.W., *Handbook of separation process technology.* 1987, Chichester;New York;: Wiley.

100. Gholap, R.V., D.S. Kolhe, R.V. Chaudhari, G. Emig, and H. Hofmann, *A new approach for the determination of liquid-solid mass-transfer coef in multiphase reactors.* Chemical Engineering Science, 1987. **42**(7): p. 1689-1693.

101. Sano, Y., N. Yamaguchi, and T. Adachi, *Mass transfer coefficients for suspended particles in agitated vessels and bubble columns.* Journal of Chemical Engineering of Japan, 1974. **7**(4): p. 255-261.

102. Miller, D.N., *Scale-up of agitated vessels.* Ind. Eng. Chem. Process Des. Develop., 1971. **10**(3): p. 365-375.

103. Sádaba, I., M. López Granados, A. Riisager, and E. Taarning, *Deactivation of solid catalysts in liquid media: the case of leaching of active sites in biomass conversion reactions.* Green Chemistry, 2015. **17**(8): p. 4133-4145.

104. Stegeman, D., F.E.v. Rooijen, A.A. Kamperman, S. Weijer, and K.R. Westerterp, *Residence Time Distribution in the Liquid Phase in a Cocurrent Gas-Liquid Trickle Bed Reactor.* Ind. Eng. Chem. Res, 1996. **35**: p. 378-385.

105. Gupta, A.S. and G. Thodos, *Direct analogy between mass and heat transfer to beds of shperes.* A.I.Ch.E Journal, 1963. **9**(6): p. 751-754.

106. Morsi, B.I., *Mass transfer Coefficients in a Trickle-bed Reactor with High and Low Viscosity Organic Solutions.* The Chemical Engineering Journal, 1989. **41**: p. 41-48.

107. Goto, S. and J.M. Smith, *Trickle-Bed reactor Performance. Part I: Holdup and Mass Transfer Effects.* A.I.Ch.E Journal, 1975. **21**(4): p. 8.

108. Metaxas, K. and N. Papayannakos, *Gas-Liquid Mass Transfer in a Bench-Scale Trickle Bed Reactor used for Benzene Hydrogenation.* Chemical Engineering & Technology, 2008. **31**(10): p. 1410-1417.

109. Satterfield, C.N., *Trickle-Bed Reactors.* AIChemE Journal, 1975. **21**(2): p. 20.

110. Julcour-Lebigue, C., F. Augier, H. Maffre, A. Wilhelm, and H. Delmas, *Measurements and Modeling of Wetting Efficiency in Trickle-Bed*

Reactors_liquid viscosity and bed packing effects. Ind. Eng. Chem. Res, 2009. **48**: p. 6811-6819.

111. Fogler, H.S., *Elements of chemical reaction engineering.* 2nd ed. 1992, Englewood Cliffs: Prentice-Hall.

112. Satterfield, C.N., M.W.V. Eek, and G.S.Bliss, *Liquid-solid mass transfer in packed beds with downward concurrent gas-liquid flow.* A.I.Ch.E Journal, 1978. **24**(4): p. 709-717.

113. Miyashita, H., K. Saeki, H. Ueda, and T. Mizushina, *Transport phenomena in laminar flow of a liquid film on a horizontal cylinder.* The Society of Chemical Engineers, Japan 1975. **1**(6): p. 611-615.

114. Gierman, H., *Design of laboratory hydrotreating reactors scaling down of trickle-flow reactors.* Applied Catalysis, 1988. **43**: p. 277-286.

115. McMillan, L., *The palladium catalysed hydrogenation of multi-functional aromatic nitriles*, in *School of Chemistry*. 2011, The University of Glasgow: Glasgow.

116. H.M. McNair and J.M. Miller, *Basic gas chromatography*. 1997, New York;Chichester;: Wiley.

117. Wilke, C.R. and P. Chang, *Correlation of diffusion coefficients in dilute solutions.* A.I.Ch.E Journal, 1955. **1**(2): p. 265-270.

118. Yaws, C.L., *Yaws' Handbook of Thermodynamic and Physical Properties of Chemical Compounds*. 2003, Knovel.